Upstream River Responses to Low Head Dam Removal

by

Robert Alan Amos

A thesis
presented to the University of Waterloo
in fulfillment of the
thesis requirement for the degree of
Master of Applied Science
in
Civil Engineering

Waterloo, Ontario, Canada, 2008

Author's Declaration

I hereby declare that I am the sole author of this thesis. This is a true copy of the thesis, including any required final revisions, as accepted by my examiners.

I understand that my thesis may be made electronically available to the public.

ABSTRACT

Field and modelling investigations of eight failed or removed dams have been undertaken to examine the upstream effects of low head dam decommissioning on channel morphology. Failed or decommissioned sites were selected such that no upstream interventions or channel mitigation had been applied since the time of decommissioning resulting in a physically-based analog consistent with the passive dam removal restoration approach. Field surveys of the sites, which failed between 2 years and 70 years ago, included longitudinal profiles, cross-sections and bed material pavement sampling on each riffle, run, and headcut.

Findings demonstrate that vertical disturbances typically in the form of headcuts frequently extend well beyond the backwater limits of most reservoirs. Although in most cases, critical velocity and shear stress thresholds were exceeded, the localized increases in friction slope where headcuts occurred demonstrated that the velocities associated with larger flows exceeded critical thresholds more often than critical shear stress thresholds. Findings show that if the grain size distributions of the underlying alluvial geologic units are close to that of critical velocity thresholds, when headcuts are initiated (with their resulting increase in friction slope), they can result in continued channel degradation upstream of impoundment regions.

Acknowledgments

I would like to thank my supervisor Dr. Bill Annable for teaching me the process of academic excellence associated with field based research. Thanks for instilling in me the values of this process found through hard work, many hours, and many, many revisions.

I would like to thank my dear friends and research colleagues for assisting me with the countless hours of field work. Whether it was walking kilometers upstream through the thalweg, digging rocks out of the water and backpacking them out, or getting up before the sun for an early start, your enthusiasm and interest was incredible. Thanks to: Mason Marchildon, Terry Ridgway, Pete Thompson, Laddie Kuta, and Mike Fabro.

The support from my family and dearest girlfriend Danielle has kept me grounded in life outside of school. Thanks so much for your love and compassion.

Lastly, thanks to my roommate the Gaffer. What fun!

Table of Contents

1 INTRODUCTION 1
2 BACKGROUND 5
2.1 Rationales for Dam Removal 5
2.2 Methods of Dam Removal 7
2.2.1 Removal Alternatives of the Physical Barrier 9
2.2.2 Impoundment Composition and Remediation Considerations 11
2.3 Upstream Geomorphic and Hydraulic Responses Following Passive Dam Removal 13
2.3.1 Modes of Headcut Migration 21
2.3.2 Lateral Migration of Channels Following Dam Removal 27
2.4 Sediment Transport and Tractive Force Analysis 29
2.5 Longitudinal Hydraulic and Sedimentological Channel Evolution Responses to Passive Dam Removal 35
3 FIELD AND ANALYSIS METHODS 44
3.1 Field Surveys 46
3.1.1 Longitudinal Profiles 47
3.1.2 Cross-Sectional Profiles 48
3.1.3 Sediment Sampling 49
3.2 Numerical Analysis Methods 53
3.2.1 Discharge Frequency Estimates 56
3.2.3 Tractive Force and Permissible Velocity Analysis 61
4 RESULTS AND DISCUSSION 63
4.1 Upstream Disturbance Propagation 63
4.2 Power, Velocity and Shear Profiles 65
4.3 Tractive Force and Velocity Results 77
5 CONCLUSIONS and RECOMMENDATIONS 89
5.1 Recommendations 90
6.0 References 91
Appendix A: Croton Dam on Big Creek at Delhi 98
Appendix B: Hawkesville Dam on Conestoga River at Hawkesville 105
Appendix C: Huttonville Dam on Credit River at Huttonville 111
Appendix D: Chilligo Dam on Ellis Creek at Cambridge 119
Appendix E: Greenfield Dam on Nith River at Greenfield 126
Appendix F: Sutton Dam on Patterson Creek at Simcoe 132
Appendix G: Teeswater Dam on Teeswater River at Teeswater 137
Appendix H: Bognor Dam on Walter's Creek at Bognor 145

List of Tables

Table 1. Approximate threshold conditions for granular material by particle size (modified from Julien, 1995) 33
Table 2. List of dam study sites, river names, valley slope and dominant upstream physiography. 45
Table 3. General channel bed grain size distributions based upon the median bed-material particle size (after Bunte and Abt, 2001). 53
Table 4. Flood flow frequency each site. 59
Table 5. Summary of bed material and sizes, exceeding critical shear stress thresholds for Q_{BF}, Q_2, and Q_{20} within and upstream of site impoundments. Note: if particle sizes are identified in the table, they exceed critical thresholds at one or more morphological features 86
Table 6. Summary of bed material, and sizes, exceeding critical velocity thresholds for Q_{BF}, Q_2, and Q_{20} within and upstream of site impoundments. Note: if particle sizes are identified in the table, they exceed critical thresholds at one or more morphological features 86

List of Figures

Figure 1. Rationales for dam removals in the U.S.A. (modified from Pohl, 2002). 6
Figure 2. Proposed systematic approach for dam removal decision making 9
Figure 3. Dam removal using staged reduction. 10
Figure 4. Typical reservoir sedimentation pattern (modified from Julien, 1995). 11
Figure 5. Three scenarios founding abrupt change in channel invert following dam removal. 14
Figure 6. a) Cross-sectional and b) longitudinal upstream evolution of channel morphology through a reservoir following dam removal (modified from Doyle et al., 2002). 15
Figure 7. Average channel velocity profiles for increasing discharge within each stage of the channel evolution model suggested by Doyle et al., 2002. Q_{BF}, Q_2, Q_{20}, Q_{50}, Q_{100} values represent the bankfull, 2-year, 20-year, 50-year, and 100-year discharge frequency magnitudes respectively. 18
Figure 8. Derivation of total sediment load surcharge curve to predict effective discharge (modified from Biedenharn and Copeland, 2000). 20
Figure 9. The influence of various combinations of resistant and nonresistant bed material on headcut migration (modified from Bush and Wolman, 1960). 22
Figure 10. The physical parameterization of a of a headcut profile (modified from Begin et al., 1980). 24
Figure 11. Modes of headcut migration for a) rotating headcuts and b) stepped headcuts (modified from Stein and Julien, 1993). 26
Figure 12. Channel centreline migration over time to define channel activity (modified from Shields et al., 2000). 28
Figure 13. Relation of applied and resisting forces on a particle resting on a supporting surface (modified from Leopold et al., 1964). 30
Figure 14. Shields particle motion diagram (modified from Julien, 1995). 31
Figure 15. Bed surface for nonuniform grain size mixtures (modified from Julien, 1995). 34
Figure 16. Comparison of different hiding functions (modified from Shvidchenko et al., 2001). 35
Figure 17. Typical a) unit stream power, b) average channel velocities, and c) main channel velocities for the five stages of channel evolution after Doyle et al. [2002] for a discrete range in flows between bankfull (Q_{BF}) and the 100-year (Q_{100}) magnitude discharge events. 39
Figure 18. Typical a) average channel shear and b) main channel shear for the five stages of channel evolution after Doyle et al. [2002] for a discrete range in flows between bankfull (Q_{BF}) and the 100-year (Q_{100}) magnitude discharge events 40
Figure 19. Typical a) unit stream power, b) averge channel velocities, and c) main channel velocities for the five stages of channel evolution after Doyle et al. [2002] for 100 different incremental discharges between $0 < Q < Q_{100}$ 42
Figure 20. Typical a) average channel shear and b) main channel shear for the five stages of channel evolution after Doyle et al. [2002] for 100 different incremental discharges between 43

Figure 21. Locations of study sites within Southern Ontario. 45
Figure 22. Example plan view of a field survey of Teeswater River at Teeswater. 47
Figure 23. Longitudinal profile of Teeswater River at Teeswater. 48
Figure 24. Locations of bed material samples along a riffle. 50
Figure 25. Locations of bed material samples along a headcut. 50
Figure 26. Example pavement sample distributions of the uppermost riffle (Riffle 1) of Credit River at Huttonville. 52
Figure 27. Comparison of a) HEC-RAS calibrated vs. regional analysis method for bankfull discharge and b) adjusted Manning's roughness coefficient vs. estimated Manning's roughness coefficient using Limerinos [1970]. 56
Figure 28. Conestoga River at Hawkesville sub-watershed DEM within the Upper Grand River watershed. 58
Figure 29. Comparison of yearly instantaneous maximum discharges, Weibull Plotting Position, Log Pearson-III Analysis, Gingras et al. [1994] and Annable [1996] methods of discharge estimation for the $Q_{1.5}$, Q_2, Q_{20} and Q_{100} return periods for Environment Canada gauge stations proximal to study sites at a) Big Creek near Delhi (02GC006) b) Conestoga River at Glen Allan (02GA028) and c) Credit River at Norval (02HB025). 60
Figure 30. Ratio of maximum upstream headcut extent to normalized reservoir limit. .. 64
Figure 31. Results of a) unit stream power, b) average velocity, c) main channel velocity for incremental discharge analyses between $0 < Q < Q_{100}$, and d) thalweg elevation along the longitudinal profile for the Credit River at Huttonville (site 3). 67
Figure 32. Results of a) average channel shear stress and b) main channel shear stress for incremental discharge analyses ranging between $Q < Q < Q_{100}$ along the longitudinal profile for the Credit River at Huttonville (site 3). 68
Figure 33. Average channel velocities of a stable upstream cross-section and the envelope of incised channel cross-sections for discharges ranging between $Q < Q < Q_{100}$ for the Credit River at Huttonville (site 3). 68
Figure 34. Main channel velocities of a upstream stable cross-section and the envelope of incised cross-sections for discharges ranging between $Q < Q < Q_{100}$ for site 3. 70
Figure 35. Results of unit stream power of flows which overtop banks vs. normalized longitudinal channel profile distance. 73
Figure 36. Results of a) average channel velocity and b) main channel velocity of flows which overtop banks vs. normalized longitudinal channel profile distance.. 74
Figure 37. Results of a) average channel shear and b) main channel shear of flows which overtop banks vs. normalized longitudinal channel profile distance. 75
Figure 38. Results of a) main channel shear vs. τ_{c50} threshold and b) main channel shear vs. $\tau_{c\,84}$ threshold along the normalized longitudinal profile at Q_{BF}. 78
Figure 39. Results of a) main channel shear vs. $\tau_{c\,50}$ threshold and b) main channel shear vs. $\tau_{c\,84}$ threshold along the normalized longitudinal profile at Q_2. 79
Figure 40. Results of a) main channel shear vs. $\tau_{c\,50}$ critical threshold and b) main channel shear vs. $\tau_{c\,84}$ critical threshold along the normalized longitudinal profile at Q_{20}. 80

Figure 41. Results of a) maximum permissible particle size at Q_{BF} vs. the range of measured d_{50} values and b) maximum permissible particle size at Q_{BF} vs. the range of measured d_{84} values along the normalized longitudinal profile. 81
Figure 42. Results of a) maximum permissible particle size at Q_2 vs. the range of measured d_{50} values and b) maximum permissible particle size at Q_2 vs. the range of measured d_{84} values along the normalized longitudinal profile..... 82
Figure 43. Results of a) maximum permissible particle size at Q_{20} vs. the range of measured d_{50} values and b) maximum permissible particle size at Q_{20} vs. the range of measured d_{84} values along the normalized longitudinal profile. 83

Notation

Symbol	Unit	Description
a	[-]	sediment rating curve regression fitting parameter
A	[L^2]	channel cross-sectional area
A'	[-]	empirical coefficient
b	[-]	sediment rating curve regression fitting parameter
B	[$M\ L^{-3}$]	soil bulk density
ds	[L]	particle size
di	[L]	particle size where i denotes percentage finer
C	[-]	coefficient of friction
DA	[L^2]	effective drainage area
E	[$M\ L^{-2}T^{-1}$]	detachment rate per unit area
f	[-]	Darcy-Weisbach friction factor
F_N	[$M\ LT^{-2}$]	force normal to the bed slope
F_O	[$M\ LT^{-2}$]	fricitonal stress opposing motion
F	[-]	Froude number
g	[$L\ T^{-2}$]	acceleration due to gravity
G	[-]	specific gravity of bed material
h	[L]	initial drop height of the headcut
h_n	[L]	normal flow depth
h_u	[L]	flow depth at the crest of the headcut
P	[$M\ L^1T^{-1}$]	stream power
$\hat{P}$	[$M\ T^{-1}$]	unit stream power
Q_{BF}	[$L^3\ T^{-1}$]	bankfull discharge
Q_i	[$L^3\ T^{-1}$]	observed discharge
Q_{EFF}	[$L^3\ T^{-1}$]	effective discharge
Q_F	[$L^3\ T^{-1}$]	channel forming discharge
Q_{Si}	[$M\ T^{-1}$]	sediment transport rate related to discharge Q_i
q_s	[$M\ L^{-1}T^{-1}$]	rate of sediment transport per unit width
Qs	[$L^3\ T^{-1}$]	bed material discharge
R	[L]	hydraulic radius
R_c	[L]	radius of curvature
S_f	[-]	friction slope
S_v	[-]	valley slope
S_o	[-]	bed slope

t	[T]	time interval
T	[L]	top width of channel discharge
Td	[T]	time for the impingement scour to develop horizontally and reach the toe of the vertical face
Tu	[T]	time for upstream vertical scour to reach the toe of the vertical face
u_*	[L/T]	shear velocity
V	[L T^{-1}]	flow velocity
ν_m	[L T^{-1}]	kinematic viscosity of fluid
W	[L]	top width of bankfull channel
x	[L]	distance along the channel
y	[L]	elevation
Yo	[L]	constant elevation by which the baselevel is lowered at x = 0

Greek

Λ	[L]	wetted perimeter
ξ	[-]	empirical coefficient
ρ_m	[M L^{-3}]	fluid density (1000kg/m^3)
τ^*	[dimensionless]	Shield's parameter
τ_C	[M $L^{-1}T^{-2}$]	critical shear strength
τ_o	[M $L^{-1}T^{-2}$]	shear at the bed
γ_s	[M $L^{-2}T^{-2}$]	bulk unit weight of the sediment (2650 kg/m^3)
γ_w	[M $L^{-2}T^{-2}$]	specific weight of water (9810 kg/m^3)
$\emptyset$	[-]	critical angle of repose
Ω	[-]	sinuosity

1 INTRODUCTION

Dams have been integral to the advancement of mankind for hundreds of years by providing sources of power, water supply, flood control, irrigation, and navigation; amongst many other uses. Correspondingly, the siting and construction of dams have segmented the majority of rivers in the Northern Hemisphere resulting in large-scale environmental disruption (Dynesius, 1994). The environmental impacts dams can have on their surrounding physical and biological environments are well documented (Petts, 1984; Ligon, 1995; Bednarek, 2001).

In more recent times, the removal of dams has garnered considerable attention; primarily related to structures which are no longer fulfilling their primary design purpose. The acceleration in structure removals reflects expiring life expectancies, the desire to restore ecological connectivity, and national policies directed at mitigating environmental impacts of riverine structures. Several studies have also been focused on the ecological effects, sediment transport responses, and channel adjustments downstream of impoundments post removal (Dynesius, 1994; Ligon, 1995; Pansic et al., 1998; Dolye et al., 2003; Doyle, 2005; Cui et al., 2005; Ashley, 2006).

In general, dam restoration projects consist of removing the physical barrier and the re-establishment of a stable channel; floodplain; and sediment continuity within the impoundment footprint. There are two typical approaches to channel recovery which are commonly referred to as active and passive restoration. Active restoration entails the design and construction of a river channel to either it's historical or new stable channel

morphology and removing the impounded sediments to pre-dam topographic conditions. Passive restoration involves channelization through the impoundment sediments via initiating erosional processes (i.e. headcuts) at the dam face to form a channel. Over time with the upstream propagation of headcuts, an incised channel forms through the impoundment sediments, which, eventually tends toward a state of dynamic morphologic stability. The active restoration strategy, however, is notably more costly than the passive approach rendering the passive approach to often being the preferred remediation alternative.

The passive restoration approach, however, can have several negative impacts to the local ecology and river stability if not properly considered and mitigated in the design and construction process. Headcuts initiated at the dam face migrate upstream to achieve base level lowering within the impoundment and initially create an incised channel. The scale of the headcuts, and associated incision, is dependent upon the extent of base level lowering necessary to achieve channel stability in addition to establishing discharge and sediment continuity between the upstream and downstream reaches of the impoundment. Incised channels, of which headcuts are a physical identifier, have distinctive characteristics which affect the hydraulic, sedimentological and geomorphical processes and typically indicate periods of channel instability or disequilibrium (Simon and Darby, 1999). An incised channel typically has increased bank heights and enlarged cross-sections with increased channel discharge capacity relative to a bankfull channel and flood plain dominated morphology. The incised channel morphology results in higher shear stresses; velocities; and unit stream power during moderate to high flood flows as

the floodplain is rendered inaccessible (Simon, 1998). Consequently, an excess of sediment transport capacity occurs within the incised channel reaches relative to the amount of sediment supplied. This initiates an increased sediment yield within the incised channel (i.e. within the reservoir impoundment) to the downstream reaches. This degradational process can affect the impoundment and downstream reaches over several years until dynamic channel stability is attained and often results in declines of both hydraulic and ecosystem function (Shields et al., 2000; Beechie et al., 2007). The degradational processes can also have socio-economic ramifications resulting from land loss, the undercutting of bridges, road crossing or other man made structures.

It is commonly believed that headcuts and channel incision related to the passive restoration approach diminish in size and terminate at the upstream extent of the impoundment. However, depending upon such factors as headcut size, headcut slope, local hydraulic grade lines, local geology, geometric characteristics, and flood forming flows, headcuts may continue to migrate beyond the upstream limits of the impoundment. Therefore, the act of inducing headcuts at the dam face to initiate a passive restoration strategy may have upstream effects well beyond the intended limits of the reservoir impoundment leading to continued channel degradation.

The purpose of this study is to examine if channel disturbances related to the decommissioning of low head dams exist, utilizing the passive restoration approach, upstream of reservoir impoundments. If channel disturbances are found, a secondary objective of this work is to provide remediation strategies to mitigate such upstream

disturbances. As there are a limited number of dam restoration projects with sufficient time lines to study the effects of upstream channel degradation, an examination of channel morphologies and evolutions using the analog of removed or failed dams with no upstream interventions to the headcut driven channel formation processes will be studied. As channel evolution is dependent upon numerous criteria such as local geology, valley slopes, particle sizes and gradations, reservoir sediment levels and channel forming flow depths, failed or removed dams will be studied on a broad spectrum of environmental factors.

2 BACKGROUND

The literature review provided within this thesis is assembled into the following sections:

- Rationales for dam removal;
- Methods of dam removal;
- Geomorphic and hydraulic responses to channelization through reservoir impoundments;
- Tractive force analysis; and
- Longitudinal channel evolution responses to dam removal.

2.1 Rationales for Dam Removal

Pohl [2002] compiled a database of dams within the U.S.A. and analyzed both spatial and temporal trends in dam removal strategies. Pohl found that dam removal initiatives were strongly related geographically to ecological values and funding opportunities for the dismantling of structures. Four principle motivations were identified: environmental initiatives to re-establish riparian corridor connectivity, dam safety, economics, and dam failures. Pohl [2002] also identified an escalation of dam removals in the 1990s, as illustrated in Figure 1, for environmental reasons due to social and environmental policy changes.

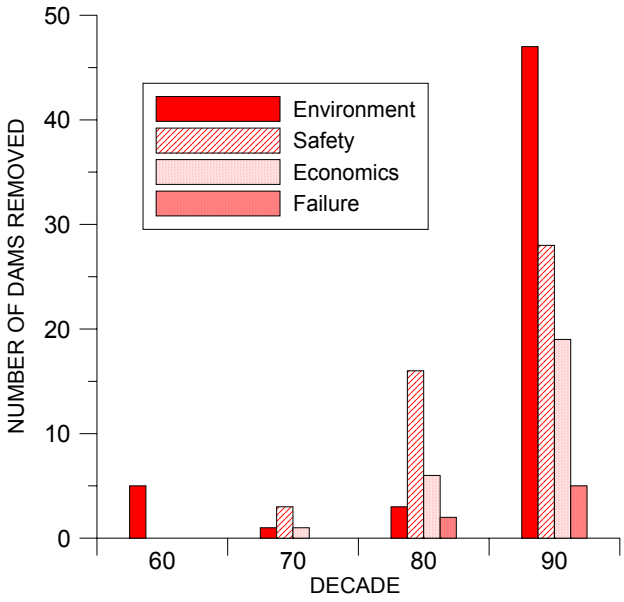

Figure 1. Rationales for dam removals in the U.S.A. (modified from Pohl, 2002).

A study was conducted by the American Association of State Highway and Transportation Officials [2005] to summarize existing research on low head dam removal projects. They found that the majority of removals that have occurred in the United States are not accompanied by environmental impact studies, even though it was found that the primary rational behind dam removal is related to ecological benefit. Of 129 agencies surveyed, 50 responses were received. Results of the study concluded:

- Dam removals were relatively uncommon before the 1980s but have escalated significantly in the 21st century. The recent acceleration of dam removals reflects problems associated with aging structures, growing interest in restoring rivers and fish passage, new funding opportunities to support dam removal, and national policies aimed at improving the safety of aging structures and mitigating the environmental impacts of these structures.
- The three most common reasons for dam removals in order of frequency were: ecology, economics, and safety.

- Most of the dams removed have a structural height smaller than six meters. This is in agreement with observations made by the Heinz Center [2002]. The majority of low head dams (79%) were completely removed with the remaining structures either being breached or partially removed. Further, the study found that the deconstruction cost typically accounted for approximately 50% of the total removal cost, where the remaining costs were related to sediment management, stream channel restoration and monitoring.

Public reaction to dam removal is often quite varied. Commonly, a portion of the public opposes removal based upon issues such as loss of recreation opportunities, reduced access to aquatic environments, alteration of aesthetic parameters, private land owner concerns, loss of cultural or historic values, and costs related to removal. In contrast, support is often found for environmental enhancements to water quality and fish migration, along with residents and government agencies concerned with dam safety, liability and litigation (Canadian Dam Association, 2005).

2.2 Methods of Dam Removal

Standard methods and/or generic guidelines do not exist for the removal of dams and reservoir restorations; similar to the state of the science for river restoration (Copeland et al., 2000). In order to achieve the desired effects from dam removal; be it related to environmental restoration, minimizing public health and safety risks, reducing liability, or minimizing maintenance costs to dam owners, dam removal is highly site specific and

techniques must vary to suit the socio-economic, local ecological and geomorphologic conditions.

Socio-economic considerations include the funding sources for dam removal, the impending risk and liability of dam failure, public support or protests, public safety, functionality, and ownership. Ecological aspects consider changes in: flow regime; water temperature; sediment and pollutant releases and super-saturations; aquatic habitats; and the migration of fish and other aquatic organisms. The geomophological implications include: downstream sedimentation and upstream erosion; channelization through the impoundment; bank stability; lateral and transverse channel adjustment and degradation; and attaining a natural channel in a state of quasi-equilibrium for the given surrounding geology and valley slopes.

Although many of the socio-economic, ecological and geomorphological considerations overlap in a dam removal project, they are seldom congruent (Bednarek, 2001). The Heinz Center [2002] developed a systematic approach to assess the feasibility of a dam removal. This approach establishes goals, identifies major issues of concern and assesses potential outcomes of the river ecology and morphology as outlined in Figure 2.

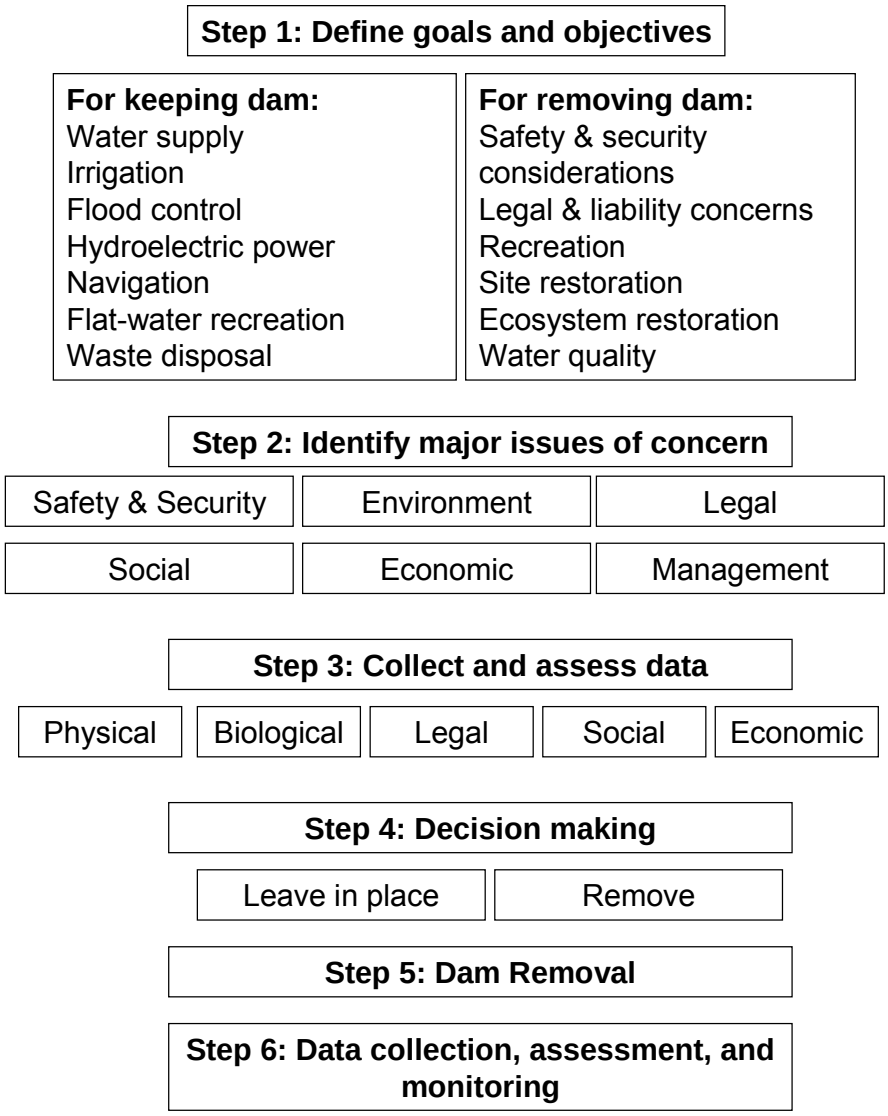

Figure 2. Proposed systematic approach for dam removal decision making (after Heinz Center, 2002).

2.2.1 Removal Alternatives of the Physical Barrier

There are several common methods for removing the physical structure of a dam, whether it is a series of notched or staged reductions of the spillway crest as part of a gradual dam removal (Figure 3), using controlled explosives or heavy machinery for immediate removal, or the simple removal of gates or stop logs. An alternative to

removing the physical barrier is to divert the river around the dam completely if sufficient land is available.

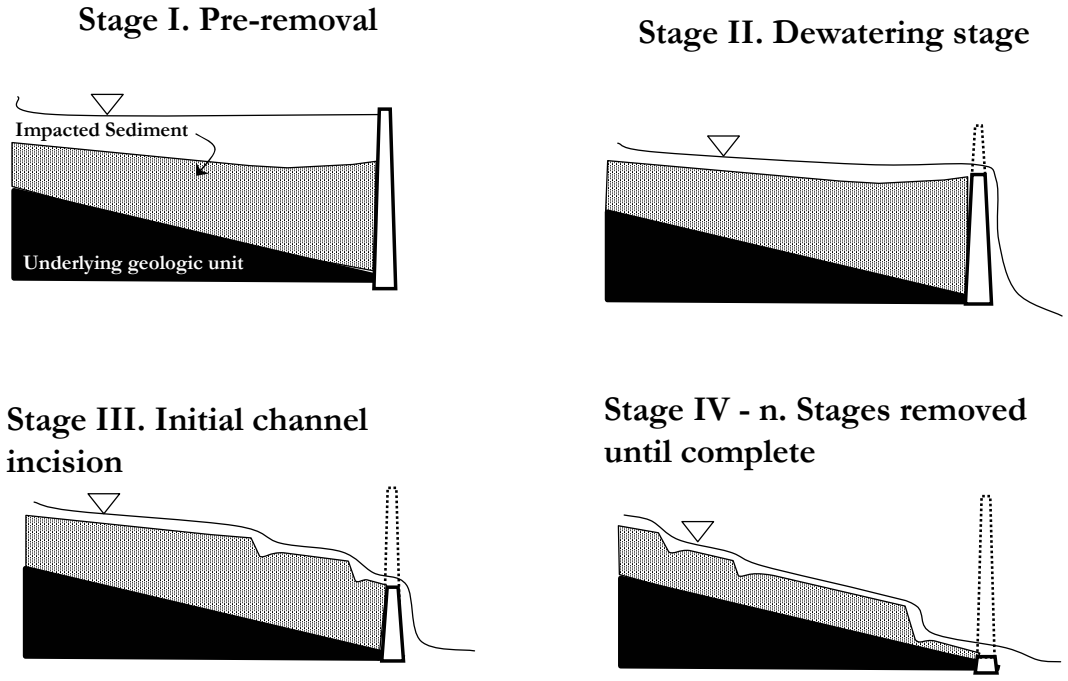

Figure 3. Dam removal using staged reduction.

Removals can also be limited to partial removal or dam breaches if complete removal is deemed not to be the preferred option. In these scenarios, the majority of the physical structure is left intact, and either a vertical notch is cut through the entire height of the dam face (typically consistent with the downstream bankfull channel width) or the height of the spillway is reduced to the upstream height of the deposited sediments. Partial removal is often considered a preferred restoration alternative to avoid the costs of full removal, to stabilize upstream reservoir sediments (particularly if contaminated sediment concerns exist), and to retain some structure for historic or cultural purposes.

2.2.2 Impoundment Composition and Remediation Considerations

Dams affect the transport of both sediment and organic material. Upon construction of a dam, channel velocities decrease approaching the dam face, the gradually varied flow profile depicts an M1 profile for a mildly sloping channel, and a reduction in sediment transport capacity results. Sediments entering a reservoir commonly deposit throughout its full length, both raising the bed elevation and reducing the channel bed slope over time as sediment transport from upstream reaches continues. Sediments within a reservoir are mainly comprised of fine silt and sand near the dam face, transported by density currents, while coarser material often settles closer to the inflow of the reservoir (Julien, 1995; Kondolf, 1997) often forming small deltas. In some cases impoundments completely fill with sediment, rendering the primary function of the dam (water retention) ineffective. Figure 4 depicts a typical reservoir sedimentation pattern.

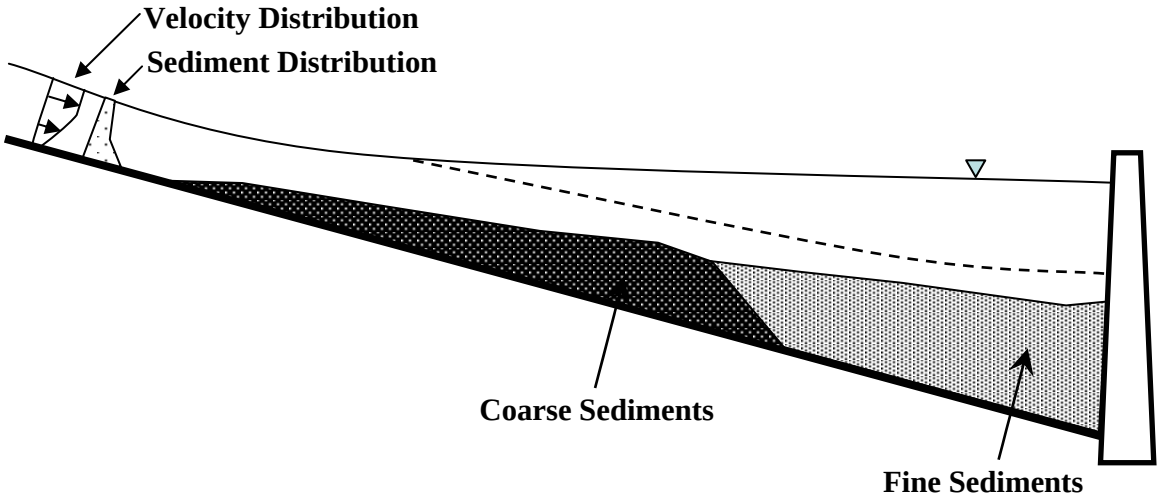

Figure 4. Typical reservoir sedimentation pattern (modified from Julien, 1995).

A notable concern of most dam removals is the fate of sediments and pollutants stored within the reservoir impoundment. Rapid flushing of fine sediments and mobilization of

potential pollutants accumulated from the impoundment region upstream of the dam face to downstream channel reaches may cause considerable channel aggradation and have severe ecological and water quality effects (Wohl, 2000). Cheng and Granata [2004] also identifies that the downstream release of sediments can have prohibitive effects upon infrastructure and water intakes.

A primary objective of dam restoration is to minimize sedimentation to downstream reaches. This is commonly achieved within the impoundment region by developing a dynamically stable channel and floodplain using one of two general methods. The first method considers the construction of a channel and floodplain within the impoundment region consistent with the historical topography and / or stable upstream morphology by excavating a channel and the preponderance of the sediments to the pre-dam conditions. This is referred to as the active channel recovery method (Stanley and Doyle, 2002; Selle et al., 2007). The active channel recovery method typically requires sizable investigations (both spatially and temporally), engineered designs, and often significant disposal fees for contaminated sediments and construction costs that often render this alternative financially prohibitive.

An alternative approach, commonly referred to as the passive channel recovery method (Stanley and Doyle, 2002; Selle et al., 2007) does not require the removal of the entire structure or impounded sediments. This approach entails channelization through the impoundment sediments while leaving the majority of deposited material in place, and allows a channel to evolve to a state of quasi-equilibrium (Leopold et al., 1964) with

time. Although a channel can be constructed through the impoundment sediments using natural channel design techniques, the passive method typically subscribes to the initiation of headcuts at the dam face (via notches in the dam face) resulting in a channel evolving through the impoundment sediment with time tending towards a state of quasi-equilibrium. This approach utilizes little, if any, mechanical means of channel construction and relies solely upon the migration of a headcut or headcuts to recreate the channel and associated floodplains. In turn, the dispositions of impounded sediments rely solely on downstream conveyance and depositional patterns (Selle et al., 2007). If the rate and volumes of downstream sedimentation can be controlled while meeting the remaining objectives of the project, the passive approach garners considerable interest as a cost effective remediation alternative.

2.3 Upstream Geomorphic and Hydraulic Responses Following Passive Dam Removal

The focus of the discussion herein will consist of the upstream hydraulic, sedimentological and geomorphological outcomes of passive impoundment channelization initiated by headcut migration. Headcuts are initiated from an abrupt change in channel invert caused by either aggradation within the impoundment, illustrated in Figure 5c, degradation below the dam (Figure 5b), or a combination of the two (Figure 5a).

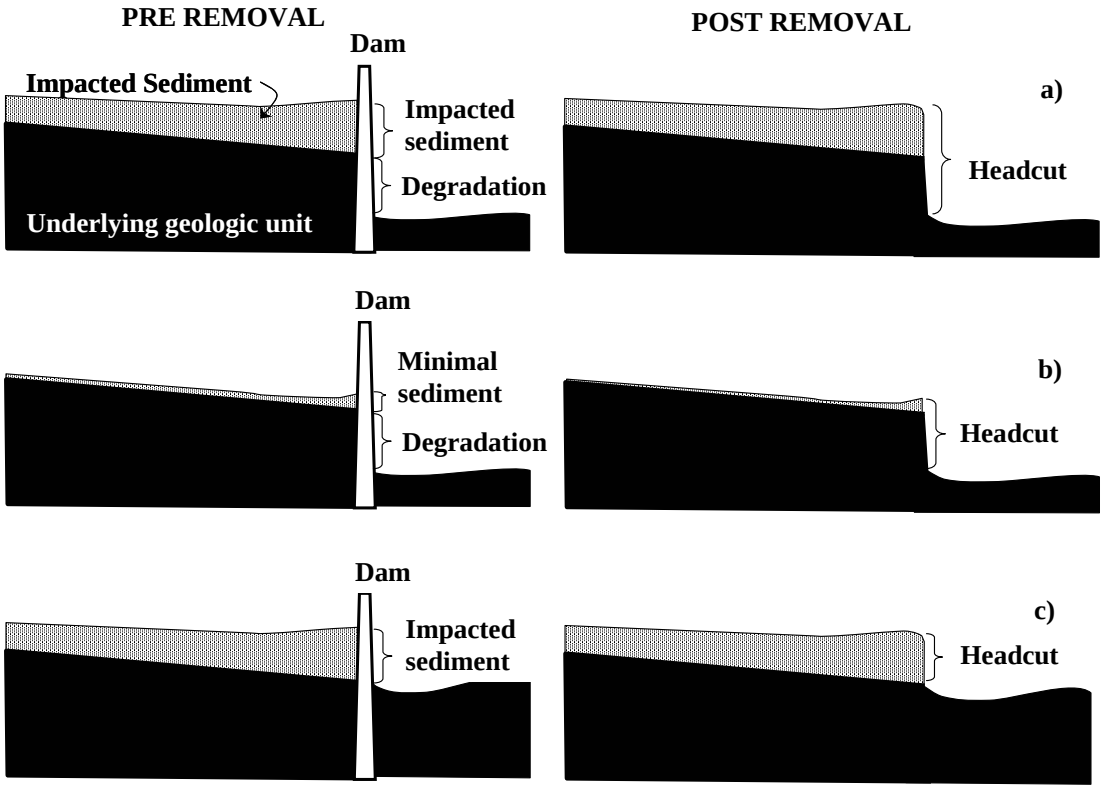

Figure 5. Three scenarios founding abrupt change in channel invert following dam removal.

Doyle et al. [2003] identified that passive dam removals with impoundments principally composed of fine sediments are geomorphically analogous to that of alluvial channels responding to base level lowering, specifically alluvial channel incision. Researchers in the fields of fluvial hydraulics and geomorphology have long observed and studied spatial and temporal channel adjustments in response to disturbances such as base level lowing (Schumm, 1969; Emerson, 1971; Simon and Darby, 1999). Channels responding to such perturbations tend to follow a series of generalized geomorphic responses related to discharge and sediment continuity, geotechnical stability and geomorphic processes. The series of channel adjustments are commonly referred to as the channel evolution model (CEM) (Schumm et al., 1984). Doyle et al. [2002] modified the CEM to depict the geomorphic responses which are consistent with the channel evolution upstream of a dam

where base level lowering has been instigated by the development of a headcut at the dam face (Figure 6). As illustrated in Figure 6b, channel evolution propagates upstream in response to base level lowering at the dam face. Several morphologic features such as headcuts and knickpoints (smaller scale versions of headcuts) are observed along the longitudinal profile which indicates continued vertical instability and degradation in the channel profile.

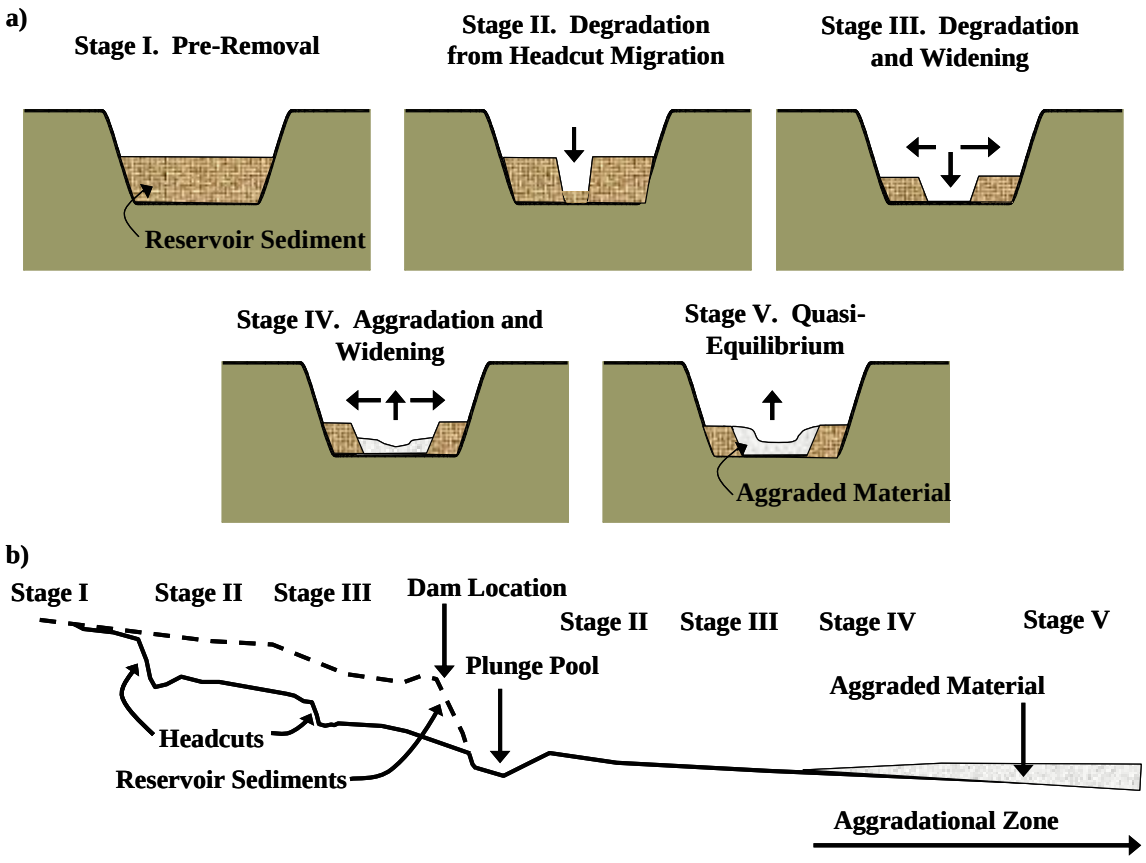

Figure 6. a) Cross-sectional and b) longitudinal upstream evolution of channel morphology through a reservoir following dam removal (modified from Doyle et al., 2002).

Rapid longitudinal channel degradation ensues as the headcut or headcuts migrate through the impoundment (Stage II), while the wetted perimeter of the cross-section upstream of the advancing headcut remains largely undisturbed maintaining a Stage I

channel morphology (Doyle et al., 2003). The Stage I channel morphology is characterized by a bankfull channel with an associated floodplain that is commonly either a riffle-pool or step-pool dominated morphology. Continued channel degradation begins to decrease the channel gradient (by increasing sinuosity) resulting in increased bank heights and steeper channel side slopes. This continued geomorphic response leads to channel widening by mass-wasting and bank failure (Stage III) once bank heights and angles exceed their critical angles of repose and critical shear stress thresholds (Simon and Darby, 1999). As channel degradation continues to migrate further upstream, the reaches closer to the dam face begin to aggrade (Stage IV) resultant from elevated sediment loads from upstream reaches where Stage III is occurring. The evolution of Stage V continues to experience aggradation, reductions in channel slope and decreasing bank height, and channel side slope angles by meander extension (Simon and Darby, 1999). Over time, a new dynamic equilibrium channel and floodplain develops in Stage V which is similar in cross-sectional profile to Stage I but at a lower base elevation.

The geomorphic response throughout the stages of the CEM is often expressed using Lane's stream power proportionality (Lane, 1955):

$$\gamma_w Q_F S_o \propto \gamma_S Q_s d_i \qquad [1]$$

where Q_F is the channel forming discharge [$L^3 T^{-1}$], S_o is the bed slope [-], Q_s is the bed material discharge [$L^3 T^{-1}$], d_i is the characteristic particle size [L], and γ_W [$M L^{-2}T^{-2}$] and γ_S [$M L^{-2}T^{-2}$] are the specific weights of water and sediment respectively. The initial disturbance is caused by the localized increase in bed slope at the headcut causing an

increase in the sediment discharge and permissible particle size. This describes the evolution from the first to the second stage of channel evolution. In each subsequent stage, an imbalance is present causing corresponding shifts in the other variables expressed in Equation 1. As the channel tends towards a more stable state, such that a new dynamic equilibrium is attained in Stage V, a new balance is attained in Equation 1 which has adjusted to the surrounding topographic, geologic and hydraulic environment. Differences exist in the sediment routing and carrying capacity characteristics within each stage of the channel evolution sequence which is strongly related to bank heights and access to the adjacent floodplain. Flows that frequently overtop their banks onto floodplains (Stages I and V) maintain lower in-channel velocities and shear stresses relative to the incised channel reaches where there is limited access to the floodplain (Stages II, III, IV). Figure 7 illustrates the resulting average velocities for increasing discharge for the five different stages of channel evolution. In Stage II where vertical incision occurs, there is limited access to the adjacent floodplain and higher flows are contained within the limits of the channel. As a result, velocities continue to increase with increasing discharge. In Stages III and IV where channel widening ensues, the range in discharge may still be contained within the channel cross-section with no access to the floodplain; however, with the increasing cross-sectional area, velocities begin to decrease relative to Stage II. Points of inflection in Stages I, IV and V indicate flow conditions where floodplain access is achieved. A similar response is observed for average channel shear stress whereby the hydraulic radius increases more dramatically in Stages II, III and IV relative to Stages I and V. In the stages of channel evolution where velocities and shear stresses increase, there is an increased tendency for channel

degradation to occur for the reason that velocity and shear stress thresholds may be exceeded relative to the bed material sizes and cohesiveness required to maintain channel bed and bank stability.

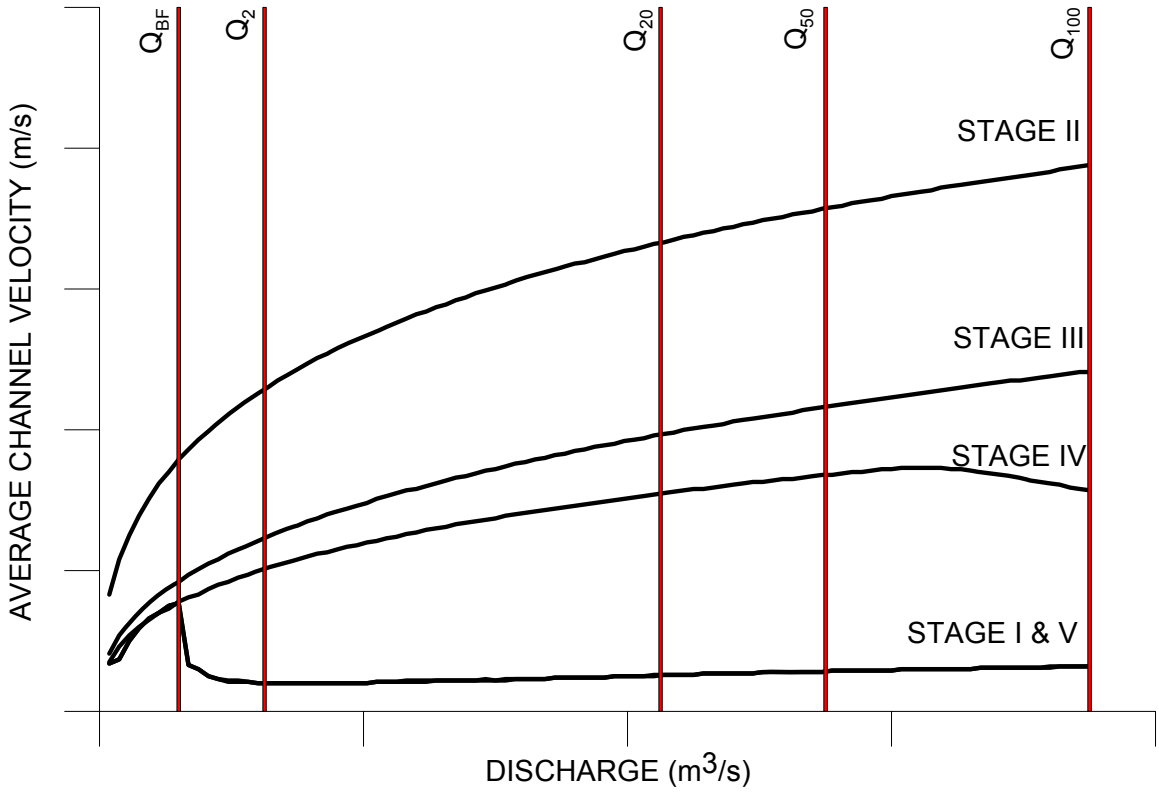

Figure 7. Average channel velocity profiles for increasing discharge within each stage of the channel evolution model suggested by Doyle et al., 2002. Q_{BF}, Q_2, Q_{20}, Q_{50}, Q_{100} values represent the bankfull, 2-year, 20-year, 50-year, and 100-year discharge frequency magnitudes respectively.

Inherent within Figure 7 is the observation that where inflections occur in the velocity profiles (and in the corresponding shear stress profiles), there are particular discharges that dominate the rate of channel evolution known as the channel forming discharge (Q_F). The channel forming discharge is defined as the theoretical discharge, if maintained indefinitely, that would produce the same channel geometry as the natural long-term hydrograph (Copeland et al., 2000). This discharge is significant as many researchers and practitioners use this single representative discharge to determine the stable channel

geometry (Copeland et al., 2000). In channel Stages I and V, bankfull discharge (Q_{BF}) [$L^3 T^{-1}$] dominates the channel evolution which is defined as the discharge, over a long period of time that defines the dynamically-stable equilibrium channel (Leopold et al., 1964). In floodplain dominated stream morphologies, this stage is commensurate with the top of the bank just prior to flows entering the flood plain, thus $Q_{BF} = Q_F$. The recurrence interval or frequency of flows that overtop the banks in the unstable sections (Stages II – IV) is often much greater than the recurrence interval of bankfull discharge associated with the stable sections and occurs too infrequently to define the channel form. In these channel morphologies, effective discharge Q_{EFF} [$L^3 T^{-1}$] dominates the evolution of the channel evolution (i.e. $Q_F = Q_{EFF}$). Effective discharge is defined as the discharge, or range of discharges, that transports the largest proportion of annual sediment loads over the long period of time (Wolman and Miller, 1960). A graphical representation of the bed material load histogram, as a function of sediment transport and frequency of the transport used to define effective discharge, after Biedenharn and Copeland [2000], is illustrated in Figure 8.

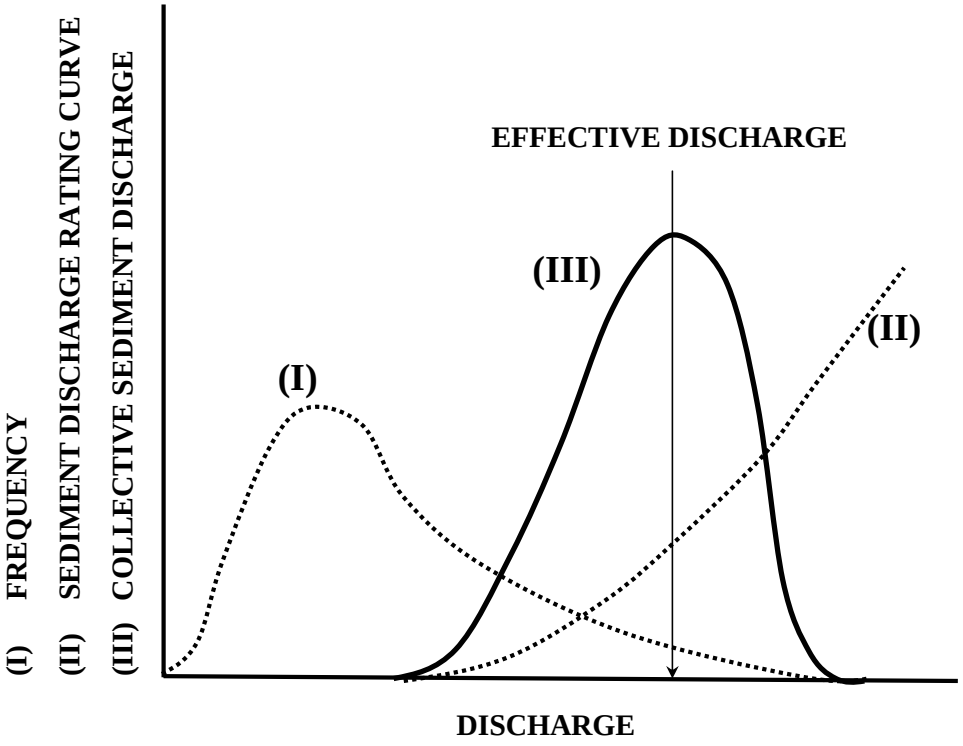

Figure 8. Derivation of total sediment load surcharge curve to predict effective discharge (modified from Biedenharn and Copeland, 2000).

Determining the effective discharge is a theoretical calculation which cannot be field validated. Effective discharge is typically determined by performing a partial duration series analysis on a sufficiently long time series (typically greater than 42 years of record) to determine the flow frequency distribution. After both the partial (pdf) and cumulative (cdf) distribution frequencies have been determined, the sediment pdf and cdf are calculated by use of a rating curve typically in the form of:

$$Q_{Si} = aQ_i^b \qquad [2]$$

where Q_{Si} [M T^{-1}] is the sediment transport rate related to discharge observed (Q_i) [L^3 T^{-1}] and a and b are sediment rating curve regression fitting parameters. The sediment pdf is plotted as a function of discharge, and the local maxima of the resulting histogram is

defined as the effective discharge (Q_{EFF}) as illustrated in Figure 8. It should be noted that in channel evolution stages I and V $Q_F = Q_{BF} = Q_{EFF}$.

2.3.1 Modes of Headcut Migration

Vertical channel migration, either in the form of degradation or aggradation, is determined with respect to the channel thalweg. Brush and Wolman [1960] assert that the shear forces acting along the channel boundary is the primary factor causing vertical erosion, consequential to surpassing the critical shear strength (τ_C) [M $L^{-1}T^{-2}$] of the channel bed composition. The rate of sediment transport per unit width of channel q_s [M $L^{-1}T^{-1}$] is a function of shear stress along the channel bed defined by:

$$q_s = f(\tau_0) \quad [3]$$

where τ_0 [M $L^{-1}T^{-2}$] is the shear at the channel bed boundary defined by:

$$\tau_o = \gamma_w R S_f \quad [4]$$

where R [L] is the hydraulic radius of the channel defined by R = A/ Λ where A [L^2] and Λ [L] are the channel cross-sectional area and wetted perimeter respectively of the submerged cross-section. S_f [-] is the friction slope for the conditions of gradually varied flow.

Headcutting caused by base level lowering creates a localized change in friction slope (S_f) which often leads to the bed shear exceeding the critical bed shear threshold τ_C [M $L^{-1}T^{-2}$] such that $\tau_0 > \tau_C$. Under these conditions, a headcut will migrate upstream. According to Leopold et al. [1964], there are two modes that headcut migration may be

predisposed to follow: migration of a vertical headcut where the vertical form is maintained in an upstream propagation; or migration of an initially vertical headcut that flattens along its migration path until eliminated. Factors that determine the migration mode are characteristics of the bed material sediments and the hydraulic properties of the channel cross-section. The importance of the bed material properties, including the cohesiveness of underlying layers on the mode of headcut migration, is illustrated in Figure 9 as offered by Brush and Wolman [1960].

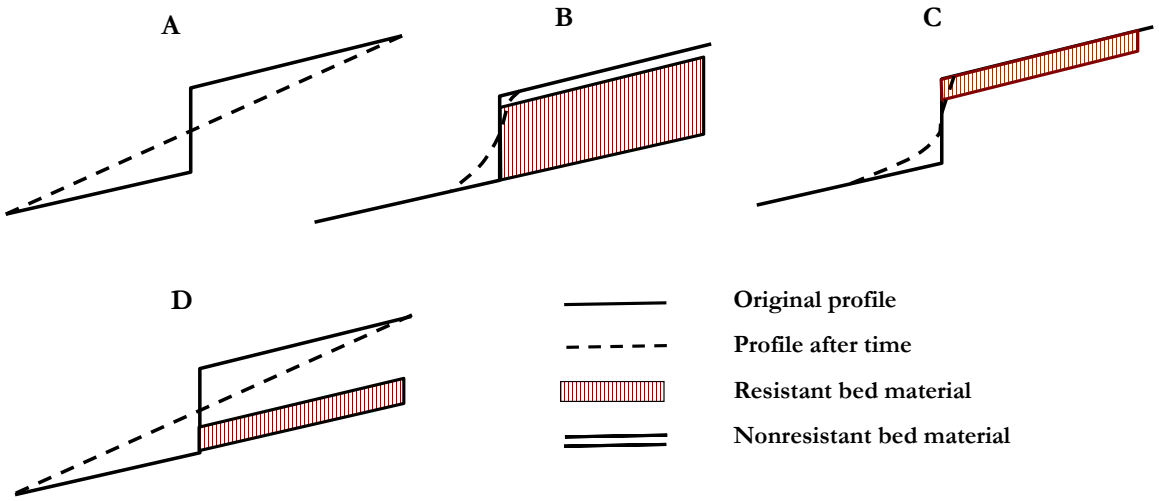

Figure 9. The influence of various combinations of resistant and nonresistant bed material on headcut migration (modified from Bush and Wolman, 1960).

Brush and Wolman [1960] observed that the behavior of a headcut or knickpoint migration is governed by the discharge regime of the river and composition of the bed and bank materials. As illustrated in Figure 9, profile A is applicable to homogeneous materials such as those found in large alluvial valleys. This profile eventually attains the average channel slope as the headcut migrates upstream and diminishes in size and extent over time. Profile B includes a resistant stratum located below the nonresistant surface bed material that is exposed at the oversteepened reach. This profile, over time, typically

maintains a headcut or knickpoint profile and has a relatively slow rate of upstream channel retreat. Profile C, is similar to that of profile B with the exception that the upstream resistant bed material overlies a more erodible underlying unit. Similar to profile B, the headcut shape of profile C remains relatively intact. The rate of upstream channel migration of profile C is dependent upon the rate of erosion of the underlying upstream layer, related to toe scour, causing the overriding layer to cantilever and fail. Lastly, profile D is a variant of the three preceding profiles. The channel response may behave similar to that of profile A if the resistant layer is located below the vertical centre of the over-steepened reach and the resulting channel bed slope is sufficiently shallow such that $\tau_0 < \tau_C$. Conversely, if the resistant layer is positioned above the centre of the over-steepened reach, the profile of the headcut and the localized channel bed slope may remain and continue to migrate upstream if the localized friction slope remains sufficiently large such that $\tau_0 > \tau_C$ along the channel thalweg.

Begin et al. [1980] numerically evaluated upstream headcut migration for the two general profiles of sustained headcut migration and flattening with upstream channel distance. Their work was based upon the assumptions of sediment continuity between upstream and downstream reaches with no localized sediment sinks or sources from lateral inflows. The equation used by Begin et al. [1980] which retains its over-steepened profile was defined as:

$$\frac{dx}{dt} = \frac{q_{sd}}{\gamma_s h} \qquad [5]$$

where x [L] is the distance along the channel (positive in the upstream where x = 0 at the outlet), t [T] is the time interval, h [L] is the height of the headcut as illustrated in Figure

10, q_{Sd} and q_{SU} are the unit sediment discharges of the downstream and upstream reaches respectively relative to the location of the headcut where q_S and γ_S have been previously defined.

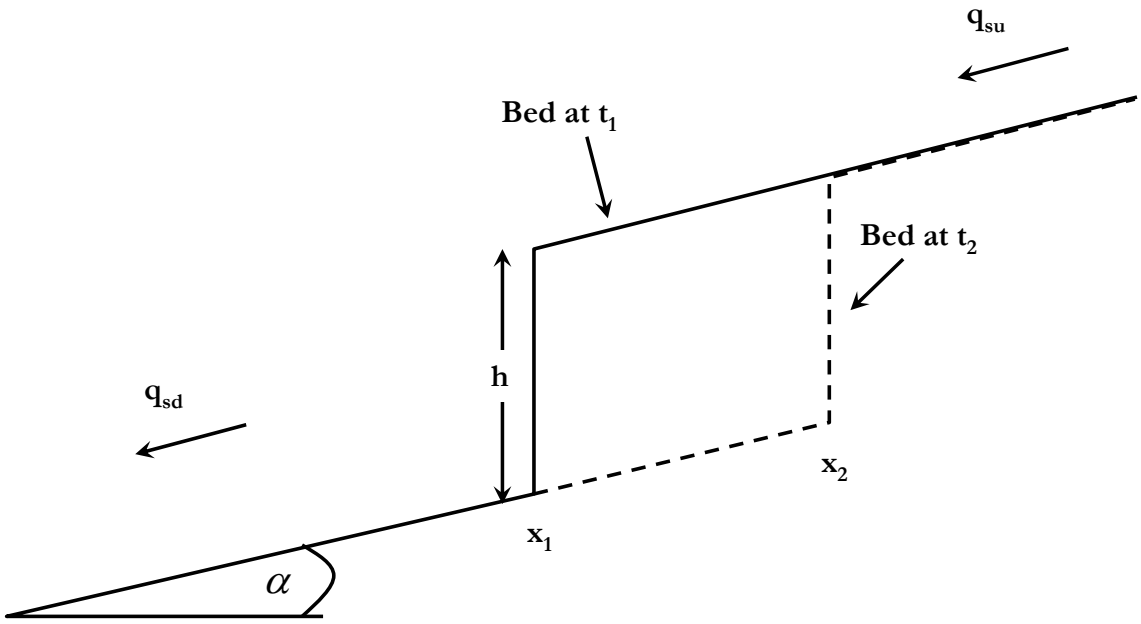

Figure 10. The physical parameterization of a of a headcut profile (modified from Begin et al., 1980).

For the headcut flattening scenario, Begin et al. [1980] also provide equations for predicting the rate of vertical degradation [Equation 6] and maximum upstream degradation [Equation 7] as defined by:

$$-\frac{\partial h}{\partial t} = \frac{Y_o x}{2\sqrt{\pi k t^3}} \exp\left(\frac{-x^2}{4kt}\right)\left(1-\frac{2x^2}{4kt}\right) \quad [6]$$

$$X(\max) = \sqrt{2k}\sqrt{t} \quad [7]$$

respectively where Y_o [L] is a constant elevation by which the baselevel is lowered at x = 0, and k is defined as:

$$k = q_s C\left(\frac{\gamma_w 3 f}{8\gamma_s 2g}\right)^{1/2} \quad [8]$$

where f [-] is the Darcy-Weisbach friction factor, g [L T^{-2}] is the acceleration due to gravity, and C [-] is the coefficient of friction, and all other terms have been previously been defined.

Stein and Julien [1993] studied the migration of headcuts similar to those considered by Begin et al. [1980]; however, in this study they considered stepped headcuts that retain their vertical faces or rotating headcuts that flatten along migration They characterized the type of headcut, based upon the relative erosion rates in the accelerated region at the face of the headcut and along the impingement region (defined as the effected reaches both immediately upstream and downstream of the headcut). They defined T_U [T] as the time for upstream vertical scour to reach the toe of the vertical face of the headcut, as illustrated in Figure 15, and T_d [T] as the downstream timescale for the impingement scour to develop horizontally and reach the toe of the vertical face of the headcut. Further, Stein and Julien [1993] defined that the headcuts are maintained if $T_U > T_d$, and rotating headcuts when $T_d < T_U$.

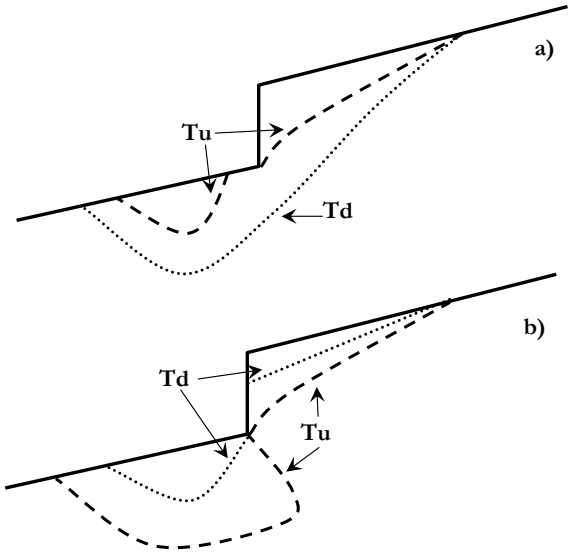

Figure 11. Modes of headcut migration for a) rotating headcuts and b) stepped headcuts (modified from Stein and Julien, 1993).

In further works by Stein and Julien [1993], they studied headcut migration employing sediment detachment theory to determine erosion time and length scales when the primary control of headcut migration is based upon bed material grain size characteristics. Their approach was consistent with that offered by Foster and Meyer [1975] who applied critical shear stress criteria to determine the detachment rate of sediment particles per unit area E [M $L^{-2}T^{-1}$] defined as:

$$E = k(\tau_o - \tau_c)^{\varepsilon} = k\left[\tau_o\left(1 - \frac{\tau_c}{\tau_o}\right)\right]^{\varepsilon} \quad [9]$$

where k and ξ are empirical coefficients. The Stein and Julien [1993] headcut migration mode equation is expressed by:

$$\frac{T_u}{T_d} = \frac{A'_u\, B_u h k_d \tau_d^{\varepsilon d}\left(1 - \frac{\tau_{cd}}{\tau_d}\right)^{\varepsilon d}}{A'_d\, B_d X_n k_u \tau_u^{\varepsilon u}\left(1 - \frac{\tau_{cu}}{\tau_u}\right)^{\varepsilon u}} \quad [10]$$

where subscripts u and d denote upstream and downstream reaches relative to the location of the headcut, A' is an empirical coefficient, and B [M L^{-3}] is soil bulk density. Stein and Julien [1993] identified that if the ratio of $T_u / T_d > 1$, downstream erosion is dominant over upstream erosion and a headcut retreat will maintain its vertical form. Where $T_u / T_d < 1$, a headcut was found to rotate and diminish in form with upstream propagation.

2.3.2 Lateral Migration of Channels Following Dam Removal

MacBroom [2005] asserts that at sites where low head dams have been removed, channel degradation occurs primarily in the early stages of evolution by rapid vertical incision (Stage II of the revised channel evolution model offered by Doyle et al. [2002]), which creates a steep slope (relative to the surrounding valley slope), low sinuosity stream channel. In subsequent stages of channel evolution over time, the channel adjusts its pattern laterally to fit its flow, particle sizes and gradation, and slope; consistent with Stages III - V of the revised channel evolution model offered by Doyle et al. [2002].

Channel migration is often detrimental to various types of floodplain land-use (Shields et al., 2000). Lateral adjustment of a channel upstream of a former dam are consistent with Stages III - V of the revised channel evolution model offered by Doyle et al. [2002] whereby the subsequent increase in migration rate decreases channel slope and decreases the cross-sectional area of the effective discharge channel which is tending towards a state of dynamic equilibrium between discharge continuity, sediment continuity and slope. Channel widening and migration, by mass-wasting, occurs once bank heights and

angles exceed the critical shear strength threshold of the bank material (Simon and Darby, 1999), also commonly referred to as basal end-point control.

Sheilds et al. [2000] defines the rate of channel movement (or channel activity) as:

$$\textbf{Channel Activity} = \frac{\textbf{(Shaded Area)}}{\textbf{(Length of } t_1\textbf{)}(t_2 - t_1)} \qquad [11]$$

where channel activity [L T^{-1}] is the mean rate of lateral migration along a river reach as illustrated in Figure 12 where the channel centrelines at times t_1 and t_2 are the temporal changes in channel location.

Rates of channel activity have been empirically and analytically related to combinations of channel geometry, principally relating mean bend radius of curvature (Rc) [L], normalized by the mean channel width (W) [L], to migration rates (Hickin and Nanson, 1975; Julien, 2002). Findings show that the greatest rates of channel migration occur when $2 \leq Rc/W \geq 3$, and decrease as $Rc/W > 3$.

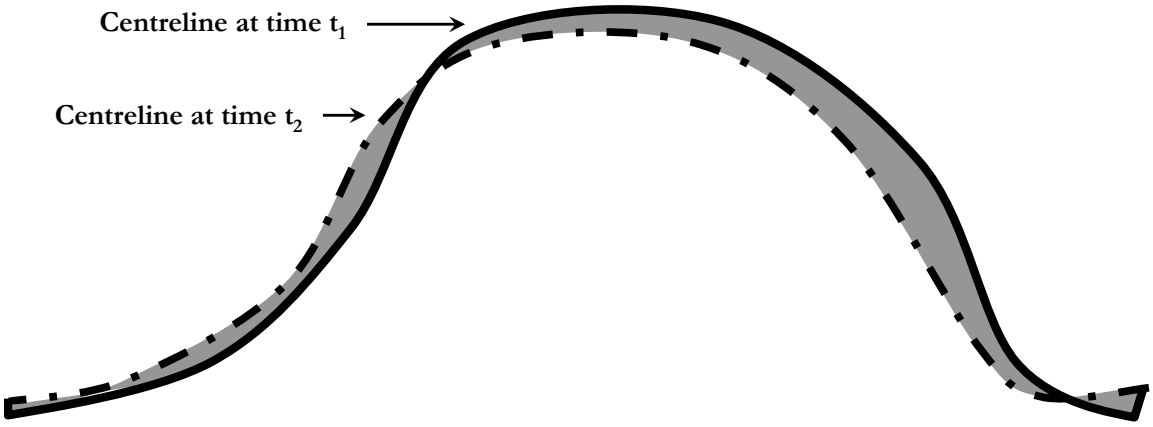

Figure 12. Channel centreline migration over time to define channel activity (modified from Shields et al., 2000).

Although general agreements have been found between R_C / W and the rates of channel migration which relate to the intensity of secondary flow in bends and basal end-point control, Shields et al. [2000] assert that the nature of the heterogeneity in boundary materials and channel geometry fail to explain the large variation in migration rates, especially over shorter time periods. Nanson and Hickin [1983] suggests that the lateral upstream river adjustments following dam removal are defined by the basal sediment size and stream power P [$M L^{1}T^{-1}$] as defined by:

$$P = \gamma_w Q S_f \qquad \textbf{[12]}$$

where Q is the range in discharges above the low flow conditions where sediment transport and the ensuing mass wasting processes dominate channel evolution and basal sediment size. Beatty [1984] further subscribes that mass wasting typically generates much of the lateral adjustments within an impoundment, a condition which is typified by great uncertainty and unpredictability in migration rates.

2.4 Sediment Transport and Tractive Force Analysis

Leopold et al. [1964] states that any mechanical system having no mean acceleration must obtain an equilibrium of applied forces. In the case of solids immersed in fluids, the excess weight of the solids must be transmitted to the ground either by direct contact, flux of fluid momentum, or a combination of both. Incipient motion of a single particle is defined as the threshold conditions between erosion and sedimentation. Moreover, Papanicolaou [2002] defines the critical condition just less than that necessary to initiate sediment movement as the threshold, and incipient motion as the commencement of movement of bed particles that previously were at rest instigated by changing flow

conditions. At incipient motion, the coefficient of friction is defined as ratio of forces $F_N/F_O = 1$ as illustrated in Figure 13:

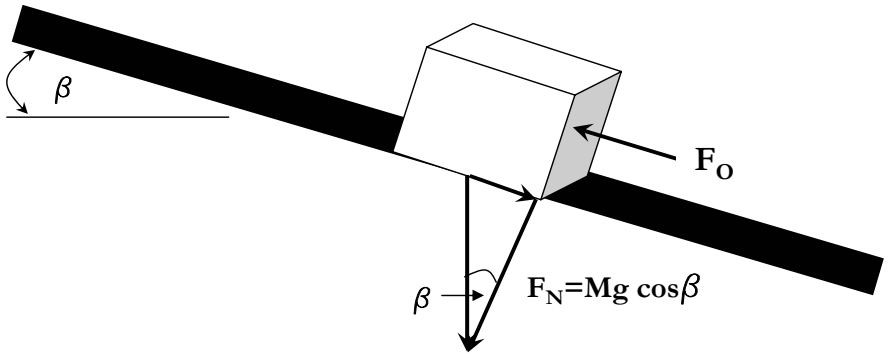

Figure 13. Relation of applied and resisting forces on a particle resting on a supporting surface (modified from Leopold et al., 1964).

where F_O [M LT^{-2}] is defined as the frictional stress opposing motion of a particle, and F_N [M LT^{-2}] is the force normal to the bed slope for a simple two-dimensional particle. Fluid flow around sediment particles exert forces which initiate particle motion and are resisted by the particle weight and shape (Julien, 1995). Motion of a particle along the channel bed is initiated when the hydrodynamic moment of forces acting on a particle causing boundary shear (τ_o) exceeds the resisting moment shear maximum (τ_c). As the slope of the supporting surface increases, as is the case along the bed of a headcut, the frictional force opposing motion must increase at a rate proportional to cosβ, thus the resisting force decreases and channel erosion ensues.

The Shields parameter (τ_*) is a dimensionless shear stress which compares experimental results of particle movement thresholds to predict incipient motion, as defined by:

$$\tau_* = \frac{\tau_o}{(\gamma_s - \gamma_m)d_s} = \frac{\rho_m u_*^2}{(\gamma_s - \gamma_m)d_s} \qquad [13]$$

where u_* [L T^{-1}] is the shear velocity, d_s [L] is the representative particle size diameter, and ρ_m [M L^{-3}]is the density of the fluid. The Shields method [1936] defines the ratio of the hydrodynamic forces to the submerged weights when the moment arms are equivalent. The Shields curve has replicate parameters on both sides of the equation, thus requiring an iterative approach for a solution (Marsh, 2004). Furthermore, Shields [1936] determined the critical shear stress corresponding to the beginning of motion ($\tau_o = \tau_c$) for a range of particle sizes depending upon whether the encompassing flow condition is either laminar or turbulent as illustrated in Figure 14:

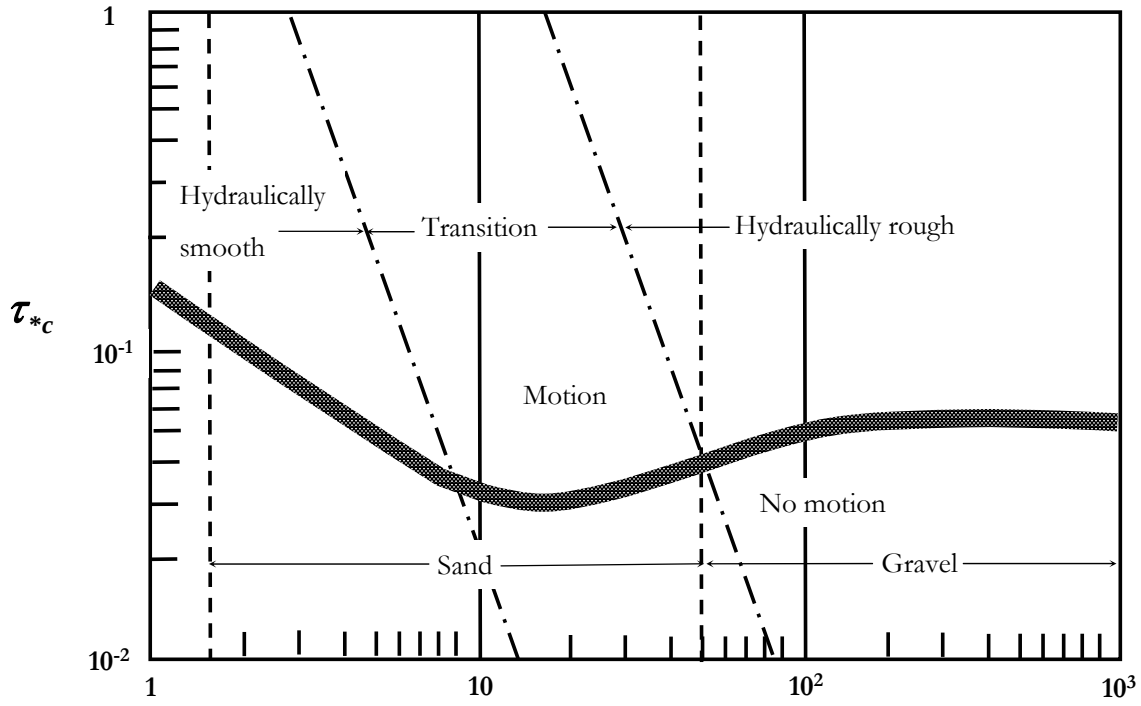

Figure 14. Shields particle motion diagram (modified from Julien, 1995).

where the critical values (τ_{*C}) of the Shields parameter are approximated as:

$$\begin{aligned} \tau_{*_c} &= 0.5\tan\phi; && d_* < 0.3 \\ \tau_{*_c} &= 0.25 d_*^{-0.6}\tan\phi; && 0.3 < d_* < 19 \\ \tau_{*_c} &= 0.013 d_*^{0.4}\tan\phi; && 19 < d_* < 50 \\ \tau_{*_c} &= 0.6\tan\phi; && d_* > 50 \end{aligned} \quad [14]$$

where d_* is the dimensionless particle diameter defined as:

$$d_* = ds\left[\frac{(G-1)g}{v_m^{\,2}}\right]^{1/3} \quad [15]$$

and v_m [L/T] is the kinematic viscosity of fluid, G [-] is the specific gravity of the bed material, and $\emptyset$ is the critical angle of repose [-] of the bed material of interest.

Figure 14 can be summarized into a tabular format consistent with that outlined in Table 1 for bed material sizes (d_s) and approximate threshold conditions for granular particles at 20^0C.

Table 1. Approximate threshold conditions for granular material by particle size (modified from Julien, 1995)

Class name	*ds (mm)*	d_*	Φ (deg)	τ_{*c}	τ_c (Pa)	u_{*c} (m/s)
Boulder						
Very large	>2048	51800	42	0.054	1790	1.33
Large	>1024	25900	42	0.054	895	0.94
Medium	>512	12950	42	0.054	447	0.67
Small	>256	6475	42	0.054	223	0.47
Cobble						
Large	>128	3235	42	0.054	111	0.33
Small	>64	1620	41	0.052	53	0.23
Gravel						
Very coarse	>32	810	40	0.05	26	0.16
Coarse	>16	404	38	0.047	12	0.11
Medium	>8	202	36	0.044	5.7	0.074
Fine	>4	101	35	0.042	2.71	0.052
Very fine	>2	50	33	0.039	1.26	0.036
Sand						
Very coarse	>1	25	32	0.029	0.47	0.0216
Coarse	>0.5	12.5	31	0.033	0.27	0.0164
Medium	>0.25	6.3	30	0.048	0.194	0.0139
Fine	>0.125	3.2	30	0.072	0.145	0.0120
Very fine	>0.0625	1.6	30	0.109	0.110	0.0105
Silt						
Coarse	>0.031	0.8	30	0.083	0.083	0.0091
Medium	>0.016	0.4	30	0.065	0.065	0.0080

In describing the particle size distribution of bed material composed of nonuniform-noncohesive sediment mixtures, Julien [1995] describes the relationships between critical particle size movement and the heterogeneity of the bed material surface as illustrated in Figure 15. The first grain size mixture presented in Figure 15a (No Motion) illustrates the applied shear stress is unable to move any of the particles and is composed of the original bed material. In the second scenario (Figure 15b) the shear is increased triggering motion of the finer particles. As a result of transporting only the finer material, the remaining surface forms an amour layer which is coarser than the original d_{50} bed material and in turn shields the finer underlying particles from erosion. This is the condition whereby a headcut retreats upstream at a slow rate such that $\tau_0 < \tau_C$ for $d_i < d_{50}$.

The final case presented in Figure 15c illustrates the condition where sufficient bed shear exists to initiate movement of all bed material particle sizes. The amour layer is no longer maintained in this scenario and the displacement of the finer particles to the surface creates a plane in which the coarse particles can easily roll. This is the condition when a headcut retreats at the fastest rate upstream, when S_f is sufficiently large such that $\tau_0 > \tau_C$ for all bed material sizes and gradations.

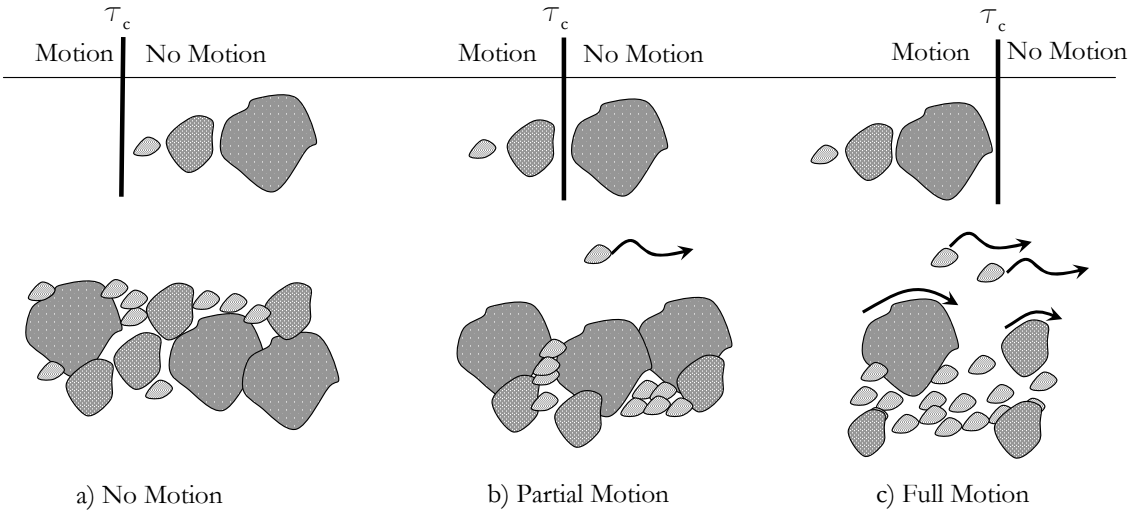

Figure 15. Bed surface for nonuniform grain size mixtures (modified from Julien, 1995).

The critical value of shear stress (τ_C) for different grain sizes has been related to the 50th percentile (d_{50}) based upon a bed material grain size analysis (Egiazaroff, 1965; Parker et al., 1982; Komar, 1987; Ashworth and Ferguson, 1989; Kuhnle, 1992; Wilcock and Southard, 1997) which is commonly expressed as:

$$\tau_{*ci} / \tau_{*c50} = z(d_i / d_{50}) \qquad [16]$$

where τ_{*Ci}, is the critical shear stress threshold of the bed material particle diameter d_i and τ_{*C50} is the critical shear stress threshold value of the d_{50} bed material diameter respectively. Furthermore, *z* is referred to as a hiding function, which varies widely

(Shvidchenko et al., 2001) and is largely related to particle shape and grain size gradation. Typical ranges in hiding functions are outlined in Figure 16.

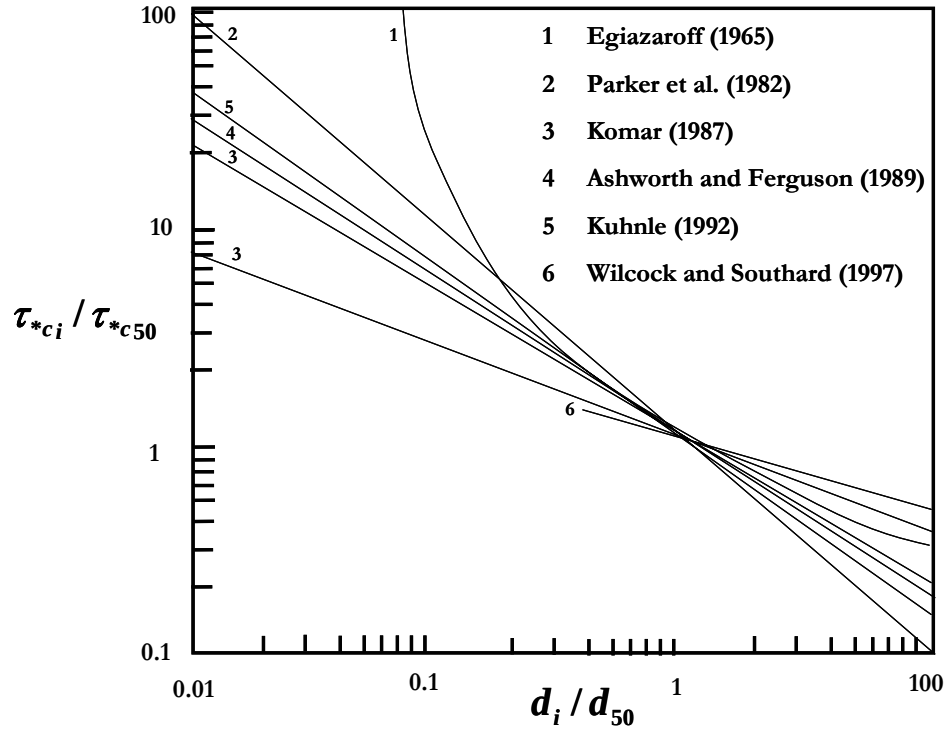

Figure 16. Comparison of different hiding functions (modified from Shvidchenko et al., 2001).

2.5 Longitudinal Hydraulic and Sedimentological Channel Evolution Responses to Passive Dam Removal

With both the theory and physical conceptualizations of how channel degradation may occur upstream of a dam (Sections 2.3 and 2.4), the channel evolution model proposed by Doyle et al. [2002] (Figure 6) can be interpreted throughout the longitudinal profile of a river channel. A conceptually based HEC-RAS© model was developed with channel geometry consistent with Figure 6 to elucidate the hydraulic and sedimentological processes occurring throughout a river channel upstream of a dam consistent with a passive restoration recovery approach.

Figure 17 and Figure 18 illustrate the unit stream power ($\hat{P}$) [M T^{-1}] as defined by:

$$\hat{P} = \frac{\gamma_w Q S_f}{T} \quad [17]$$

where T [L] is the top width of the channel, the average channel velocity ($\overline{V}$) [L T^{-1}], the main channel velocity (V_{MAIN}) [L T^{-1}], the average channel shear (τ_O), and the main channel shear (τ_{OMAIN}). In Stages I and V of the channel evolution sequence, the V_{MAIN} and $\tau_{O\,MAIN}$ are consistent with the bankfull channel hydraulic geometry. Five discrete flows are illustrated in each CEM stage ranging between bankfull discharge (Q_{BF}) and the 100-year return period (Q_{100}).

Figure 17a illustrates that the lowest unit stream power occurs in Stages I and V where bankfull discharge dominates the flow regime. These are the regions where the channel is considered to be in a state of quasi-equilibrium. It should also be noted that when the discharge state exceeds bankfull, the top width of the channel dramatically increases across the floodplain, thereby maintaining a low unit stream power and a low potential for channel degradation to occur. Stage II has the highest unit stream power for each discharge value, which also relates to the channels evolutionary stage where there is no or limited floodplain relief. The newly formed channel has yet to widen and contains all discharges within the same channel width. This is also the stage where the highest rates of vertical erosion occur. The unit stream power in Stages III and IV consistently decrease as channel widening begins to occur through meander extension. By stage IV the stream power is sufficiently low such that bed material deposition begins to occur with the continued decrease in unit stream power.

The average channel velocity and main channel velocity have similar responses to those of the unit stream power for the different discharges, as illustrated in Figure 17b and Figure 17c respectively. For Stages II – IV, the main channel velocities may be sufficiently large, such that they exceed the critical particle size thresholds (d_C) and the volumes of bed material transport in these reaches exceeds the flux entering the reservoir system from upstream. Consequently, with a discrepancy in sediment continuity, channel degradation ensues. It is also noteworthy to identify that the average bankfull channel discharge results in the highest average channel velocity (Figure 17b) in Stages I and V although the main channel discharge (Figure 17c) continues to increase with increasing discharge. This is common within a floodplain dominated channel morphology and also typifies the channel morphology where bankfull discharge and effective discharge are synonymous with the channel forming flow (i.e. $Q_F = Q_{BF} = Q_{EFF}$). In evolution Stages II – IV where the flow depth and velocities continue to increase with increasing discharge, there exists the ability to transport greater volumes of sediment. These are the stages where effective discharge dominates the channel evolution (i.e. $Q_F = Q_{EFF}$).

The average channel shear and main channel shear also have similar responses to that of the unit stream power, average channel velocity and main channel velocity for the different discharges as illustrated in Figure 18a and Figure 18b respectively. When discharges exceed the bankfull depths in Stages I and V, the wetted perimeter significantly increases as the flows begin to inundate their respective floodplains. With the significant increases in wetted perimeters (Λ) the hydraulic radii (R) begin to decrease with increasing stage above bankfull depth resulting in the shear stress

remaining relatively low in Stages I and V. Conversely, in Stages II – IV with increasing discharge, there is no or limited access to floodplains. As a result, in Stages II – IV, the flow depth continues to increase with increasing discharge and the wetted perimeter does not increase as quickly, relative to Stages I and V, resulting in increased shear stress. The highest rates of channel shear which occur in Stage II diminish as the evolutionary sequence tends towards stage IV where sediment deposition may begin to dominate the evolution of the channel morphology.

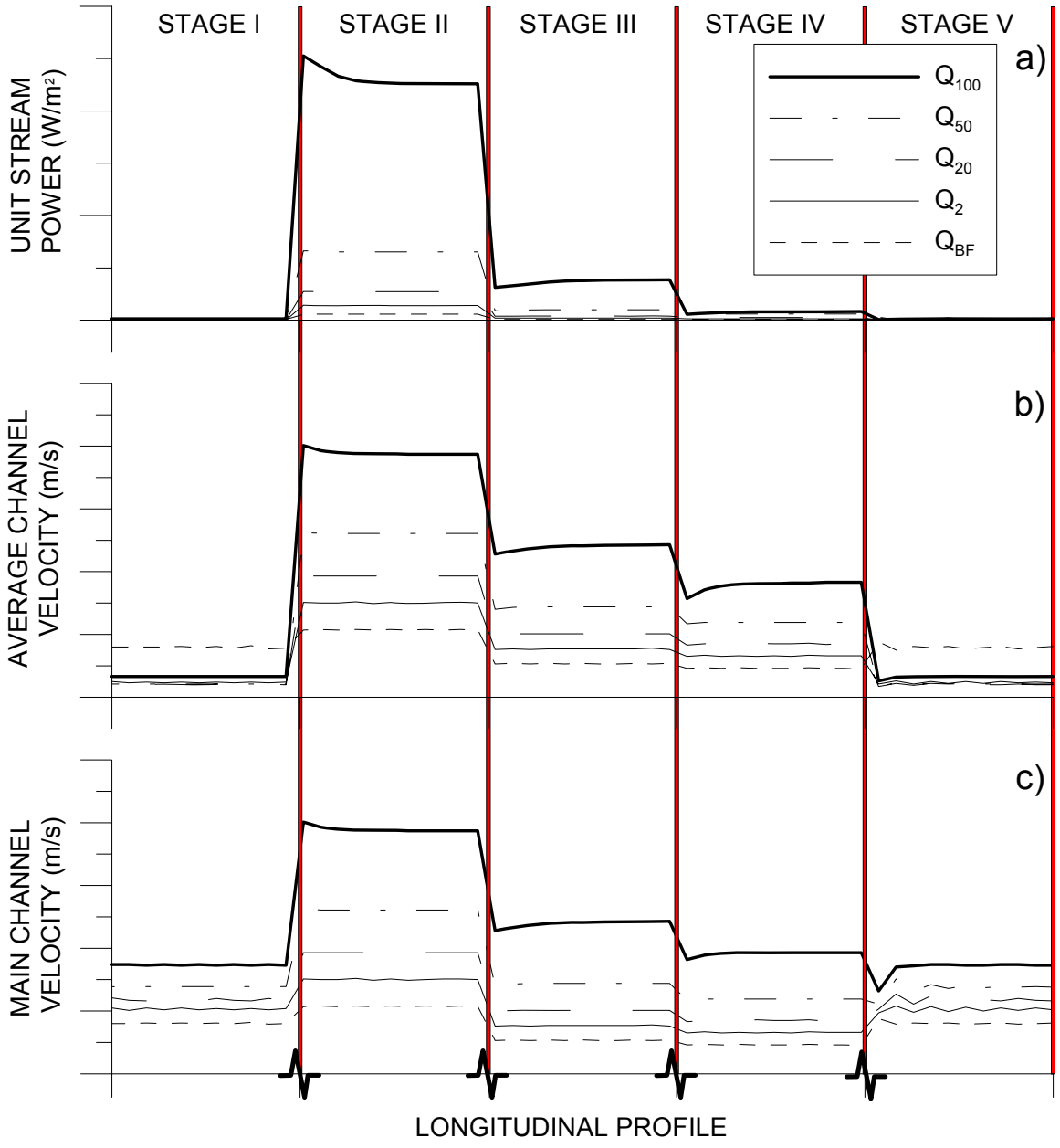

Figure 17. Typical a) unit stream power, b) average channel velocities, and c) main channel velocities for the five stages of channel evolution after Doyle et al. [2002] for a discrete range in flows between bankfull (Q_{BF}) and the 100-year (Q_{100}) magnitude discharge events.

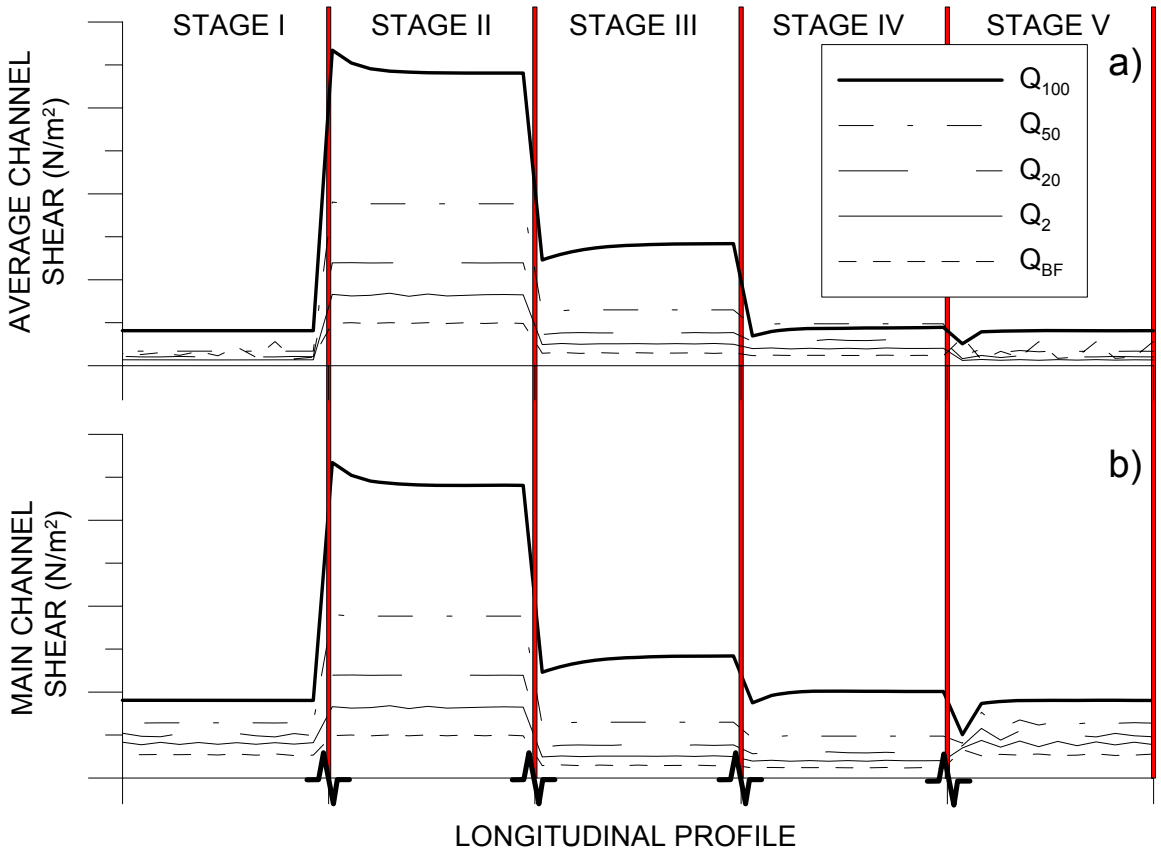

Figure 18. Typical a) average channel shear and b) main channel shear for the five stages of channel evolution after Doyle et al. [2002] for a discrete range in flows between bankfull (Q_{BF}) and the 100-year (Q_{100}) magnitude discharge events.

Another method of interpreting and illustrating the unit stream power, average channel velocity, main channel velocity, average channel shear, and main channel shear which is similar to those illustrated in Figure 17 and Figure 18 is by analyzing the hydraulic responses along the longitudinal profile for 100 equally partitioned incremental discharges ranging between $0 < Q \leq Q_{100}$. This method of analysis captures the average, standard deviation, bankfull, minimum, and maximum flows typically encountered at each cross-section, which are then illustrated using box-and-whisker plots of the hydraulic parameters. Figure 19 and Figure 20 define similar profiles of unit stream power, velocity and shear at each stage of the CEM illustrating the range of the 100 separate discharge analyses. This is also the standard reporting method used throughout

the remainder of this research to present the hydraulic results over the range of discharges from $0 < Q \leq Q_{100}$.

The analyses based upon this method further illustrate that in Stages I and V, the bankfull average channel velocity remains the highest (Figure 19b) for the entire range in discharges considered whereas the unit stream power (Figure 19a), main channel velocity (Figure 19c), average shear stress (Figure 20a), and main channel shear associated with bankfull discharge (Figure 20b) are either the lowest or close to the lowest values for the range in discharges. The small range in standard deviations of the hydraulic parameters in Stages I and V also addresses the damping effects of the floodplain on hydraulic responses in these channel morphologies. The smaller total and standard deviation ranges in hydraulic parameters of Stages I and V identify that there will not be as dramatic of a response in the channel evolution for the entire range in flows; relative to Stages II - IV. The greater range in standard deviations and total ranges of the hydraulic parameters in Stages II – IV indicate a larger vulnerability to channel degradation based upon the magnitude and recurrence interval of particular discharge events of interest. At some location within the standard deviation ranges of hydraulic parameters in Stages II – IV is the discharge associated with the effective discharge that dictates channel evolution. It is also noted in Stages II – IV that hydraulic conditions associated with bankfull discharge are notably below each standard deviation, further indicating that Q_{BF} is not a significant discharge of the channel evolution in these stages.

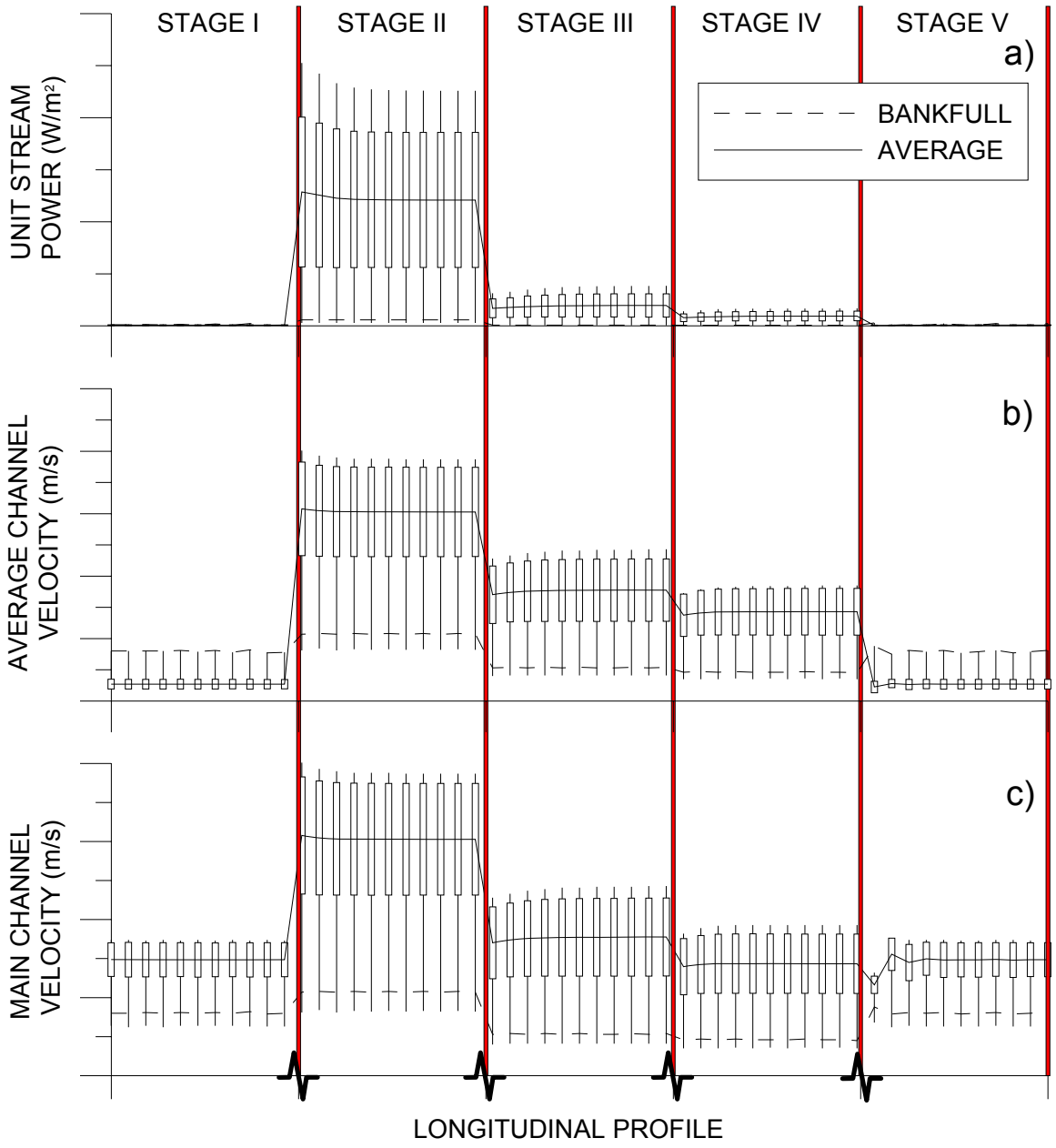

Figure 19. Typical a) unit stream power, b) averge channel velocities, and c) main channel velocities for the five stages of channel evolution after Doyle et al. [2002] for 100 different incremental discharges between $0 < Q \leq Q_{100}$

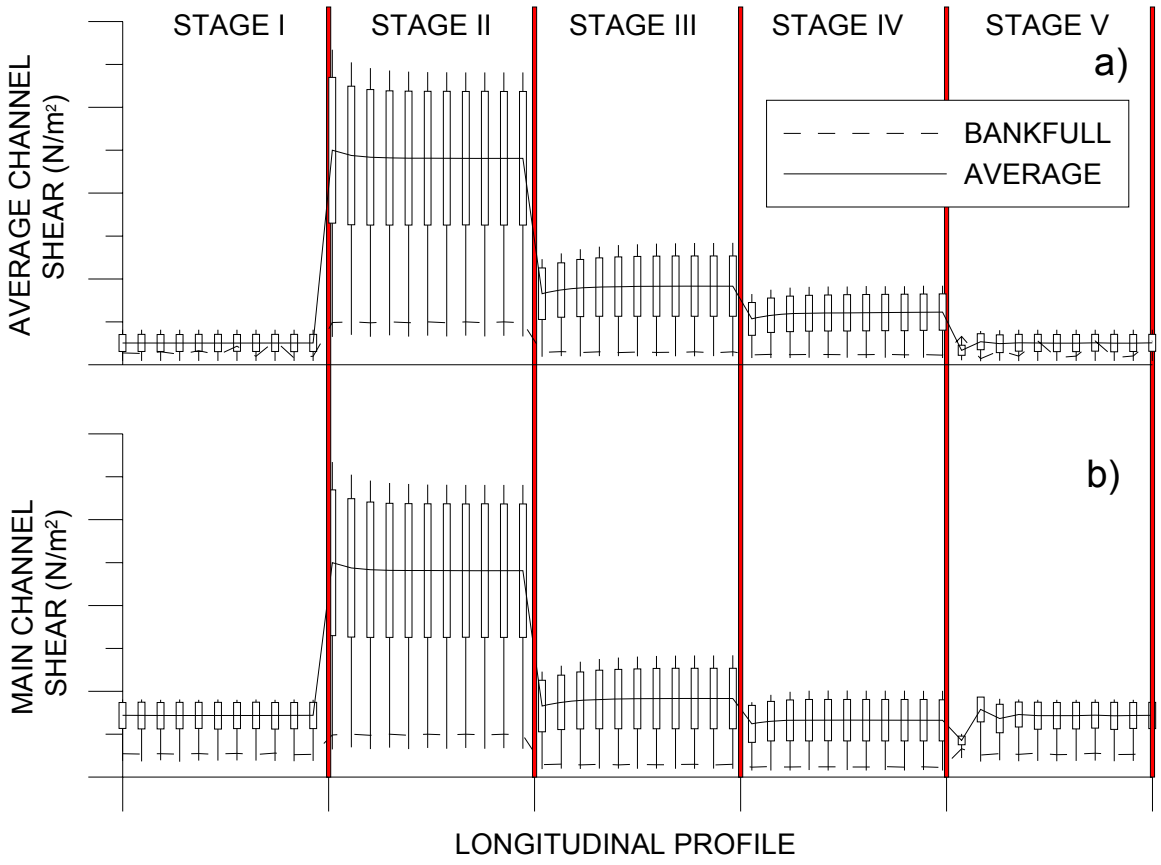

Figure 20. Typical a) average channel shear and b) main channel shear for the five stages of channel evolution after Doyle et al. [2002] for 100 different incremental discharges between

$$0 < Q \leq Q_{100}$$

3 FIELD AND ANALYSIS METHODS

Upon canvassing local and provincial agencies, 20 decommissioned / failed dams were identified in Southern Ontario south of the Canadian Shield in glacio-fluvial deposits. The dams identified had either been removed or failed from severe flooding, abandonment, or lack of operations maintenance. In order to meet the objectives of this study no upstream interventions, restorations or rehabilitation could have occurred since the time of dam failure or removal till present day. The primary selection criteria results in a morphologic response with minimal anthropogenic disturbances, analogous to the passive dam remediation approach consistent with an abrupt dam removal and without any upstream works undertaken. Further, sites were chosen to cover a broad range of valley slopes and underlying geology (i.e. differing grain sizes) as these are often principle factors in channel evolution and sediment transport. Based upon the above criteria, eight dam sites were identified from both aerial and field reconnaissance which are listed in Table 2 with their associated valley slopes and predominate upstream catchment area physiography (Chapman and Putnam, 1966). The general locations of the dams are illustrated in Figure 21. Detailed site locations of each of the dam sites are outlined in Appendices A – H.

Table 2. List of dam study sites, river names, valley slope and dominant upstream physiography.

Ref. No.	Dam Name	River Name and Neighboring Town	Valley Slope (m/m)	Physiography
1	Croton Dam	Big Creek at Delhi	1.80E-03	Sand Plain
2	Hawkesville Dam	Conestogo River at	1.90E-03	Till Moraine
3	Huttonville Dam	Credit River at Huttonville	2.70E-03	Till Plain
4	Chilligo Dam	Ellis Creek at Cambridge	3.10E-03	Spillway
5	Greenfield Dam	Nith River at Greenfield	1.70E-03	Kame Moraine
6	Sutton Dam	Patterson Creek at Simcoe	2.05E-03	Sand Plain
7	Teeswater Dam	Teeswater River at Teeswater	2.40E-03	Kame Moraine
8	Bognor Dam	Walter's Creek at Bognor	8.00E-03	Drumlinized Till Plain

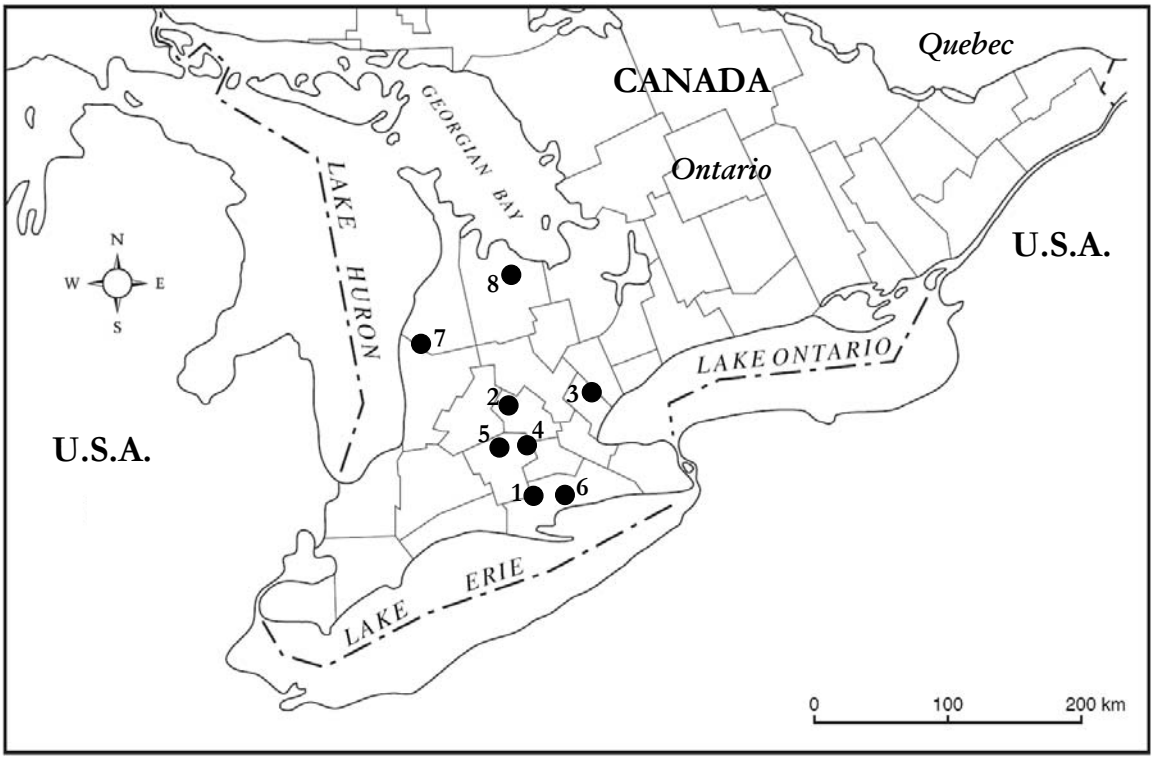

Figure 21. Locations of study sites within Southern Ontario.

Background studies were conducted for each site using the Geographic Information Systems (GIS) program ArcGIS® and AutoCAD®. Time series aerial photographs were acquired for each site, ranging from 1954 – 2002 photographs provided by the Ontario department of Lands, Ontario Ministry of Natural Resources and the local conservation authorities. Hard copy aerial photographs were scanned and georeferenced for time-

series morphometric analysis which included channel activity and effective catchment area land use change.

3.1 Field Surveys

Longitudinal profiles and a series of cross-sections were surveyed at each site consistent with methods outlined by Annable [1996] using a Set 5E Sokkia® total station, data logger and single-optic prism pole. Each survey began downstream of each former dam at either a hydraulic control or approximately one meander wavelength downstream of each dam. The upstream limit of each study terminated at either a hydraulic control (such as a culvert or a bridge) or where the channel demonstrated dynamically stable characteristics (Leopold et al., 1964) for approximately 2 meander wavelengths upstream of the uppermost headcut.

Total station surveys were geo-referenced to NAD 1983 UTM Zone 17N coordinates acquired with a Trimble® Geo XT GPS unit at the starting and ending control benchmarks of each survey. A typical plan view survey of the channel profile, cross-sections and additional field attributes are illustrated in Figure 22 for the Teeswater site at Teeswater, Ontario. Appendices A - H detail the total station surveys conducted at each site.

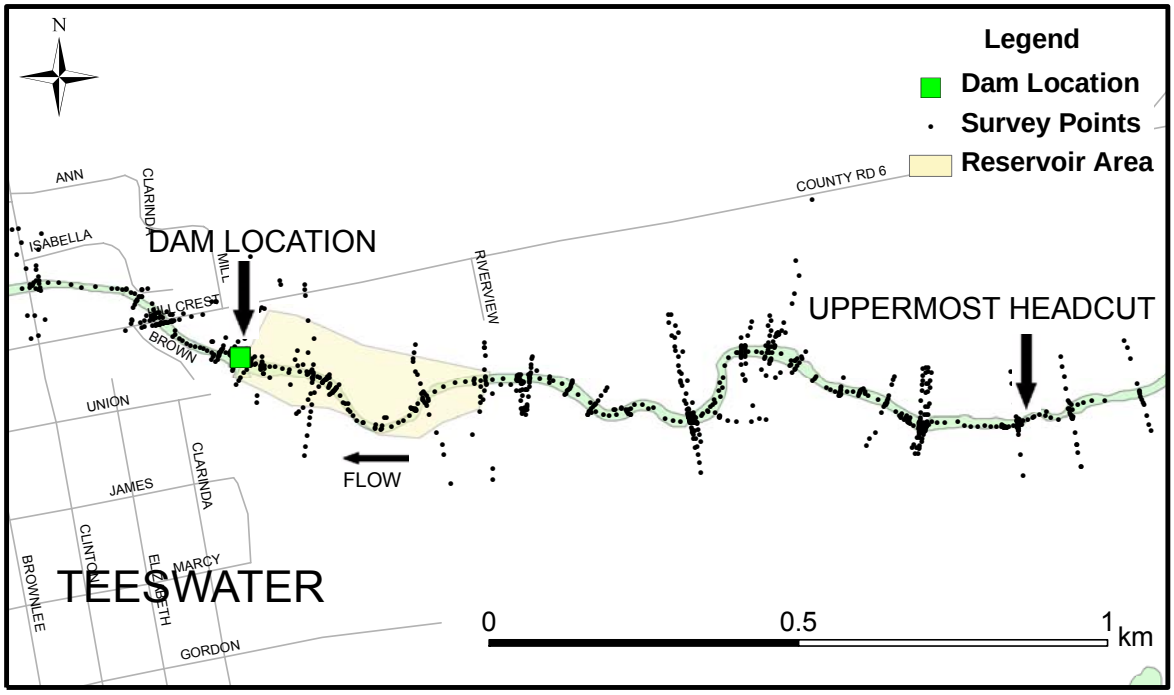

Figure 22. Example plan view of a field survey of Teeswater River at Teeswater.

3.1.1 Longitudinal Profiles

Thalweg measurements were obtained along the study reach at approximately every bankfull channel width, in addition to the maximum inverts of pools, notable changes in channel slope, and at the tops and bottoms of riffles and headcuts respectively consistent with the methods outlined by Annable [1996]. Using thalweg measurements, a longitudinal profile was developed for every site as illustrated in Figure 23 for the Teeswater dam. Appendices A - H also detail each of the longitudinal profiles.

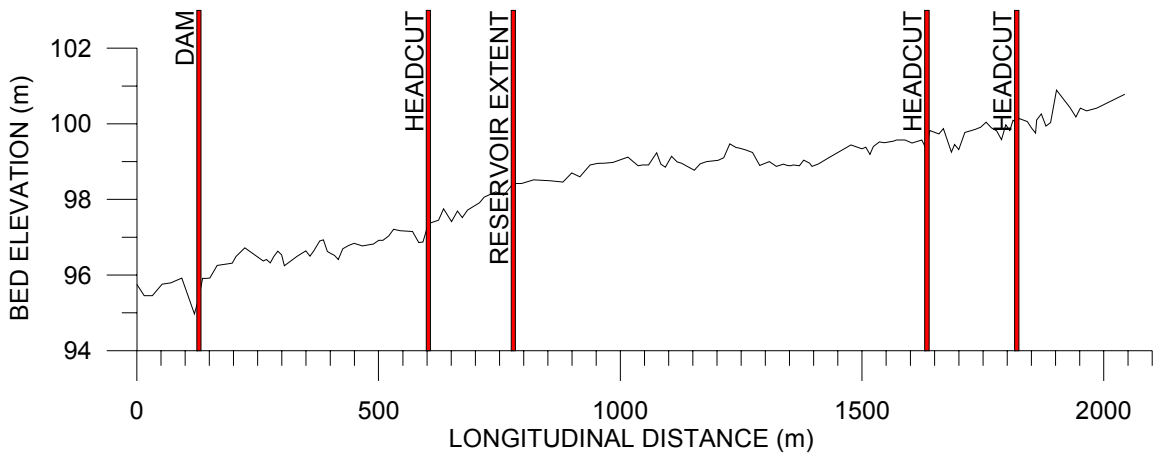

Figure 23. Longitudinal profile of Teeswater River at Teeswater.

The lengths and slopes of riffles, runs, headcuts, knickpoints, inter-riffle and inter-pool lengths were determined from the longitudinal profile. Slopes and lengths were determined from the average elevation of the three survey points at the top and bottom of each morphological feature respectively.

3.1.2 Cross-Sectional Profiles

Cross-sections define the geometric boundary conditions of a river or stream perpendicular to flow along the channel and adjacent floodplains. Cross-sections were defined and measured perpendicular to the channel within the upper third of each riffle, run or headcut and extended out into the floodplains in sufficient detail to define cross-sections for undertaking hydraulic analysis using Hydrologic Engineering Center's River Analysis System (HEC-RAS® 4.0) for flood conditions. At each cross-section, characteristics such as top and bottom of banks, bankfull stage, and thalweg were defined, in addition to all notable breaks in slope and terraces identified in the field. Ideally, the extent of each cross-section was surveyed from, at minimum, the top of

valley walls to the channel thalweg. In cases where it was not possible to extend the survey to the top of the valley walls, due to line of sight limitations with the total station, the extents of the cross-section along the floodplain were extrapolated using topographic maps at a scale of 1:10 000 once the field surveys were geo-referenced.

3.1.3 Sediment Sampling

Bed material sampling was undertaken to obtain particle size distributions of riffles, runs, and headcuts within each disturbed reach in addition to reaches upstream of the erosional effects or the uppermost headcut. Sampling methods were consistent with those offered by Klingeman and Emmett [1982] and Annable [1996] for the gravel- and cobble-bed streams; and by Ashmore [1988] for the sand-bed channels. Two-to-three random locations (dependent on channel width) across both the upper and lower thirds of each feature were sampled and their locations geographically referenced using a Trimble® GeoXT. Figure 24 and Figure 25 illustrate the typical locations where samples were collected along riffles and headcuts respectively.

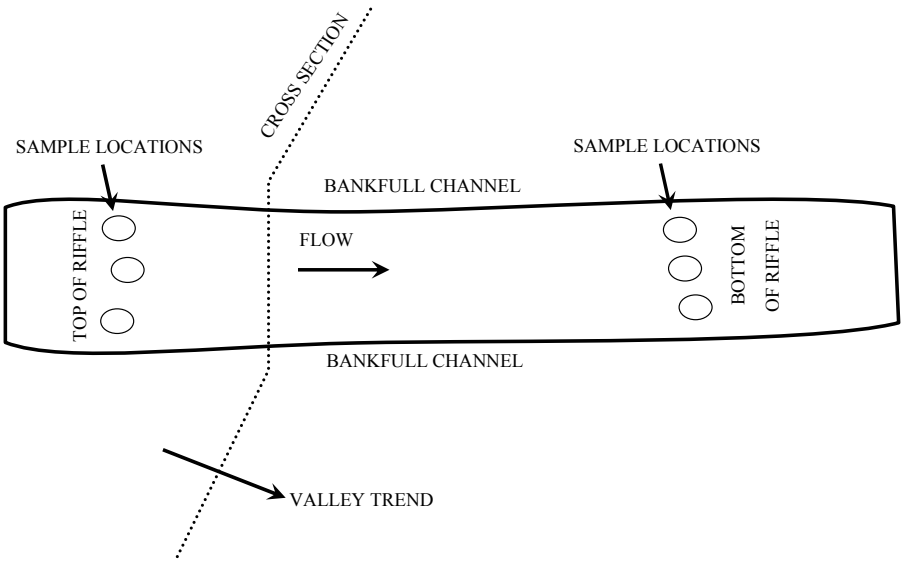

Figure 24. Locations of bed material samples along a riffle.

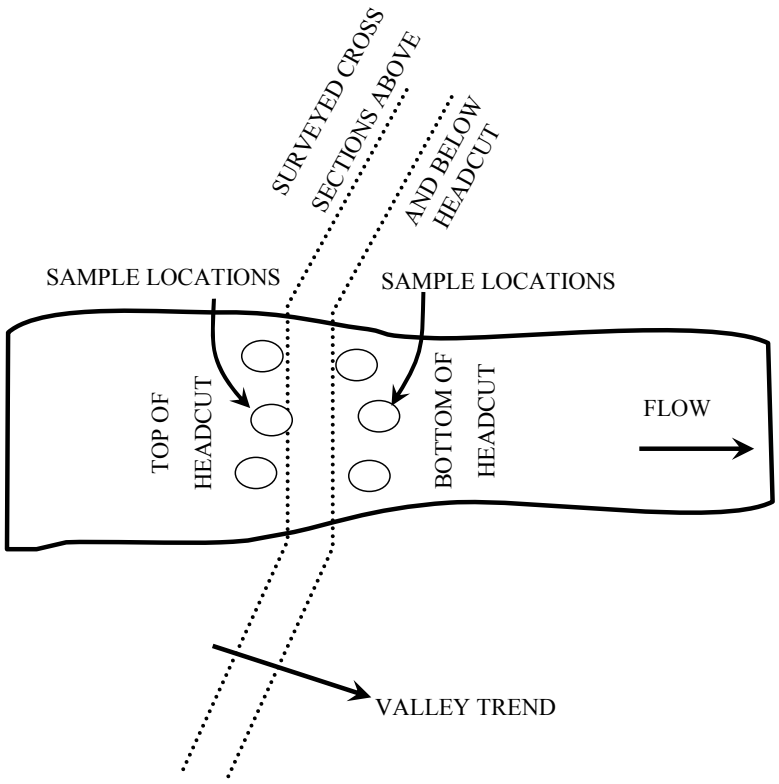

Figure 25. Locations of bed material samples along a headcut.

Notable exceptions to the methods above were in the cases where the bed material was principally comprised of boulders too large to be extracted for laboratory analysis. In these cases, a modified version of the Wolman [1954] pebble count method was employed. The modified Wolman pebble count method consisted of two passes between the bankfull channel limits along the bed of the channel on the morphological feature of interest randomly sampling approximately 50 particles. The three principle particle axes of each particle were measured (a-axis, b-axis, c-axis) which relate to the largest, intermediate and smallest particle axis lengths respectively, and the particle converted to its spherical volume equivalent. Using this volume estimate, the mass was estimated using a bulk density of 2650 kg/m^3. Grain size analyses were conducted on each sediment sample collected using dry sieving methods at 0.5ϕ intervals (Friedman and Sanders, 1978) for particles smaller than 32mm (d_i < 32mm), where

$$\phi = \log_2(d_i). \qquad [18]$$

Particles greater than 32mm were measured and massed individually in the field and segregated into 0.5 ϕ intervals. Both field and dry sieve data on each sample were combined after the various sampling and particle sorting methods and the d_5, d_{16}, d_{25}, d_{50}, d_{75}, d_{84}, d_{95} percentiles determined. The mean, standard deviation, kurtosis and skewness of each sediment sample were also calculated in addition to a composite grain size distribution (Friedman and Sanders, 1978) of each morphological feature (i.e. riffles, runs, headcuts, knickpoints). Figure 26 illustrates the analysis results of sediment sampling of a riffle, along with the respective sampling locations. Appendices A – H contain these analyses for each site.

An aggregate grain size distribution for each study reach was also calculated by combining the masses of each size interval from all of the bed material samples (regardless of location). The mean particle diameter (d_{50}) from the reach based aggregate grain size analysis was then used to determine the general reach grain size classification consistent with the methods offered by Bunte and Abt [2001]. Table 3 outlines the general reach grain size classifications.

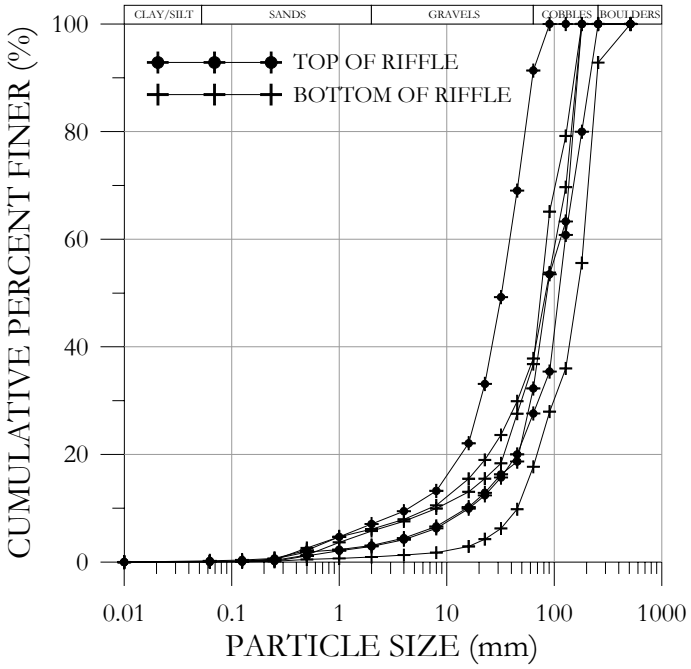

TOP		BOTTOM	
d	mm	d	mm
5	4.68	5	1.05
16	22.77	16	21.39
25	33.75	25	33.25
50	67.59	50	63.62
75	171.29	75	93.74
84	180.26	84	122.18
95	191.88	95	133.89

d	mm	d	mm
5	3.86	5	0.91
16	29.68	16	13.98
25	46.49	25	30.48
50	91.69	50	66.96
75	133.44	75	121.01
84	171.87	84	127.39
95	189.04	95	135.65

d	mm	d	mm
5	3.67	5	22.13
16	24.31	16	47.53
25	44.98	25	66.39
50	67.83	50	132.87
75	124.04	75	181.69
84	129.43	84	189.46
95	136.33	95	247.42

Figure 26. Example pavement sample distributions of the uppermost riffle (Riffle 1) of Credit River at Huttonville.

Table 3. General channel bed grain size distributions based upon the median bed-material particle size (after Bunte and Abt, 2001).

Ref. No.	Dam Name	River Name	d_{50}(mm)	Class
1	Croton Dam	Big Creek at Delhi	1.7	Sand
2	Hawkesville Dam	Conestogo River at Hawkesville	81	Cobble
3	Huttonville Dam	Credit River at Huttonville	65	Cobble
4	Chilligo Dam	Ellis Creek at Cambridge	31	Gravel
5	Greenfield Dam	Nith River at Greenfield	69	Cobble
6	Sutton Dam	Patterson Creek at Simcoe	0.3	Sand
7	Teeswater Dam	Teeswater River at Teeswater	32	Gravel
8	Bognor Dam	Walter's Creek at Bognor	60	Gravel

Reservoir sediments were also collected along the exposed incised channel banks within the impoundment regions. Samples were collected using a spade at approximately the vertical centre of the incised channel banks. Samples were collected from two separate locations along the incised channel; the first location was collected proximal to the dam face and the other near the upstream limit of the abandoned reservoir. Grain size analyses were performed on each impoundment sample using hydrometer testing methods consistent with those described by the American Society for Testing Materials [1958].

3.2 Numerical Analysis Methods

Field data collected from each of the eight study sites as presented in Section 3.1 were then used to define each of the modelling domains and the boundary conditions for the hydraulic and sediment transport analysis using HEC-RAS® 4.0.

HEC-RAS® has been developed to undertake one-dimensional hydraulic modelling which include: steady flow, transient flow and basic sediment transport analyses. The current research developed and applied a HEC-RAS model for each of the study sites to

investigate the hydraulic characteristics of the study reaches over a series of discharges ranging between $0 < Q \leq Q_{100}$.

In the development of each site model, additional cross-sections were required to reduce conveyance ratio errors. Cross-sections were added at locations where numerical errors were identified by using the representative cross-sectional form of the adjacent upstream and downstream cross-sections and adjusting the elevation of the thalweg of the synthetically generated cross-section to be consistent with the field measured thalweg elevation.

In some instances, a location of hydraulic control was not identified in the field to provide downstream boundary conditions. In these situations, a downstream hydraulic control flow condition was assumed, however, the downstream limit of the site model was extended downstream such that normal depth was achieved immediately downstream of the dam for discharge conditions ranging between $0 < Q \leq Q_{100}$. The river reach was typically extended downstream of the dam a distance equal to 40 times the top width (T) of the Q_{100} discharge event. In mild slope channel conditions, the channel extension distance is considered to be adequate to address any numerical artifacts of assuming a downstream critical flow depth (Totz and Klotz, 2003). An average channel cross-section was assumed for the downstream channel extension reach based upon surveyed cross-sections downstream of each dam. Stream channel slope (S_O) was determined from the relationship:

$$S_o = \frac{S_V}{\Omega} \qquad [19]$$

where S_V [-] is the valley slope and Ω [-] is the channel sinuosity down stream of the dams which were determined from 1:10000 topographic maps and / or digital elevation models.

Estimates of Manning's roughness coefficients (n) for each cross-sections bankfull channel were determined using the equation offered by Limerinos [1970] which relates Manning's n values to the hydraulic radius (R) and the 84th percentile of the bed material particle size (d_{84}) as defined by:

$$n = R^{1/6}\left(\frac{0.0926}{1.16 + 2.0\log\frac{R}{d_{84}}}\right) \qquad [20]$$

Manning's n values for each cross-sections left and right floodplains were estimated using a series of photographs provided by the Arcement and Schneider [1989] of vegetated floodplains for which the roughness coefficients had been verified.

Bankfull discharge from regional analysis methods (discussed in Section 3.2.1) were compared to the field calibrated bankfull discharges in the upstream stable sections of each river and compared to the HEC-RAS analysis results. Bankfull discharge model calibrations were achieved by adjusting the stream bed Manning's roughness coefficient, within acceptable tolerances, until as close of an agreement could be achieved between bankfull discharges determined from HEC-RAS, the field calibrated bankfull depth, and the localized maximum in the average channel velocity (as discussed in Section 2.5 and illustrated in Figure 19b). The results of the bankfull calibration methods are illustrated in Figure 27a, where the HEC-RAS calibrated bankfull discharge is compared to the

regional analysis method offered by Annable [1996] for $Q_{1.5}$. Correspondingly, Figure 27b illustrates the differences in Manning's roughness values using Equation 20 to predict the bed material roughness and the final calibrated values from the HEC-RAS sensitivity analyses.

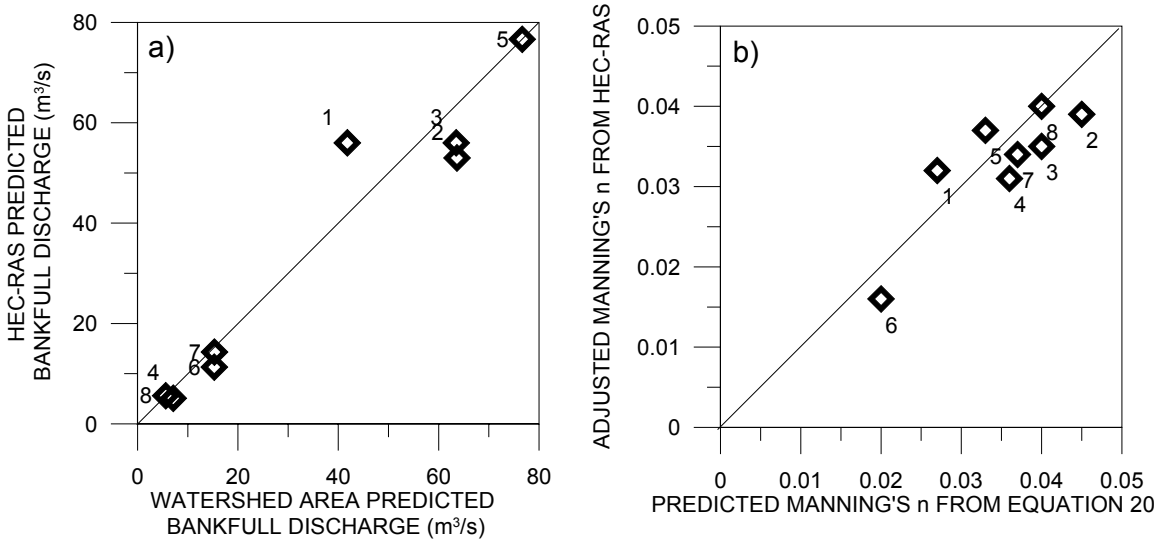

Figure 27. Comparison of a) HEC-RAS calibrated vs. regional analysis method for bankfull discharge and b) adjusted Manning's roughness coefficient vs. estimated Manning's roughness coefficient using Limerinos [1970].

3.2.1 Discharge Frequency Estimates

100 individual discharge analyses were undertaken ranging between $0 < Q \leq Q_{100}$ for each of the river reaches developed in HEC-RAS® in addition to the $Q_{1.5}$, Q_2, Q_{20}, and Q_{100} return frequencies. Typically, discharge frequency analyses (such as a Weibull plotting position or a Log-Pearson III) are commonly undertaken based upon flow data from nearby discharge gauging stations on the same river. However, of the eight sites surveyed, only four were locally occupied with hydrometric gauging stations and only three gauging stations had a sufficiently long period of record to undertake a flow frequency statistical analysis. Alternatively, where gauge stations did not exist and / or

gauges with too short of a time record to predict return frequencies or to calibrate rating curves, the watershed drainage area was used in conjunction with regionalization methods to predict flood flow recurrence intervals.

Regionalization techniques provided by Gingras et al. [1994] were employed to determine the Q_2, Q_{20} and Q_{100} return periods. These techniques relate particular flood quantiles to the effective drainage areas within the provinces of Ontario and Quebec using the equation:

$$\log Q_x = a + b \log DA \qquad [21]$$

where Q_x [L^3/T]is the flood flow of return period x [T], DA is the effective drainage area [L^2] of the watershed, and parameters a and b are regression coefficients specific to the hydrophysiographic region. For the purposes of this study and hydrogeographic region, Region 7 and 8 coefficients for a and b specified by Gingras et al. [1994] were utilized. In the case of bankfull discharge (Q_{BF}), a similar regionalization technique was offered for southern Ontario by Annable [1996] of the form:

$$Q_{BF} = 0.52 DA^{0.74} \qquad .[22]$$

Annable [1996] also identified that $Q_{BF} \approx Q_{1.5}$ for rural rivers in southern Ontario.

Drainage areas for each site were obtained through hydrological analysis of digital elevation models (DEMs) at $10m^2$ grid scales. Hydrological analyses were performed using ArcGIS 9.1®, and the DEMs obtained from the Geological Survey of Canada to delineate the effective catchment areas. Figure 28 illustrates an example of effective catchment area delineation for the Conestoga River at Hawkesville. Based upon the

ArcGIS 9.1® analysis algorithms, the effective catchment area was determined for each watershed studied.

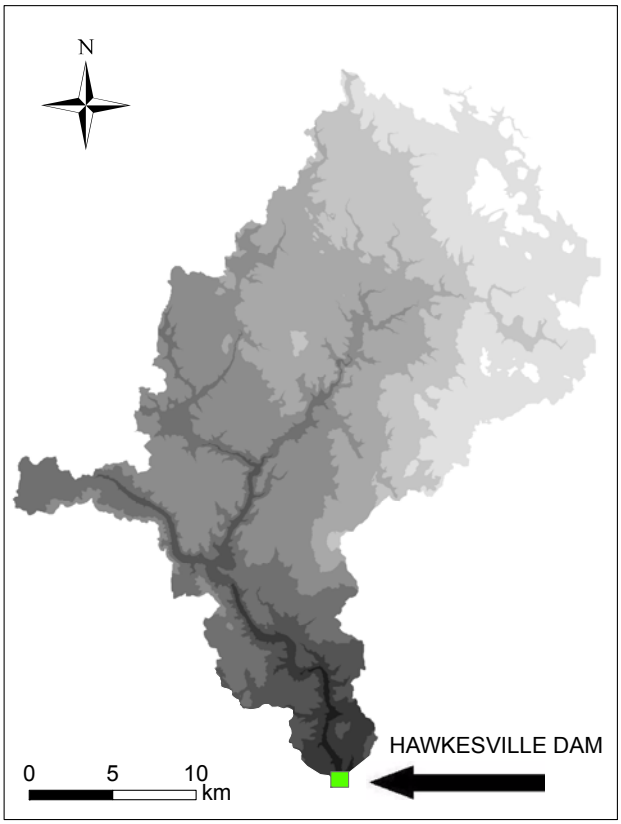

Figure 28. Conestoga River at Hawkesville sub-watershed DEM within the Upper Grand River watershed.

A summary of flood recurrence interval discharges using coefficients for Region 7 and 8 by Gingras et al. [1994] for each site are listed in Table 4.

Table 4. Flood flow frequency each site.

Ref. No.	Dam Name	River Name	Region	Area (km^2)	Return Period (m^3/s)			
					1.5	2	20	100
1	Croton Dam	Big Creek at Delhi	7	363	41.8	63.2	131.5	159.6
2	Hawkesville Dam	Conestogo River at Hawkesville	7	651	63.7	109.8	222.9	265.5
3	Huttonville Dam	Credit River at Huttonville	7	648	63.5	109.4	222.1	264.6
4	Chilligo Dam	Ellis Creek at Cambridge	7	57	7.1	10.9	24.6	31.6
5	Greenfield Dam	Nith River at Greenfield	7	842	76.6	140.0	281.3	332.3
6	Sutton Dam	Patterson Creek at Simcoe	7	90	15.3	16.9	37.2	47.2
7	Teeswater Dam	Teeswater River at Teeswater	8	123	15.3	15.8	29.1	35.0
8	Bognor Dam	Walter's Creek at Bognor	8	45	5.6	6.6	12.6	15.2
						coefficients		
			7	a	-	-0.621	-0.198	-0.032
			7	b	-	0.946	0.905	0.873
			8	a	-	-0.613	-0.274	-0.196
			8	b	-	0.867	0.832	0.833
					Annable (1996)	*Gingras et al. (1994)*		

For the three sites that were in close proximity to gauge stations (Big Creek, Conestoga River and Credit River), the Weibull Plotting position and the Log Pearson-III analysis were performed, consistent with methods offered by Bulletin 17b (U.S. Department of the Interior, 1981) and compared to the regionalization methods. The effective catchment areas at each gauge station were used in the regionalization methods rather than the effective catchment area associated with each dam location. Figure 29 illustrates the differences in the various methods considered in this research.

As illustrated in Figure 29, the regionalization methods considerably over predict both the Log Pearson-III and Weibull analysis for Big Creek (Figure 29a) and the Credit River (Figure 29c), and under predict in the case of the Conestoga River (Figure 29b). The regionalization method offered by Annable [1996] is the closest to those calculated using the Log Pearson-III and Weibull analysis methods which provides the initial estimate of bankfull discharge for calibration purposes. The remaining regionalization methods offered by Gingras et al. [1994] varies widely relative to the flow frequencies predicted using either the Log Pearson-III or the Weibull analysis. It should be noted, however,

that the accuracy of either the Q_{20} or the Q_{100} is not relevant in the HEC-RAS model accuracy or calibration. In particular the Q_{100} values obtained from the regionalization method offered by Gingras et al. [1994] simply provided an upper bound to estimate the Q_{100} such that 100 individual hydraulic analyses could be undertaken between $0 < Q \leq Q_{100}$ in evenly spaced intervals. The hydraulic responses of interest relevant to this study (where flows would overtop either the bankfull channel or the impoundment sediment levels) are captured somewhere within the range between $0 < Q \leq Q_{100}$, and then be used for analysis purposes.

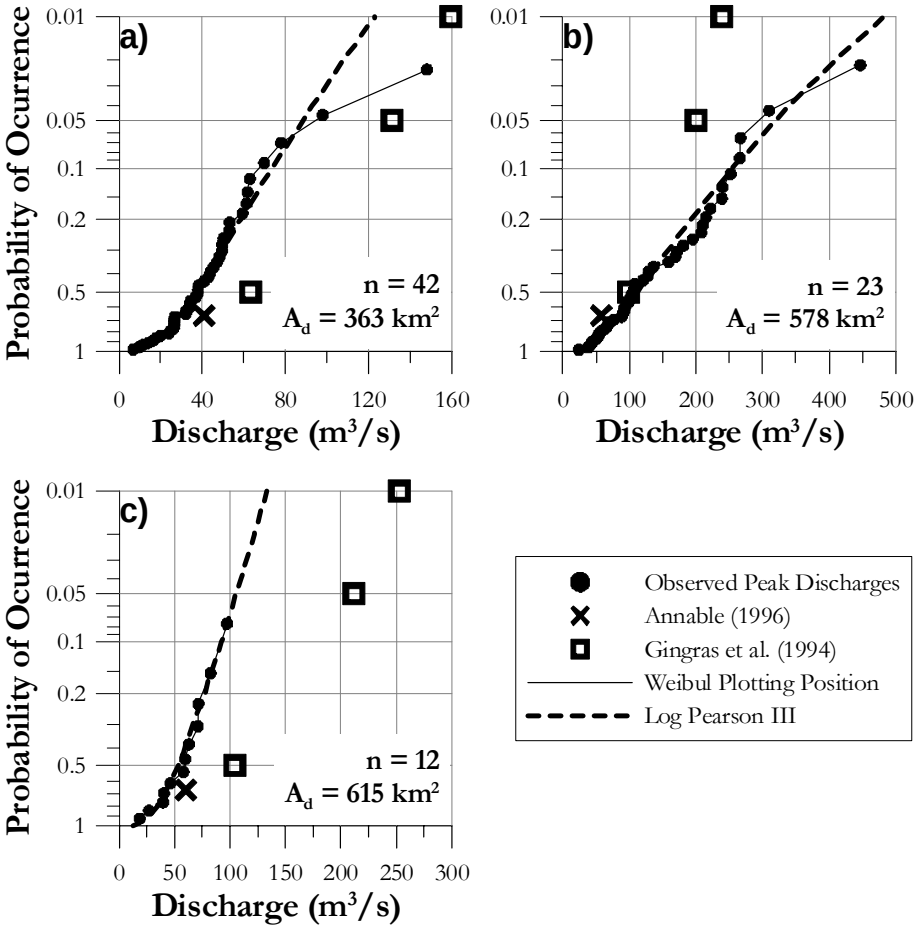

Figure 29. Comparison of yearly instantaneous maximum discharges, Weibull Plotting Position, Log Pearson-III Analysis, Gingras et al. [1994] and Annable [1996] methods of discharge estimation for the $Q_{1.5}$, Q_2, Q_{20} and Q_{100} return periods for Environment Canada gauge stations proximal to study sites at a) Big Creek near Delhi (02GC006) b) Conestoga River at Glen Allan (02GA028) and c) Credit River at Norval (02HB025).

3.2.3 Tractive Force and Permissible Velocity Analysis

The stability of the bed material along a river reach is affected through shearing forces and permissible velocity. For both shear forces and velocities, critical values were calculated to determine the threshold values to differentiate between particle motion or stability.

The threshold shear value (τ_{cds}), was calculated as a function of Shields parameter as defined by Julien (1995):

$$\tau_{cds} = \tau_{*c}(\gamma_s - \gamma_m)d_s \quad [23]$$

Furthermore, critical shear is specific for each particle size, and in turn was calculated for τ_{*c5}, τ_{*c16}, τ_{*c25}, τ_{*c50}, τ_{*c75}, τ_{*c84}, τ_{*c95} particle sizes from each sample. These values were compared to the bed shear within the main channel defined using Duboy's equation:

$$\tau_o = \gamma_m RS_f \quad [24]$$

which was calculated with the HEC-RAS analysis for the range of flows discussed previously.

Critical velocities (v_{cids}) [L T $^{-1}$] were determined using the equation offered by Novak and Nalluri [1984]:

$$\mathbf{v}_{cids} = 0.5\left(\frac{d_s}{R_i}\right)^{-0.4}\sqrt{gd_s(G-1)} \quad [25]$$

for each of the different discharges (Q_i) studied, where R_i represents the hydraulic radius of a given hydraulic analysis at a given cross-section. As critical velocity is both a

function of hydraulic radius and particle size, a suite of critical velocities exist for each flood flow and particle size respectively. The main channel velocity (V_i) and associated hydraulic radii (R_i) calculated in HEC-RAS were used to determine the critical particle size (d_{cv}) that would remain stable on the channel bed for the range in discharges between $0 < Q_i \leq Q_{100}$ using the equation defined by Novak and Nalluri [1984]:

$$\mathbf{d}_{cv} = \boldsymbol{R_i}^{-4}\left(\frac{4\mathbf{V}_i^2}{\boldsymbol{g(G-1)}}\right)^5 \qquad [\ 26\ ]$$

The critical particle values for the range in flows analyzed were then compared to the range of particle size percentiles determined by the sediment analysis (i.e. d_5, d_{16}, d_{25}, d_{50}, d_{75}, d_{84}, d_{95}) at each sample location to determine the particle size class associated with the critical cessation velocity.

4 RESULTS AND DISCUSSION

This chapter presents the hydraulic and sedimentological results obtained for each study site. Unit stream power, velocity and shear stress analyses are presented for flows ranging between $0 < Q \leq Q_{100}$. Subsequently, results of permissible and critical velocities and shear stress are presented and further interpreted with respect to continued upstream headcut migration. As all of the study sites range in longitudinal profile lengths (ranging between 1050m and 5600m), a normalized length comparison was developed for analysis purposes. For each study site, the distance along each thalweg longitudinal profile, starting at the dam face, was normalized with respect to the thalweg length between the dam face and the backwater limit of each reservoir. Using this approach, ratios of zero and one consistently occur at the dam face and the backwater limits of the reservoirs respectively (i.e. the region of the impoundments). Positive ratios reflect distances progressing upstream of the dam face, whereas negative values represent reaches progressing downstream of the dam face. The reference numbers identified in each graph refer to each site studied as outlined in Table 2.

4.1 Upstream Disturbance Propagation

Upstream disturbances initiated from dam failure are presented using field observations of headcuts and knickpoints. The longitudinal ratio here is defined as the maximum upstream extent of observed headcutting, relative to the dam face, normalized by the thalweg length of the reservoir. Figure 30 illustrates the longitudinal ratio versus the number of years since the dam was functional.

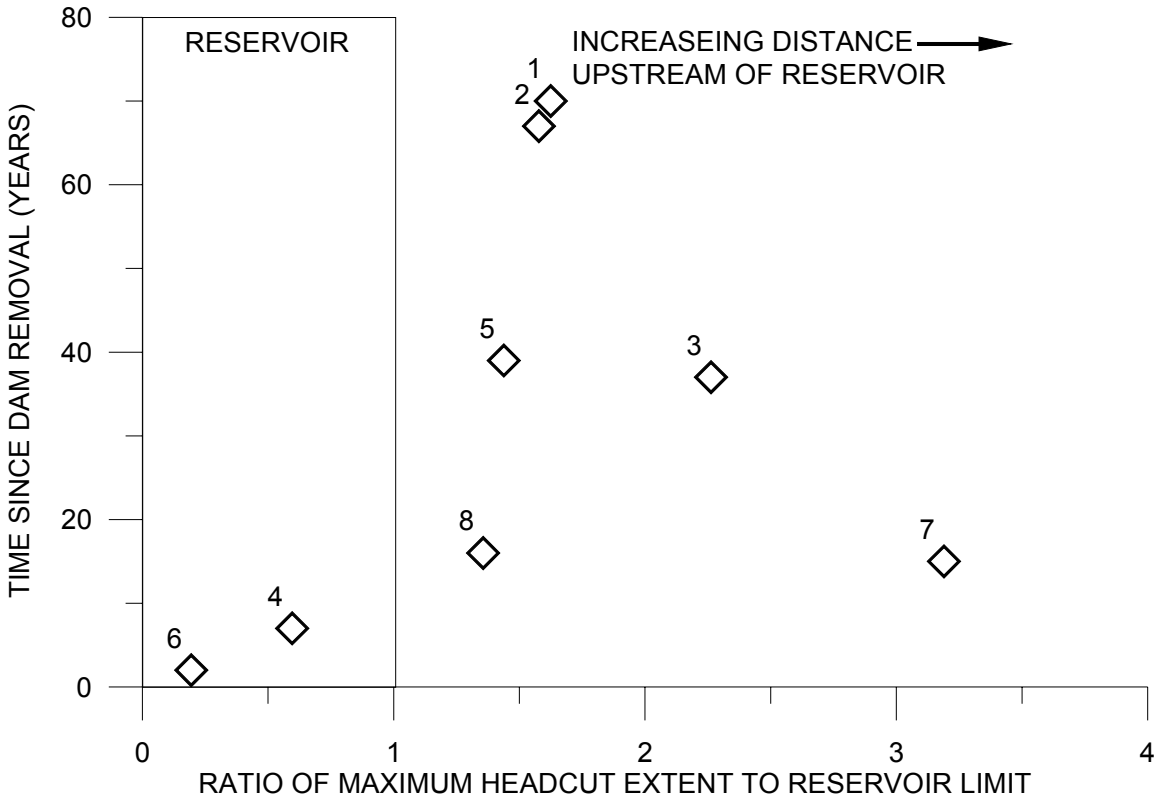

Figure 30. Ratio of maximum upstream headcut extent to normalized reservoir limit.

Vertical disturbances in the forms of headcuts and knickpoints initiated from dam removal or failure were identified at six of the eight study sites beyond the backwater limits of the reservoir. This confirms the hypothesis that headcuts and upstream vertical channel disturbances initiated from dam removal, consistent with the passive restoration approach, can extend beyond the backwater limits of the reservoirs. In most cases, the headcuts upstream of each reservoir are maintaining a vertical bed separation (although decreasing in vertical relief with upstream distance) rather than rotating and diminishing as discussed in Section 2.1. In the cases of sites 4 and 6, where headcut migration has not propagated upstream of the reservoir limits, both of these sites have had the least amount of time for upstream degradational processes to occur. In the subsequent sections of the

discussion, the sedimentological, shear stress and cessation velocities analyzed will be evaluated for each site and interpretations discussed with respect to the extent of upstream degradation (including Sites 4 and 6).

4.2 Power, Velocity and Shear Profiles

Analysis of unit stream power ($\hat{P}$), average channel velocity ($\overline{V}$), main channel velocity (V_{MAIN}), average channel shear (τ_O), and main channel shear (τ_{OMAIN}) were undertaken using the HEC-RAS models developed for each site to interpret the hydraulic responses along the longitudinal profiles of the 100 equally partitioned incremental discharges ranging between $Q < Q \leq Q_{100}$. The results of these analyses are presented in Figure 31 Figure 32 for Site 3 (Huttonville Dam on the Credit River). Appendices A – H contain similar plots for the remaining seven sites.

The bankfull delineation in each of the figures represents the hydraulic response of bankfull discharge (Q_{BF}) at each cross-section and how it compares to the hydraulic responses of the remaining group of unique discharges analyzed. As mentioned in Section 3.2.1, bankfull discharge was field determined from the stable upstream reaches and validated within each HEC-RAS analysis as the local maximum in the average channel velocity for the entire suite of discharges analyzed, as illustrated in Figure 33. The longitudinal profile is also included in Figure 31d to illustrate the bed variability along the reach in addition to the locations of headcuts and other field features of relevance.

It should further be noted that a longitudinal profile was not undertaken by wading the channel for site 1 similar to the other seven sites. Rather, channel cross-sections were surveyed using a Sokkia® Set 5E total station and their locations geo-referenced using a differentially corrected first order accurate GPS. Cross-sections were exclusively surveyed for this reach as there was significant tree fall (woody debris) and channel incisement making the navigation through the channel very prohibitive over the 4km incised channel reach.

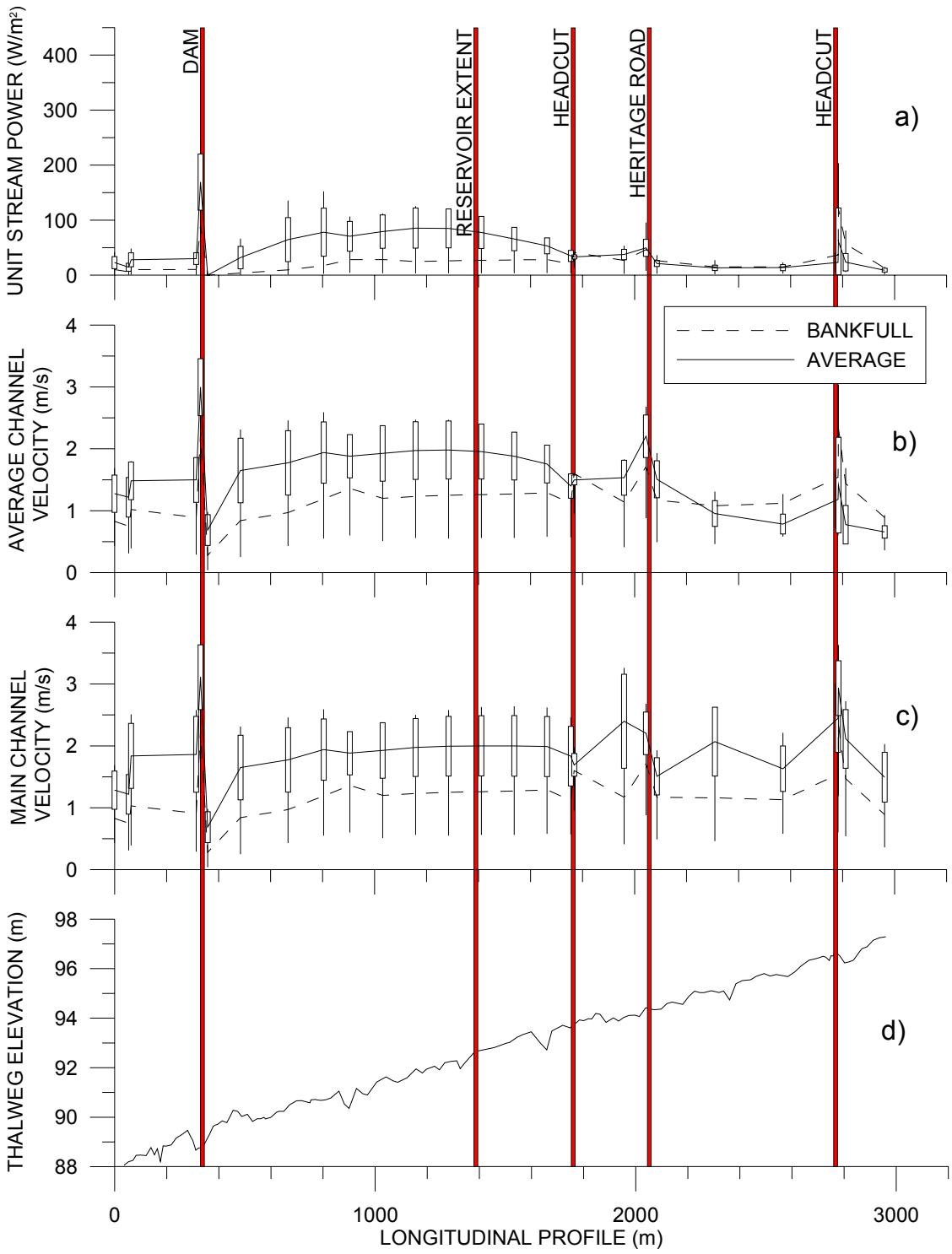

Figure 31. Results of a) unit stream power, b) average velocity, c) main channel velocity for incremental discharge analyses between $0 < Q \leq Q_{100}$, and d) thalweg elevation along the longitudinal profile for the Credit River at Huttonville (Site 3).

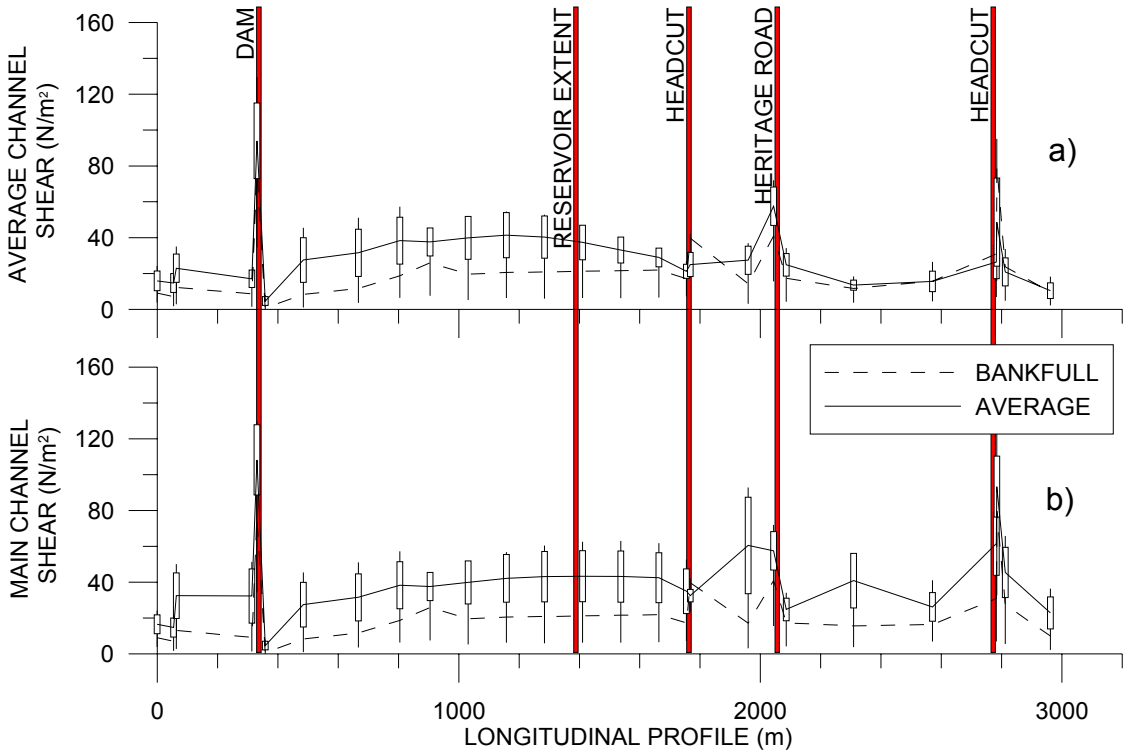

Figure 32. Results of a) average channel shear stress and b) main channel shear stress for incremental discharge analyses ranging between $Q < Q \leq Q_{100}$ along the longitudinal profile for the Credit River at Huttonville (Site 3).

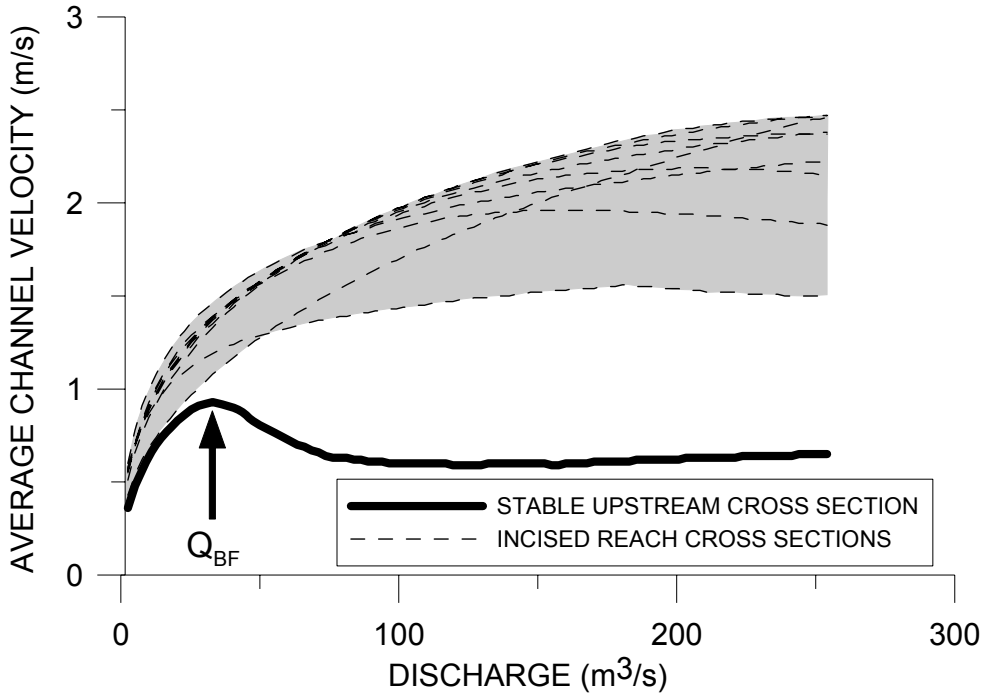

Figure 33. Average channel velocities of a stable upstream cross-section and the envelope of incised channel cross-sections for discharges ranging between $Q < Q \leq Q_{100}$ for the Credit River at Huttonville (Site 3).

Figure 31 a, b and c illustrate that the lowest unit stream power, highest average channel velocity and lowest main channel velocity occur upstream of the uppermost headcut where a stable bankfull channel was observed. This is further supported by the smallest range in standard deviations for the three previously mentioned hydraulic parameters suggesting that floodplain conveyance is occurring at larger discharges to attenuate flood flows and maintain channel stability. Conversely, throughout the impoundment reach upstream to Heritage Road, notable increases in each of the hydraulic parameters are identified in Figure 31 a, b and c; and each of the standard deviations in hydraulic parameters respectively. These channel responses are consistent with the idealized example presented in Section 2.5 for the incised channel reaches of the CEM (Stages II – IV). Within the incised channel reaches, the hydraulic parameters associated with Q_{BF} presented in Figure 31 a, b and c indicate that Q_{BF} does not predominant as a channel forming flow. Rather within the incised reaches, the effective discharge predominates the channel forming processes (i.e. $Q_{EFF} = Q_F$), typically found at some discharge within the standard deviation range of each hydraulic parameter analyzed. It should be further noted; that the effective discharge was not explicitly calculated at any site. Sediment rating curves did not exist at any of the sites; and only three of the eight sites were occupied with a hydrometric monitoring station possible for undertaking a partial series duration analysis.

The entire range in flows between $0 < Q \leq Q_{100}$ are contained within the incised channel reach and are all conveyed in the main channel, whereas the uppermost stable section accesses the floodplains when the discharge exceeds $Q \approx 41$ m^3/s. As the channel

velocities increase with increasing discharge for the incised channel reaches (as illustrated in Figure 33, larger particles are able to be entrained within the bedload transport fractions. The velocities within the incised channel reach are compared to those where bankfull discharge (and its associated velocity as illustrated in Figure 33) dominate the channel evolution in a floodplain channel morphology. As a result of the differences between velocities in the incised vs. bankfull reaches, and in turn the sizes and the mass of material able to be transported in each reach, a discontinuity exists in sediment transport from the upstream stable to incised channel reaches. Since the upstream reaches are not able to transport sufficient mass and sizes to maintain sediment continuity within the incised channel reaches, channel degradation by mass transport ensues leading to further channel incision and widening. This response is common to transport regardless if the average channel velocity (Figure 33) or main channel velocities are considered (Figure 34).

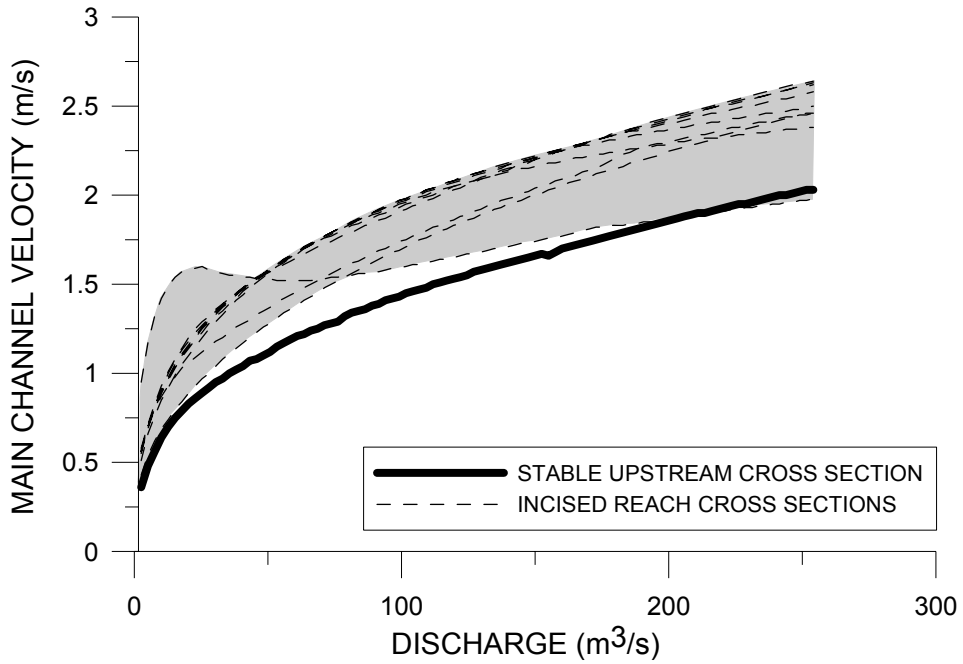

Figure 34. Main channel velocities of a upstream stable cross-section and the envelope of incised cross-sections for discharges ranging between $Q < Q \leq Q_{100}$ for Site 3.

Upon detailed examination of the longitudinal profile in Figure 31d, channel bed slope (S_o) within the reservoir was calculated at $S_0 = 0.33\%$ as compared to the adjacent valley slope of $S_V = 0.27\%$. Channel slopes greater than their associated valley slopes are another indicator of channel degradation consistent with Stages II and III channel evolution. In stable river channels, the channel bed slope is always less than or equal to the valley slope (i.e. $S_O \geq S_V$) by reason of meander bend extension. The increase in localized bed slope through the incised reaches results in increased hydraulic responses of stream power and channel velocities potentially in excess of the surrounding geological material incipient thresholds that were deposited over centuries. Over geologic time lines, the stable bed material size and channel slope evolve to a condition whereby $S_O \geq S_V$, which is not the case in the incised channel reaches. Along the increased channel slope associated with headcut migration, the critical particle size thresholds may be exceeded to erode particles otherwise stable; leading to continued channel degradation. These results will be presented in Section 4.3.

Figure 32a and Figure 32b illustrate the average and main channel shear stress respectively along the channel profile in a similar hydraulic fashion to Figure 31a through Figure 31c. When discharges exceed Q_{BF} in the floodplain dominated morphology, the wetted perimeter (Λ) significantly increases with inverse affects on the hydraulic radius (R) resulting in shear stresses remaining relatively low for the entire range of flows. Conversely, in the cross-sections where flows exceed Q_{BF} and do not access their adjacent floodplains, flow depths continue to increase with discharge and Λ increases at a relatively lower rate to that of the stable channels reaches until overbank access is

attained. This results in main channel shear (τ_{OMAIN}) and average channel shear (τ_O) continuously increasing until floodplains are accessed where Λ significantly increases. Moreover, there is an increased tendency in the incised sections for channel degradation to occur as shear thresholds are more likely to be exceeded as a result of increasing hydraulic radii relative to the bed material sizes and cohesiveness required to maintain channel bed and bank stability.

Hydraulic responses for $\hat{P}$, $\overline{V}$, V_{MAIN}, $\tau_{OAVERAGE}$, and τ_{OMAIN} for the seven other sites are included in Appendices A – H. The hydraulic responses of the seven other sites studied are thematically similar to Site 3 (Huttonville Dam on the Credit River) which are presented in Figure 31 and Figure 32.

To further summarize the effects of vertical channel degradation identified by migrating headcuts, plots were constructed which illustrate $\hat{P}$ (Figure 35), $\overline{V}$ and V_{MAIN} (Figure 36), τ_O and τ_{OMAIN} (Figure 37) for the discharge at each channel cross-section when overbank cresting occurs (i.e. when water begins to spill out onto the adjacent flood plain) for all of the river reaches studied. In the cases of the bankfull channel reaches, this discharge is synonymous with Q_{BF}. Within the incised channel reaches, the discharge used in the analyses is the unique flow observed when an inflection occurs in the average velocity vs. discharge plots for each cross-section (similar to those presented in Figure 33 and Figure 34) and/or where a notable increase in top widths occurred with increasing discharge. In the event that a channel inflection does not occur at a given cross-section, the Q_{100} discharge was used in the analysis. Ratios greater than 1.0 on the

ordinate indicate hydraulic parameter ratios in excess of the upstream stable cross-sectional profile, hence indicating channel degradation is occurring at these locations. Moreover, cross-sections with ordinate ratios > 1 indicate effective discharge dominates the channel evolution, and $Q_{BF} < Q_F = Q_{EFF}$.

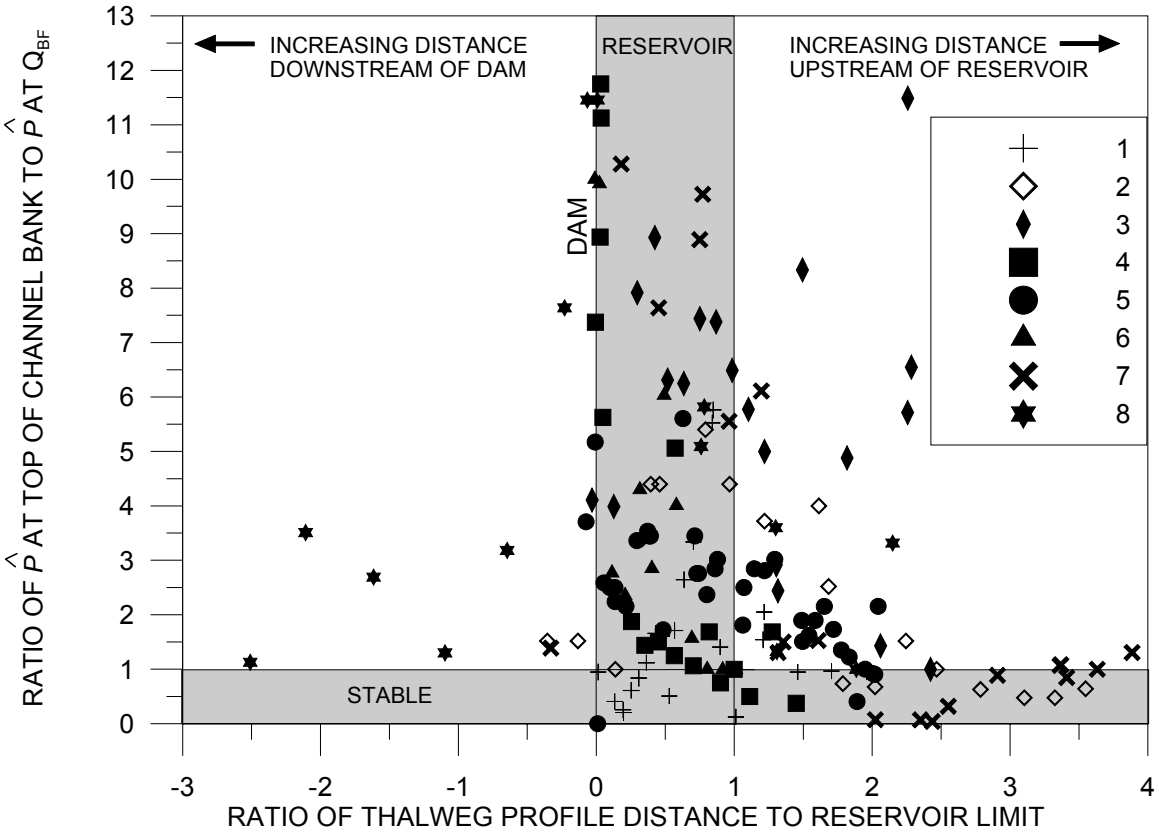

Figure 35. Results of unit stream power of flows which overtop banks vs. normalized longitudinal channel profile distance.

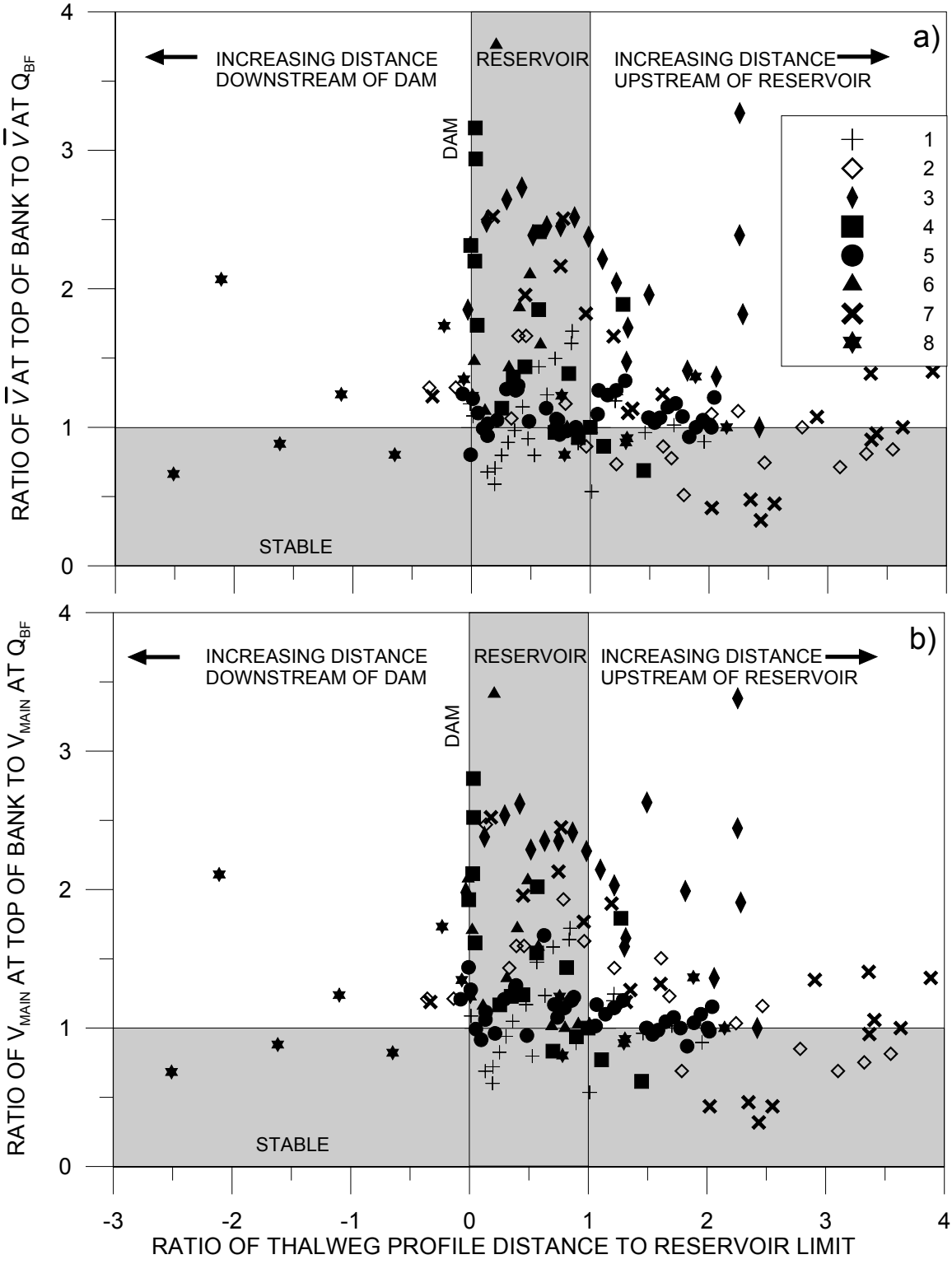

Figure 36. Results of a) average channel velocity and b) main channel velocity of flows which overtop banks vs. normalized longitudinal channel profile distance.

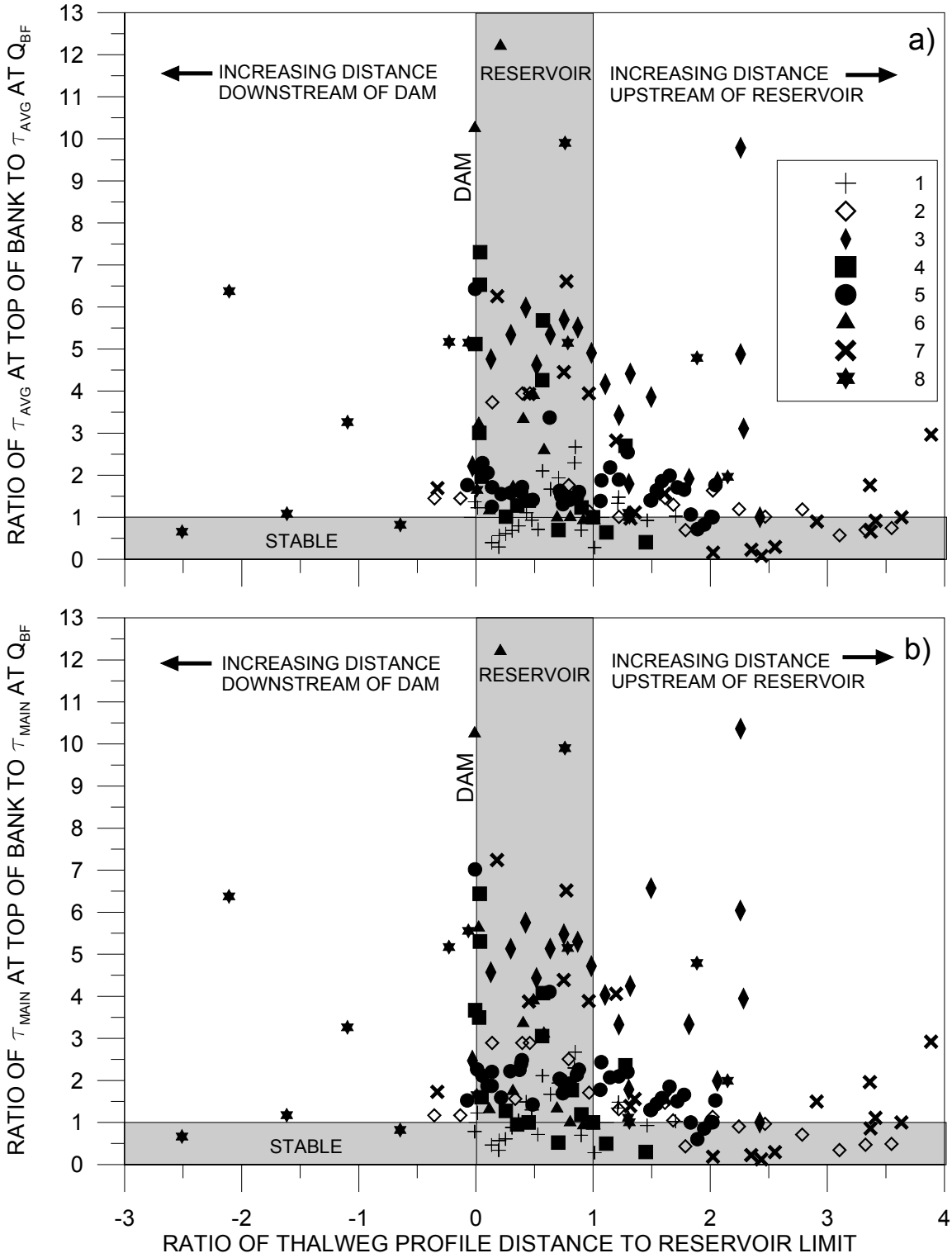

Figure 37. Results of a) average channel shear and b) main channel shear of flows which overtop banks vs. normalized longitudinal channel profile distance.

The hydraulic parameter ($\hat{\boldsymbol{P}}$, $\overline{\boldsymbol{V}}$, $V_{MAIN,}$ τ_O, τ_{OMAIN}) responses at each site are similar, with the exception of site 1, and maintain ratios >1 on the ordinate immediately upstream of the dam, indicative of channel evolution Stages II - III. Elevated hydraulic characteristics at flows that overtop banks above bankfull discharge are consistent with incised channels causing increased sediment carrying capacity and decreased channel sinuosity resulting in steeper bed slopes or some combination thereof. Where ratios exceed unity, effective discharge dominates the channel evolution. Additionally, at these cross-sections there is an increased tendency for further channel degradation to occur, as thresholds of greater particle sizes and cohesiveness are exceeded for flows greater than bankfull. The trend of cross-sections tends towards unity with increasing distance upstream of the reservoir.

Site 1 is the exception in the hydraulic responses relative to the other seven sites. Examining the cross-sections for site 1 immediately upstream of the dam in Figures 35, Figure 36 and Figure 37, overbank flow ratios are < 1. These cross-sections have been evolving for approximately 70 years (since the time of failure) and demonstrate Stage IV or Stage V characteristics. As cross-sections are examined in sequence of increasing distance upstream from the dam, the effects of incision gradually increase (tending towards stages III and II of the CEM sequence). Moreover, Figure 6b in Section 2.3 demonstrates this longitudinal evolution of channel morphology, where downstream reaches are in a state of quasi-equilibrium and upstream reaches are increasing in both vertical and cross-sectional profiles consistent with the location of the uppermost headcut.

4.3 Tractive Force and Velocity Results

This section presents shear stress and velocity hydraulic results for modeled flood flows of Q_{BF}, Q_2 and Q_{20}. Results are presented as the ratios of each event's hydraulic responses to critical thresholds for d_{50} and d_{84} particle sizes of the observed bed material at riffles, runs and headcuts. Figure 38, Figure 39 and Figure 40 present the results of the shear stress analysis for the three increasing discharges previously cited. Similarly, Figure 41, Figure 42 and Figure 43 present the results of the critical particle sizes as a function of cessation velocity (critical velocity) for the three flows previously cited.

Ratios on the ordinate greater than 1 indicate that critical thresholds have been exceeded and particle motion is expected. Each range in ratio represents the variations in critical values for the suite of sediment samples collected on each morphological feature. The symbol depicted in each range represents the average determined for a given morphological feature.

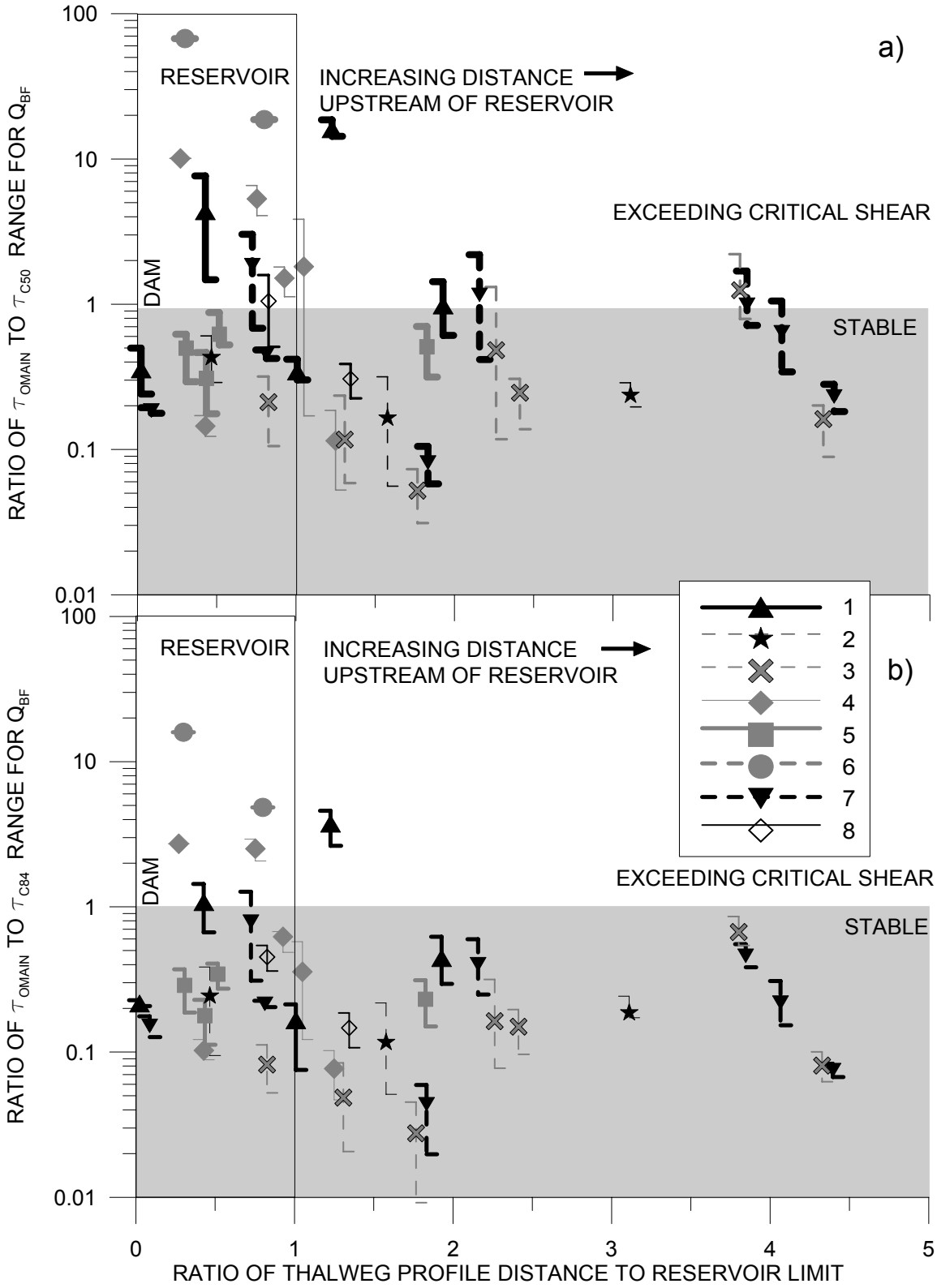

Figure 38. Results of a) main channel shear vs. τ_{c50} threshold and b) main channel shear vs. $\tau_{c\,84}$ threshold along the normalized longitudinal profile at Q_{BF}.

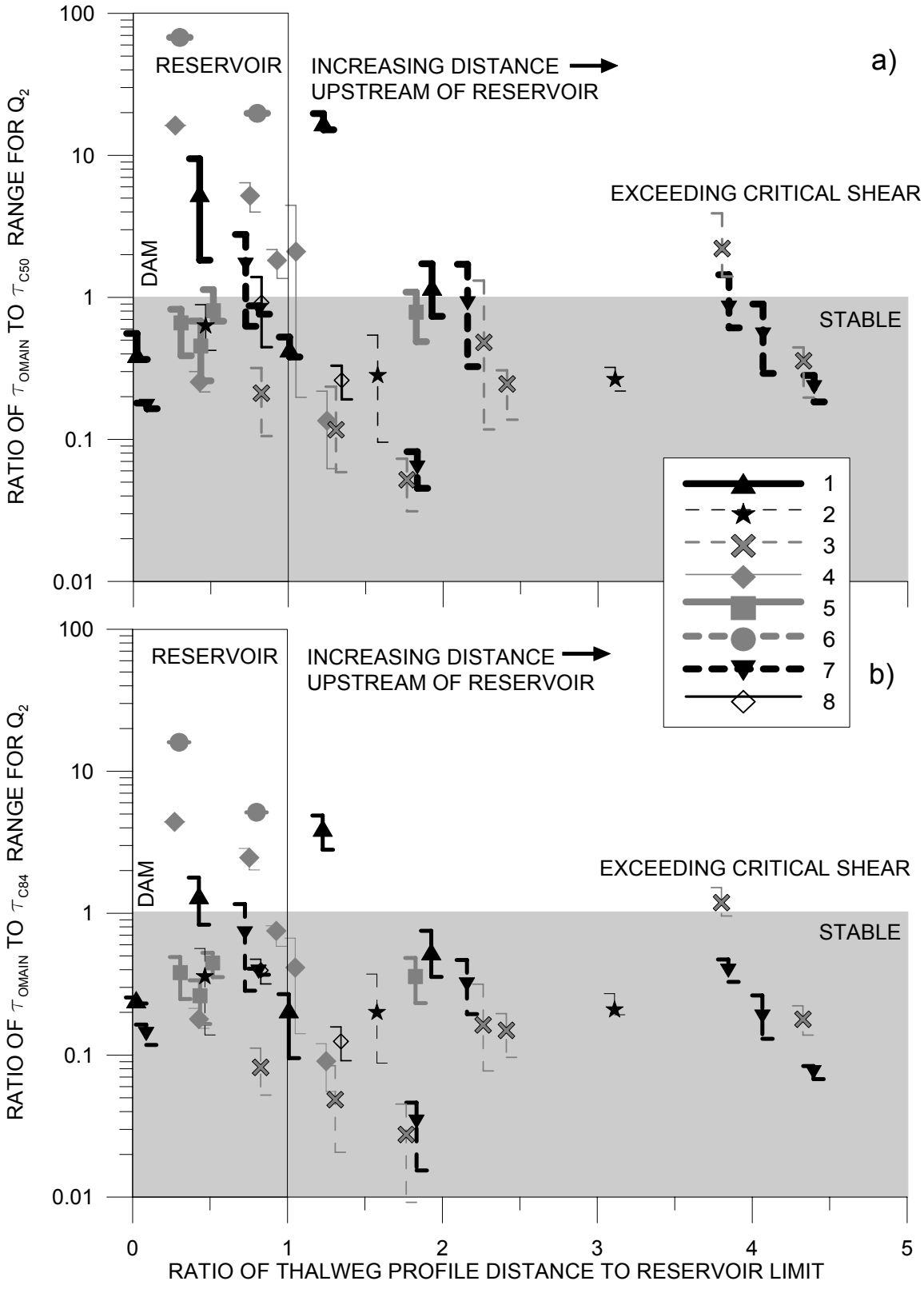

Figure 39. Results of a) main channel shear vs. $\tau_{c\,50}$ threshold and b) main channel shear vs. $\tau_{c\,84}$ threshold along the normalized longitudinal profile at Q_2.

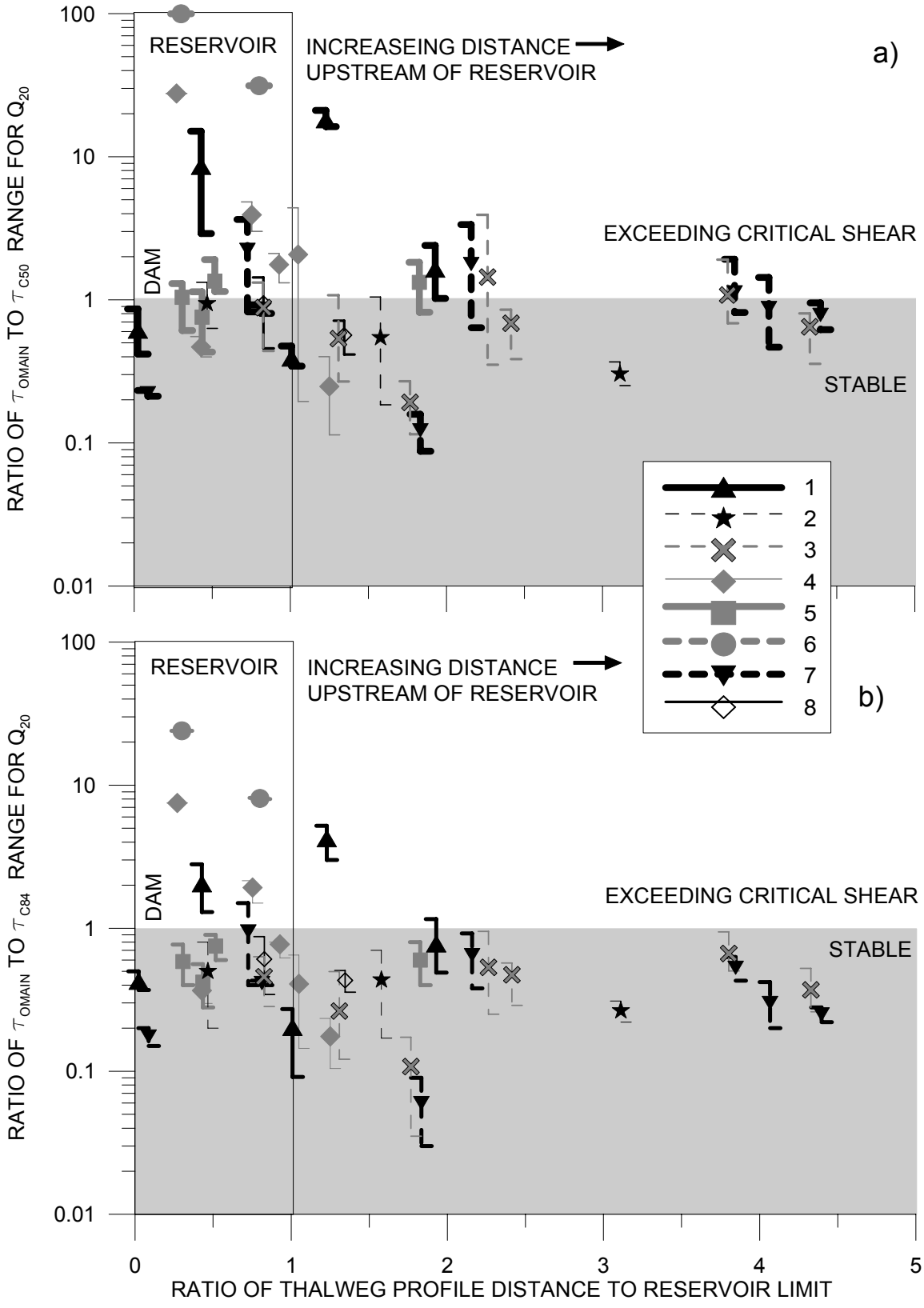

Figure 40. Results of a) main channel shear vs. $\tau_{c\,50}$ critical threshold and b) main channel shear vs. $\tau_{c\,84}$ critical threshold along the normalized longitudinal profile at Q_{20}.

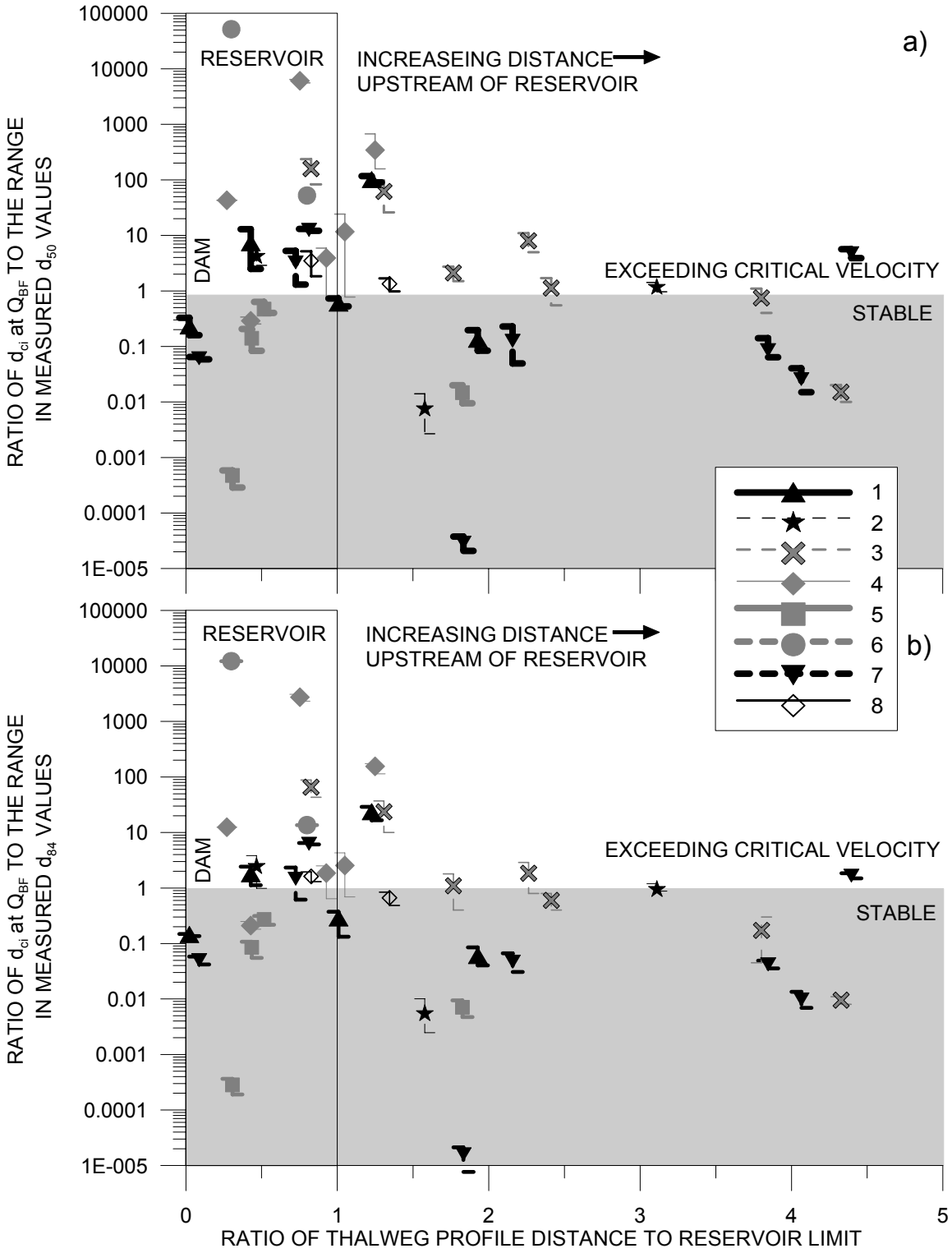

Figure 41. Results of a) maximum permissible particle size at Q_{BF} vs. the range of measured d_{50} values and b) maximum permissible particle size at Q_{BF} vs. the range of measured d_{84} values along the normalized longitudinal profile.

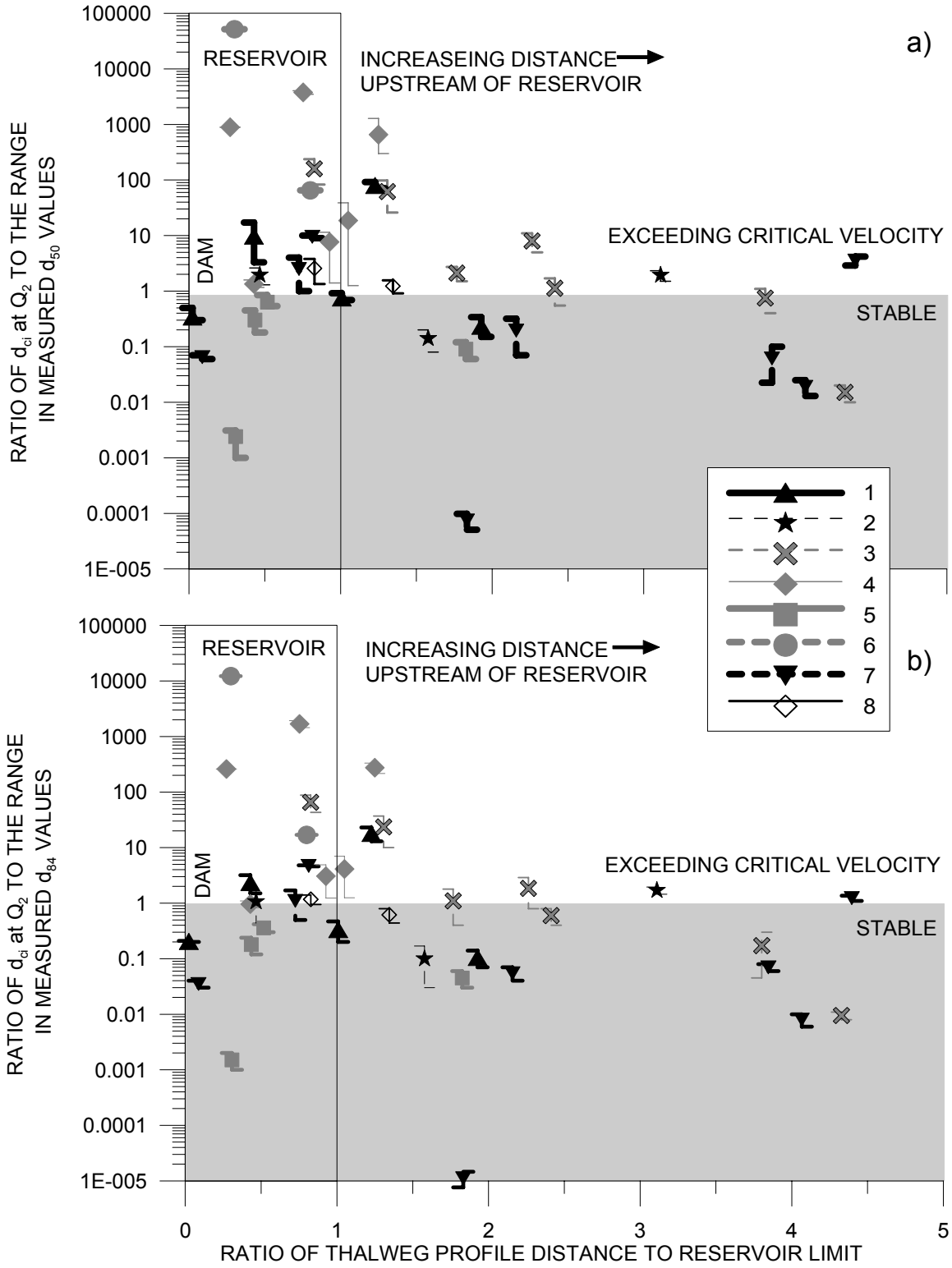

Figure 42. Results of a) maximum permissible particle size at Q_2 vs. the range of measured d_{50} values and b) maximum permissible particle size at Q_2 vs. the range of measured d_{84} values along the normalized longitudinal profile.

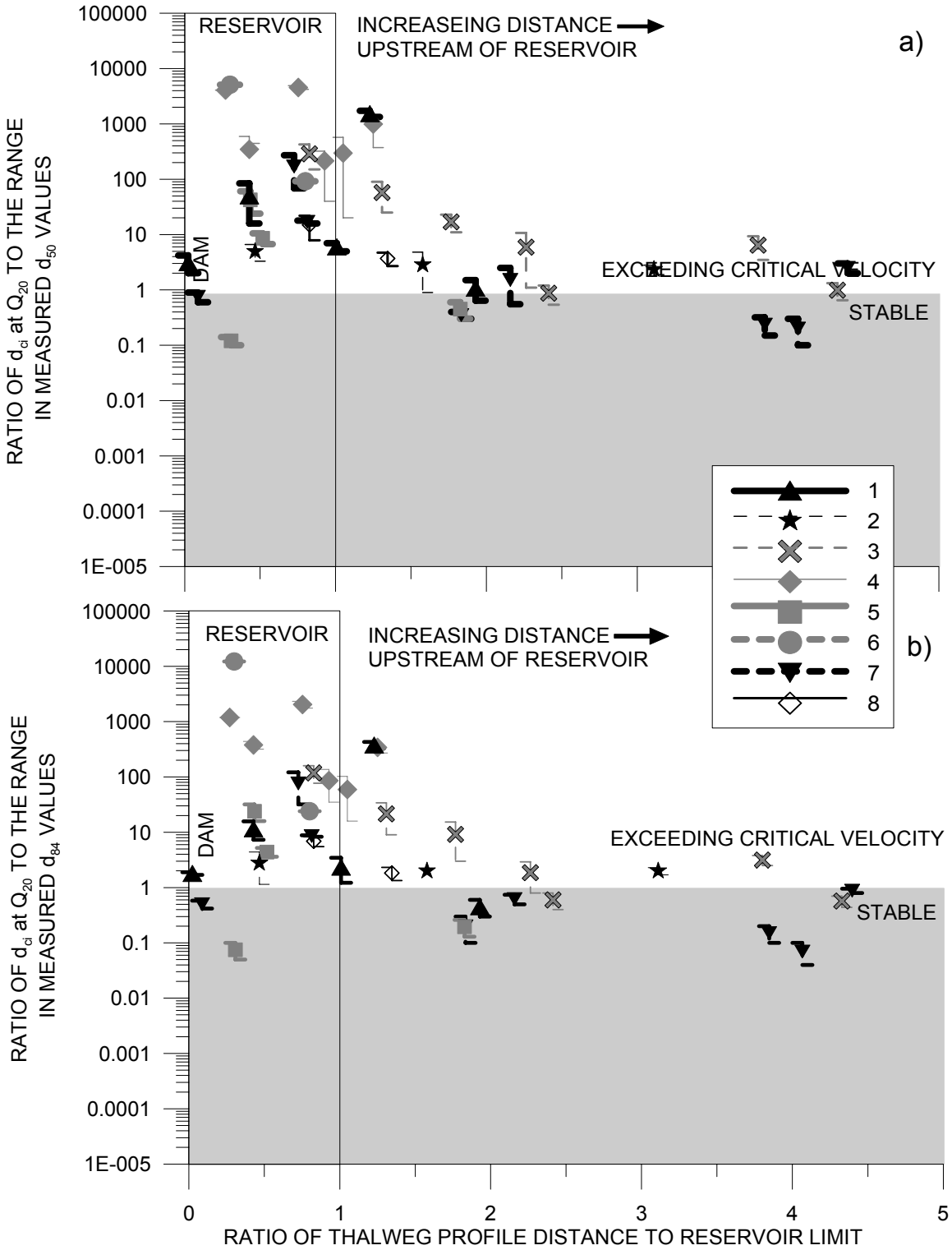

Figure 43. Results of a) maximum permissible particle size at Q_{20} vs. the range of measured d_{50} values and b) maximum permissible particle size at Q_{20} vs. the range of measured d_{84} values along the normalized longitudinal profile.

A common trend observed in Figure 38 – Figure 43 is that with increasing discharge, a greater number of the morphological features (i.e. headcuts, runs and riffles) begin to incrementally exceed both their critical shear stress and velocity thresholds. As many of the sites range in age between 2 years and 20 years, continued and enhanced channel degradation is predicted with the hydraulic responses between the Q2 and Q20 year return periods. Further, the general trends presented in Figure 38 – Figure 43 also indicate that, in most cases, the particle sizes comprising the bed material, and their associated critical thresholds, are more often exceeded relative to the critical shear thresholds for the range in flows studied.

General trends, most apparent within the velocity results for Q_{20} (Figure 43) illustrate higher surpluses in the permissible thresholds of particles within the incised sections of the reservoir compared to cross-sections upstream with less incision. Within the reservoir, the greatest surpluses (greatest ratios) occur at sites 6 and 4; the youngest two dam failure sites. This is consistent among the results of shear and velocity. The analyses of morphological features within the reservoir at both of these sites are experiencing the effects of Stage II channel evolution. Sites 4 and 6 are still evolving as the maximum upstream headcut at both sites have not surpassed the reservoir limit. In turn, the most recently removed dams show the greatest susceptibility to erosion during floods within the reservoir caused by highly incised, low sinuosity channels. This susceptibility will be maintained until the channel widens and increases in sinuosity, indicative of later stages of channel evolution.

The uppermost feature for each site indicates the sediment range of the stable bankfull morphology which has yet to be affected by vertical incision. Figure 38a demonstrates that at Q_{BF}, the shear along the channel bed is insufficient to degrade the stable bankfull morphology d_{50} particles at six of the eight sites (2, 3, 4, 5, 7, and 8). Moreover, Sites 2, 3, 4, 7, and 8 experience erosion of d_{50} at Q_{BF} due to shear at some features downstream. These observations support the hypothesis that sediment discontinuities of d_{50} particles at Q_{BF} are occurring at five of the sites. These discontinuities cause further degradation of the channel bed and banks, and are a principle driving force in headcut migration.

It was mentioned in Section 4.2 that Site 1 cross-sections immediately upstream of the dam had evolved to later stages of channel evolution (Stage IV or V) and experienced low hydraulic responses to floods attributed to floodplain access at lower discharge levels. Further upstream at Site 1, however, severe channel incision is still apparent as illustrated in Figure 38 – Figure 43 as ratios on the ordinate typically exceed unity. These results further the conclusion as the foremost riffle upstream of the dam at Site 1 indicates stability of d_{50} and d_{84} particles with respect to shear for Q_{BF}, Q_2, Q_{20} and velocity for Q_{BF} and Q_2. Within the incised cross-sections upstream, erosion due to the exceedances of shear and velocity thresholds are apparent for all particles at all flood flows.

To simplify the results presented in Figure 38 – Figure 43, the following summary tables were prepared for the shear stress ratios (Table 5) and critical velocity ratios (Table 6). These tables identify for each site and discharge analyzed, the particle sizes which exceed

their respective critical thresholds (i.e. values greater than unity in Figure 38 – Figure 43). Further, the tables have been divided into two sections to depict the erosion of the specified particle ranges within the impoundment and upstream of the impoundment.

Table 5. Summary of bed material and sizes exceeding critical shear stress thresholds for Q_{BF}, Q_2, and Q_{20} within and upstream of site impoundments. Note: if particle sizes are identified in the table, they exceed critical thresholds at one or more morphological features.

	Within Impoundment			Upstream of Impoundment			Time Since Failure (Years)
SITE	**Q_{BF}**	**Q_2**	**Q_{20}**	**Q_{BF}**	**Q_2**	**Q_{20}**	
1	d_{50}/d_{84}	d_{50}/d_{84}	d_{50}/d_{84}	d_{50}/d_{84}	d_{50}/d_{84}	d_{50}/d_{84}	70
2			d_{50}				67
3			d_{50}	d_{50}	d_{50}/d_{84}	d_{50}	37
4	d_{50}/d_{84}	d_{50}/d_{84}	d_{50}/d_{84}	d_{50}	d_{50}	d_{50}	7
5		d_{50}	d_{50}		d_{50}	d_{50}	39
6	d_{50}/d_{84}	d_{50}/d_{84}	d_{50}/d_{84}				2
7	d_{50}/d_{84}	d_{50}/d_{84}	d_{50}/d_{84}	d_{50}	d_{50}	d_{50}	15
8	d_{50}	d_{50}	d_{50}				16

Table 6. Summary of bed material and sizes exceeding critical velocity thresholds for Q_{BF}, Q_2, and Q_{20} within and upstream of site impoundments. Note: if particle sizes are identified in the table, they exceed critical thresholds at one or more morphological features.

	Within Impoundment			Upstream of Impoundment			Channel Slope (S_O) (-)
SITE	**Q_{BF}**	**Q_2**	**Q_{20}**	**Q_{BF}**	**Q_2**	**Q_{20}**	
1	d_{50}/d_{84}	d_{50}/d_{84}	d_{50}/d_{84}	d_{50}/d_{84}	d_{50}/d_{84}	d_{50}/d_{84}	-
2	d_{50}/d_{84}	d_{50}/d_{84}	d_{50}/d_{84}	d_{50}/d_{84}	d_{50}/d_{84}	d_{50}/d_{84}	3.6E-03
3	d_{50}/d_{84}	d_{50}/d_{84}	d_{50}/d_{84}	d_{50}/d_{84}	d_{50}/d_{84}	d_{50}/d_{84}	3.3E-03
4	d_{50}/d_{84}	d_{50}/d_{84}	d_{50}/d_{84}	d_{50}/d_{84}	d_{50}/d_{84}	d_{50}/d_{84}	3.8E-03
5			d_{50}/d_{84}				2.0E-03
6	d_{50}/d_{84}	d_{50}/d_{84}	d_{50}/d_{84}				8.0E-03
7	d_{50}/d_{84}	d_{50}/d_{84}	d_{50}/d_{84}	d_{50}/d_{84}	d_{50}/d_{84}	d_{50}/d_{84}	3.0E-03
8	d_{50}/d_{84}	d_{50}/d_{84}	d_{50}/d_{84}	d_{50}	d_{50}	d_{50}/d_{84}	8.0E-03

Comparison of Table 5 (shear) to Table 6 (velocity) show that increased levels of velocity at flood flows have greater influences on erosion than shear stress. The notable exception is site 5 where shear stress with increasing discharge has dominated the channel evolution. Site 5 is located within a kame moraine deposit which has the largest source

of course material from upstream bank erosion (relative to the other sites), and the bed material averages the second most coarse ($d_{50} \approx 69$ mm – Table 3) particle size. Further, the valley slope is the shallowest of all sites studied ($1.7x10^{-3}$ m/m – Table 2) suggesting that the combination of the course bed material sizes and the shallowest slopes would result in velocities insufficient to typically move the range in bed material sizes. Therefore, the predominant mechanism for Site 5 is by channel shear.

In the case of Site 6 (the most recent dam failure) headcuts have not been observed upstream of the impoundment region. However, in undertaking the critical shear and velocity threshold analyses, both the d_{50} and the d_{84} values exceed both critical thresholds for all flows. Considering that the local geology of this site is a sand plain deposit and the bed material at this site is primarily composed of sand ($d_{50} \approx 0.3$mm – Table 3), it is likely that this watercourse will experience continued headcutting beyond the limits of the impoundment region. Inspection of the HEC-RAS model developed for this site upstream of the impoundment indicates that both shear and velocity conditions for the Q_{BF}, Q_2 and Q_{20} exceed critical thresholds for the sand bed composition measured within and upstream of the study site. The hydraulic analysis further supports the position that upstream channel degradation should be expected at this river reach.

A similar argument to that posed for Site 6 is also consistent for Site 4 (which is the second youngest dam – 7 years). The reach is a gravel bed channel ($d_{50} \approx 31$mm – Table 3), however, as indicated in Table 5 and Table 6 the critical velocity thresholds are exceeded throughout the impoundment and upstream regions for both d_{50} and d_{84} grain

sizes. Moreover, the critical shear stress thresholds for d_{50} and d_{84} are exceeded within the impoundment in addition to the shear stress thresholds for the d_{50} values upstream of the impoundment. These results suggest that headcut migration should be expected upstream of the impoundment, however, due to the short time span since dam removal, upstream migration has not evolved to the upper reaches.

5 CONCLUSIONS and RECOMMENDATIONS

Field and modelling studies of eight removed or failed dam sites with no upstream interventions were used as the analog to passive channel restoration with a headcut driven channel formation. The results show that vertical disturbances identified by headcuts extend for considerable distances upstream of the backwater limits of six of the eight reservoir study sites. Furthermore, headcuts were observed and measured at all sites, which ranged in age between 2 years – 70 years since dam failure with the likelihood in all cases that channel degradation will continue in the future. Similar results are probable at sites where passive dam removals are implemented without any upstream intervention.

The hydraulic responses of unit stream power, velocity and shear strength within the disturbed channel reaches at flood flows that overtop banks were much greater than bankfull discharges upstream of the disturbed sections. Main channel velocities exceeding critical thresholds dominated the channel evolution processes for the range in bed material particle sizes ($0.3\text{mm} \leq d_{50} \leq 81\text{mm}$) over critical shear stress thresholds with increasing discharges. Only one site seems to have regained a stable channel morphology upstream of the dam face within the reservoir – which also corresponds to the oldest channel evolution at 70 years before present. Channel degradation and the upstream propagation of headcuts will continue at the remaining sites until new dynamic equilibriums are achieved when sediment and discharge continuity are established; and geotechnical and geomorphic stability attained for each set of unique site-based conditions.

5.1 Recommendations

To prevent vertical disturbances of the channel bed from migrating beyond the reservoir limits, grade control solutions should be incorporated into the channel restoration approach to ensure that the disturbances from dam decommissioning do not propagate upstream beyond the backwater limits. Watson and Biedenharn [1999] identified two main categories of grade control structures which either construct a hard point within the main channel, by increasing bed material size that exceeds both critical shear stress and velocity thresholds, or by introducing a hydraulic control structure to decrease the energy slope. Watson and Biedenharn [1999] further define the applicability of the type of grade control structure depends on factors such as hydraulic conditions, sediment size, channel morphology, and funding constraints, amongst many others. Neilson et al. [1991] provides a comprehensive outline on types and applications of grade control structures. If fish passage is of interest, grade control structures that facilitate this intent should be considered. Such structures may include rocky-ramps (Newbury and Gaboury, 1993) or cross-vane structures (Rosgen, 1996) if properly constructed within a bankfull cross-sectional channel profile at appropriate locations.

Furthermore, the extent of base level lowering may be controlled, to reduce the energy grade line, by a partial removal of the structure to the upper limit of the impounded sediments. This would decrease the height of headcuts initiated at the dam face and would increase the likelihood of them diminishing by the reservoir limits and decrease the likelihood of velocities and shear stress exceeding critical thresholds.

6.0 References

(AASHTO) American Association of State Highway and Transportation Officials. (2005). "A summary of existing research on low-head dam removal projects." *NCHRP Project 25-25, Task 14, National Cooperative Highway Research Program, Transportation Research Board*, p. 179.

Annable, W. K. (1996), *Morphological relationships of rural water courses in southwestern Ontario and selected field methods in fluvial geomorphology*, Ontario Ministry of Natural Resources, ISBN 077785113X, p. 92.

Arcement, G., and Schneider, V. (1989). "Guide for selecting Manning's roughness coefficients for natural channels and flood plains." *U.S. Geological Survey Water Supply Paper,* 2339.

Ashley, J. (2006). "The effects of small dam removal on the distribution of sedimentary contaminants." *Environmental Monitoring and Assessment,* 114(1), 287 - 312.

Ashmore, P. (1988). "Bed load transport in braided gravel-bed stream models." *Earth Surface Processes and Landforms,* 13(8), 677 - 695.

Ashworth, P. J., and Ferguson, R. I. (1989). "Size-selective entrainment of bedload in gravel-bed streams." *Water Resources Research,* 25(4), 627 - 634.

Beatty, D. A. (1984). "Channel migration and incision of the Beatton River." *Journal of Hydraulic Engineering,* 110(11), 1681-1682.

Bednarek, A. T. (2001). "Undamming Rivers: A review of the ecological impacts of dam removal." *Environmental Management,* 27(6), 803 - 814.

Beechie, T. T., Pollock, M. M., and Baker, S. (2007). "Channel incision, evolution and potential recovery in the Walla Walla and Tucannon River basins, northwestern USA." *Earth Surface Processes and Landforms.*

Begin, Z., Meyer, D., and Schumm, S. (1980). "Knickpoint migration due to baselevel lowering." *Journal of the Waterway, Port, Coastal, and Ocean Division,* 106(3), 369 - 388.

Biedenharn, D., and Copeland, R. (2000). "Effective discharge calculation." *Coastal and Hydraulics Engineering Technical Notes (CHETN),* 3(4), 1 - 10.

Brush, L. M., and Wolman, M. G. (1960). "Knickpoint behaviour in noncohesive material: a laboratory study." 71(1), 59 - 74.

Bunte, K., and Abt, S. (2001). "Sampling surface and subsurface particle-size distributions in wadable gravel- and cobble-bed streams for analysis in sediment transport, hydraulics, and streambed monitoring." *Rep. No. 1,* United States Department of Agriculture, Forest Service Rocky Mountain Research Station, p. 428.

Canadian Dam Association. (2005). "Dam Safety Guidelines." *http://www.cda.ca (Aug. 9, 2006)*, p. 18.

Chapman, L. J., and Putnam, D. F. (1966). *Physiography of southern Ontario,* Second Edtion, University of Toronto Press, Toronto, Ontario, Canada, ISBN 0-8020-1944-7, p. 386.

Cheng, F., and Granata, T. (2004). "Monitoring and modeling sediment transport and geomorphology changes associated with dam removal." *2004 Self-Sustaining Solutions for Streams, Wetlands, and Watersheds Conference,* American Society of Agricultural Engineers, St. Joseph, MI 49085-9659, United States, St Paul, MN, United States, pp. 208 - 213.

Copeland, R., Biedenharn, D., and Fischenich, J. (2000). "Channel-forming discharge." *Coastal and Hydraulics Engineering Technical Notes (CHETN),* 3(5), 1 - 10.

Cui, Y., Braudrick, C., and Rothert, S. (2005). "Preliminary Assessment of Sediment Transport Dynamics Following Dam Removal: A Case Study." *ASCE conference proceedings - Managing Watersheds for Human and Natural Impacts: Engineering, Ecological, and Economic Challenges*, 275 - 286.

Doyle, M. W. (2005). "Stream ecosystem response to small dam removal: Lessons from the Heartland." *Geomorphology,* 71(1), 227 - 244.

Doyle, M. W., Stanley, E., and Harbor, J. (2002). "Geomorphic Analogies for Assessing Probable Channel Response to Dam Removal." *Journal of the American Water Resources Association,* 38(6), 1567 - 1579.

Doyle, M., Stanley, E., Harbor, J., and Grant, G. (2003). "Dam Removal in the United States: Emerging Needs for Science and Policy." 84(4), 29 - 36.

Dynesius, M. (1994). "Fragmentation and Flow Regulation of River Systems in the Northern Third of the World." *Science,* 266(5186), 753 - 762.

Egiazaroff, I. V. (1965). "Calculation of nonuniform sediment concentrations." *Journal of Hydraulics Division Conference Proceedings Paper,* 91(4), 225 - 247.

Emerson, W. (1971). "Channelization: A Case Study." *Science,* 173(3994), 325 - 326.

Foster, G. R. and Meyer, L. D. (1975). "Mathematical simulation of upland erosion by fundamental erosional mechanics." *Proceedings of the Sediment-Yield Workshop - Present and prospective technology for predicting sediment yield and sources,* USDA Sedimentation Lab., Oxford, MS, 190 - 207.

Friedman, G., and Sanders, J. (1978). *Principles of sedimentology,* Wiley Publisher, New York, NY, p.792.

Gingras, D., Adamowski, K., and Pilon, P. (1994). "Regional flood equations for the provinces of Ontario and Quebec." *Journal of the American Water Resources Association,* 30(1), 55 - 67.

Heinz Center. (2002). "Dam removal: Science and decision making." The H. John Heinz III Center for Science, Economics and the Environment, p. 221.

Hickin, E. J., and Nanson, G. C. (1975). "The character of channel migration on the Beatton River." *Geological Society of America Bulletin,* 86, 487 - 494.

Julien, P. Y. (1995). *Erosion and Sedimentation.* Cambridge University Press, New York, NY, p. 280.

Julien, P. Y. (1995). *River Mechanics.* Cambridge University Press, New York, NY, p. 434.

Klingeman, P., and Emmett, W. (1982). "Gravel bedload transport processes. IN - " *Gravel-bed Rivers. Fluvial Processes, Engineering and Management,* R.D. Hey, J.C. Bathurst and C.R. Thorne, ed., John Wiley and Sons, Chichester, pp. 141 - 179.

Komar, P. D. (1987). "Selective gravel entrainment and the empirical evaluation of flow competence." *Sedimentology,* 34(6), 1165 - 1176.

Kondolf, G. M. (1997). "Hungry water: Effects of dams and gravel mining on river channels." *Environmental Management,* 21(4), 533 - 551.

Kuhnle, R. A. (1992). "Fractional transport rates of bedload on Goodwin Creek." *Dynamics of gravel-bed rivers,* P. Billi, ed., John Wiley and Sons Ltd, New York, 141-155.

Lane, E. W. (1955). "Design of stable alluvial channels." *Transactions of American Society of Civil Engineers,* 120, 1234-1260.

Leopold, L., Wolman, M., and Miller, J. (1964). *Fluvial Processes in Geomorphology.* W. H. Freeman and Company, San Francisco, p. 522.

Ligon, F. K. (1995). "Downstream ecological effects of dams." *BioScience,* 45(3), 183.

Limerinos, J. T. (1970). "Determination of the Manning coefficient from measured bed roughness in natural channels." *U.S. Geological Survey Water Supply Paper,* 1898-B.

MacBroom, J. G. (2005). "Evolution of channels upstream of dam removal sites." *2005 Watershed Management Conference - Managing Watersheds for Human and Natural Impacts: Engineering, Ecological, and Economic Challenges, Jul 19-22 2005,* American Society of Civil Engineers, Reston, VA 20191-4400, United States, Williamsburg, VA, United States, 287-298.

Marsh, N. A. (2004). "Comparison of Methods for Predicting Incipient Motion for Sand Beds." *Journal of Hydraulic Engineering,* 130(7), 616 - 621.

Nanson, G. C., and Hickin, E. J. (1983). "Channel migration and incision on the Beatton River." *Journal of Hydraulic Engineering,* 109(3), 327-334.

Neilson, F. M., Waller, T. N., and Kennedy, K. M. (1991). "Annotated bibliography on grade control structures." Technical Report HL-91-4, U.S. Army Corps of Engineers, Waterways Experiment Station, Vicksburg, MS.

Newbury, R., and Gaboury, M. N. (1993). *Stream analysis and fish habitat design : a field manual.* Newbury Hydraulics, Gibsons, B.C., p. 256

Novak, P., and Nalluri, C. (1984). "Incipient motion of sediment particles over fixed beds." *Journal of Hydraulic Research,* 22(3), 181 - 197.

Pansic, N., Austin, R. J., and Finis, M. (1998). "Sediment management for dam decommissioning." U.S Conference on Large Dams, Sediment Management and Erosion Control on Water Resources Projects, 15th Annual USCOLD Lecture Series. San Francisco, CA. 29-45. May 15-19.

Papanicolaou, A. N. (2002). "Stochastic Incipient Motion Criterion for Spheres under Various Bed Packing Conditions." *Journal of Hydraulic Engineering,* 128(4), 369 - 380.

Petts, G. (1984). *Impounded Rivers: Perspectives for ecological management.* John Wiley and Sons, Chichester, England, p. 326.

Pohl, M. M. (2002). "Bringing down our dams: Trends in American dam removal rationales." *Journal of the American Water Resources Association,* 38(6), 1511 - 1519.

Rosgen, D. L. (1996). *Applied river morphology.* Wildland Hydrology, Pagosa Springs, CO. USA., ISBN # 0965328902, p. 390.

Schumm, S. (1969). "River Metamorphisis." *Proceedings of the American Society of Civil Engineers,* 95(6352), 255 - 273.

Schumm, S. A., Harvey, M. D., and Watson, C. C. (1984). *Incised channels: morphology, dynamics, and control.* Water Resources Publications, Littleton, CO. USA., p.200.

Selle, A., Burke, M., Melchior, M., and Koonce, G. (2007). "Active vs. passive channel recovery following dam removal: a comparison of approaches", *World Environmental and Water Resources Congress 2007*, American Society of Civil Engineers, 243(40927), 356 - 366.

Shields, A. (1936). "Application of similarity principles and turbulence research to bed-load movement." *Mitteilunger Der Preussischen Versuchsanstalt f˙ur Wasserbau Und Schiffbau,* 26, 5 - 24.

Shields, F. D., Simon, A., and Steffen, L. (2000). "Reservoir effects on downstream river channel migration." *Environmental Conservation,* 27(1), 54 - 66.

Shvidchenko, A. B., Pender, G., and Hoey, T. (2001). "Critical shear stress for incipient motion of sand/gravel streambeds." *Water Resources Research,* 37(8), 2273-2283.

Simon, A. (1998). "Process-form interactions in unstable sand-bed river channels: A numerical modelling approach." *Geomorphology,* 21(2), 85 - 106.

Simon, A., and Darby, S. (1999). "The nature and significance of incised river channels." *Incised River Channels: Processes, forms, engineering and management,* John Wiley and Sons Ltd, West Sussex, England, pp. 3 - 34.

Simons, D. B. (1971). "Open Channel Flow." *Introduction to fluvial processes,* R. J. Chorley ed., pp.124 - 145.

Stanley, E. H., and Doyle, M. W. (2002). "Trading off: the ecological effects of dam removal." *Bioscience,* 52(8), 693 - 701.

Stein, O. R. (1993). "Criterion delineating the mode of headcut migration." *Journal of Hydraulic Engineering,* 119(1), 37 – 50.

Totz, C., and Klotz, D. (2003). *Floodplain modeling using HEC-RAS.* Haestad Press, Waterbury, CT. p. 696.

U.S. Department of the Interior. (1981). "Bulletin 17B: Guidelines for determining flood flow frequency." Interagency Advisory Committee on Water Data, Department of the Interior, U.S. Geological Survey, Office of Water Data Coordination, Reston, VA.

Watson, C., and Biedenharn, D. (1999). "Design and effectiveness of grade control structures in incised river channels of North Mississippi, USA. IN" *Incised River Channels: Processes, forms, engineering and management,* A. Simon, and S. Darby, eds., John Wiley and Sons Ltd, West Sussex, England, pp. 395 - 422.

Wilcock, P. R., and Southard, J. B. (1997). "Experimental study of incipient motion in mixed-size sediment." *Water Resources Research,* 24(7), 1137 - 1151.

Wohl, E. E. (2000). "Sediment deposition and transport patterns following a reservoir sediment release." *Water Resources Research,* 36(1), 319 - 333.

Wolman, M. G. (1954). "A method of sampling coarse river-bed material." *American Geophysical Union,* 35(6), 951 - 956.

Wolman, M. G., and Miller, W. P. (1960). "Magnitude and frequency of forces in geomorphic processes." *Journal of Geology,* 68, 54 - 74.

Appendices A – H

Appendix A: Croton Dam on Big Creek at Delhi

Dam Location:
Northing: 4740972m
Easting: 540213m
(Coordinate System: NAD 1983 UTM Zone 17N)

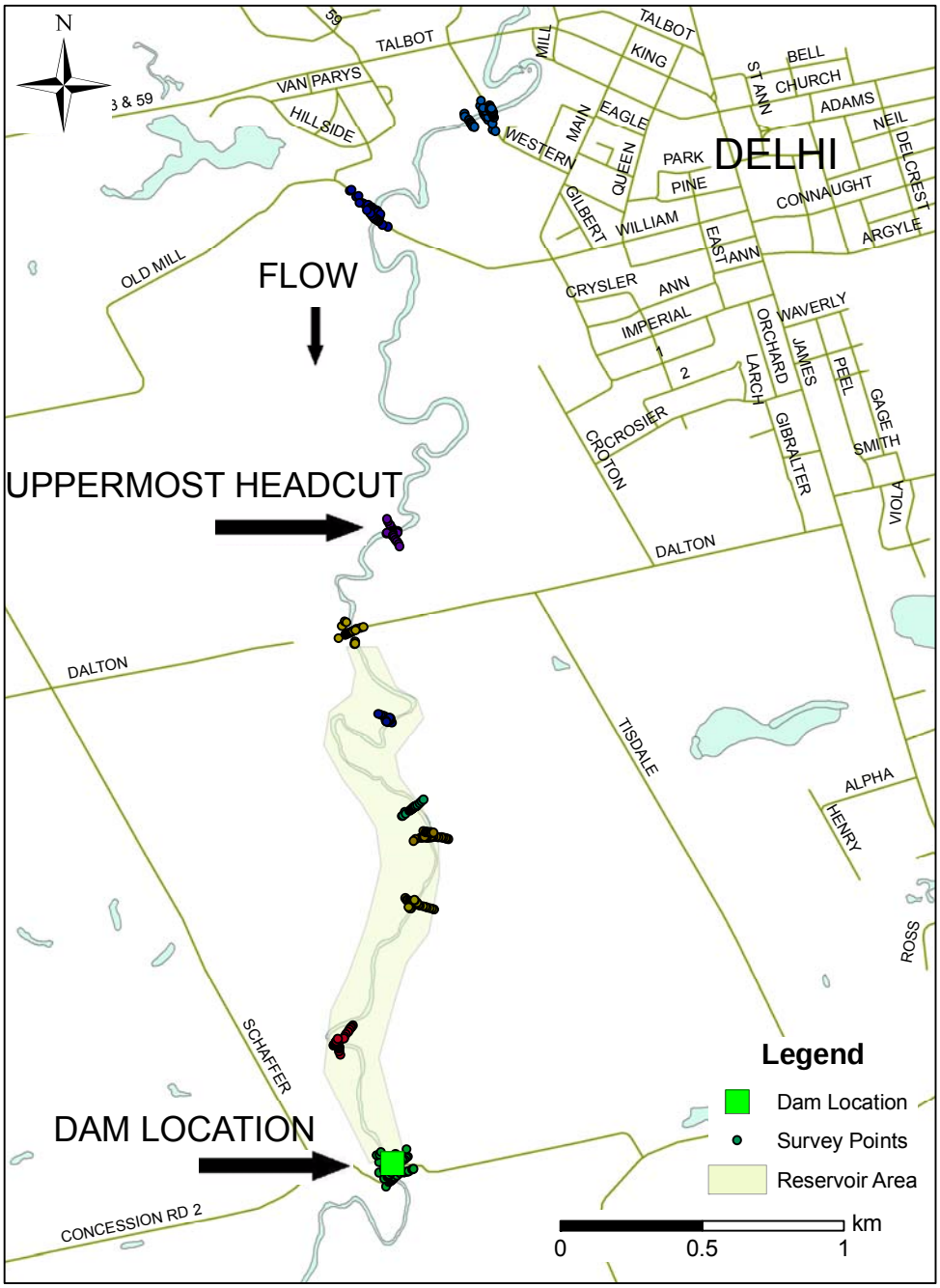

Figure A – 1. Croton Dam on Big Creek at Delhi site survey.

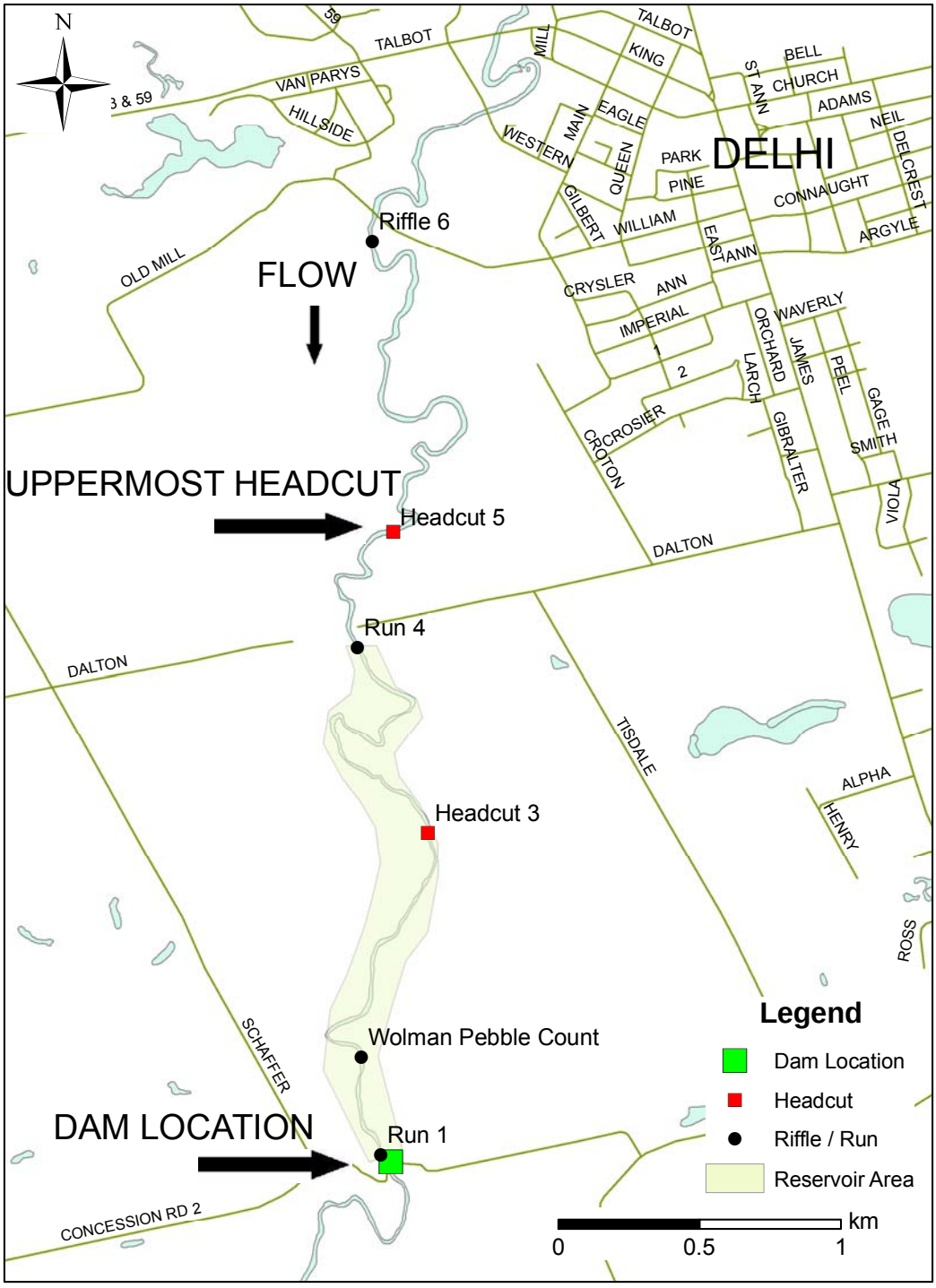

Figure A – 2. Locations of sediment samples on Big Creek in Delhi.

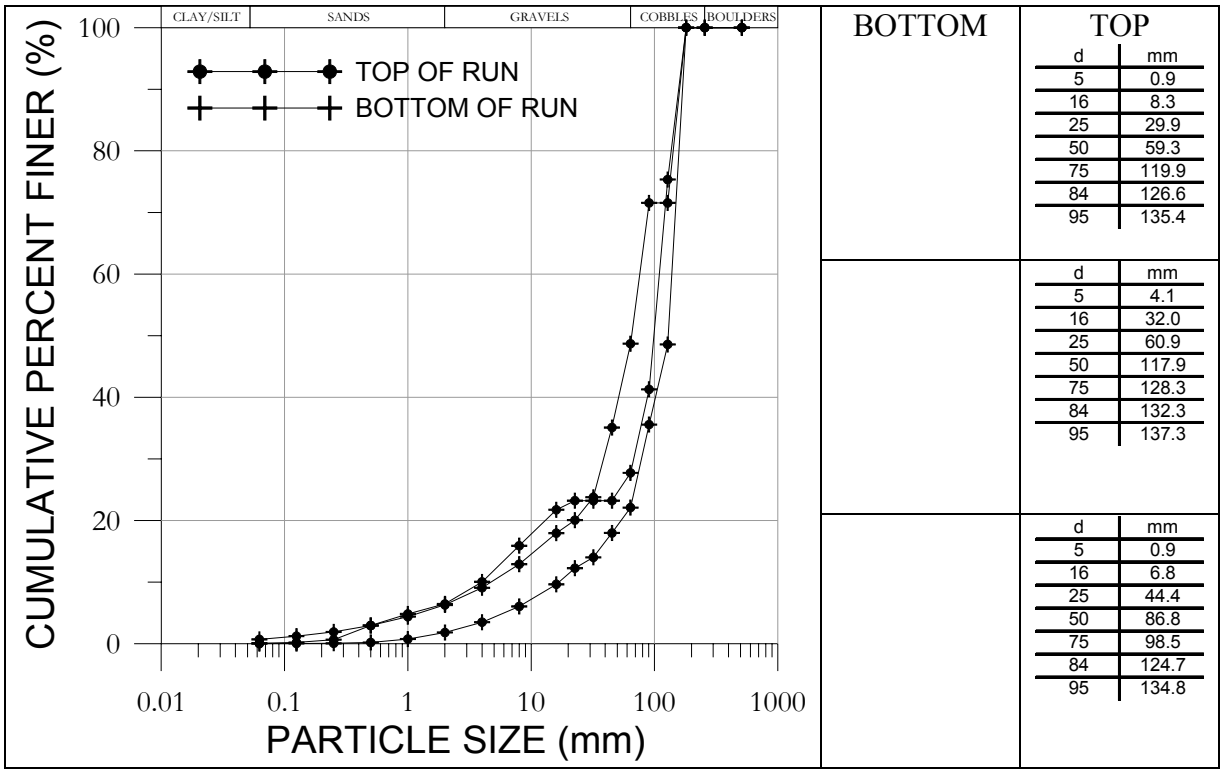

BOTTOM

TOP

d	mm
5	0.9
16	8.3
25	29.9
50	59.3
75	119.9
84	126.6
95	135.4

d	mm
5	4.1
16	32.0
25	60.9
50	117.9
75	128.3
84	132.3
95	137.3

d	mm
5	0.9
16	6.8
25	44.4
50	86.8
75	98.5
84	124.7
95	134.8

Figure A – 3. Pavement sample characteristics of Run 1.

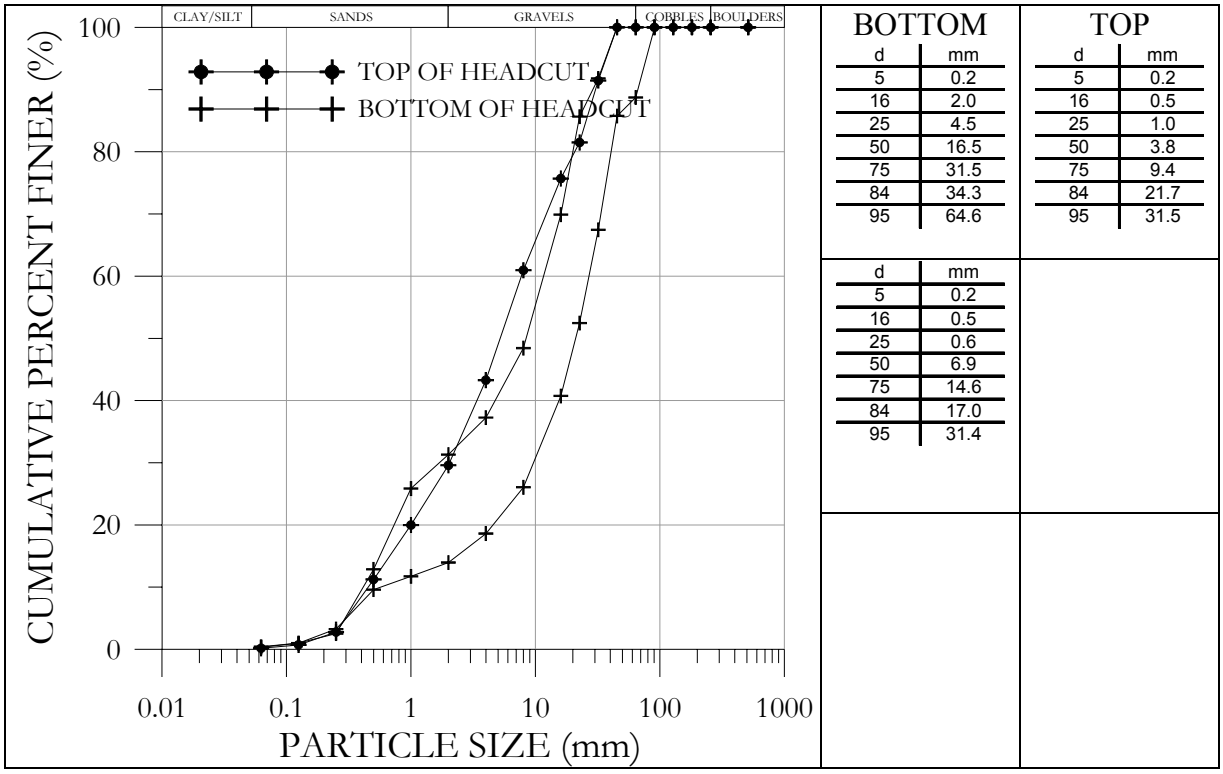

BOTTOM

d	mm
5	0.2
16	2.0
25	4.5
50	16.5
75	31.5
84	34.3
95	64.6

TOP

d	mm
5	0.2
16	0.5
25	1.0
50	3.8
75	9.4
84	21.7
95	31.5

d	mm
5	0.2
16	0.5
25	0.6
50	6.9
75	14.6
84	17.0
95	31.4

Figure A – 4. Pavement sample characteristics of Headcut 3.

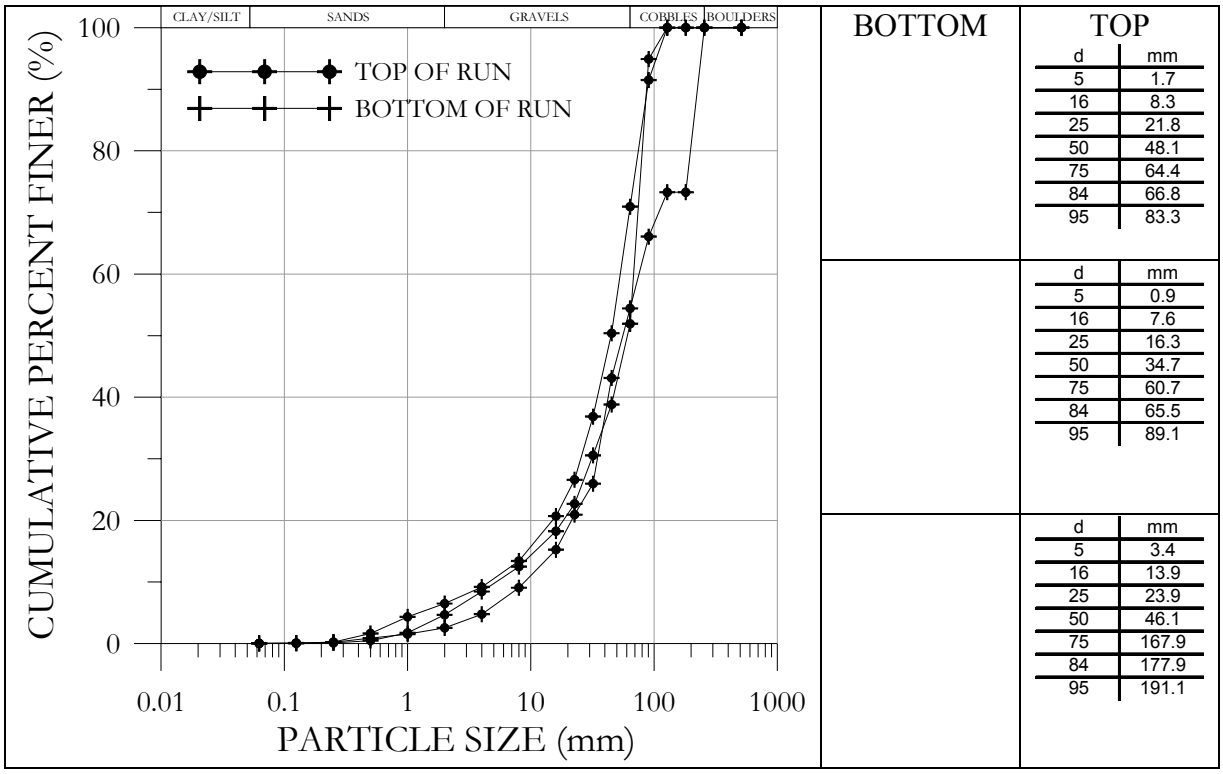

BOTTOM	TOP	
	d	mm
	5	1.7
	16	8.3
	25	21.8
	50	48.1
	75	64.4
	84	66.8
	95	83.3

	d	mm
	5	0.9
	16	7.6
	25	16.3
	50	34.7
	75	60.7
	84	65.5
	95	89.1

	d	mm
	5	3.4
	16	13.9
	25	23.9
	50	46.1
	75	167.9
	84	177.9
	95	191.1

Figure A – 5. Pavement sample characteristics of Run 4.

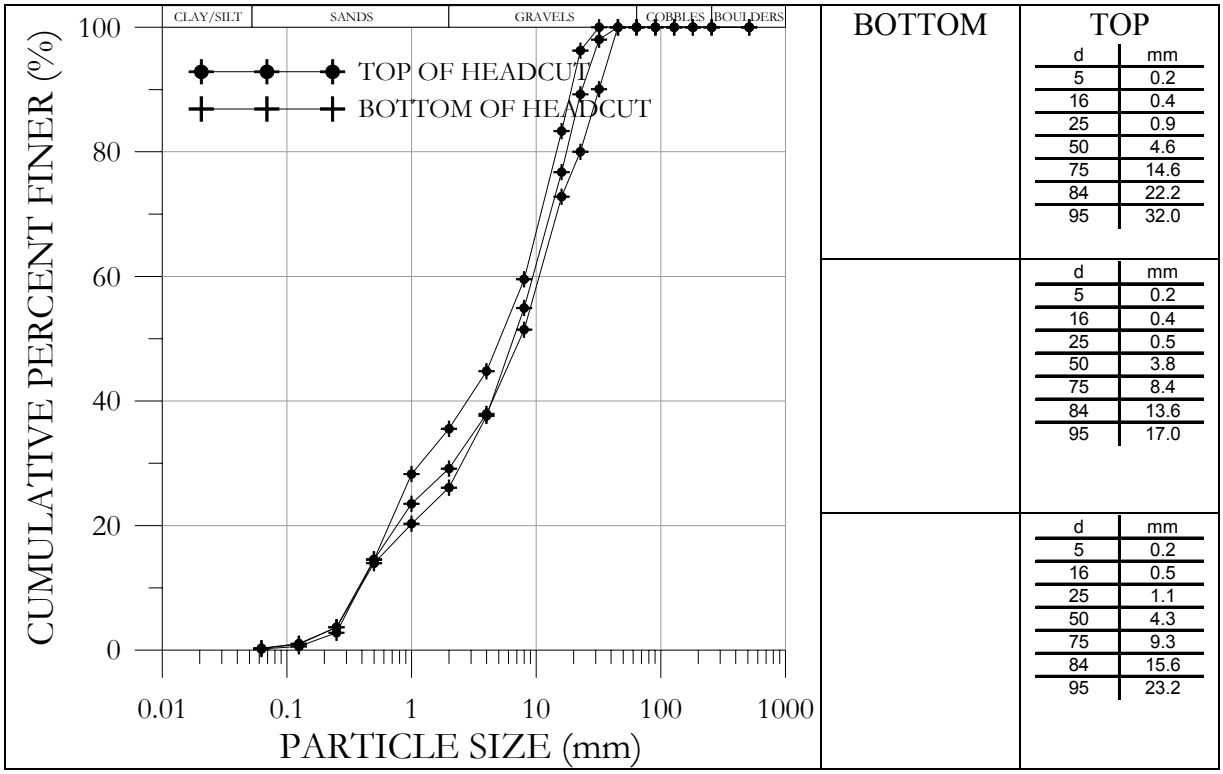

BOTTOM	TOP	
	d	mm
	5	0.2
	16	0.4
	25	0.9
	50	4.6
	75	14.6
	84	22.2
	95	32.0

	d	mm
	5	0.2
	16	0.4
	25	0.5
	50	3.8
	75	8.4
	84	13.6
	95	17.0

	d	mm
	5	0.2
	16	0.5
	25	1.1
	50	4.3
	75	9.3
	84	15.6
	95	23.2

Figure A – 6. Pavement sample characteristics of Headcut 5.

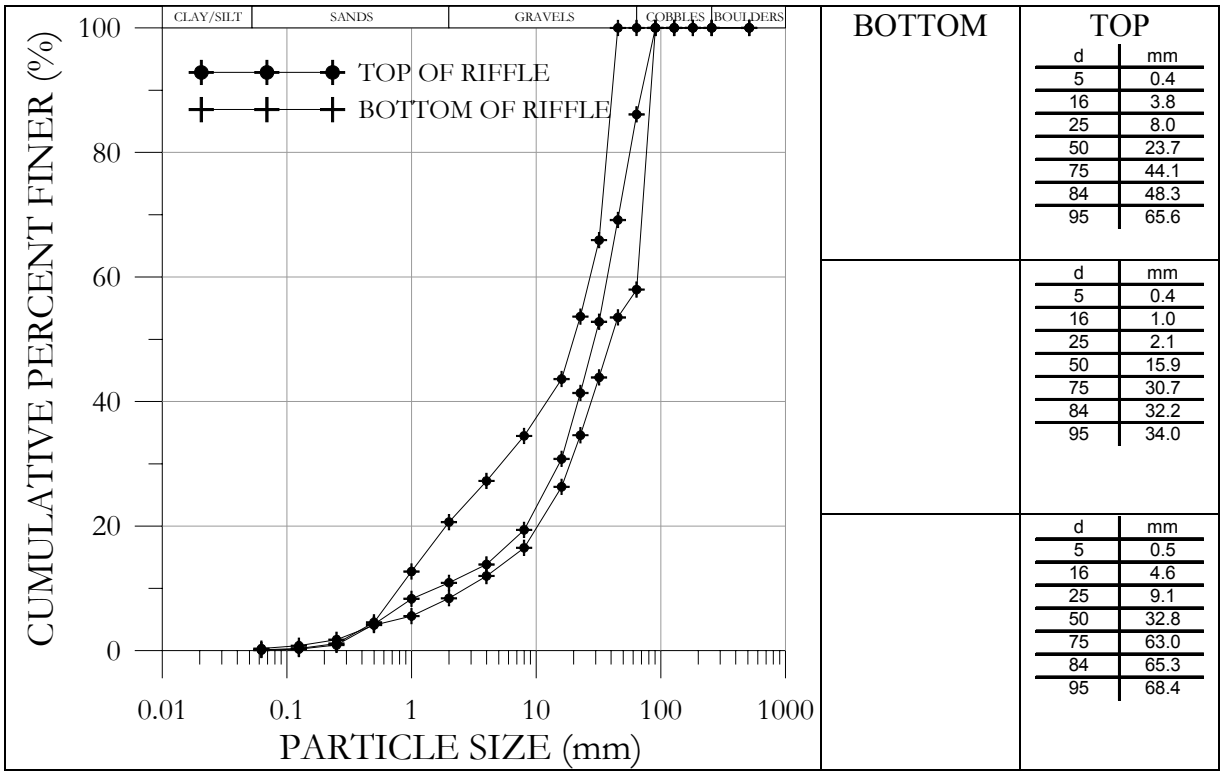

Figure A – 7. Pavement sample characteristics of Riffle 6.

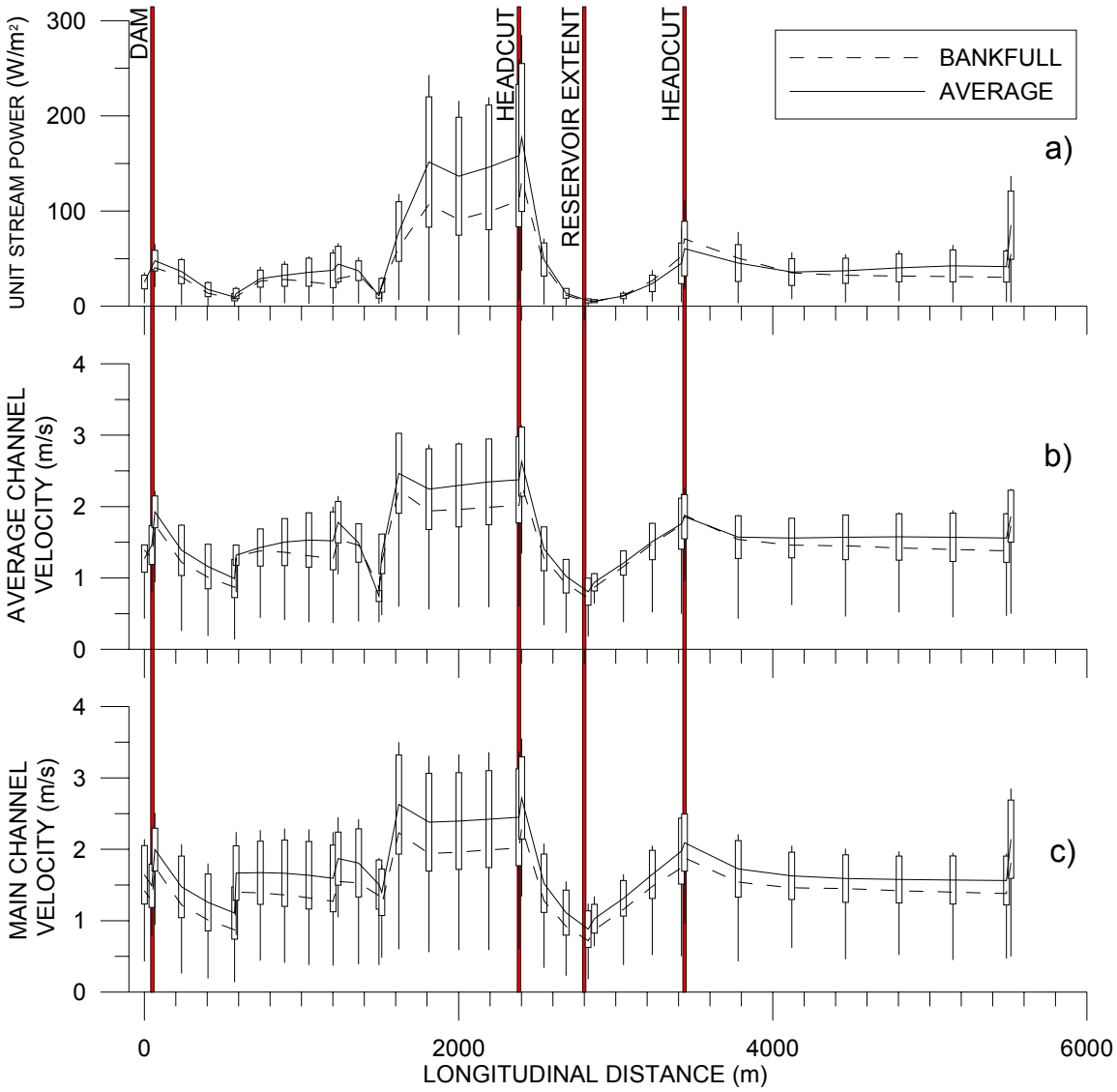

Figure A – 8. Results of a) unit stream power, b) average velocity, and c) main channel velocity for incremental discharge analyses between $0 < Q \leq Q_{100}$, along the longitudinal profile for Big Creek at Delhi.

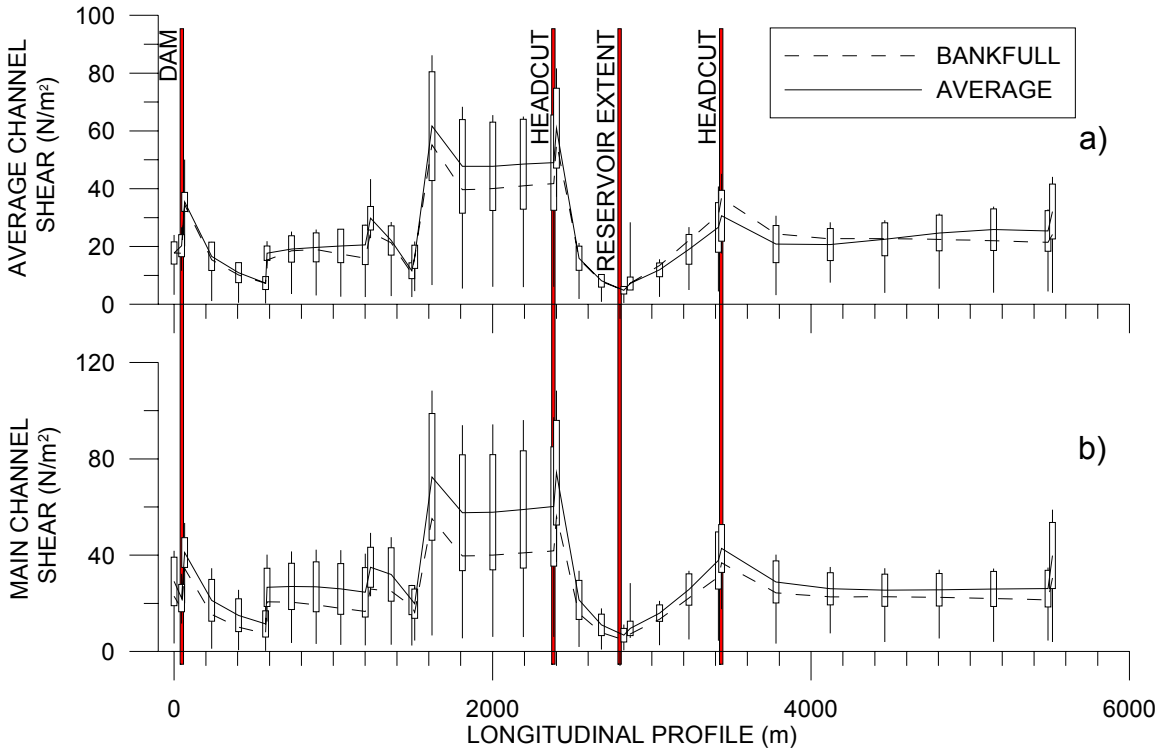

Figure A – 9. Results of a) average channel shear stress and b) main channel shear stress for incremental discharge analyses ranging between $Q < Q \leq Q_{100}$ along the longitudinal profile for Big Creek at Delhi .

Appendix B: Hawkesville Dam on Conestoga River at Hawkesville

Dam Location:
Northing: 4823911m
Easting: 529356m
(Coordinate System: NAD 1983 UTM Zone 17N)

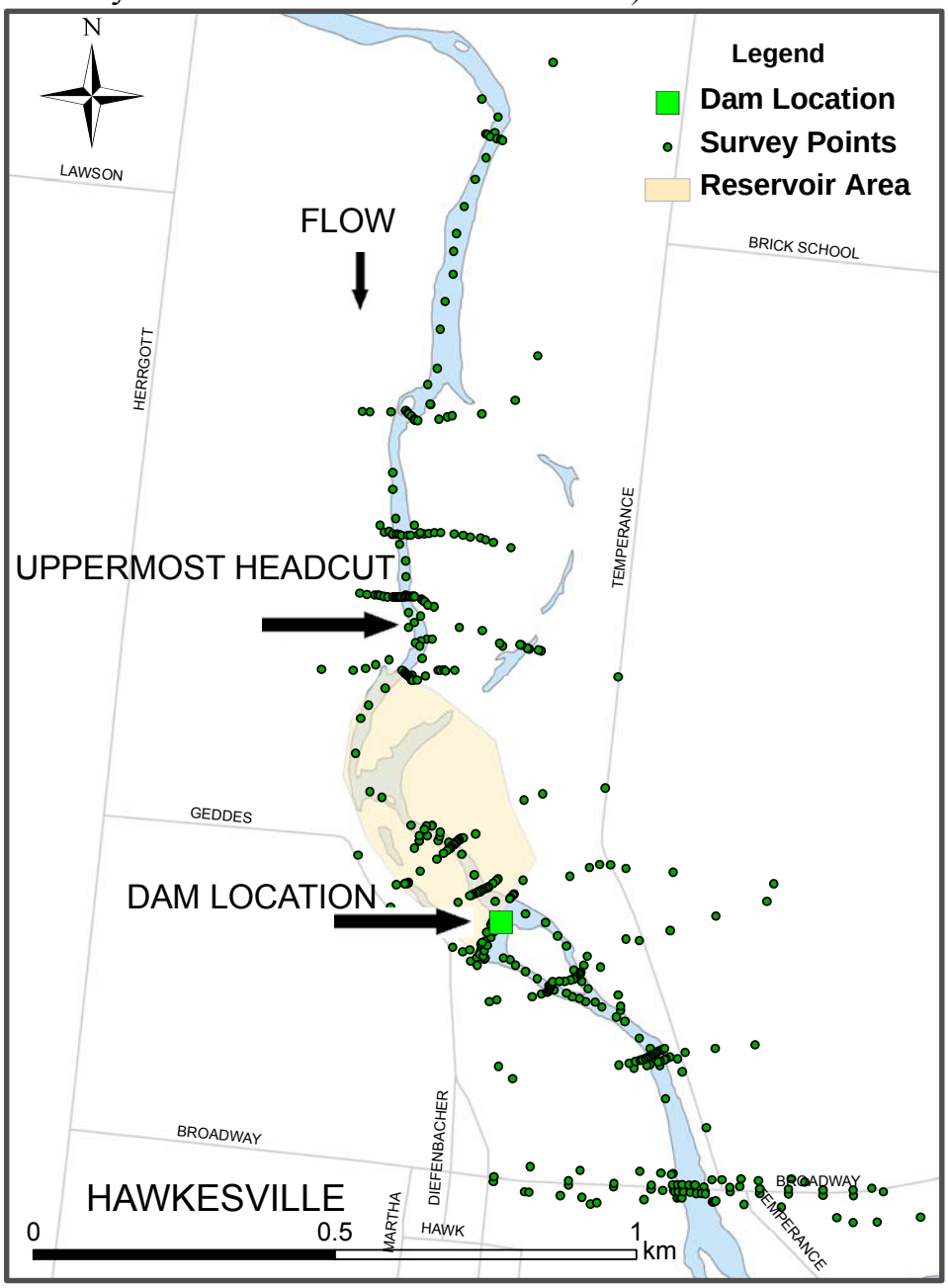

Figure B – 1. Hawkesville Dam on Conestoga River at Hawkesville site survey.

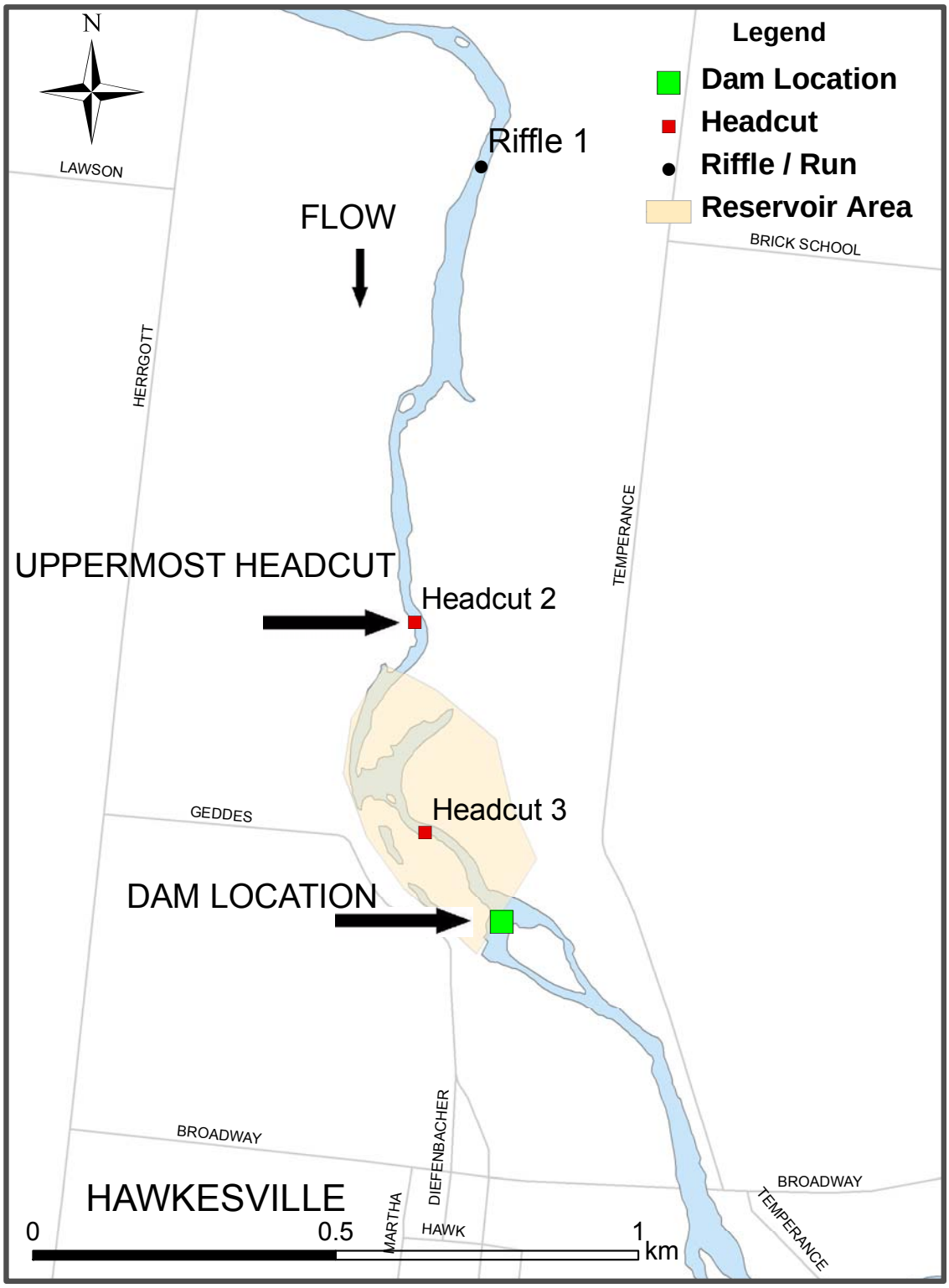

Figure B – 2. Locations of pavement samples on Conestoga River.at Hawkesville.

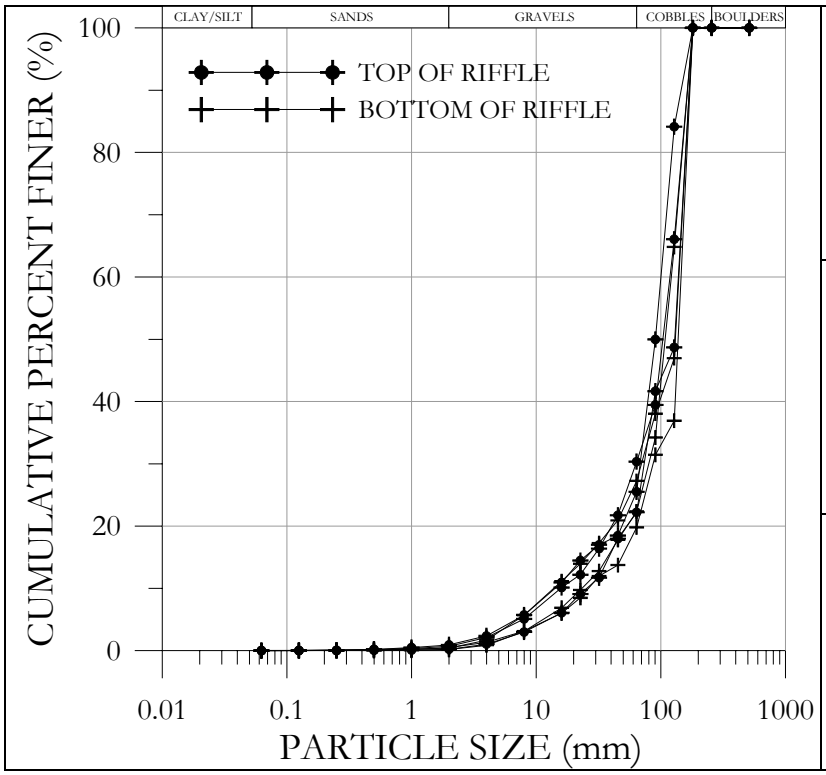

BOTTOM	
d	mm
5	8.4
16	44.3
25	63.4
50	121.7
75	130.3
84	133.6
95	137.7

TOP	
d	mm
5	8.4
16	33.0
25	60.2
50	117.9
75	128.3
84	132.2
95	137.2

d	mm
5	8.0
16	32.8
25	61.0
50	90.8
75	123.4
84	129.0
95	136.2

d	mm
5	4.7
16	24.3
25	44.3
50	88.9
75	122.9
84	128.6
95	136.1

d	mm
5	4.5
16	23.1
25	46.4
50	118.5
75	128.6
84	132.5
95	137.3

d	mm
5	4.4
16	23.0
25	48.7
50	83.0
75	94.2
84	98.6
95	132.2

Figure B – 3. Pavement sample characteristics of Riffle 1.

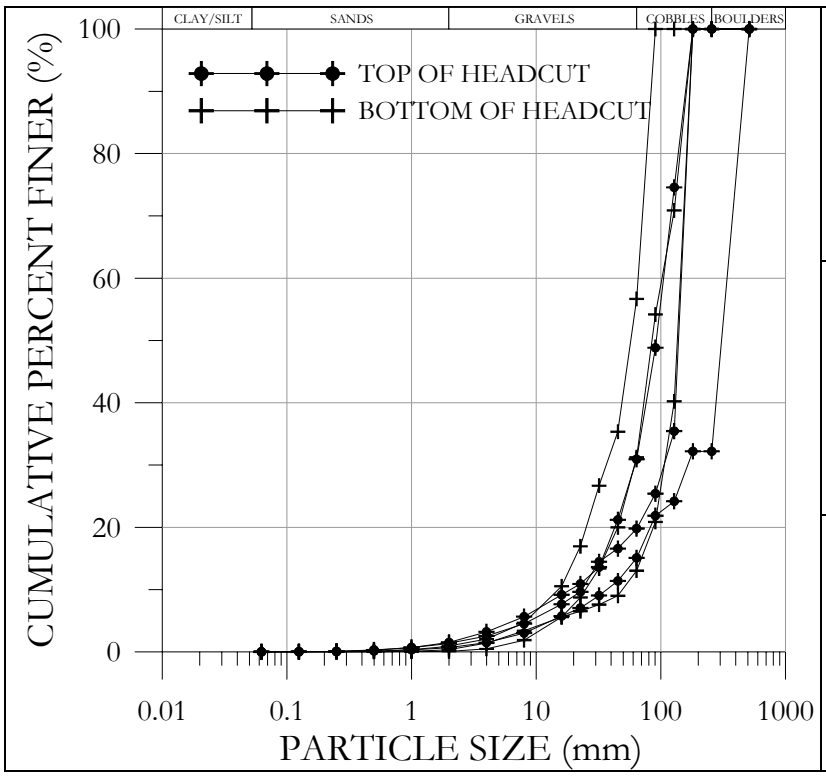

BOTTOM	
d	mm
5	8.7
16	62.7
25	86.1
50	120.7
75	129.8
84	133.3
95	137.6

TOP	
d	mm
5	8.6
16	60.1
25	119.5
50	245.7
75	261.9
84	268.0
95	275.6

d	mm
5	9.0
16	31.4
25	44.8
50	67.6
75	120.3
84	126.9
95	135.5

d	mm
5	4.3
16	31.0
25	44.4
50	83.7
75	117.7
84	125.2
95	134.9

d	mm
5	6.9
16	16.8
25	23.9
50	46.7
75	63.2
84	65.5
95	68.4

d	mm
5	7.1
16	33.3
25	68.9
50	122.1
75	130.5
84	133.7
95	137.7

Figure B – 4. Pavement sample characteristics of Headcut 2.

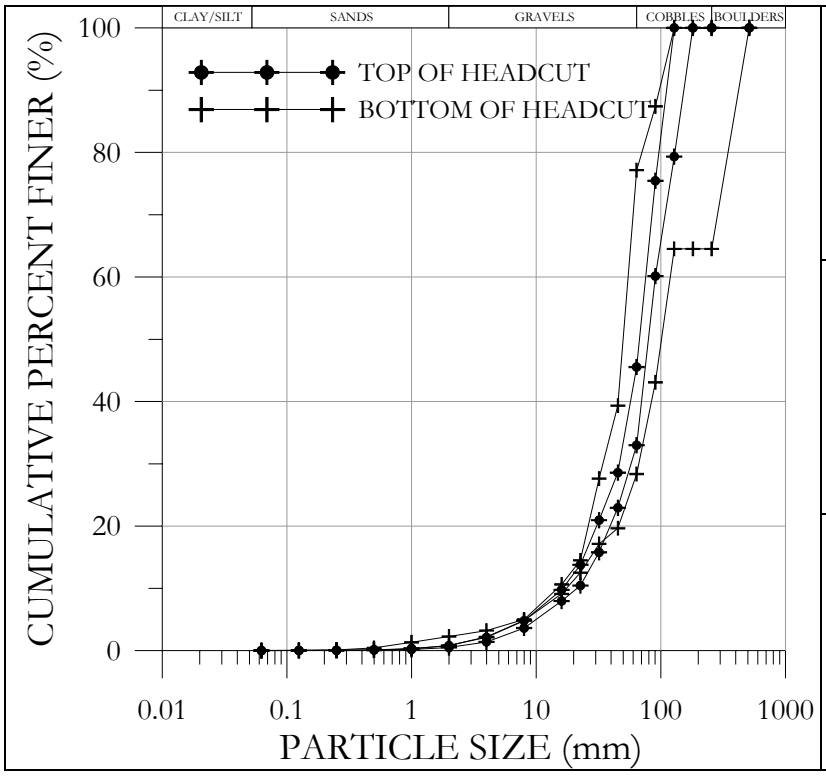

BOTTOM	
d	mm
5	4.7
16	21.2
25	23.8
50	43.6
75	48.9
84	65.9
95	92.1

TOP	
d	mm
5	6.8
16	21.9
25	32.2
50	60.2
75	69.6
84	88.2
95	95.3

d	mm
5	6.8
16	23.6
25	46.2
50	87.8
75	247.1
84	258.2
95	272.4

d	mm
5	7.5
16	29.5
25	43.0
50	65.4
75	94.9
84	122.1
95	133.9

Figure B – 5. Pavement sample characteristics of Headcut 3.

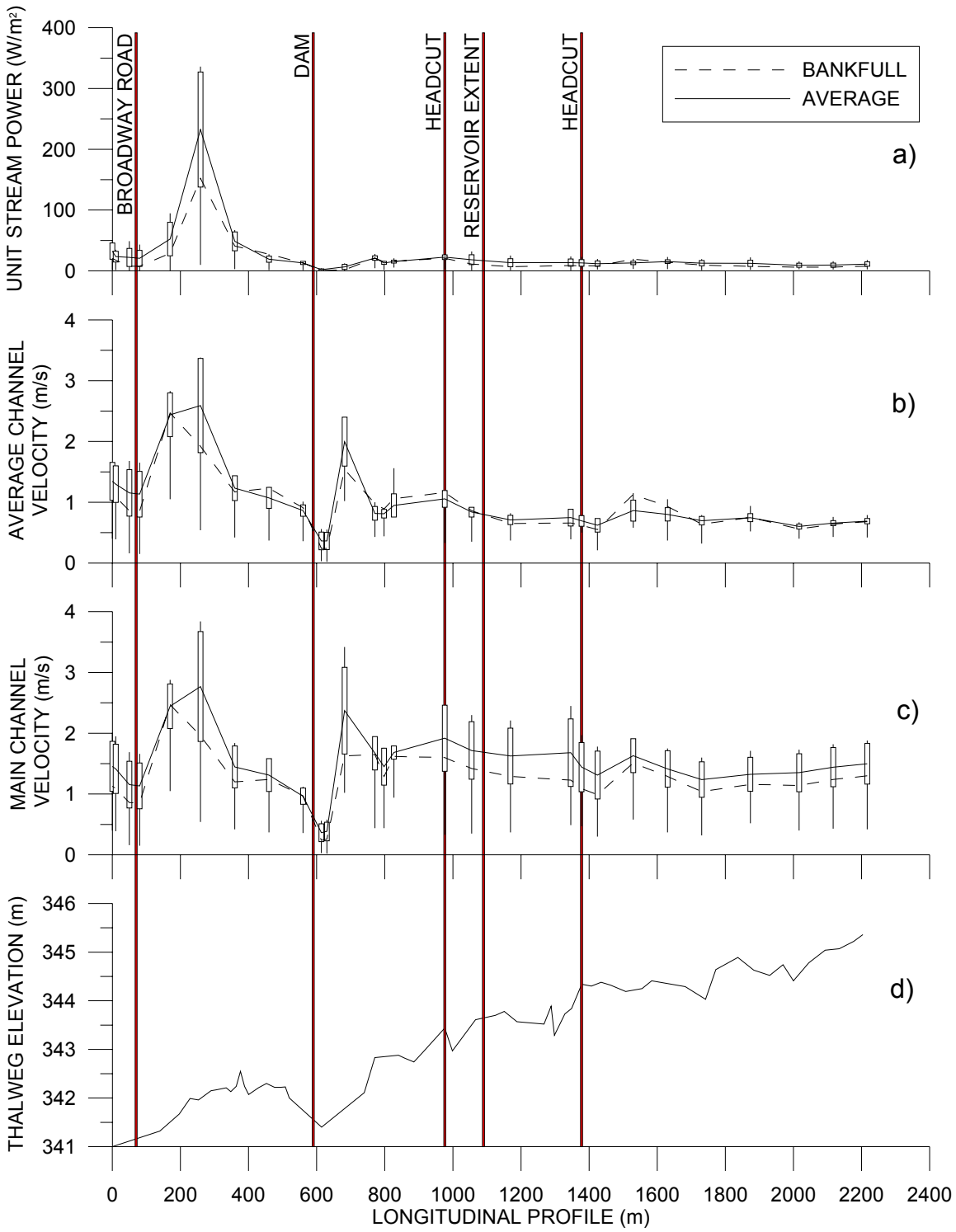

Figure B – 6. Results of a) unit stream power, b) average velocity, c) main channel velocity for incremental discharge analyses between $0 < Q \leq Q_{100}$, and d) thalweg elevation along the longitudinal profile for the Conestoga River at Hawkesville.

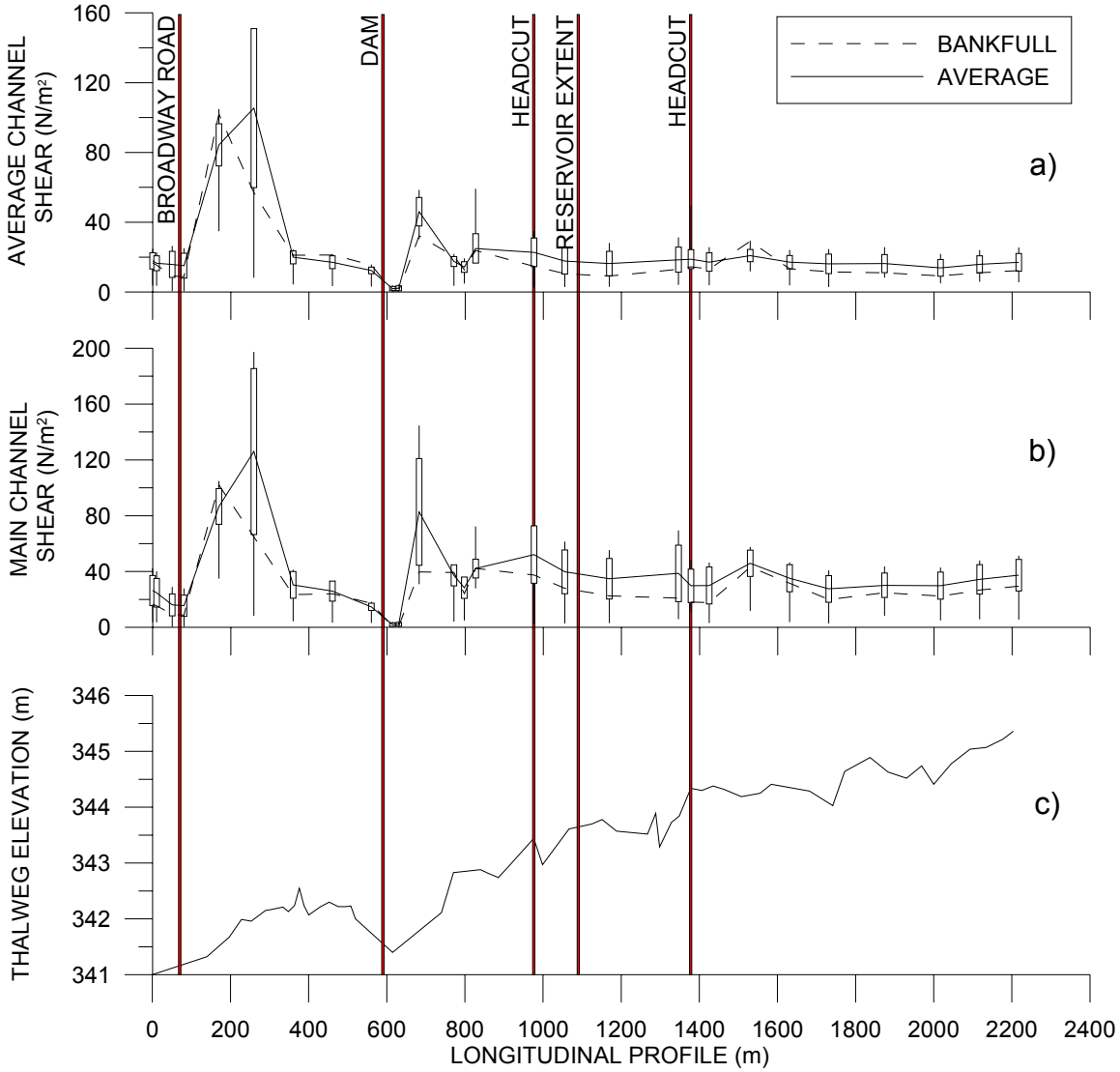

Figure B – 7. Results of a) average channel shear stress, b) main channel shear stress for incremental discharge analyses ranging between $Q < Q < Q_{100}$, and c) thalweg elevation along the longitudinal profile for the Conestoga River at Hawkesville.

Appendix C: Huttonville Dam on Credit River at Huttonville

Dam Location:
Northing: 4809470m
Easting: 553860m
(Coordinate System: NAD 1983 UTM Zone 17N)

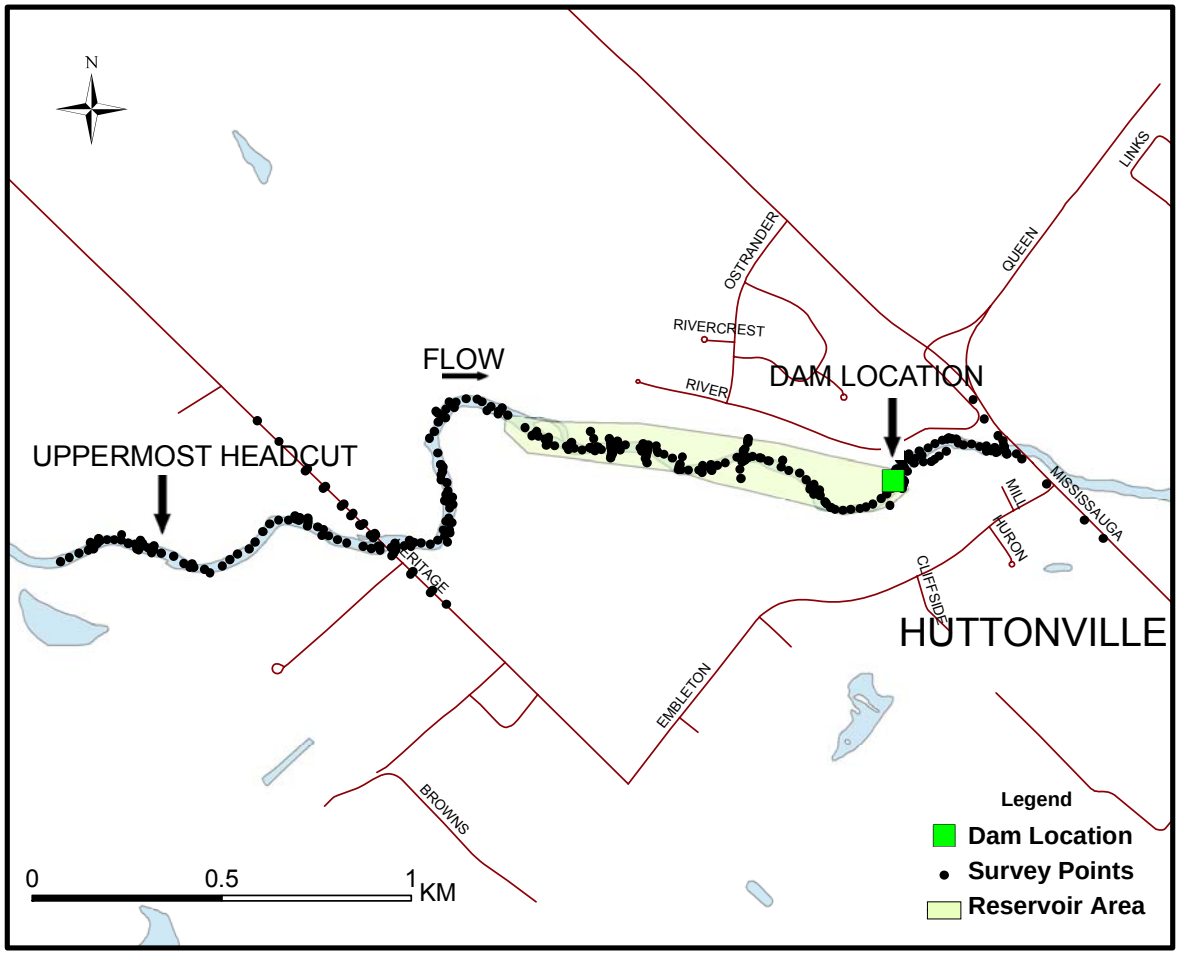

Figure C – 1. Huttonville Dam on Credit River at Huttonville site survey.

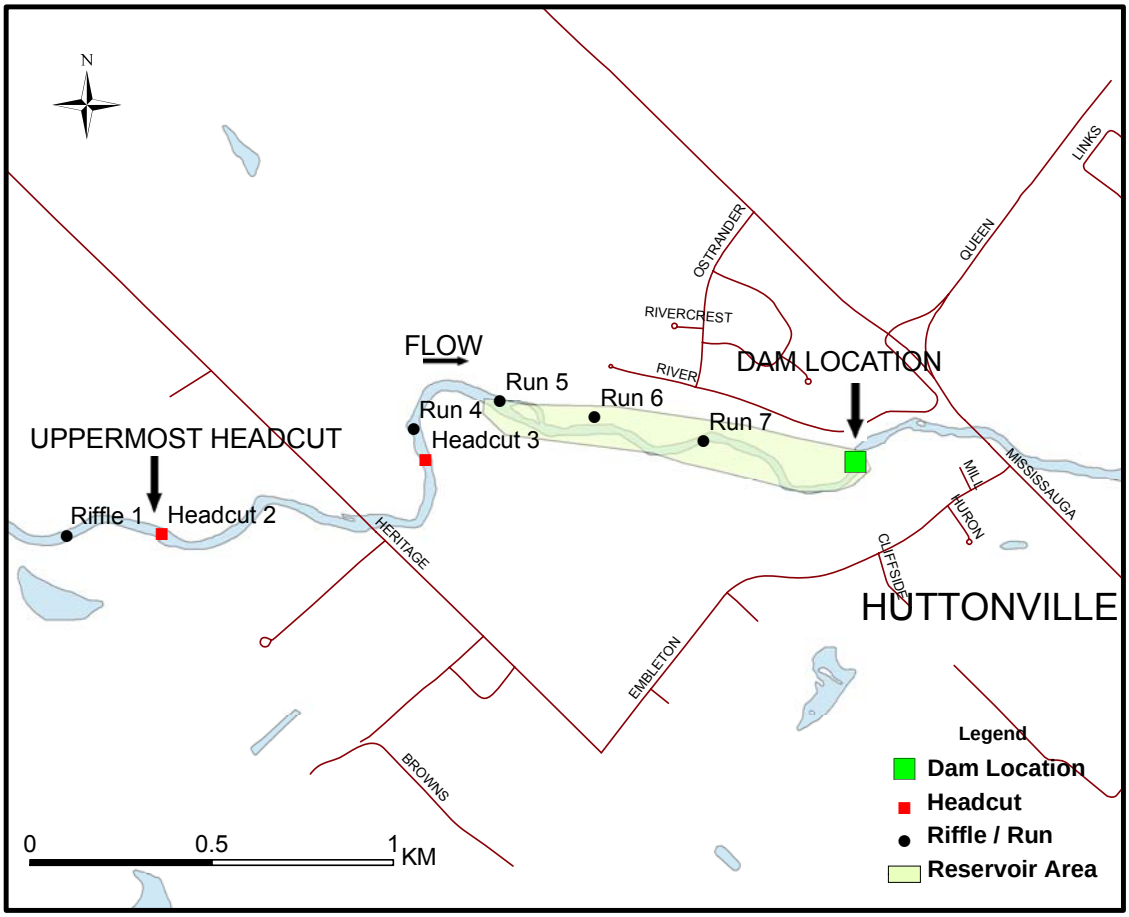

Figure C – 2. Locations of pavement samples on Credit River at Huttonville.

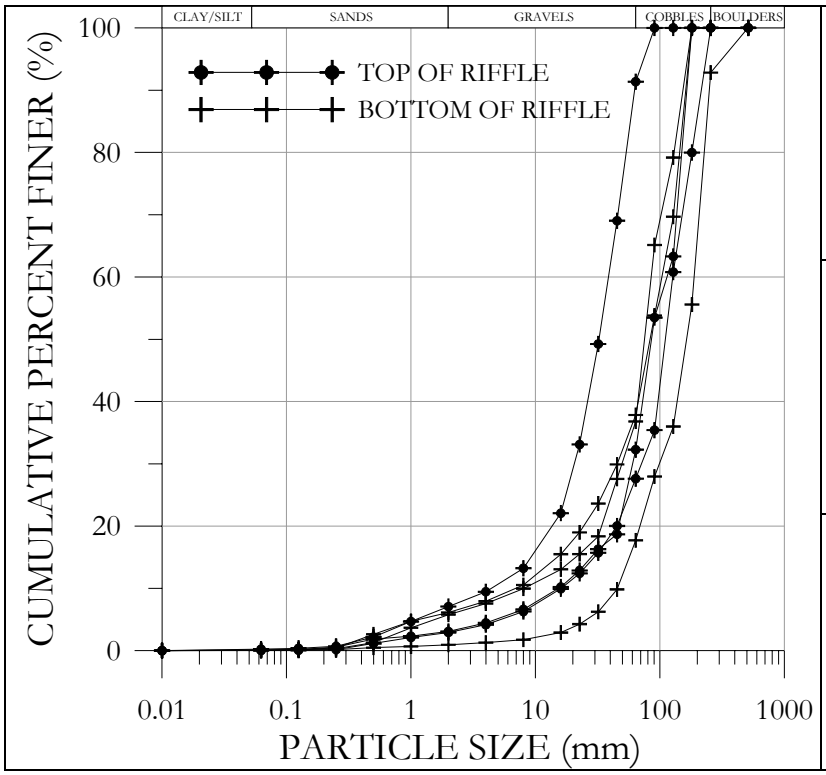

BOTTOM	
d	mm
5	1.0
16	21.4
25	33.2
50	63.6
75	93.7
84	122.2
95	133.9

TOP	
d	mm
5	4.7
16	22.8
25	33.8
50	67.6
75	171.3
84	180.3
95	191.9

d	mm
5	0.9
16	14.0
25	30.5
50	67.0
75	121.0
84	127.4
95	135.7

d	mm
5	3.9
16	29.7
25	46.5
50	91.7
75	133.4
84	171.9
95	189.0

d	mm
5	22.1
16	47.5
25	66.4
50	132.9
75	181.7
84	189.5
95	247.4

d	mm
5	3.7
16	24.3
25	45.0
50	67.8
75	124.0
84	129.4
95	136.3

Figure C – 3. Pavement sample characteristics of Riffle 1.

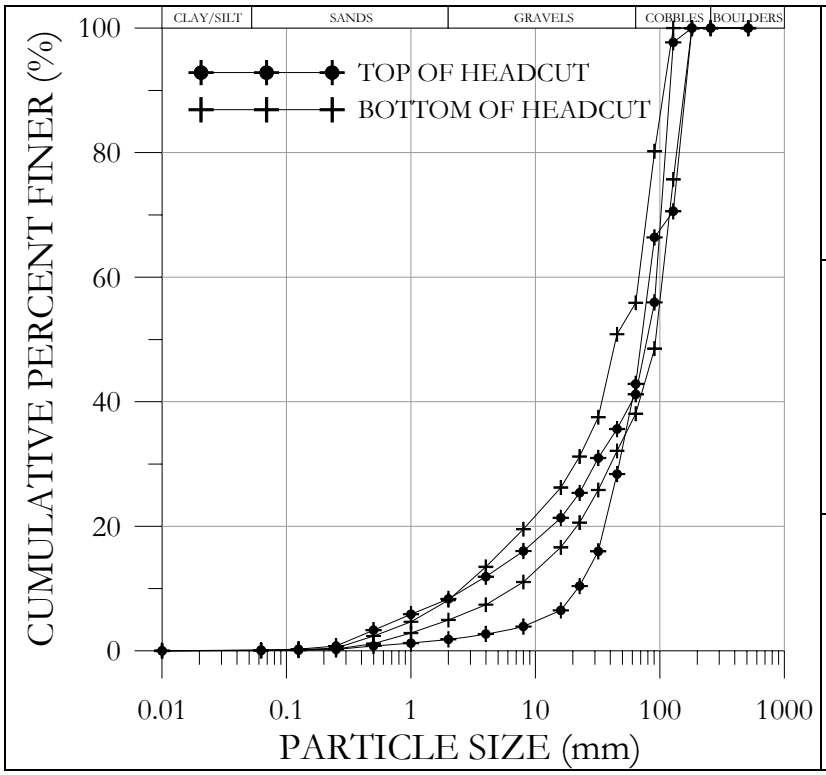

BOTTOM	
d	mm
5	0.9
16	3.9
25	8.9
50	34.5
75	67.2
84	85.8
95	94.5

TOP	
d	mm
5	7.8
16	29.4
25	33.3
50	61.9
75	120.5
84	127.0
95	135.5

d	mm
5	1.7
16	9.2
25	24.0
50	83.8
75	98.3
84	124.5
95	134.7

d	mm
5	0.5
16	4.7
25	17.0
50	65.1
75	89.8
84	93.2
95	97.6

Figure C – 4. Pavement sample characteristics of Headcut 2.

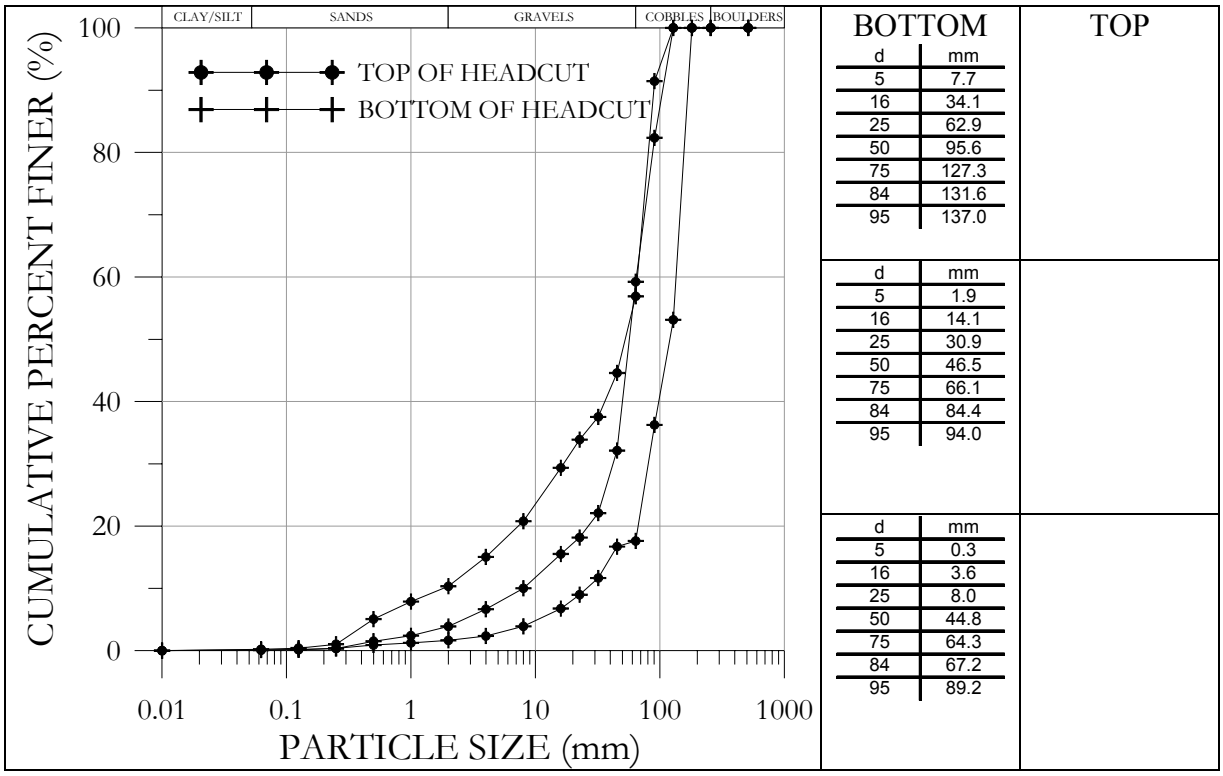

BOTTOM	
d	mm
5	7.7
16	34.1
25	62.9
50	95.6
75	127.3
84	131.6
95	137.0

d	mm
5	1.9
16	14.1
25	30.9
50	46.5
75	66.1
84	84.4
95	94.0

d	mm
5	0.3
16	3.6
25	8.0
50	44.8
75	64.3
84	67.2
95	89.2

Figure C – 5. Pavement sample characteristics of Headcut 3.

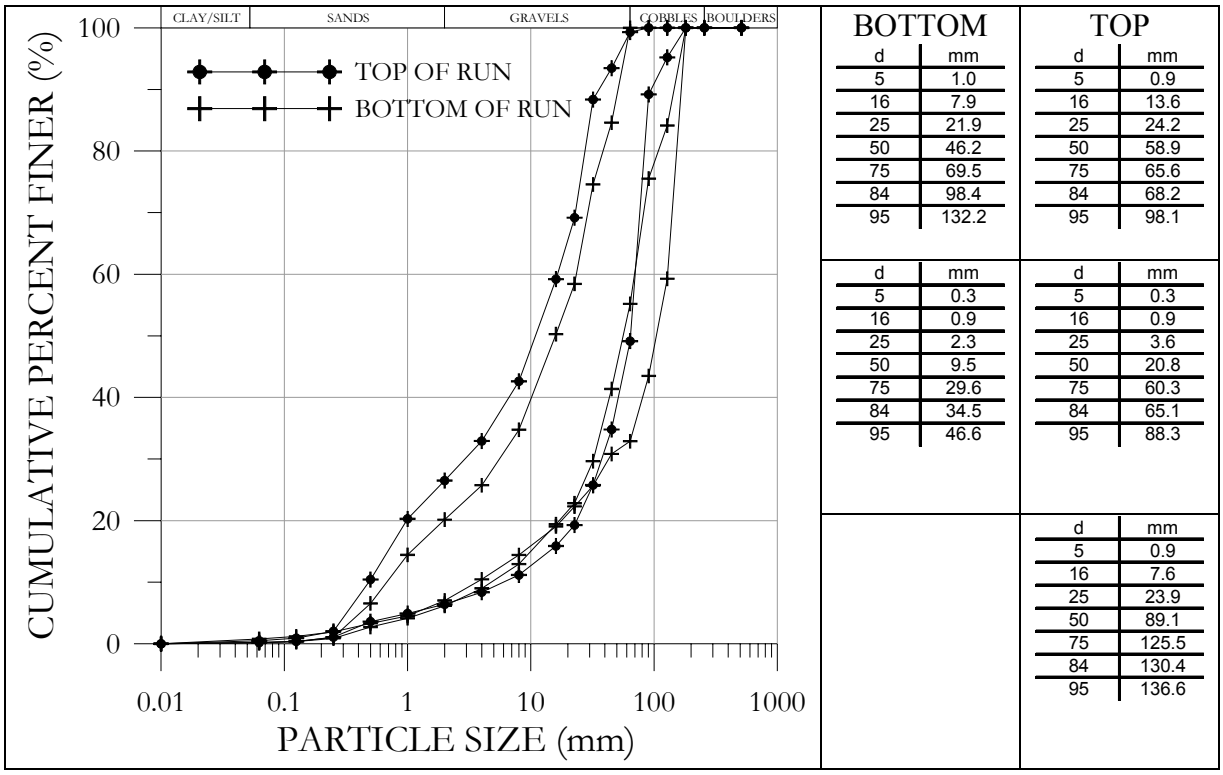

BOTTOM	
d	mm
5	1.0
16	7.9
25	21.9
50	46.2
75	69.5
84	98.4
95	132.2

TOP	
d	mm
5	0.9
16	13.6
25	24.2
50	58.9
75	65.6
84	68.2
95	98.1

d	mm
5	0.3
16	0.9
25	2.3
50	9.5
75	29.6
84	34.5
95	46.6

d	mm
5	0.3
16	0.9
25	3.6
50	20.8
75	60.3
84	65.1
95	88.3

d	mm
5	0.9
16	7.6
25	23.9
50	89.1
75	125.5
84	130.4
95	136.6

Figure C – 6. Pavement sample characteristics of Run 4.

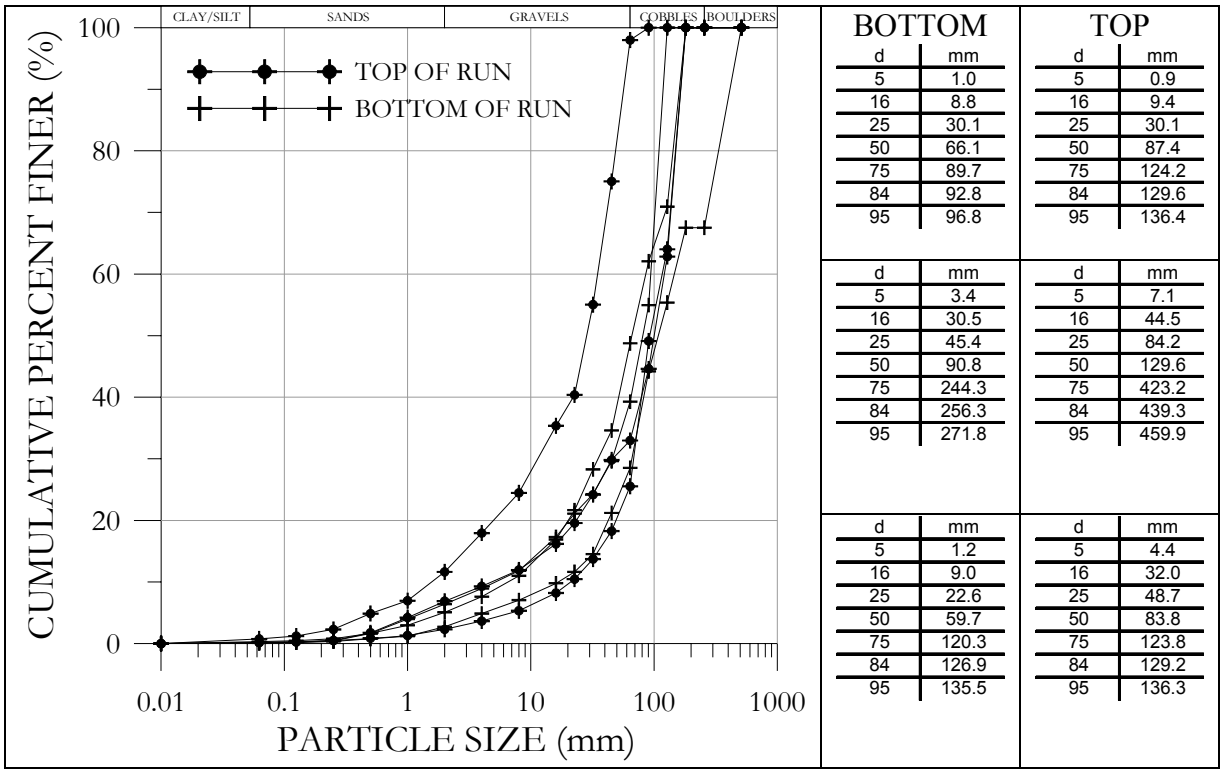

BOTTOM	
d	mm
5	1.0
16	8.8
25	30.1
50	66.1
75	89.7
84	92.8
95	96.8

TOP	
d	mm
5	0.9
16	9.4
25	30.1
50	87.4
75	124.2
84	129.6
95	136.4

d	mm
5	3.4
16	30.5
25	45.4
50	90.8
75	244.3
84	256.3
95	271.8

d	mm
5	7.1
16	44.5
25	84.2
50	129.6
75	423.2
84	439.3
95	459.9

d	mm
5	1.2
16	9.0
25	22.6
50	59.7
75	120.3
84	126.9
95	135.5

d	mm
5	4.4
16	32.0
25	48.7
50	83.8
75	123.8
84	129.2
95	136.3

Figure C – 7. Pavement sample characteristics of Run 5.

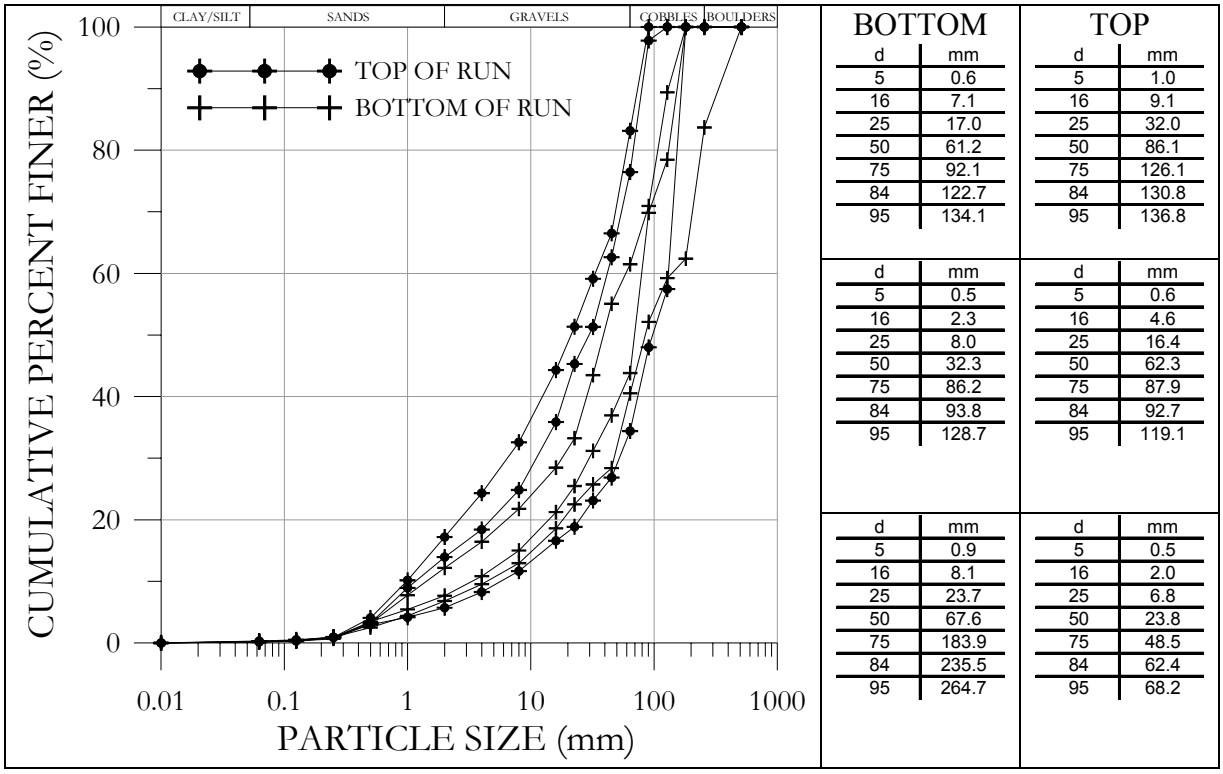

BOTTOM	
d	mm
5	0.6
16	7.1
25	17.0
50	61.2
75	92.1
84	122.7
95	134.1

TOP	
d	mm
5	1.0
16	9.1
25	32.0
50	86.1
75	126.1
84	130.8
95	136.8

d	mm
5	0.5
16	2.3
25	8.0
50	32.3
75	86.2
84	93.8
95	128.7

d	mm
5	0.6
16	4.6
25	16.4
50	62.3
75	87.9
84	92.7
95	119.1

d	mm
5	0.9
16	8.1
25	23.7
50	67.6
75	183.9
84	235.5
95	264.7

d	mm
5	0.5
16	2.0
25	6.8
50	23.8
75	48.5
84	62.4
95	68.2

Figure C – 8. Pavement sample characteristics of Run 6.

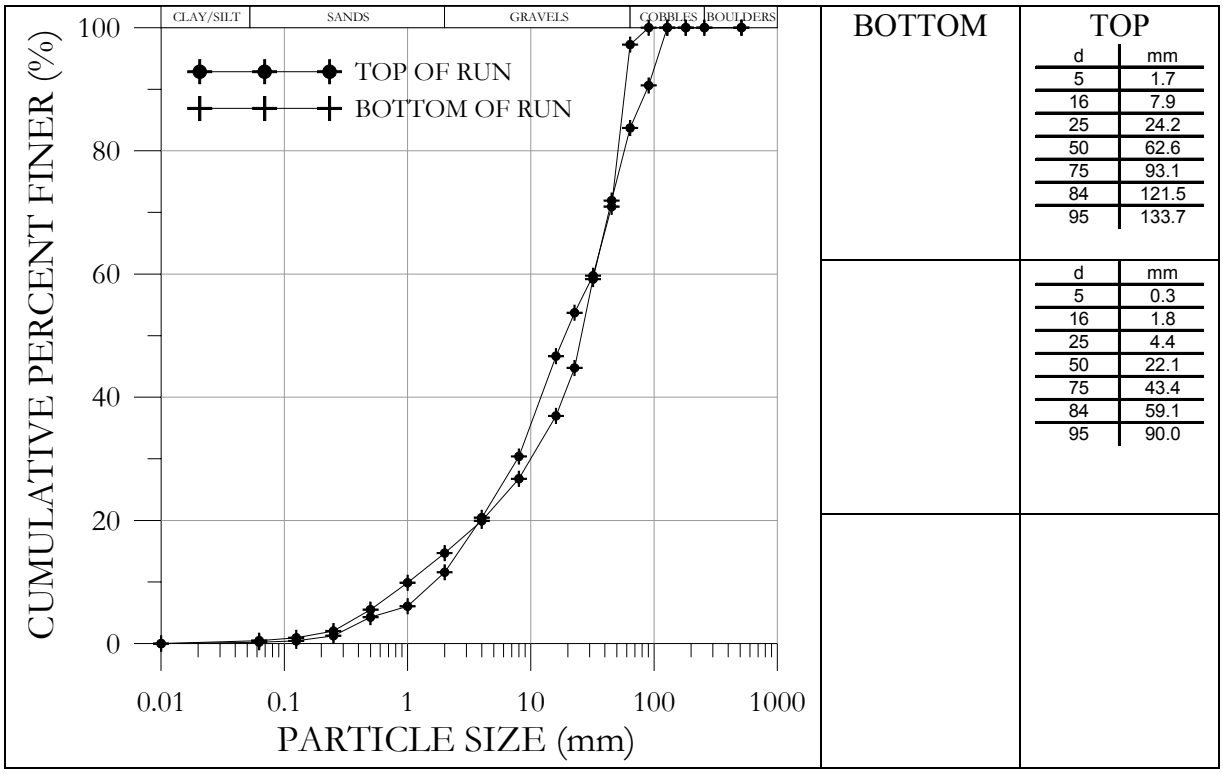

Figure C – 9. Pavement sample characteristics of Run 7.

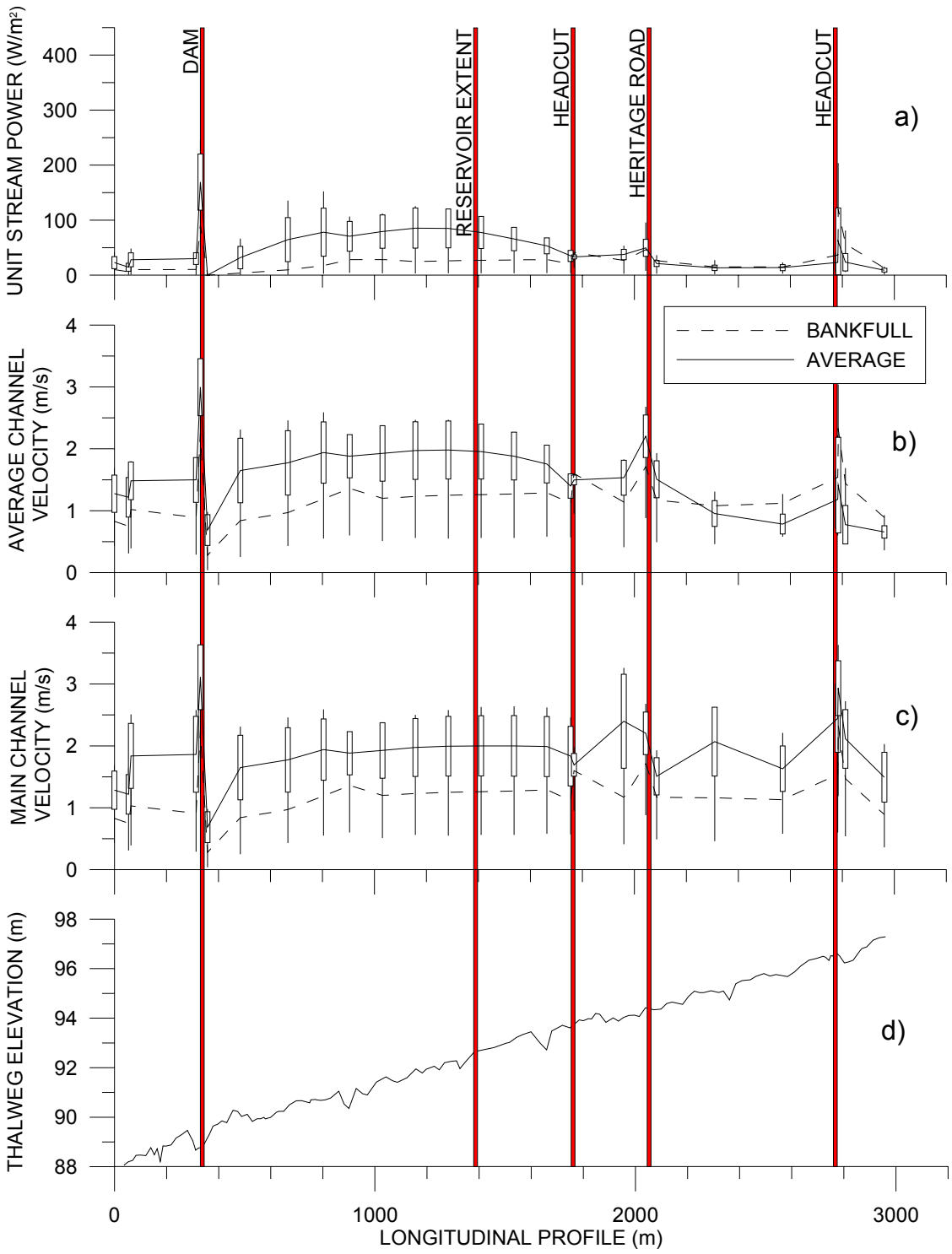

Figure C – 10. Results of a) unit stream power, b) average velocity, c) main channel velocity for incremental discharge analyses between $0 < Q \leq Q_{100}$, and d) thalweg elevation along the longitudinal profile for Credit River at Huttonville.

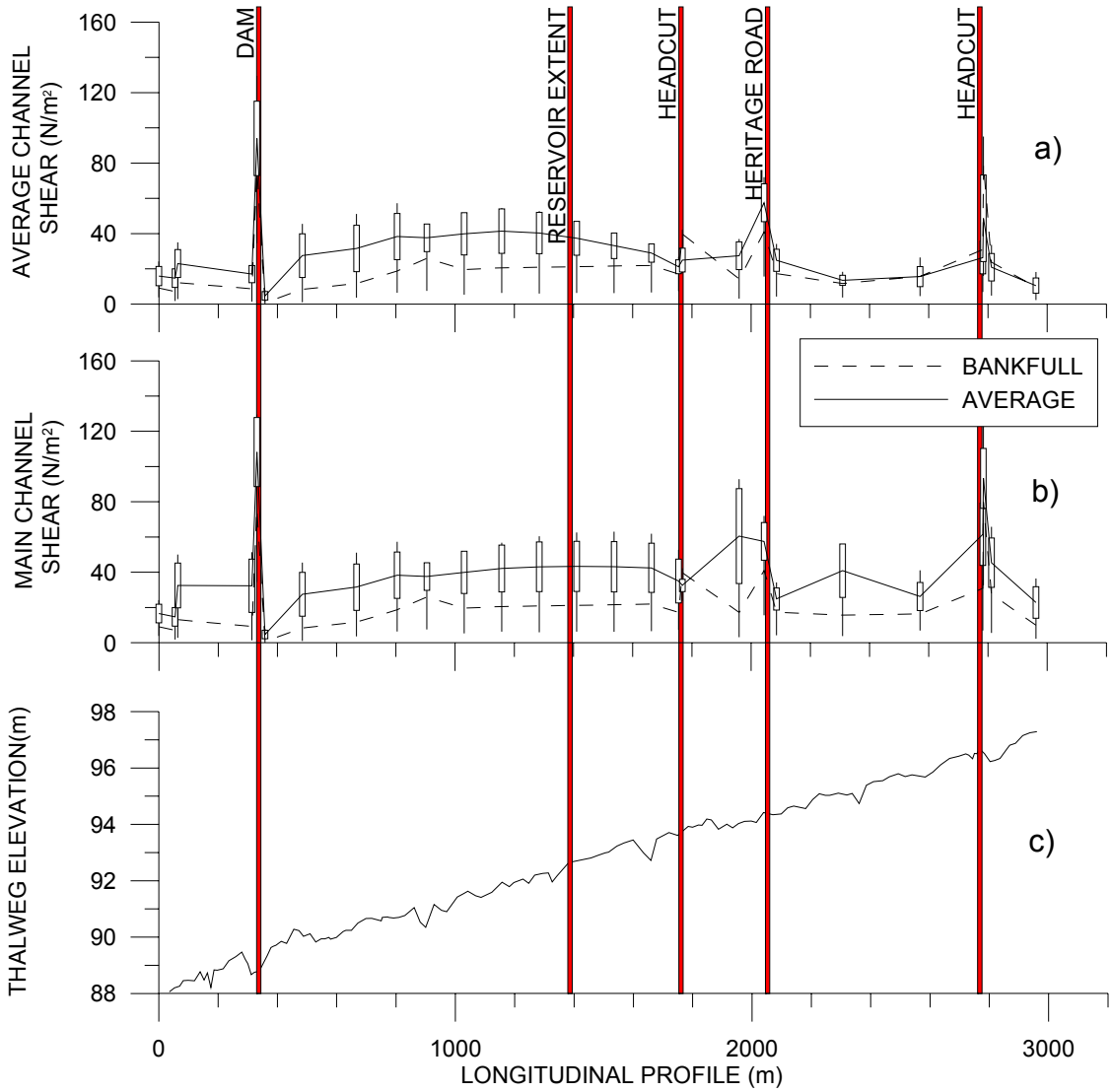

Figure C – 11. HEC Results of a) average channel shear stress, b) main channel shear stress for incremental discharge analyses ranging between $Q < Q < Q_{100}$, and c) thalweg elevation along the longitudinal profile for Credit River at Huttonville.

Appendix D: Chilligo Dam on Ellis Creek at Cambridge

Dam Location:
Northing: 4809470m
Easting: 553860m
(Coordinate System: NAD 1983 UTM Zone 17N)

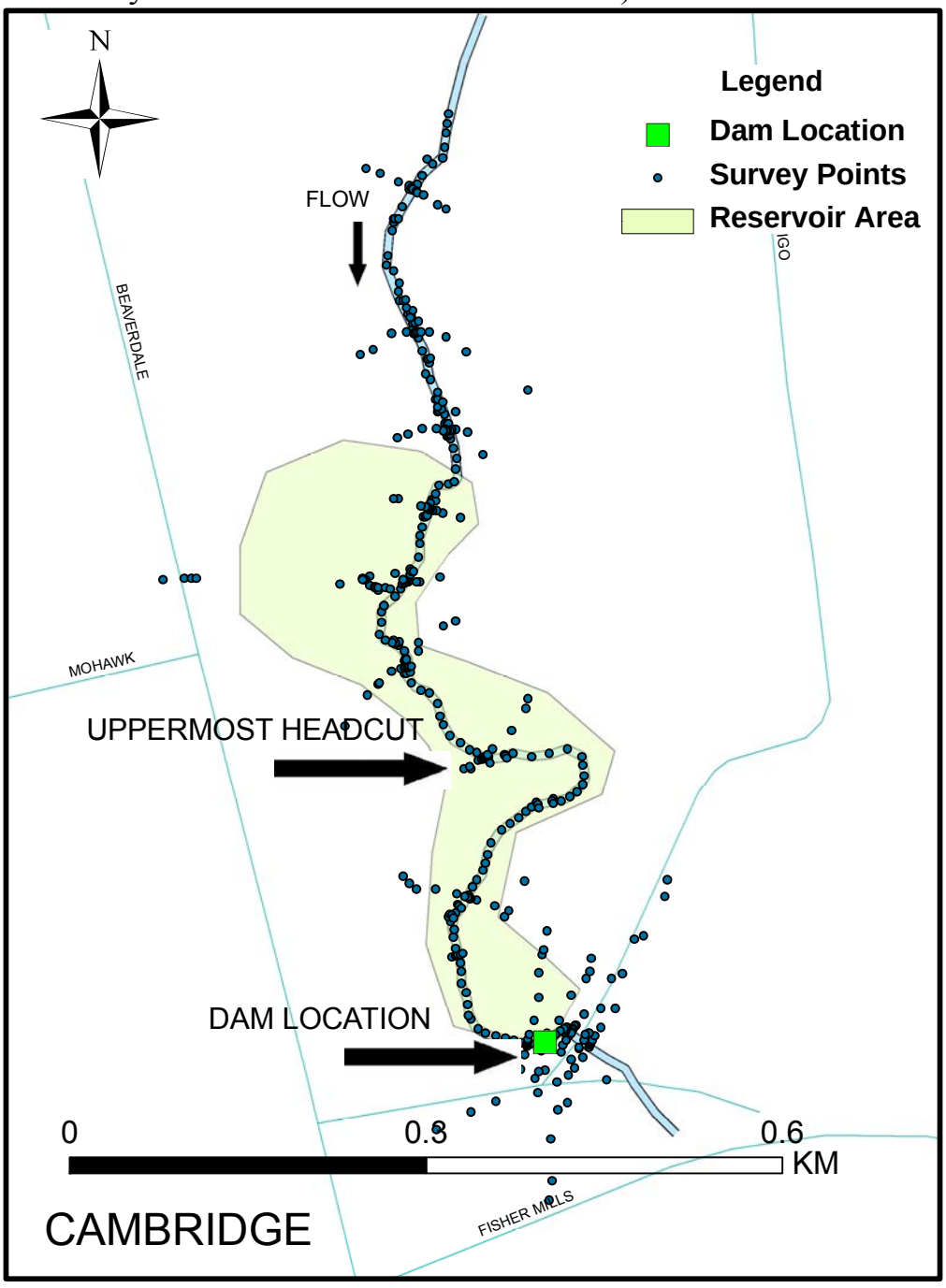

Figure D – 1. Chilligo Dam on Ellis Creek at Cambridge site survey.

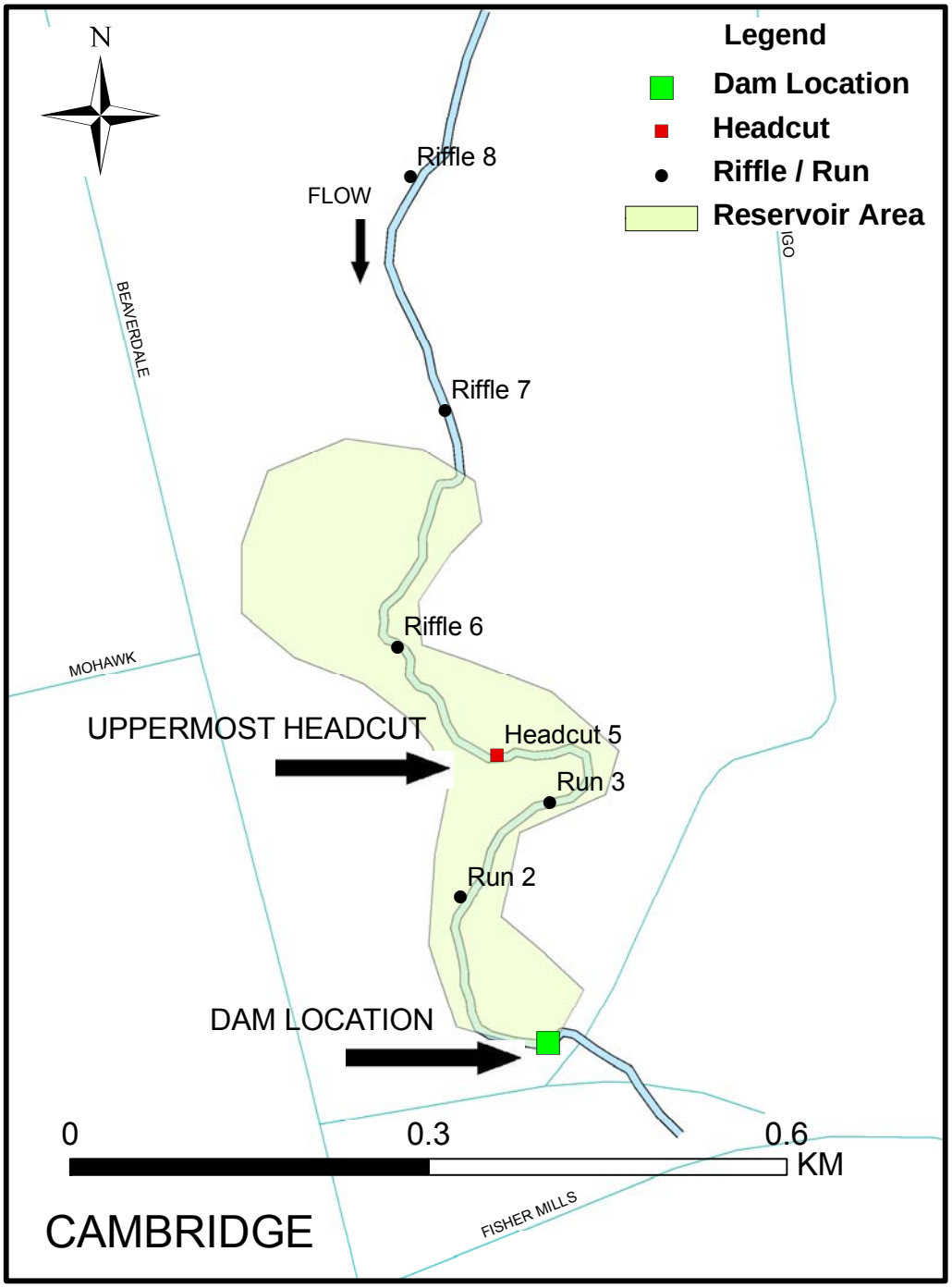

Figure D – 2. Locations of pavement samples at Chilligo Dam on Ellis Creek.

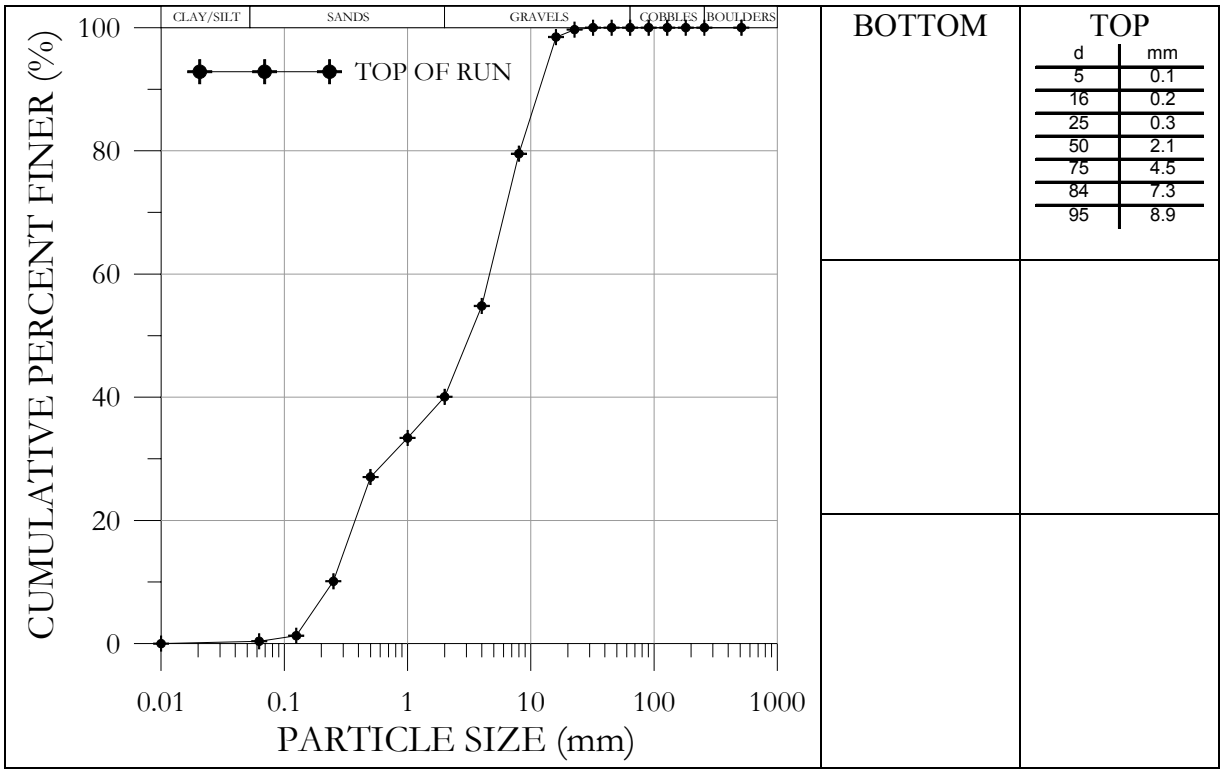

BOTTOM

TOP

d	mm
5	0.1
16	0.2
25	0.3
50	2.1
75	4.5
84	7.3
95	8.9

Figure D – 3. Pavement sample characteristics of Run 2.

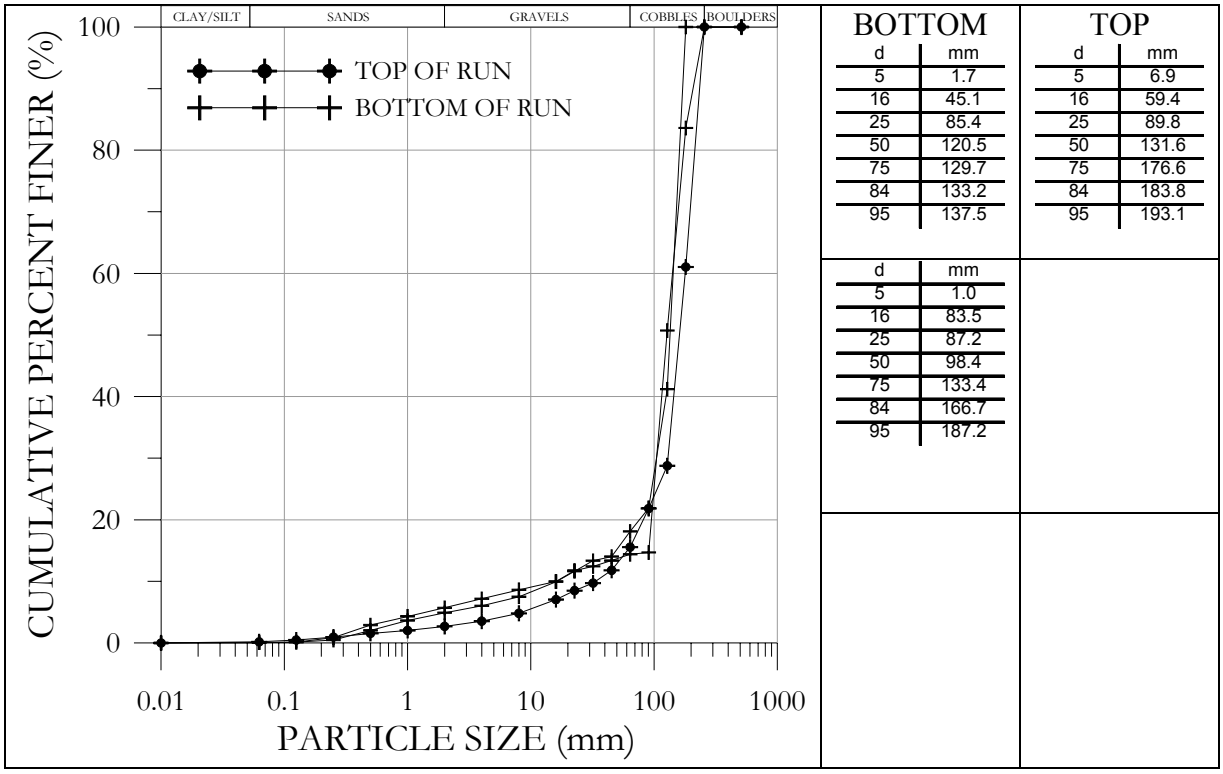

BOTTOM

d	mm
5	1.7
16	45.1
25	85.4
50	120.5
75	129.7
84	133.2
95	137.5

TOP

d	mm
5	6.9
16	59.4
25	89.8
50	131.6
75	176.6
84	183.8
95	193.1

d	mm
5	1.0
16	83.5
25	87.2
50	98.4
75	133.4
84	166.7
95	187.2

Figure D – 4. Pavement sample characteristics of Run 3.

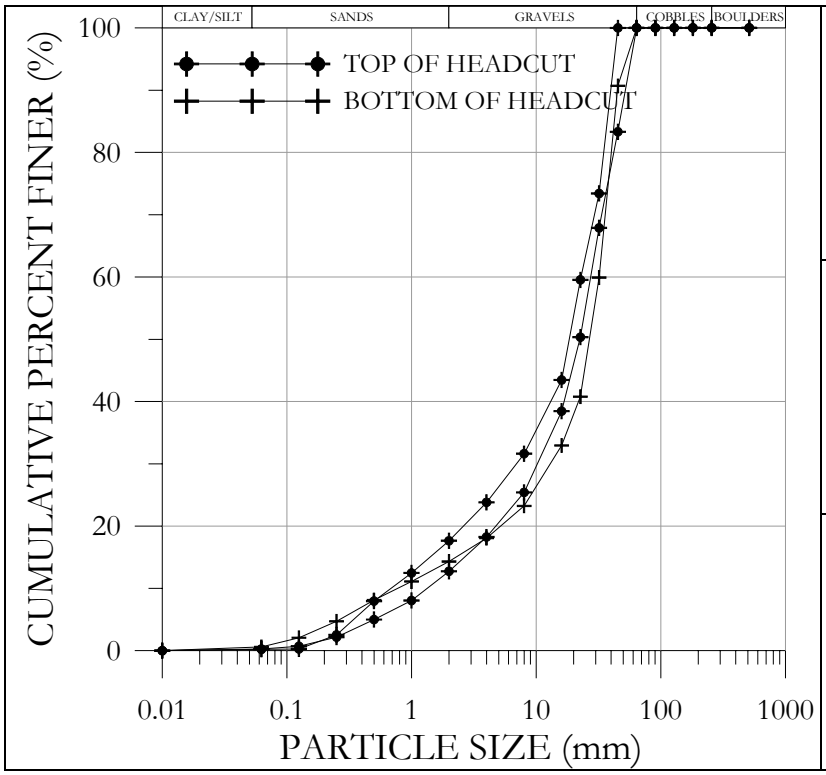

BOTTOM	
d	mm
5	0.2
16	2.0
25	7.2
50	22.6
75	31.9
84	33.6
95	45.0

TOP	
d	mm
5	0.2
16	1.1
25	3.5
50	15.0
75	29.6
84	31.4
95	33.8

d	mm
5	0.4
16	2.1
25	4.7
50	17.3
75	31.8
84	41.8
95	46.9

Figure D – 5. Pavement sample characteristics of Headcut 5.

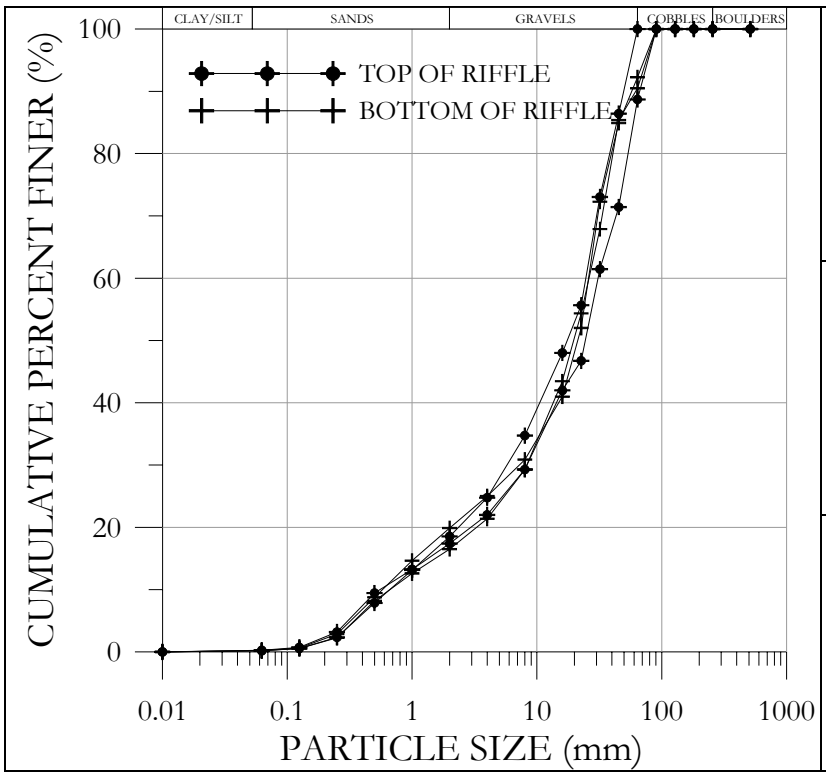

BOTTOM	
d	mm
5	0.2
16	1.1
25	3.9
50	15.7
75	31.5
84	34.4
95	63.7

TOP	
d	mm
5	0.2
16	1.1
25	3.9
50	21.6
75	43.0
84	47.1
95	64.6

d	mm
5	0.2
16	0.9
25	2.4
50	16.6
75	30.5
84	34.5
95	62.4

d	mm
5	0.2
16	1.0
25	3.4
50	14.4
75	30.1
84	33.8
95	46.3

Figure D – 6. Pavement sample characteristics of Riffle 6.

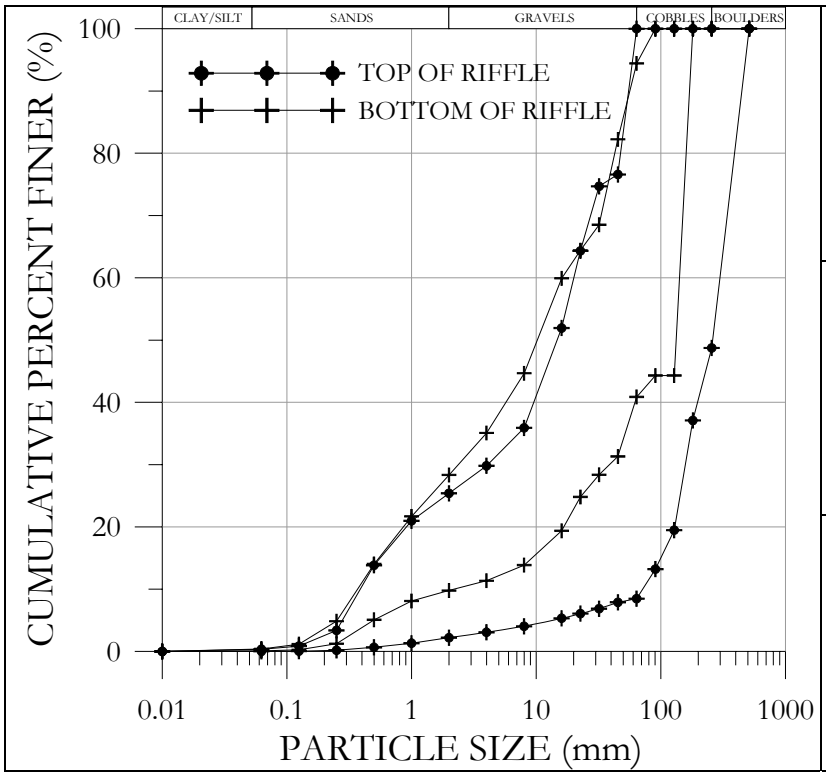

BOTTOM	
d	mm
5	0.3
16	7.7
25	21.0
50	119.5
75	129.1
84	132.8
95	137.4

TOP	
d	mm
5	0.2
16	0.5
25	1.2
50	9.1
75	30.2
84	43.8
95	47.6

d	mm
5	0.2
16	0.5
25	1.0
50	7.6
75	31.9
84	42.6
95	59.7

d	mm
5	0.5
16	9.3
25	63.5
50	133.0
75	179.4
84	185.7
95	193.7

Figure D – 7. Pavement sample characteristics of Riffle 7.

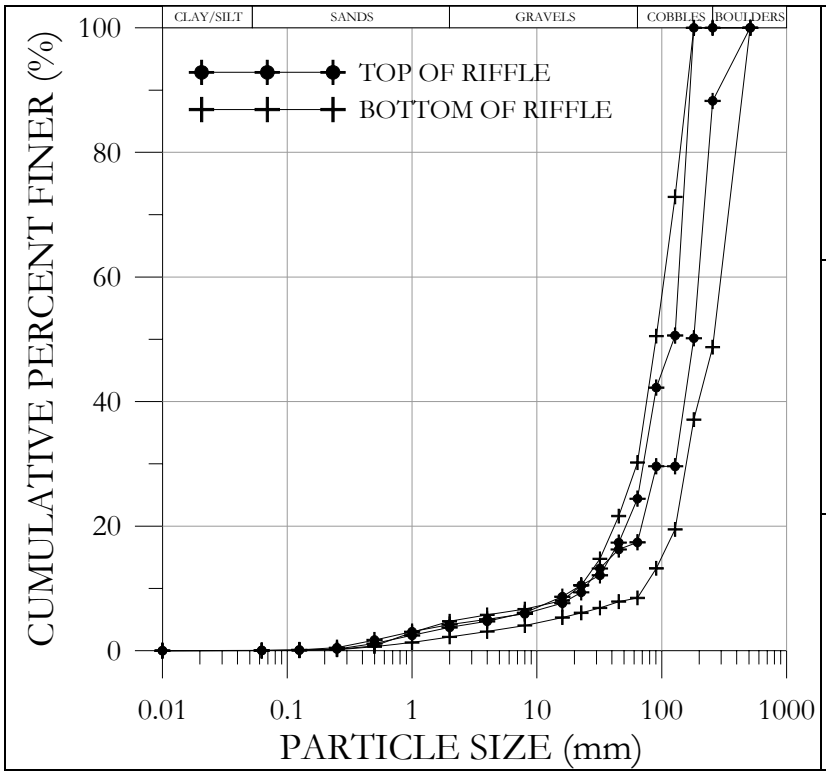

BOTTOM	
d	mm
5	8.7
16	89.6
25	123.9
50	235.8
75	256.5
84	264.5
95	274.5

TOP	
d	mm
5	3.6
16	33.4
25	59.0
50	97.5
75	127.9
84	132.0
95	137.2

d	mm
5	1.8
16	30.3
25	44.4
50	69.5
75	119.0
84	126.0
95	135.2

d	mm
5	2.3
16	34.4
25	65.4
50	139.4
75	185.8
84	193.6
95	259.3

Figure D – 8. Pavement sample characteristics of Riffle 8.

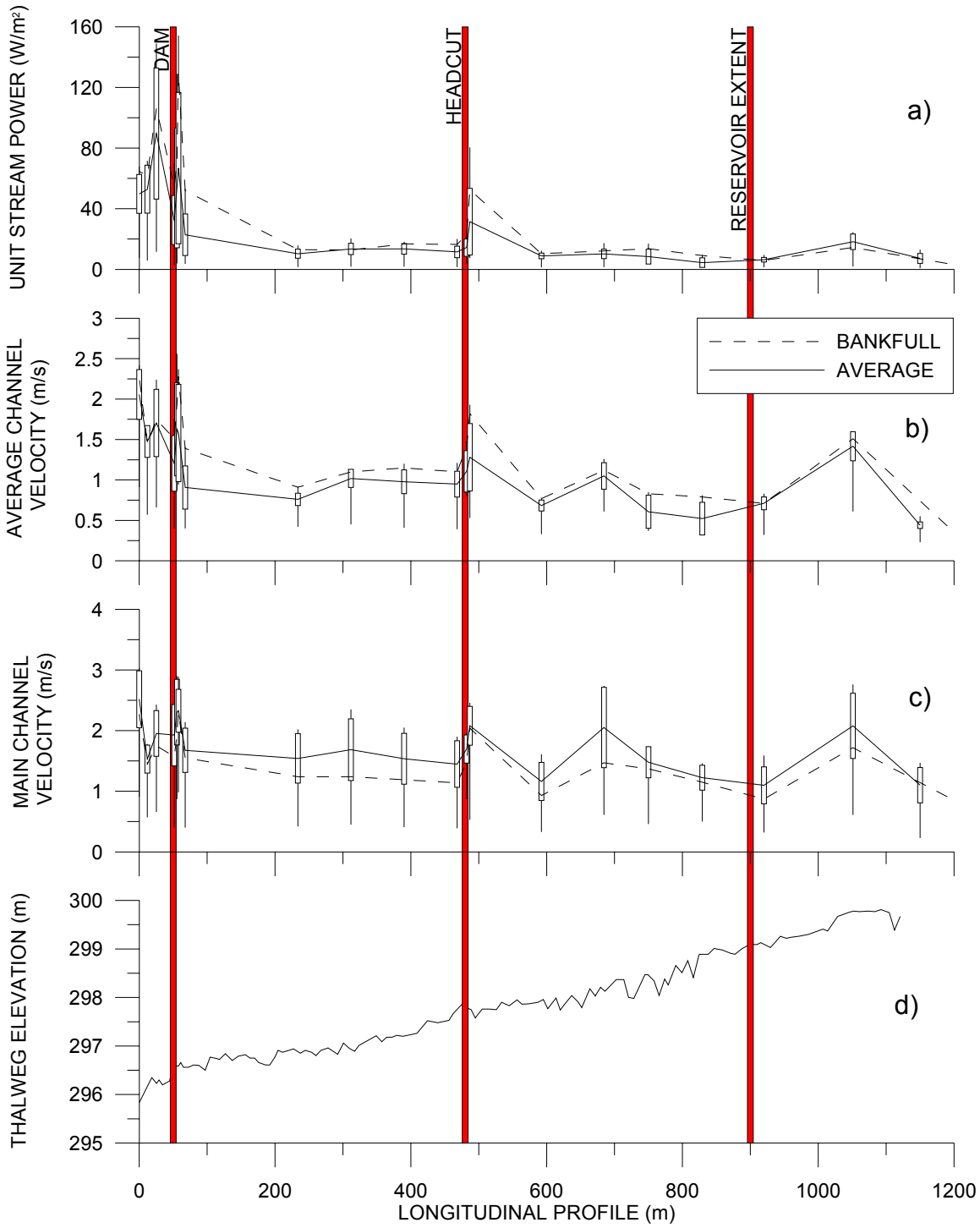

Figure D – 9 Results of a) unit stream power, b) average velocity, c) main channel velocity for incremental discharge analyses between $0 < Q \leq Q_{100}$, and d) thalweg elevation along the longitudinal profile for Ellis Creek at Cambridge.

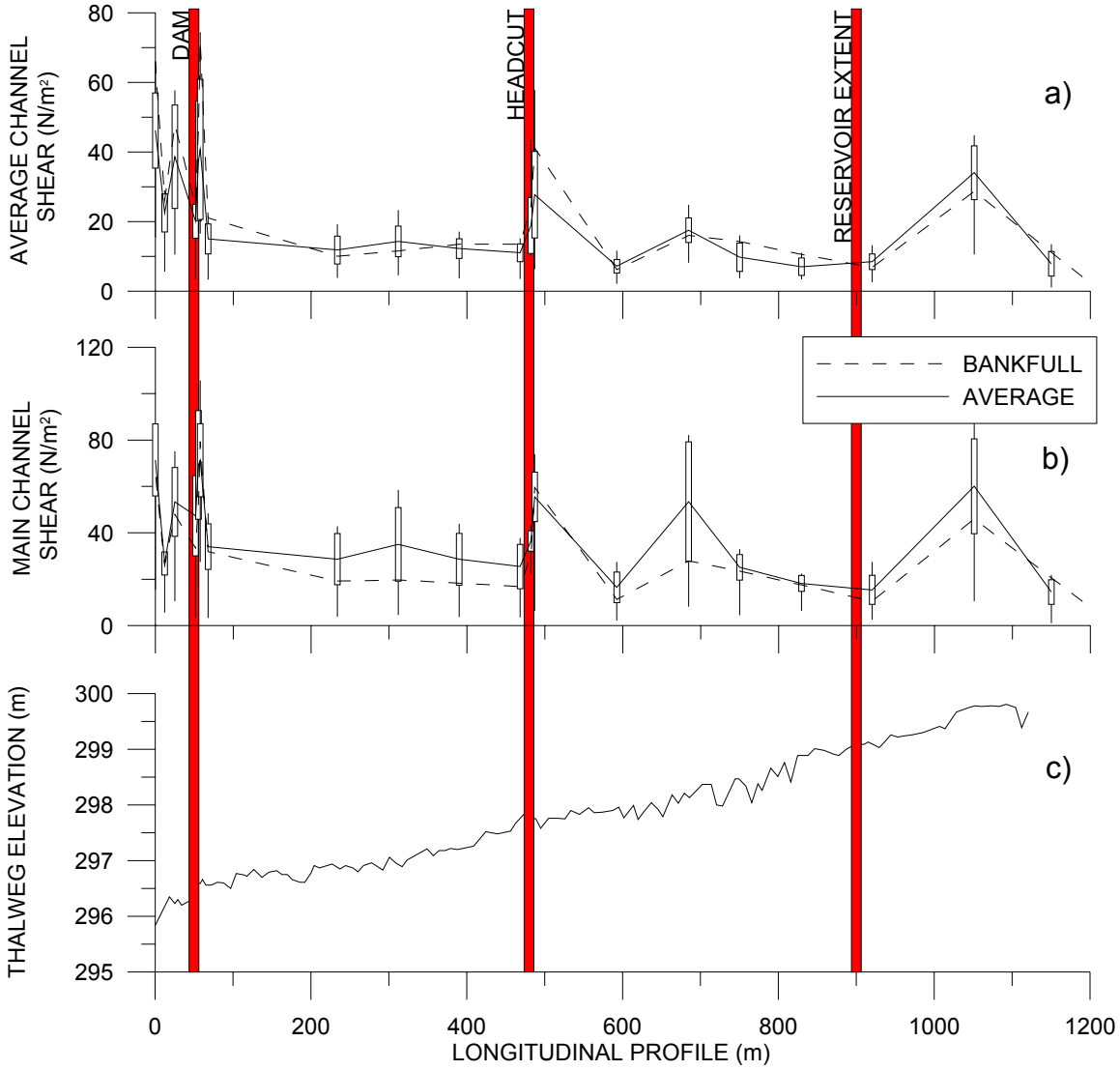

Figure D – 10. Results of a) average channel shear stress, b) main channel shear stress for incremental discharge analyses ranging between $Q < Q < Q_{100}$, and c) thalweg elevation along the longitudinal profile for Ellis Creek at Cambridge.

Appendix E: Greenfield Dam on Nith River at Greenfield

Dam Location:
Northing: 4794080m
Easting: 542633m
(Coordinate System: NAD 1983 UTM Zone 17N)

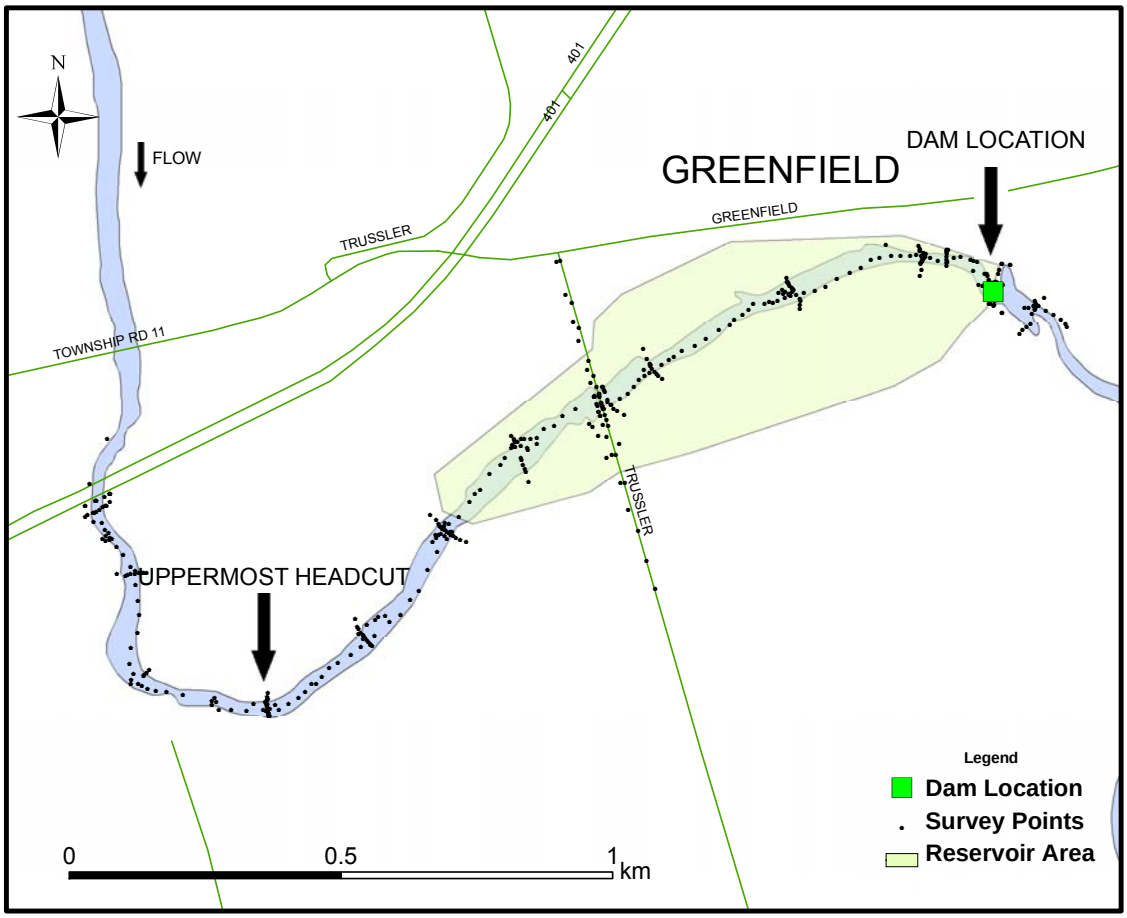

Figure C – 1. Greenfield Dam on Nith River at Greenfield site survey.

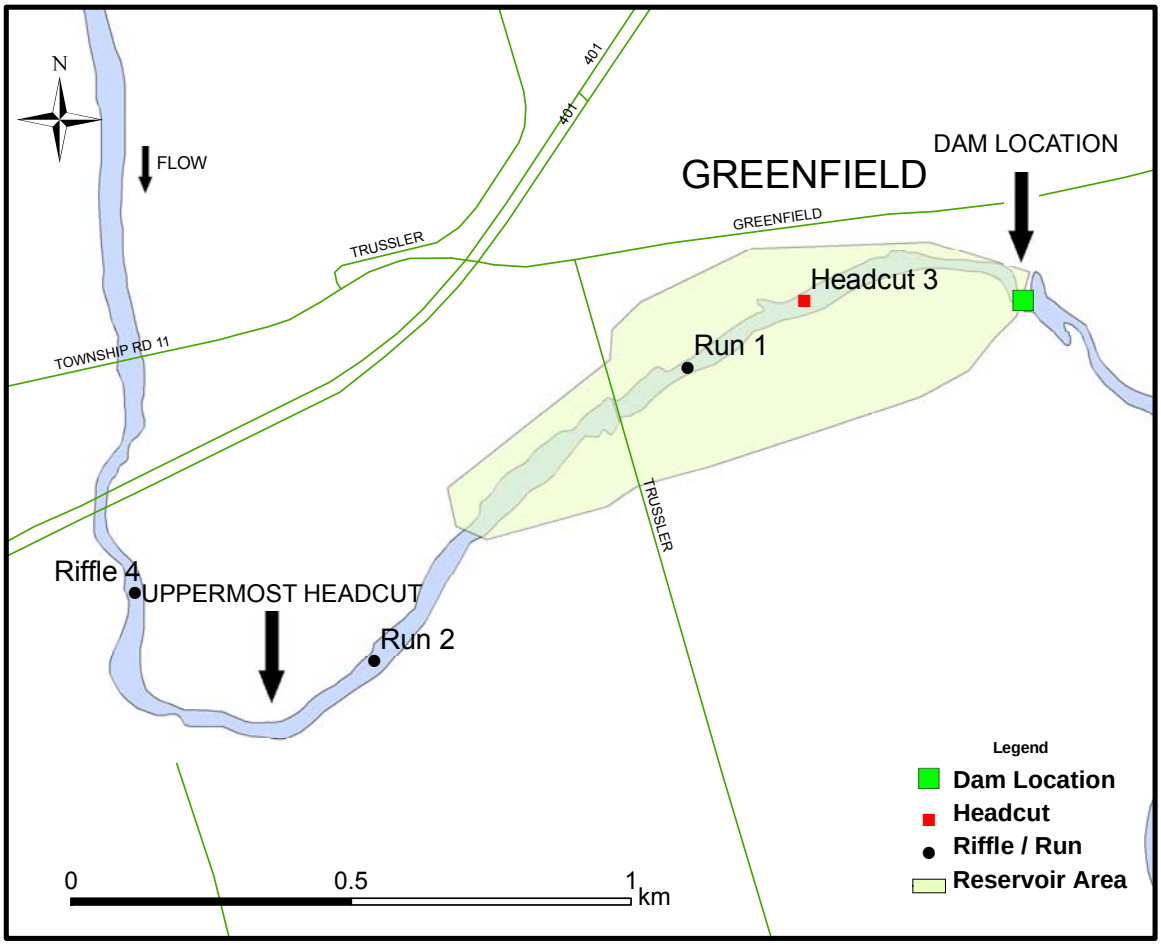

Figure E – 2. Locations of pavement samples at Greenfield Dam on Nith River.

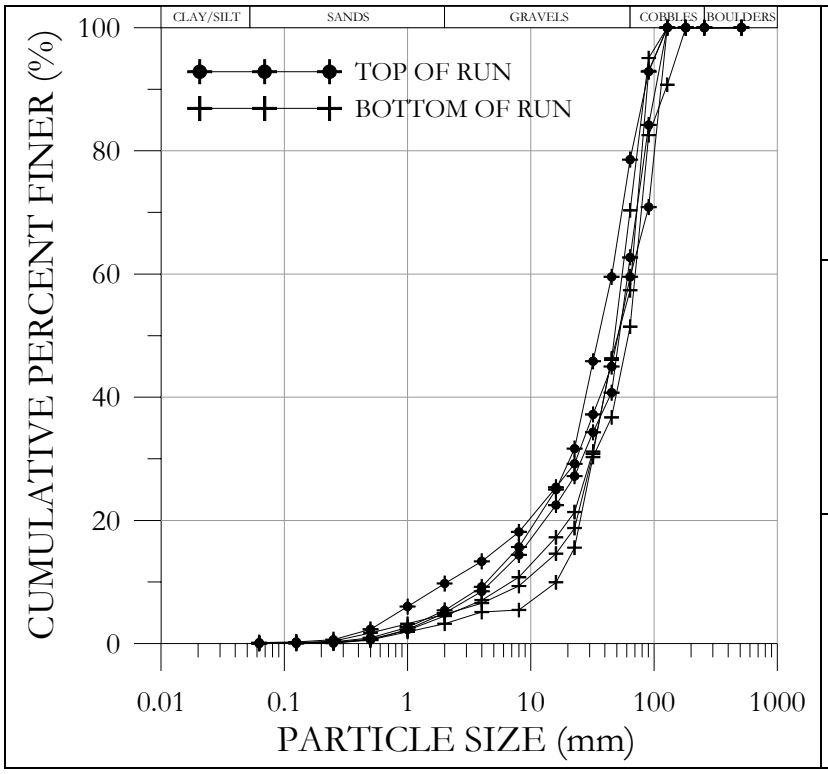

BOTTOM	
d	mm
5	1.8
16	14.7
25	22.7
50	44.0
75	63.9
84	66.8
95	87.2

TOP	
d	mm
5	1.1
16	6.8
25	9.5
50	30.9
75	47.8
84	62.7
95	87.4

d	mm
5	1.8
16	8.9
25	22.1
50	42.7
75	60.6
84	64.6
95	69.8

d	mm
5	0.5
16	4.1
25	9.3
50	44.1
75	85.1
84	89.7
95	95.8

d	mm
5	2.3
16	20.9
25	23.2
50	48.5
75	66.9
84	85.6
95	127.1

d	mm
5	1.7
16	7.2
25	15.5
50	44.6
75	64.8
84	69.7
95	93.4

Figure E – 3. Pavement sample characteristics of Run 1.

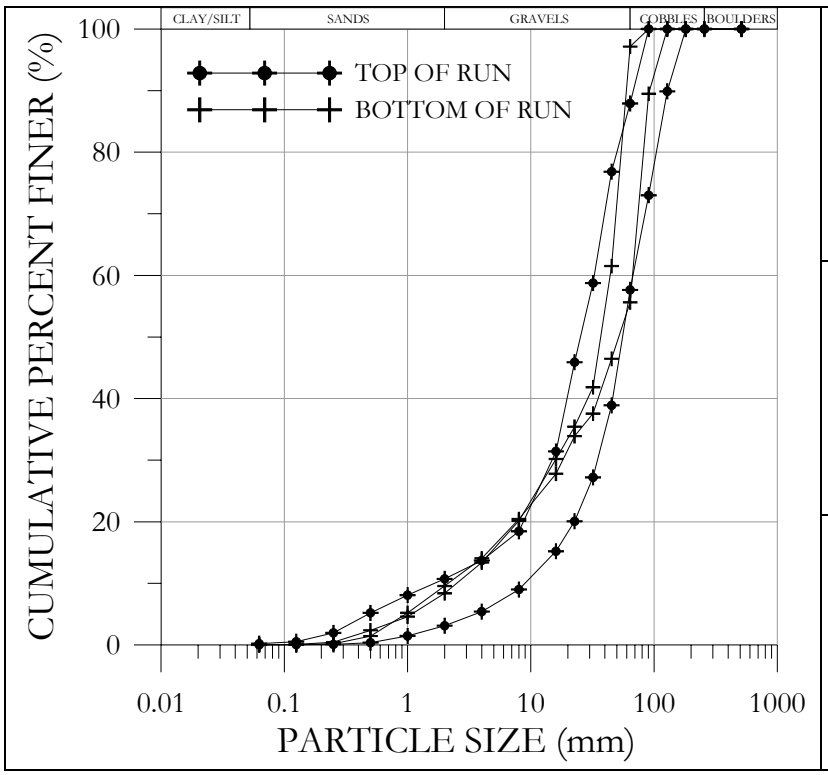

BOTTOM	
d	mm
5	0.9
16	3.8
25	8.0
50	31.5
75	44.3
84	46.3
95	48.8

TOP	
d	mm
5	0.6
16	4.3
25	8.7
50	24.2
75	44.5
84	47.8
95	64.9

d	mm
5	0.6
16	3.7
25	8.3
50	44.4
75	64.8
84	67.9
95	90.9

d	mm
5	1.0
16	8.1
25	22.2
50	60.1
75	68.0
84	90.4
95	130.1

Figure E – 4. Pavement sample characteristics of Run 2.

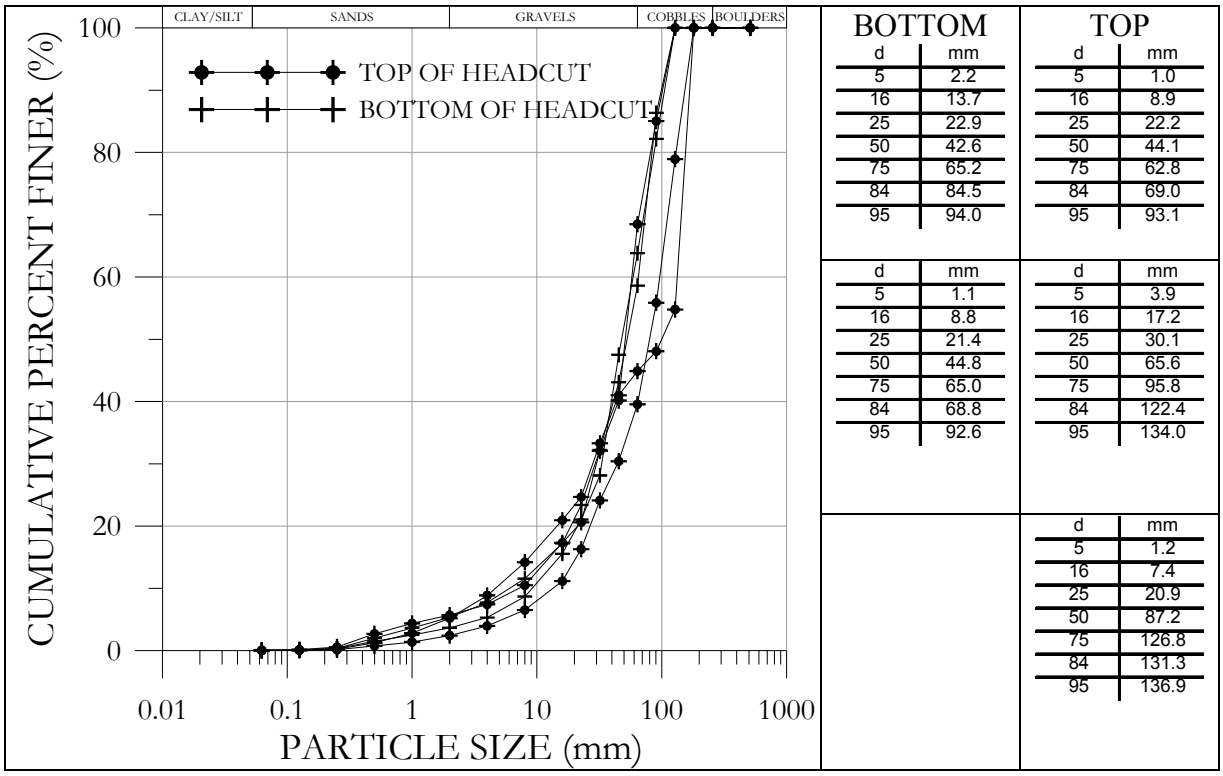

BOTTOM

d	mm
5	2.2
16	13.7
25	22.9
50	42.6
75	65.2
84	84.5
95	94.0

TOP

d	mm
5	1.0
16	8.9
25	22.2
50	44.1
75	62.8
84	69.0
95	93.1

d	mm
5	1.1
16	8.8
25	21.4
50	44.8
75	65.0
84	68.8
95	92.6

d	mm
5	3.9
16	17.2
25	30.1
50	65.6
75	95.8
84	122.4
95	134.0

d	mm
5	1.2
16	7.4
25	20.9
50	87.2
75	126.8
84	131.3
95	136.9

Figure E – 5. Pavement sample characteristics of Headcut 3.

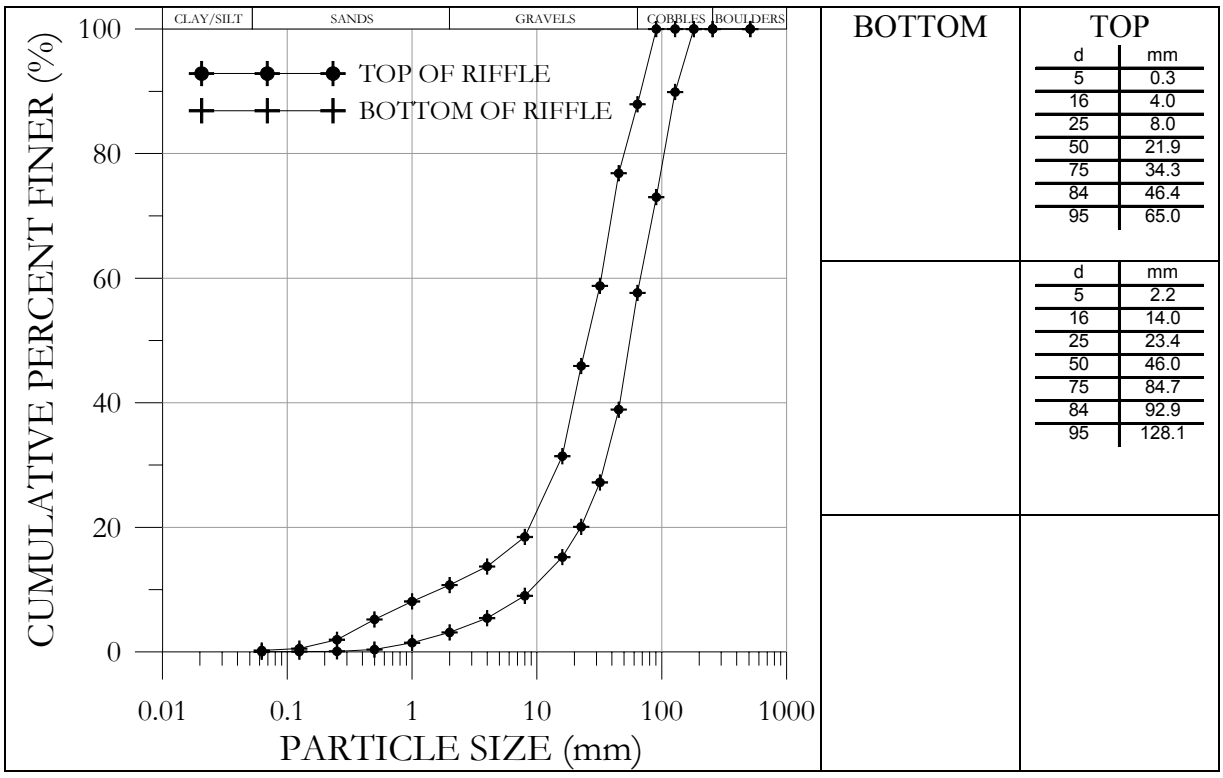

BOTTOM

TOP

d	mm
5	0.3
16	4.0
25	8.0
50	21.9
75	34.3
84	46.4
95	65.0

d	mm
5	2.2
16	14.0
25	23.4
50	46.0
75	84.7
84	92.9
95	128.1

Figure E –6. Pavement sample characteristics of Riffle 4.

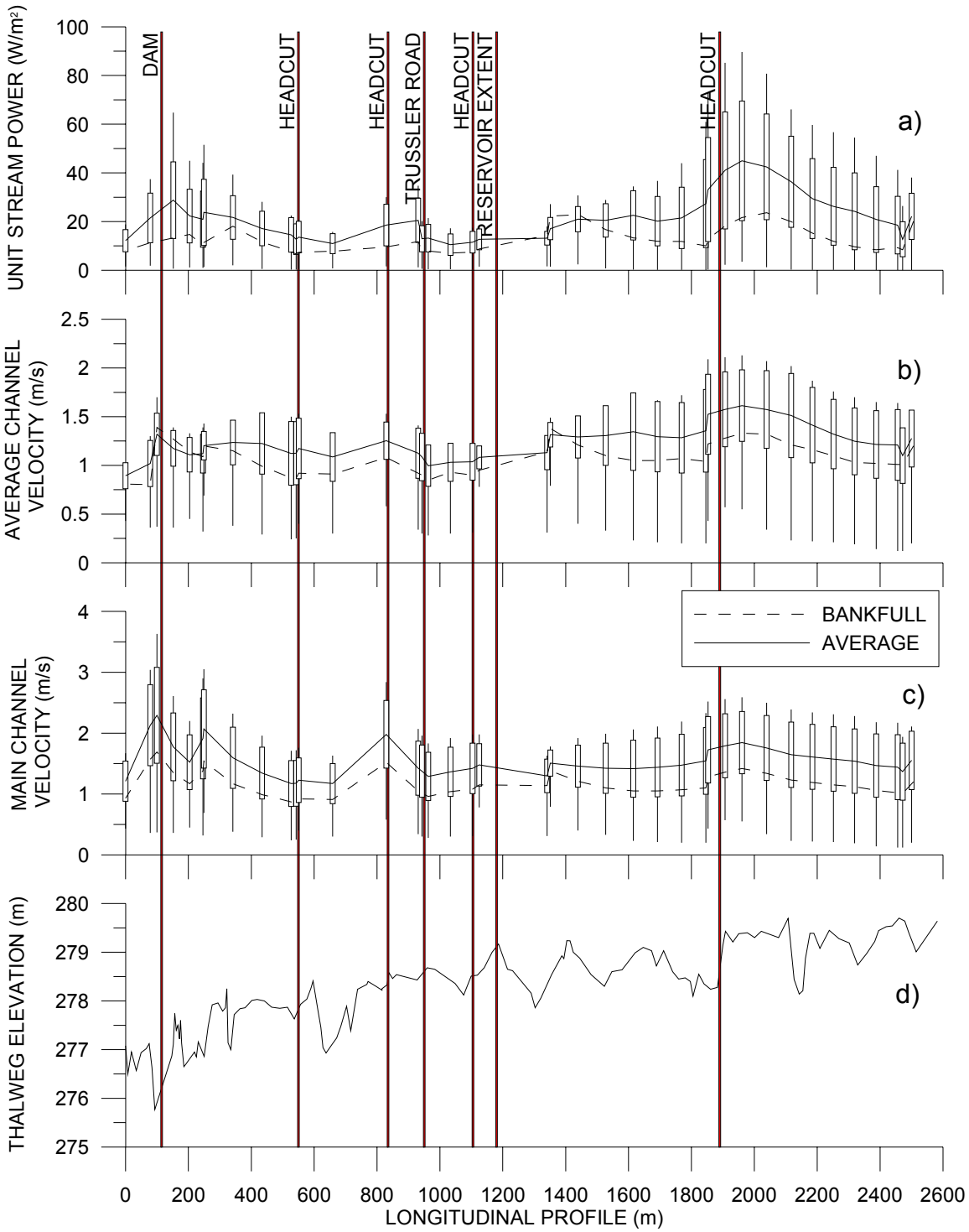

Figure E – 7. Results of a) unit stream power, b) average velocity, c) main channel velocity for incremental discharge analyses between $0 < Q \leq Q_{100}$, and d) thalweg elevation along the longitudinal profile for Nith River at Greenfield.

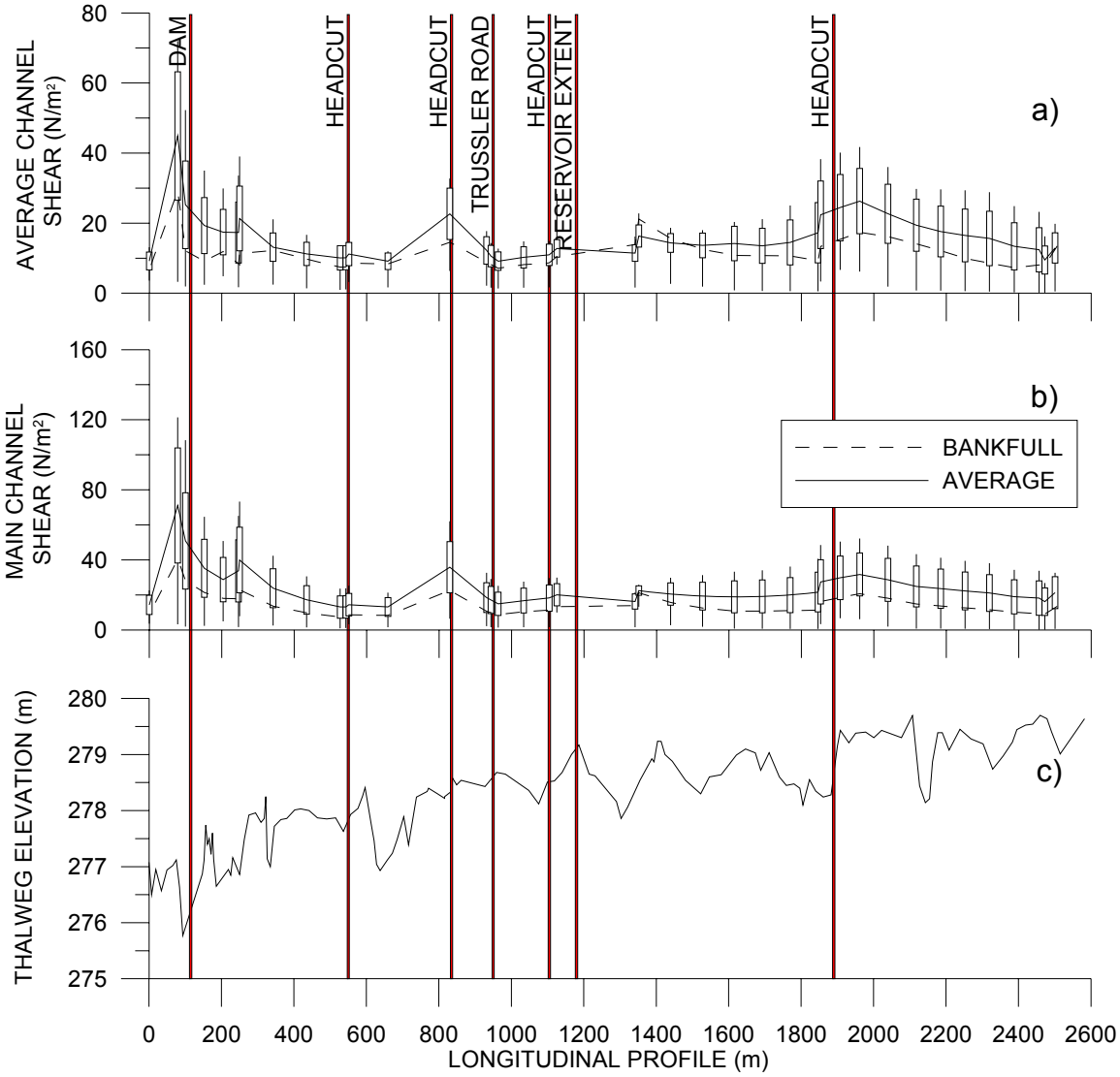

Figure E – 8. Results of a) average channel shear stress, b) main channel shear stress for incremental discharge analyses ranging between Q < Q < Q_{100}, and c) thalweg elevation along the longitudinal profile for Nith River at Greenfield.

Appendix F: Sutton Dam on Patterson Creek at Simcoe

Dam Location
Northing: 4744209m
Easting: 556476m
(Coordinate System: NAD 1983 UTM Zone 17N)

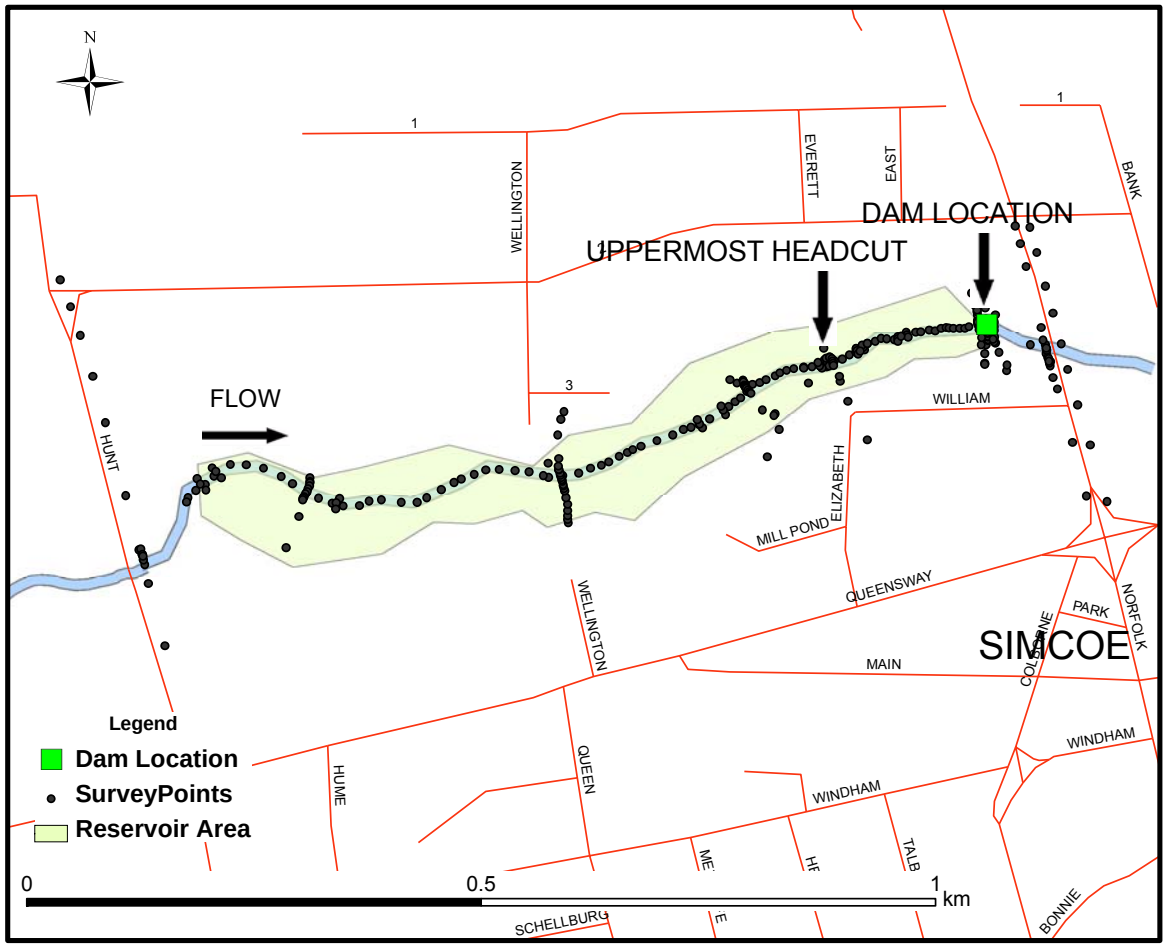

Figure F – 1: Sutton Dam on Patterson Creek at Simcoe site survey.

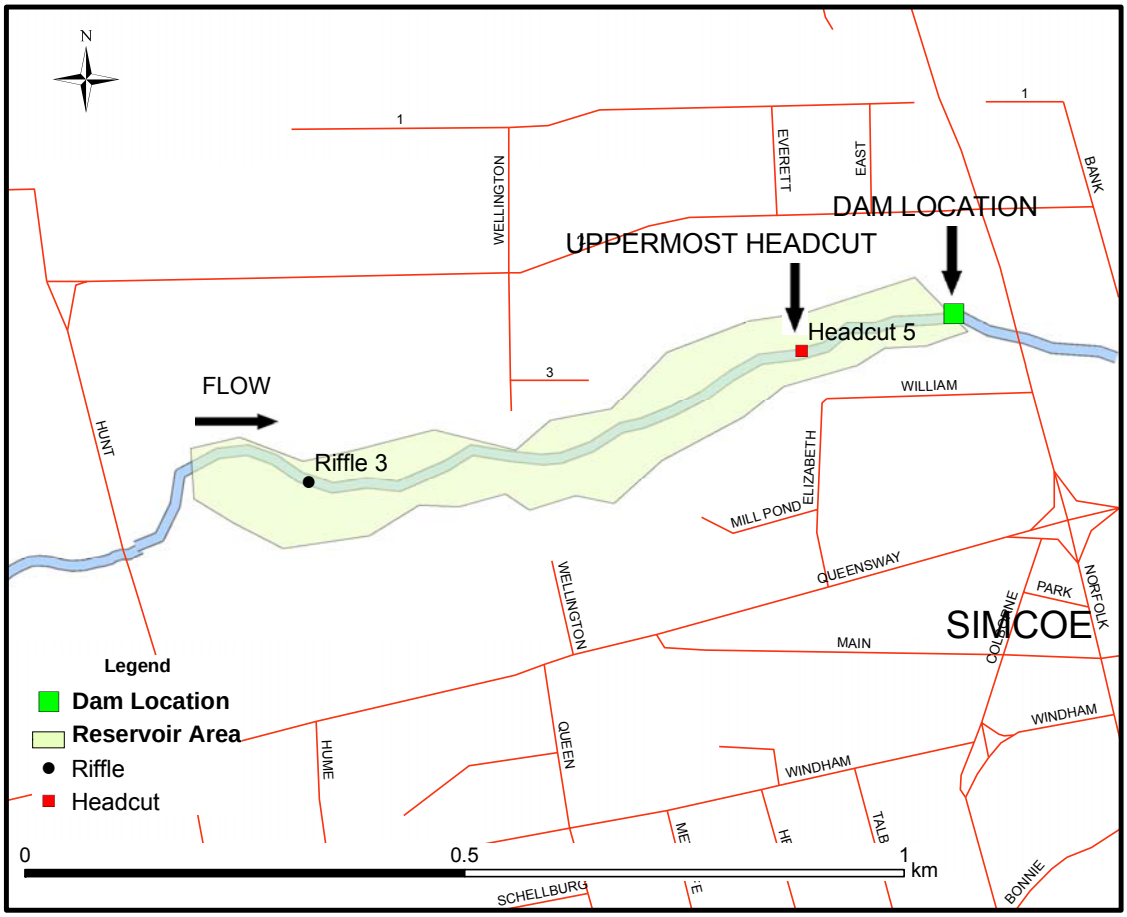

Figure F – 2: Locations of pavement samples at Sutton Dam on Patterson Creek.

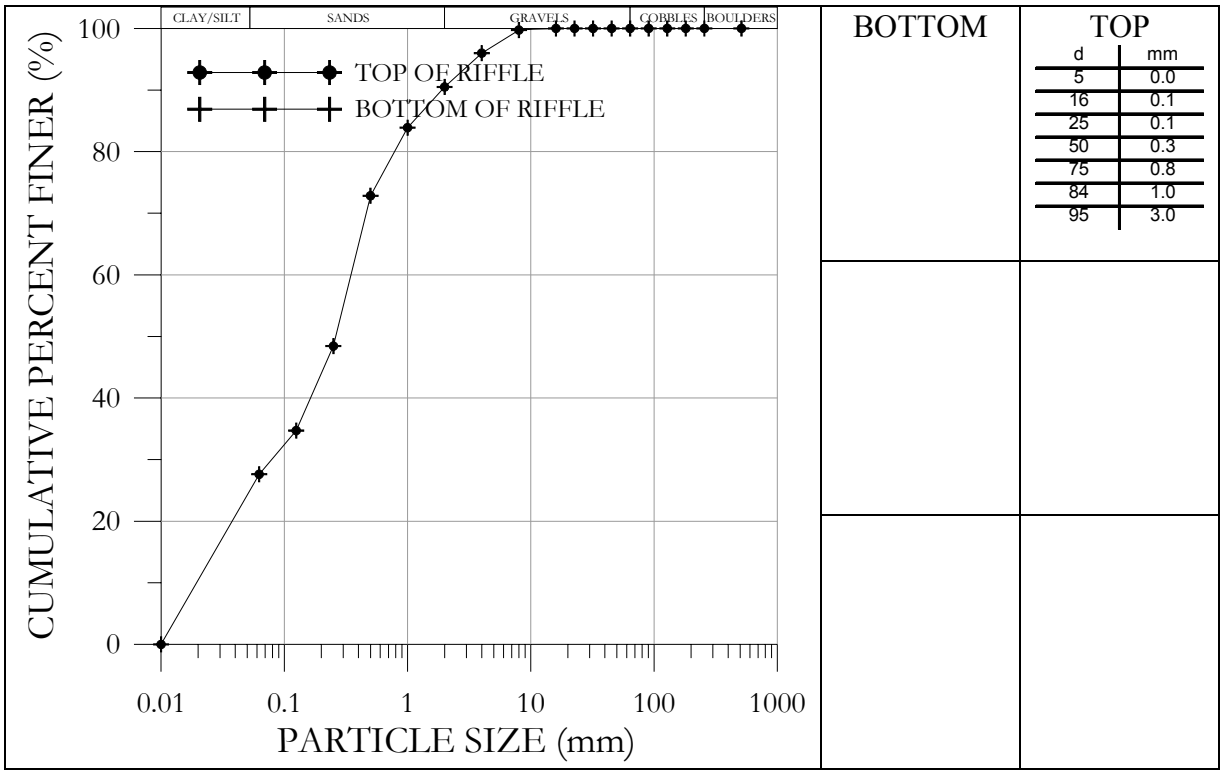

Figure F – 3. Pavement sample characteristics of Riffle 3.

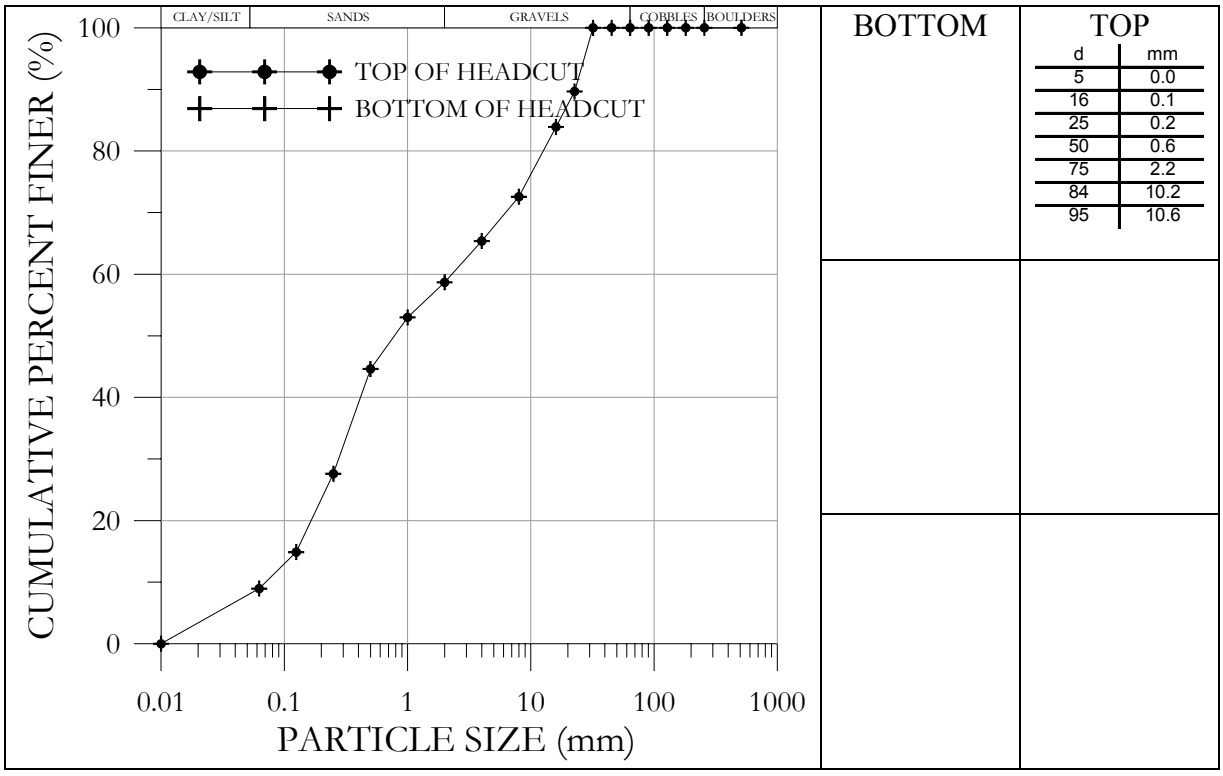

Figure F – 3. Pavement sample characteristics of Headcut 5.

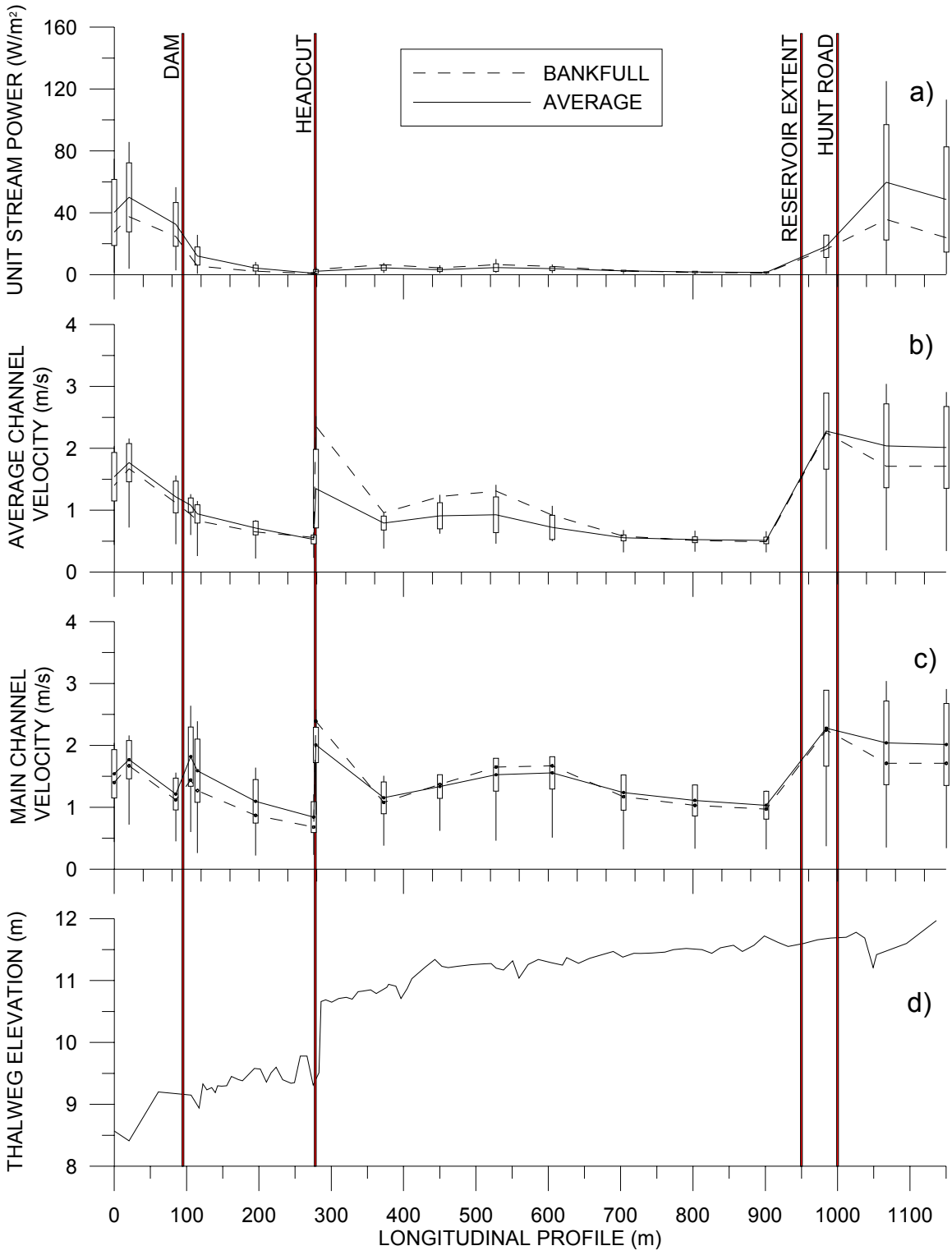

Figure F – 5. Results of a) unit stream power, b) average velocity, c) main channel velocity for incremental discharge analyses between $0 < Q \leq Q_{100}$, and d) thalweg elevation along the longitudinal profile for Patterson Creek at Simcoe.

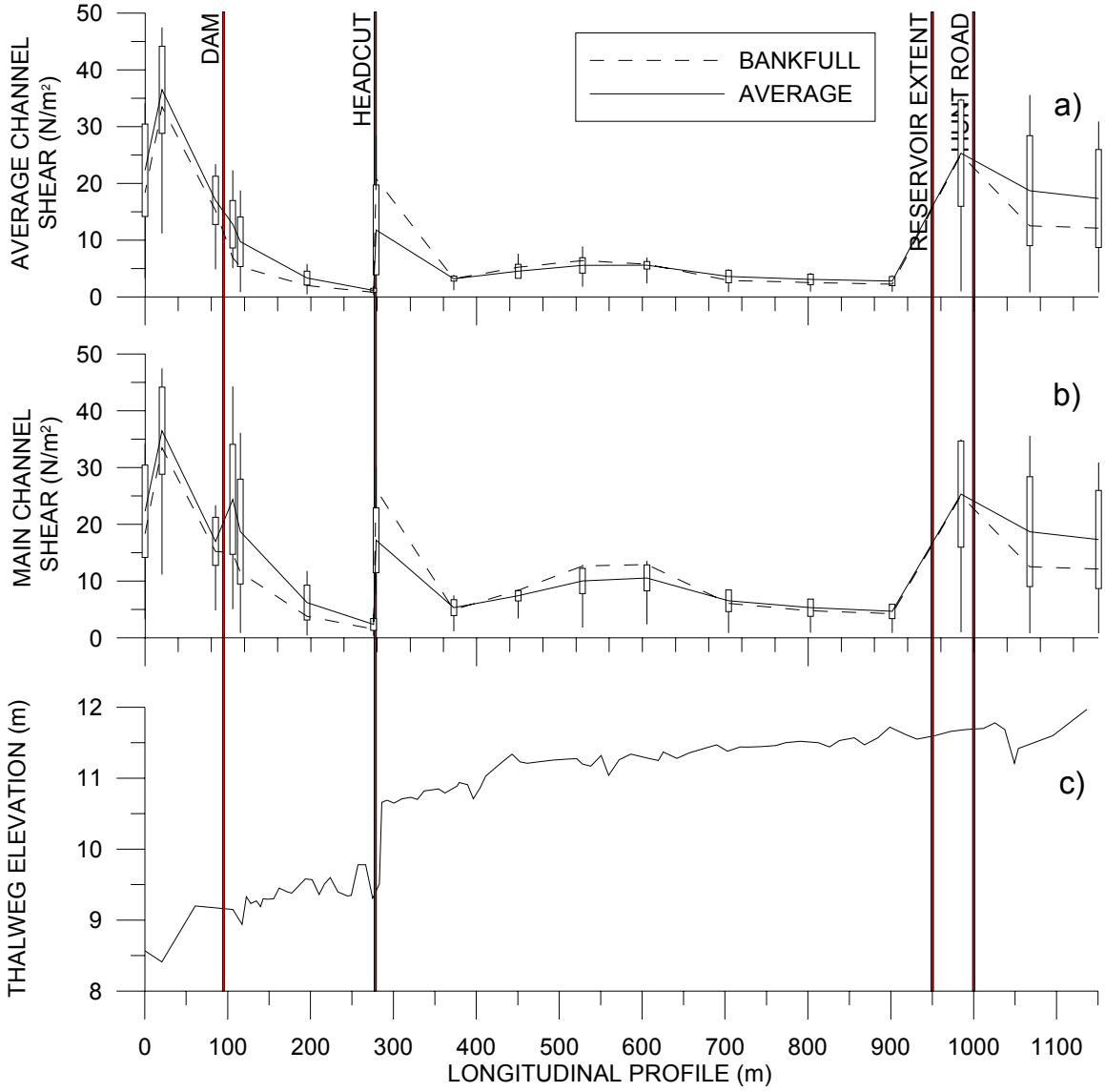

Figure F – 6. Results of a) average channel shear stress and b) main channel shear stress for incremental discharge analyses ranging between $Q < Q < Q_{100}$, and c) thalweg elevation along the longitudinal profile for Patterson Creek at Simcoe.

Appendix G: Teeswater Dam on Teeswater River at Teeswater

Dam Location:
Northing: 4871951m
Easting: 477291m
(Coordinate System: NAD 1983 UTM Zone 17N)

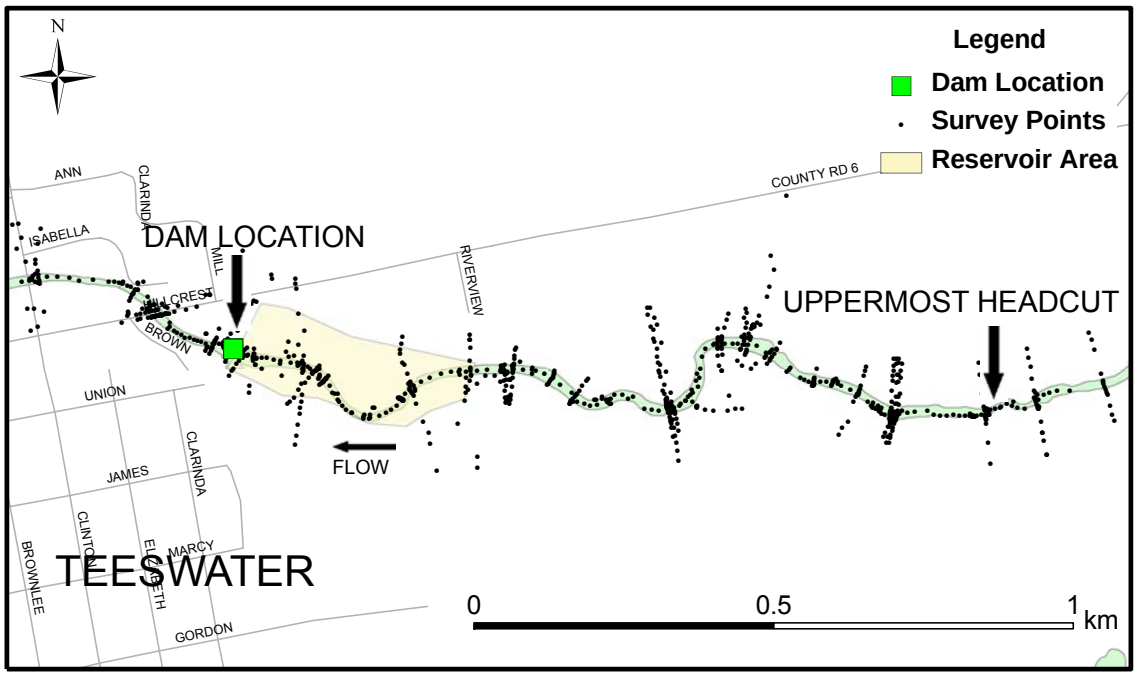

Figure G – 1: Teeswater Dam on Teeswater River at Teeswater site survey.

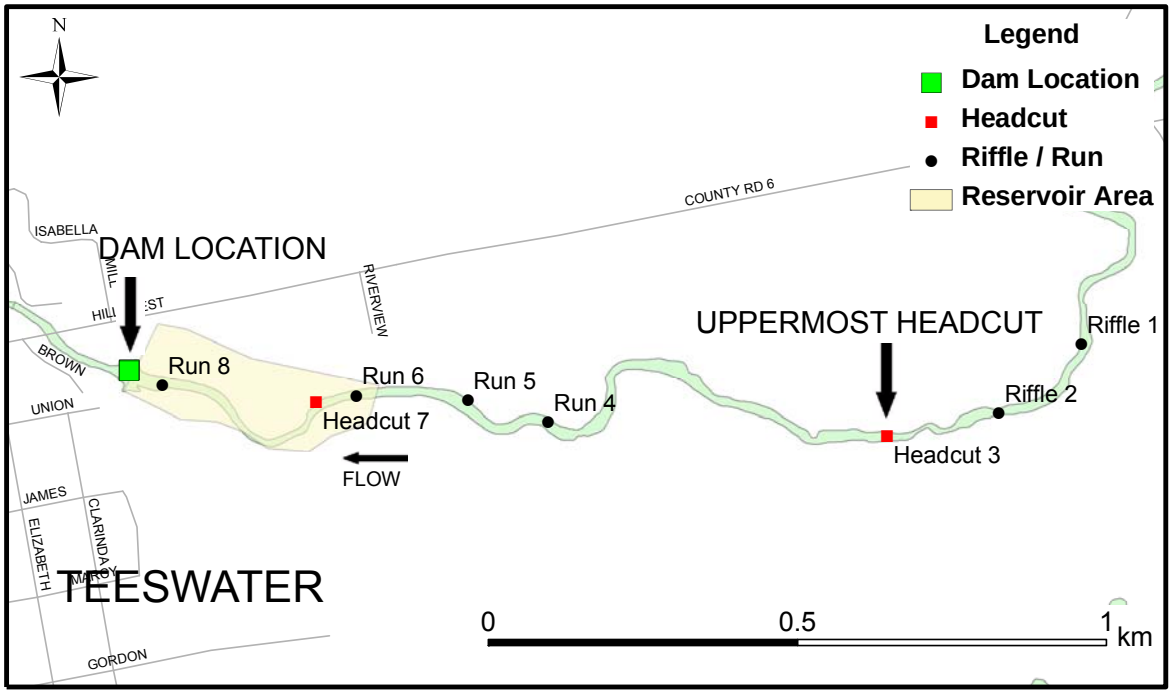

Figure G – 2: Locations of pavement samples at Teeswater Dam on Teeswater River.

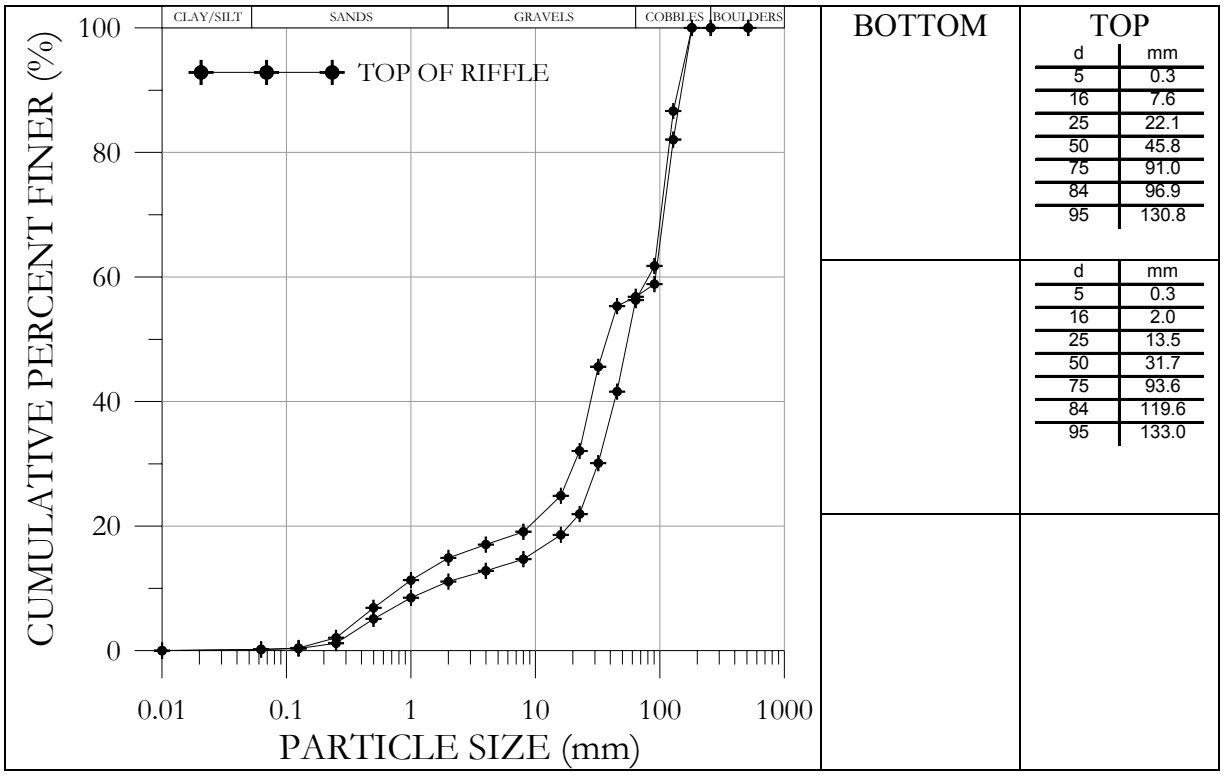

BOTTOM

d	mm
5	0.3
16	2.0
25	13.5
50	31.7
75	93.6
84	119.6
95	133.0

TOP

d	mm
5	0.3
16	7.6
25	22.1
50	45.8
75	91.0
84	96.9
95	130.8

Figure G – 3. Pavement sample characteristics of Riffle 1.

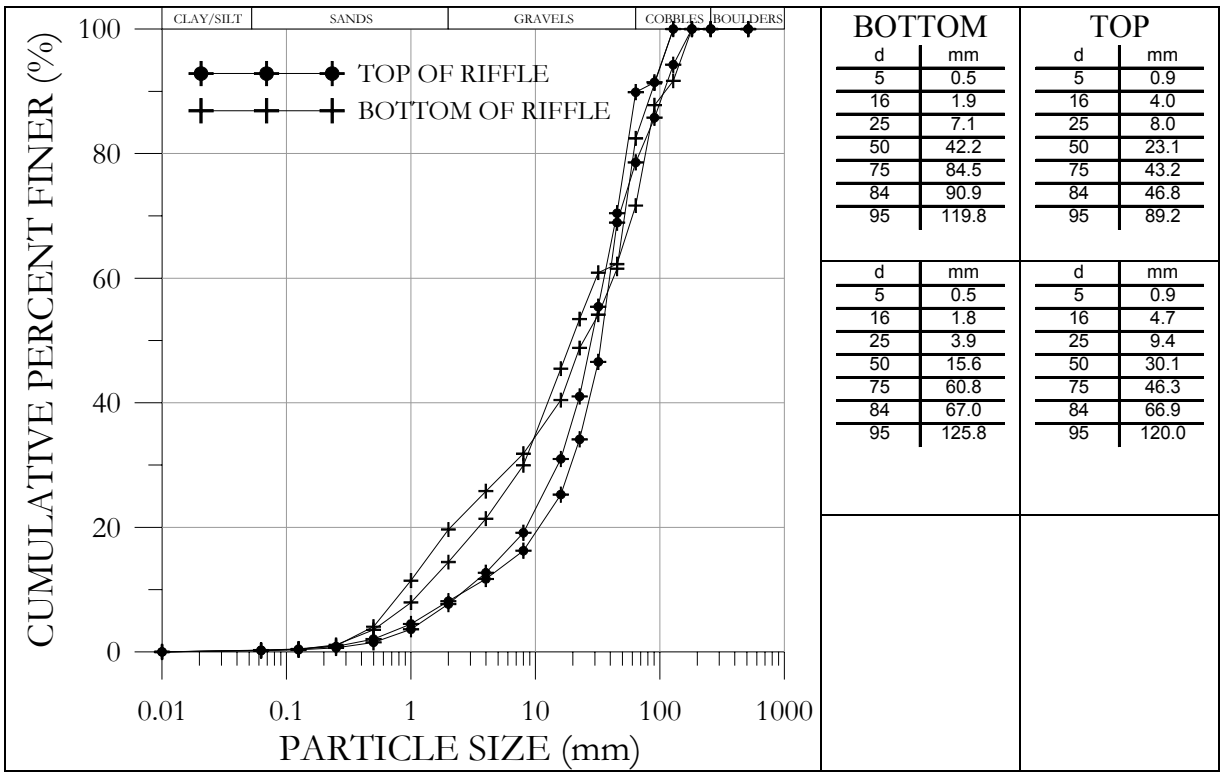

BOTTOM

d	mm
5	0.5
16	1.9
25	7.1
50	42.2
75	84.5
84	90.9
95	119.8

d	mm
5	0.5
16	1.8
25	3.9
50	15.6
75	60.8
84	67.0
95	125.8

TOP

d	mm
5	0.9
16	4.0
25	8.0
50	23.1
75	43.2
84	46.8
95	89.2

d	mm
5	0.9
16	4.7
25	9.4
50	30.1
75	46.3
84	66.9
95	120.0

Figure G – 4. Pavement sample characteristics of Riffle 2.

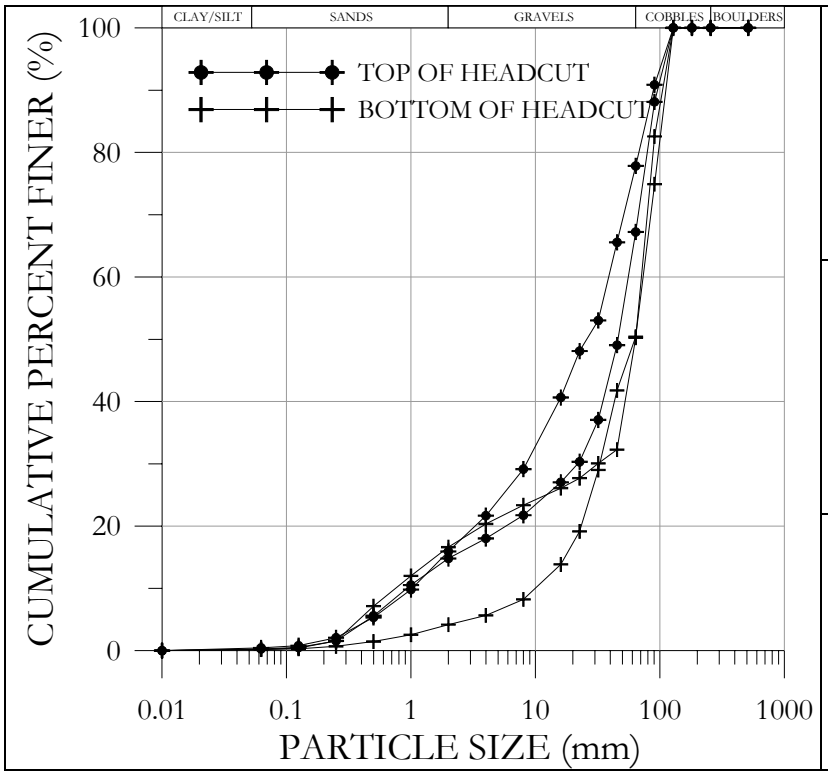

BOTTOM	
d	mm
5	0.3
16	1.1
25	8.3
50	49.2
75	67.0
84	84.2
95	93.9

TOP	
d	mm
5	0.3
16	1.9
25	8.3
50	41.9
75	62.6
84	67.4
95	91.8

d	mm
5	2.0
16	15.0
25	23.0
50	48.9
75	83.1
84	88.4
95	95.4

d	mm
5	0.3
16	1.7
25	3.9
50	22.2
75	47.4
84	63.7
95	89.8

Figure G – 5. Pavement sample characteristics of Headcut 3.

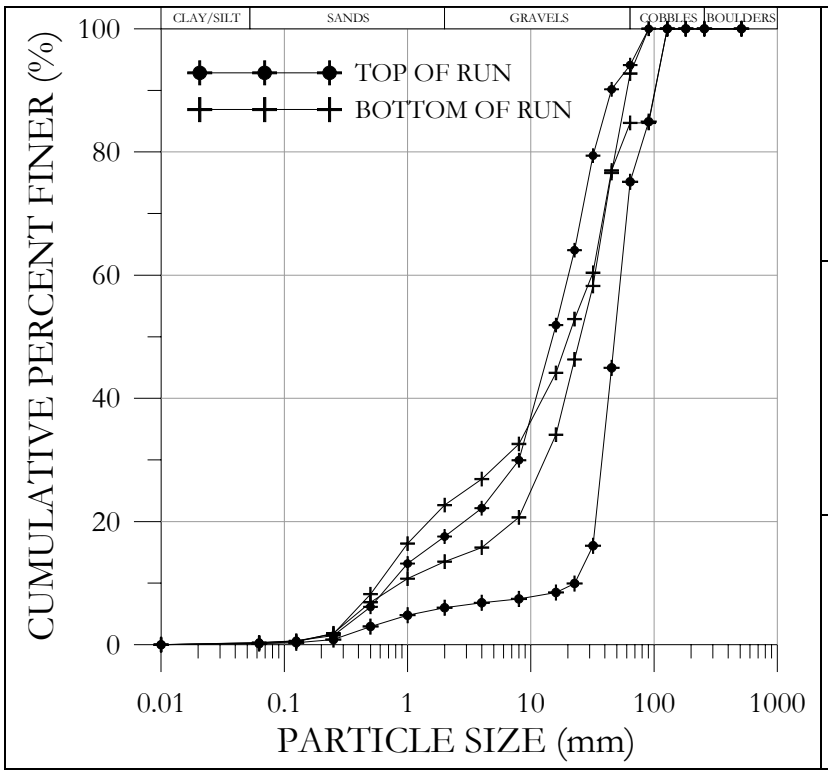

BOTTOM	
d	mm
5	0.3
16	3.4
25	7.5
50	21.9
75	34.4
84	44.9
95	62.0

TOP	
d	mm
5	0.3
16	1.1
25	3.8
50	9.2
75	23.5
84	31.6
95	60.3

d	mm
5	0.3
16	0.6
25	2.0
50	16.0
75	34.2
84	48.6
95	93.3

d	mm
5	0.9
16	24.6
25	31.0
50	42.7
75	49.3
84	68.7
95	93.2

Figure G – 6. Pavement sample characteristics of Run 4.

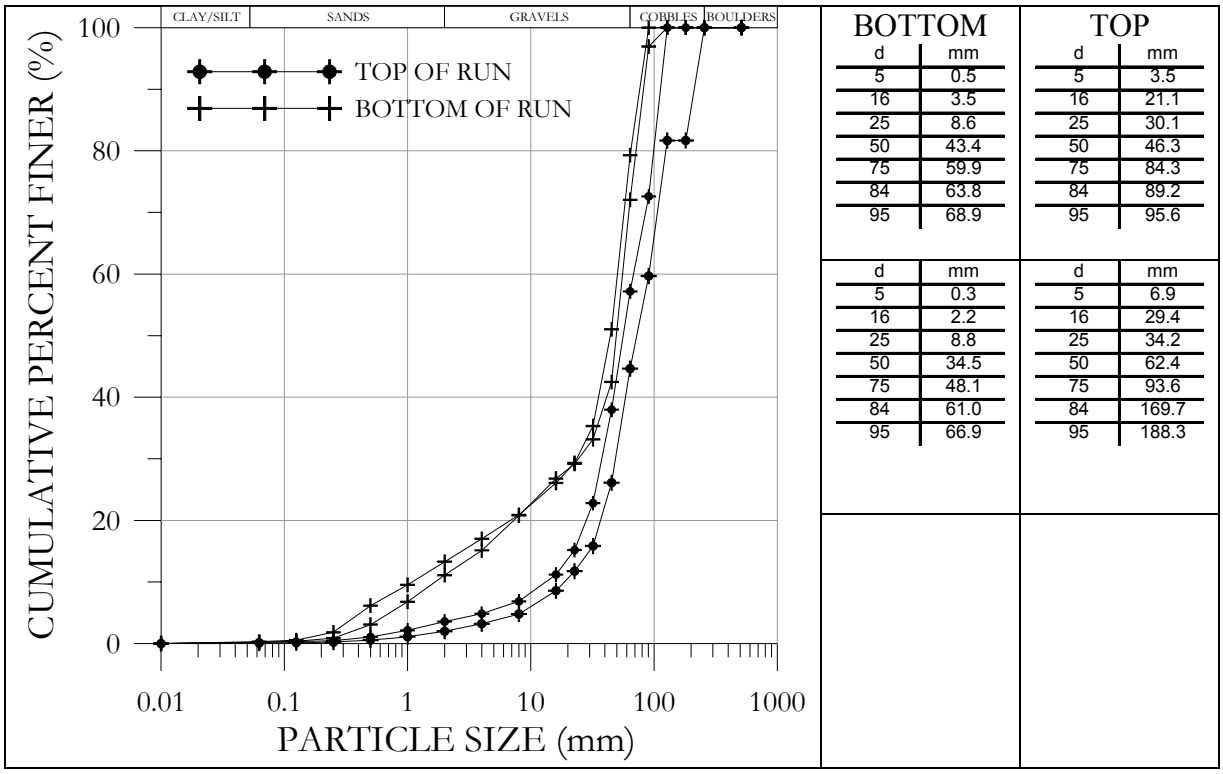

BOTTOM	
d	mm
5	0.5
16	3.5
25	8.6
50	43.4
75	59.9
84	63.8
95	68.9

TOP	
d	mm
5	3.5
16	21.1
25	30.1
50	46.3
75	84.3
84	89.2
95	95.6

d	mm
5	0.3
16	2.2
25	8.8
50	34.5
75	48.1
84	61.0
95	66.9

d	mm
5	6.9
16	29.4
25	34.2
50	62.4
75	93.6
84	169.7
95	188.3

Figure G – 7. Pavement sample characteristics of Run 5.

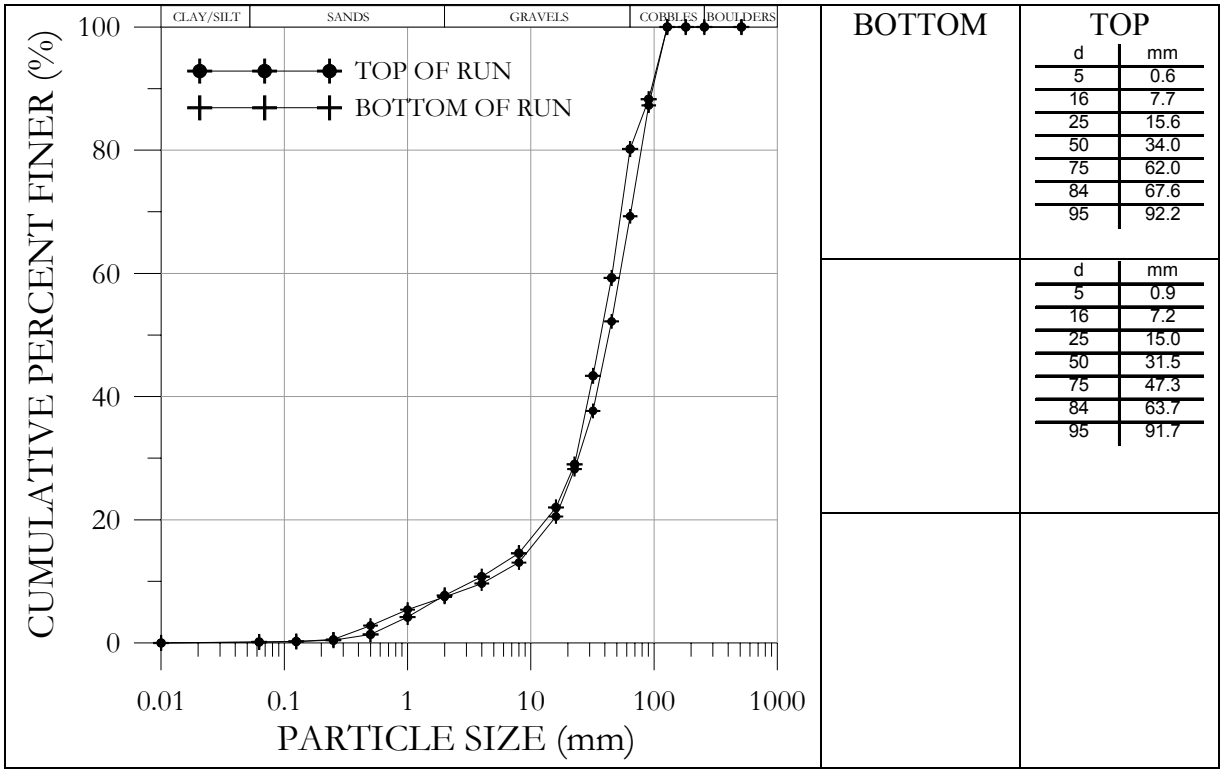

BOTTOM

TOP	
d	mm
5	0.6
16	7.7
25	15.6
50	34.0
75	62.0
84	67.6
95	92.2

d	mm
5	0.9
16	7.2
25	15.0
50	31.5
75	47.3
84	63.7
95	91.7

Figure G – 8. Pavement sample characteristics of Run 6.

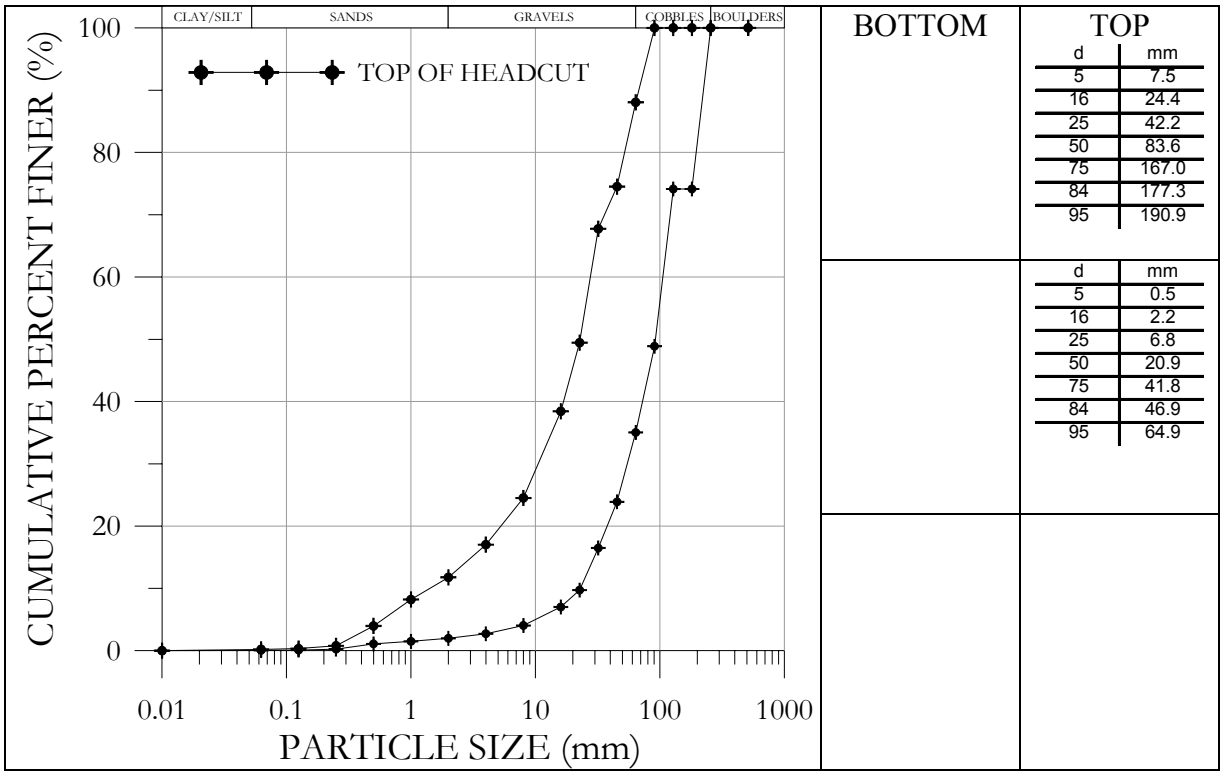

Figure G – 9. Pavement sample characteristics of Headcut 7.

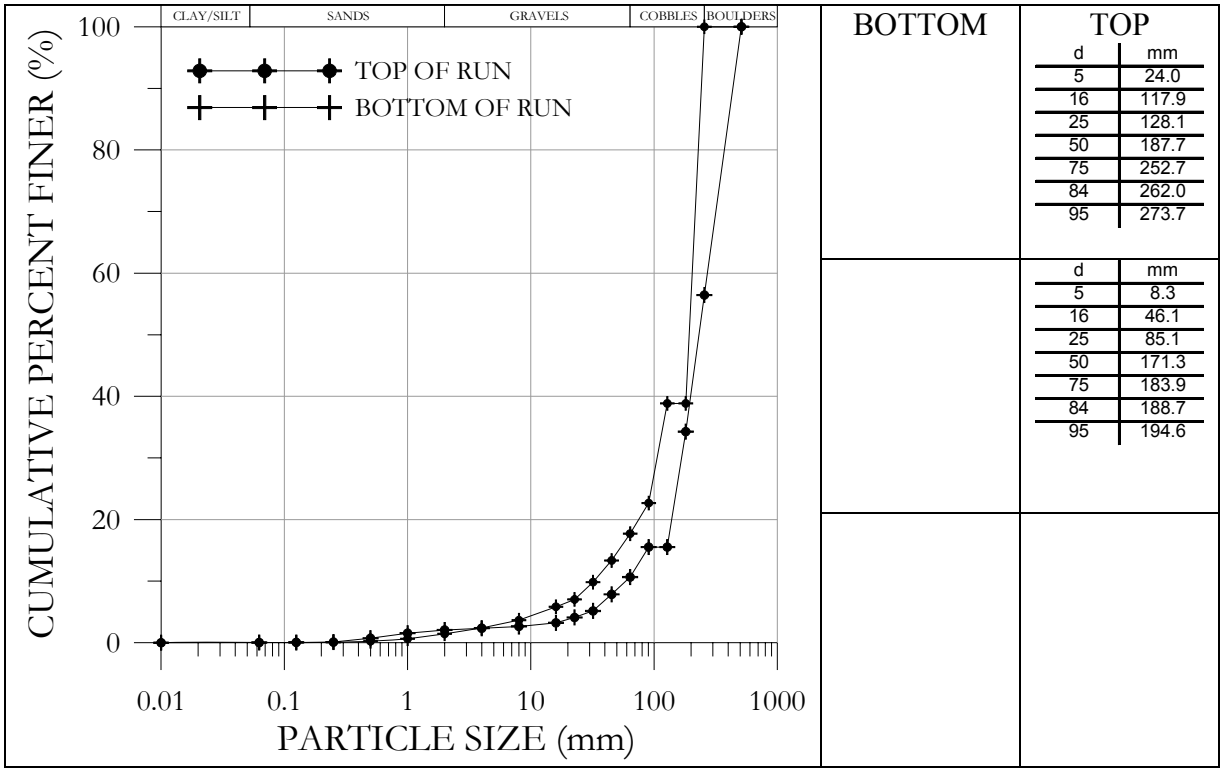

Figure G – 10. Pavement sample characteristics of Run 8.

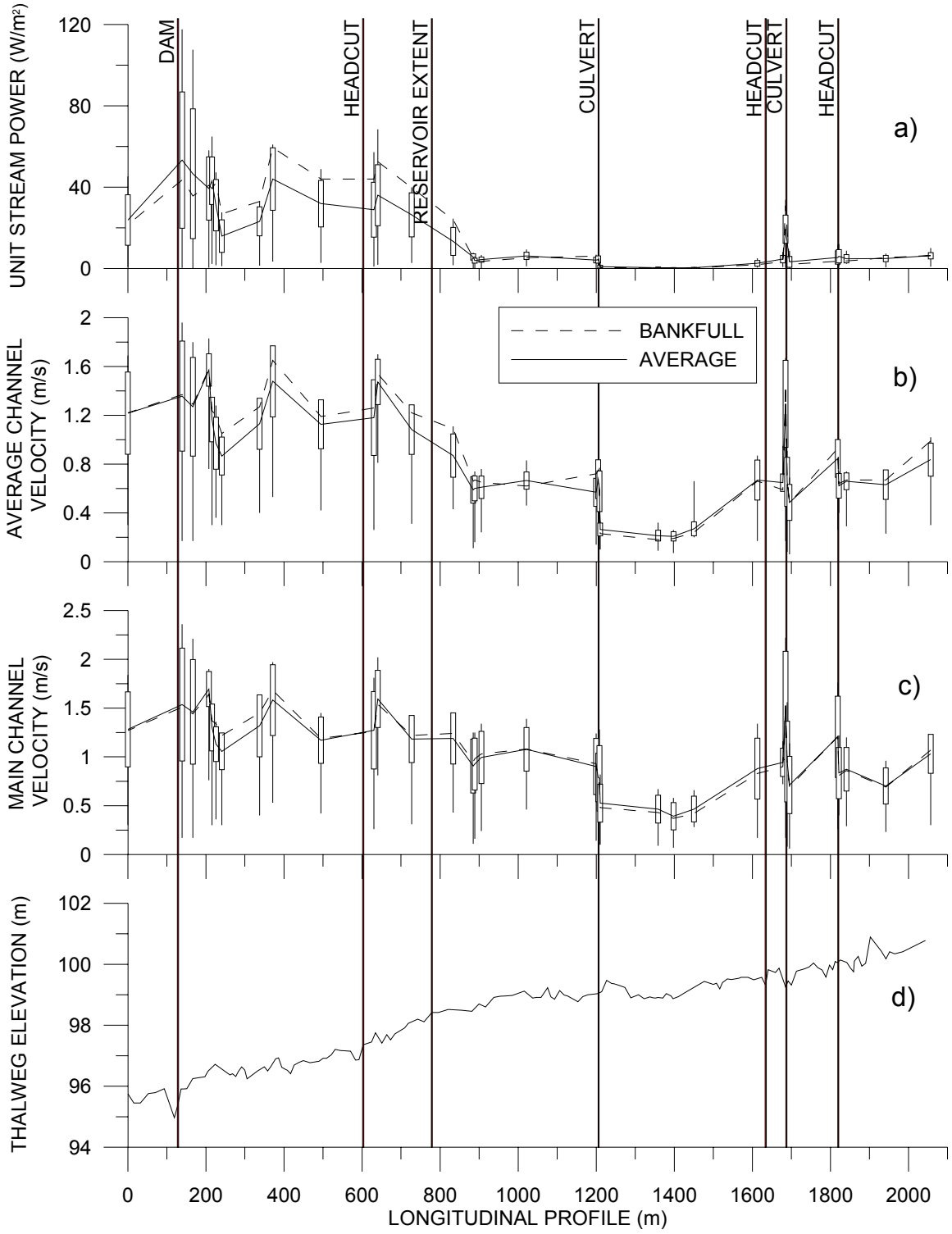

Figure G – 11. Results of a) unit stream power, b) average velocity, c) main channel velocity for incremental discharge analyses between $0 < Q \leq Q_{100}$, and d) thalweg elevation along the longitudinal profile for Teeswater River at Teeswater.

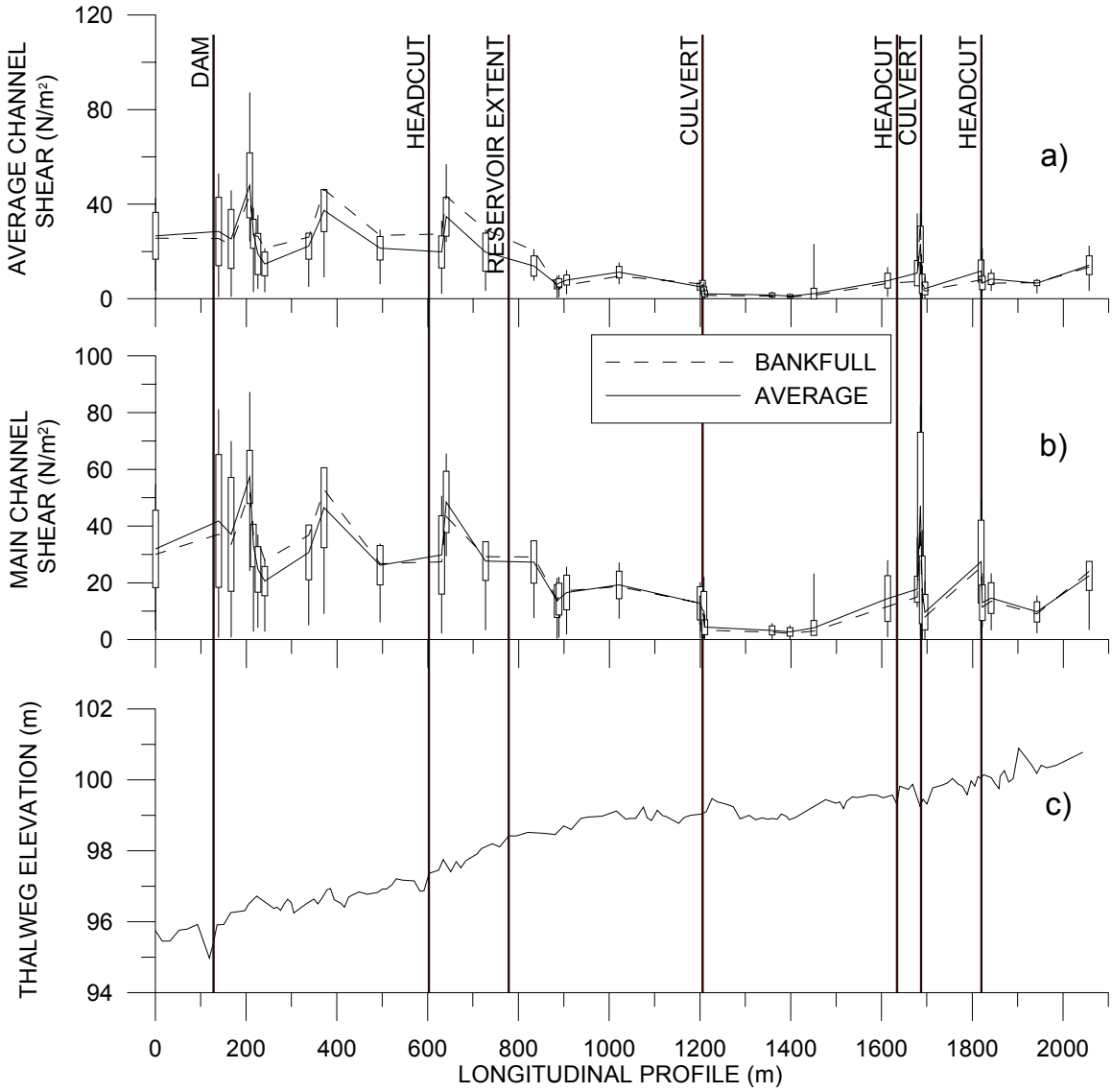

Figure G – 12. Results of a) average channel shear stress, b) main channel shear stress for incremental discharge analyses ranging between $Q < Q < Q_{100}$, and c) thalweg elevation along the longitudinal profile for Teeswater River at Teeswater for 100 equivalent flows up to 100 year flood.

Appendix H: Bognor Dam on Walter's Creek at Bognor

Dam Location:
Northing: 4930020m
Easting: 520701m
(Coordinate System: NAD 1983 UTM Zone 17N

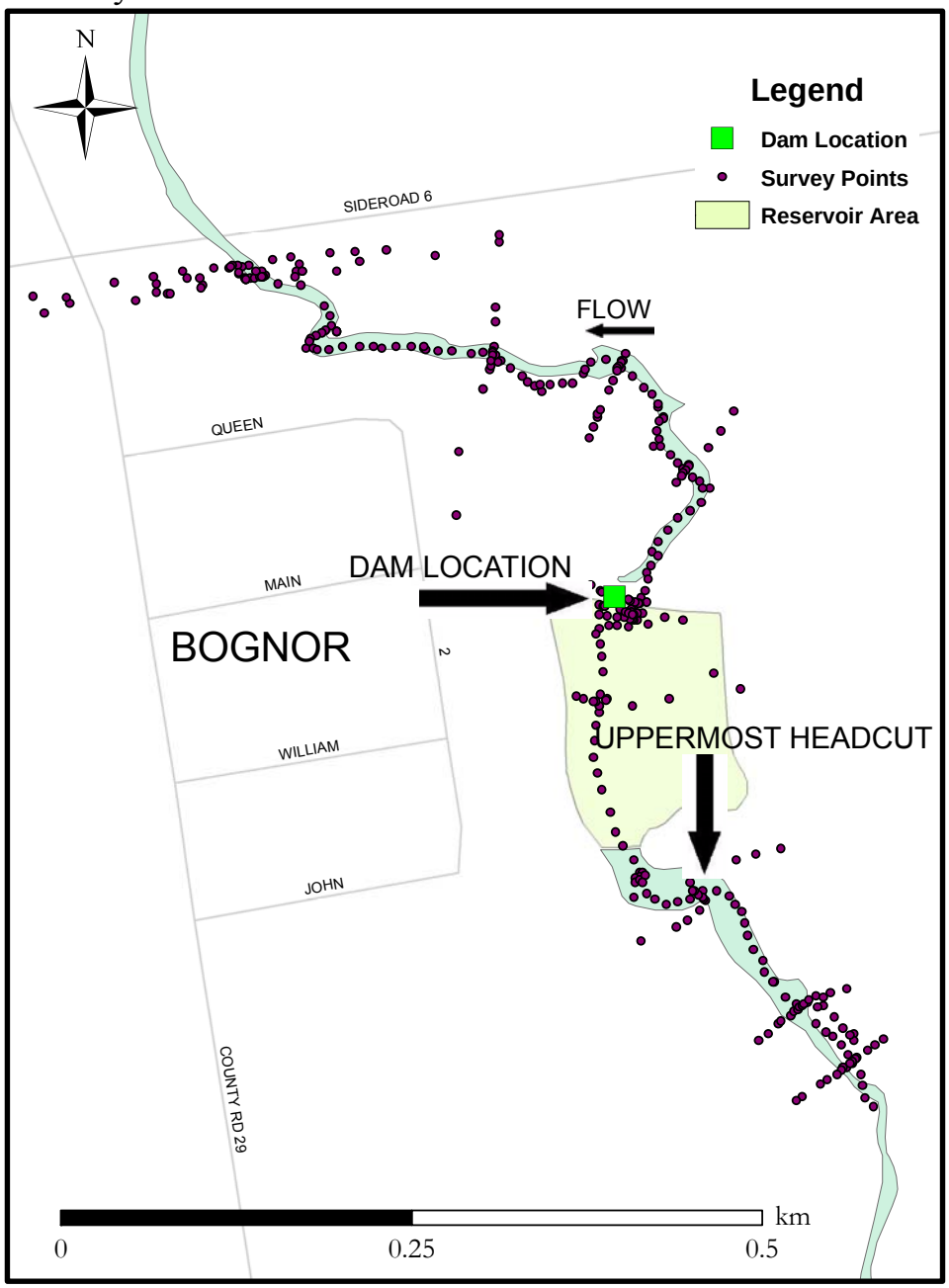

Figure H – 1: Bognor Dam on Walter's Creek at Bognor site survey.

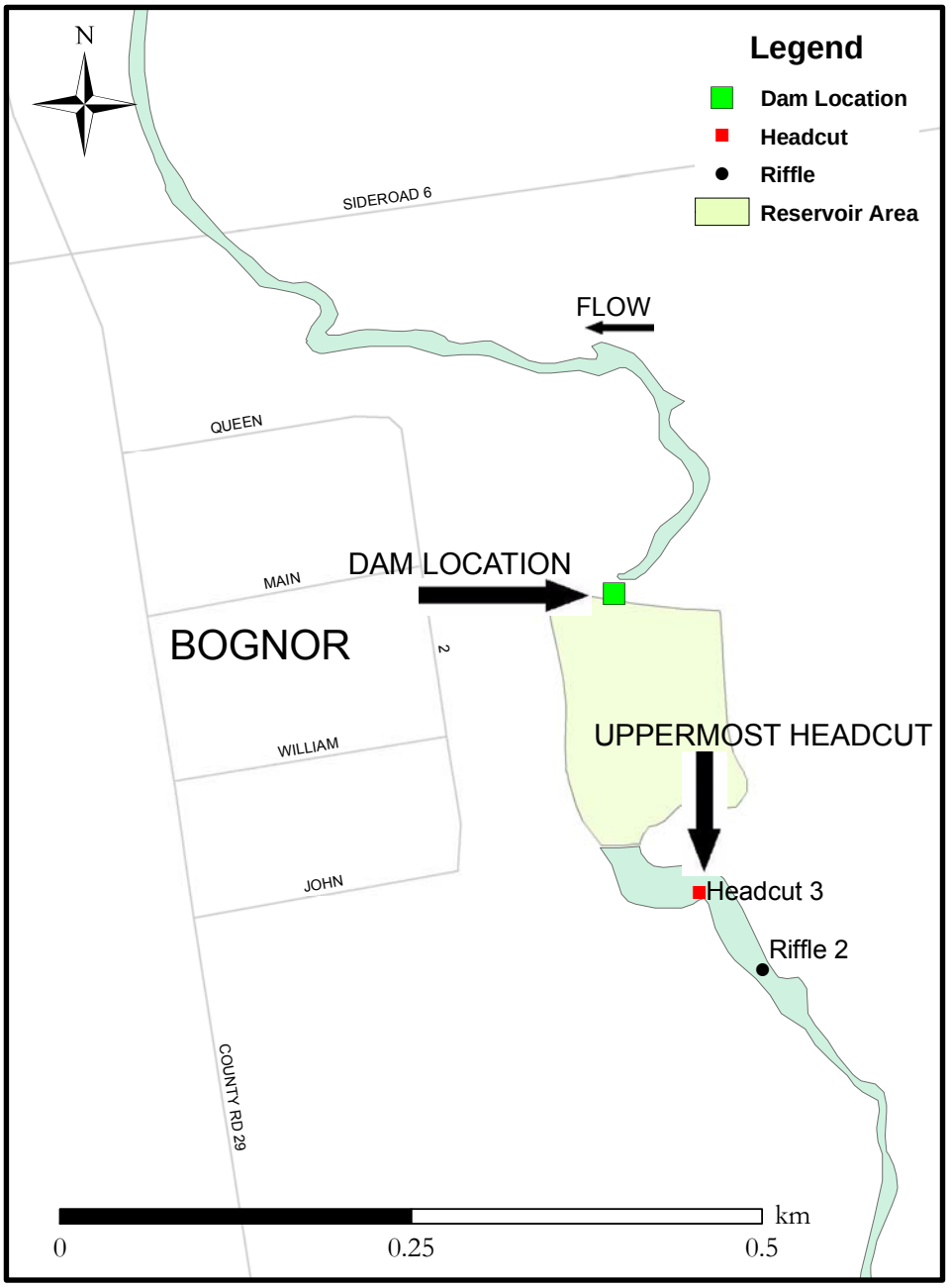

Figure H – 2: Locations of pavement samples at Bognor Dam on Walter's Creek.

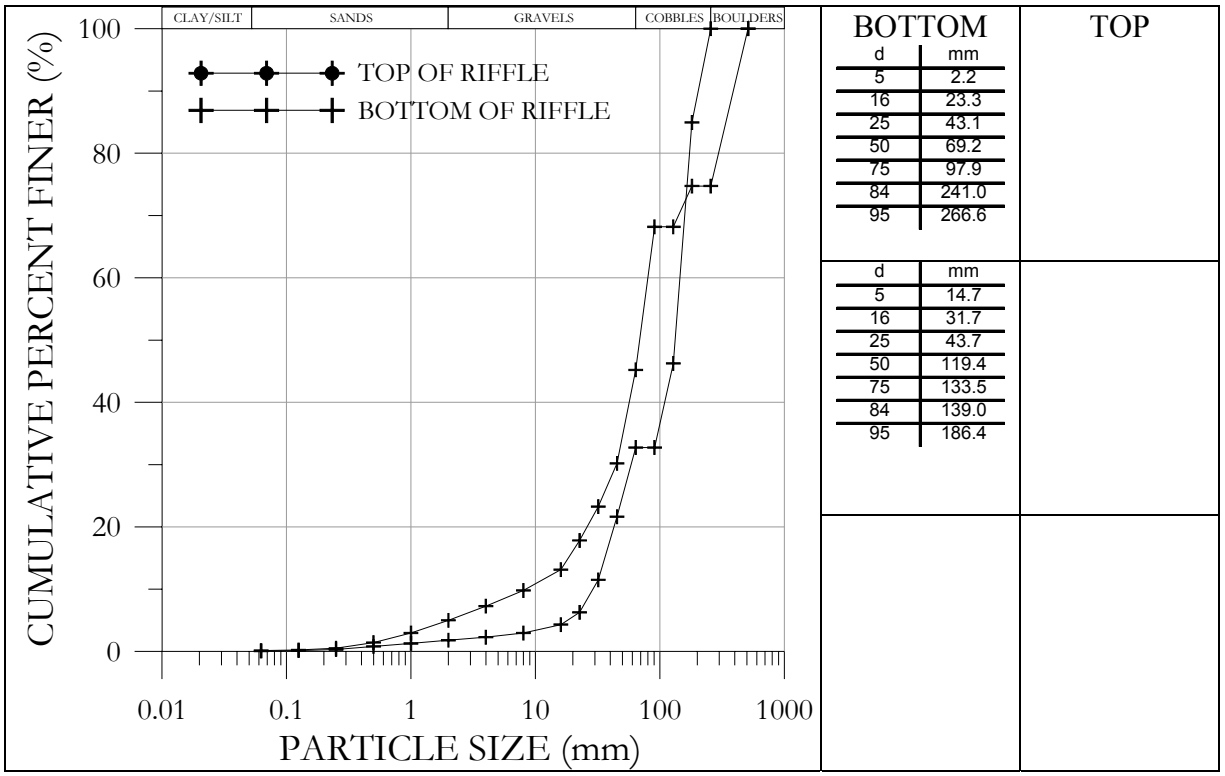

BOTTOM

d	mm
5	2.2
16	23.3
25	43.1
50	69.2
75	97.9
84	241.0
95	266.6

TOP

d	mm
5	14.7
16	31.7
25	43.7
50	119.4
75	133.5
84	139.0
95	186.4

Figure H – 3. Pavement sample characteristics of Riffle 2.

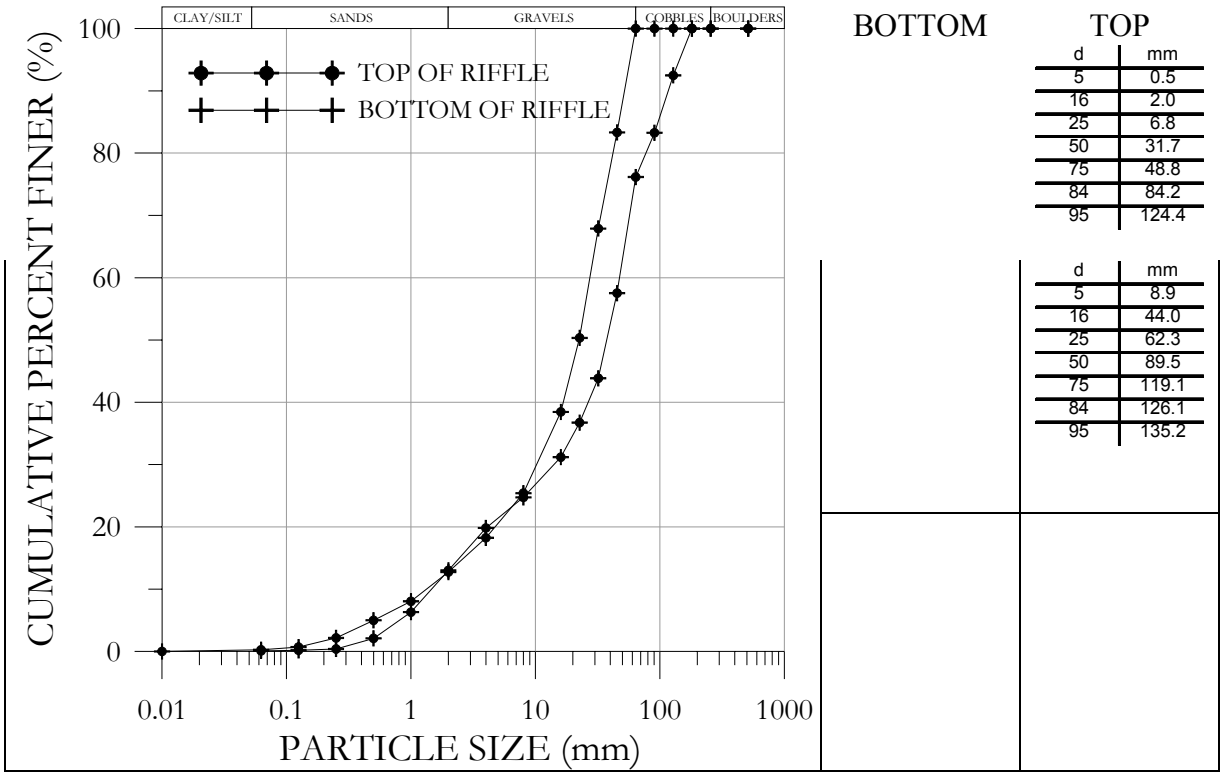

BOTTOM

TOP

d	mm
5	0.5
16	2.0
25	6.8
50	31.7
75	48.8
84	84.2
95	124.4

d	mm
5	8.9
16	44.0
25	62.3
50	89.5
75	119.1
84	126.1
95	135.2

Figure H – 4. Pavement sample characteristics of Headcut 3.

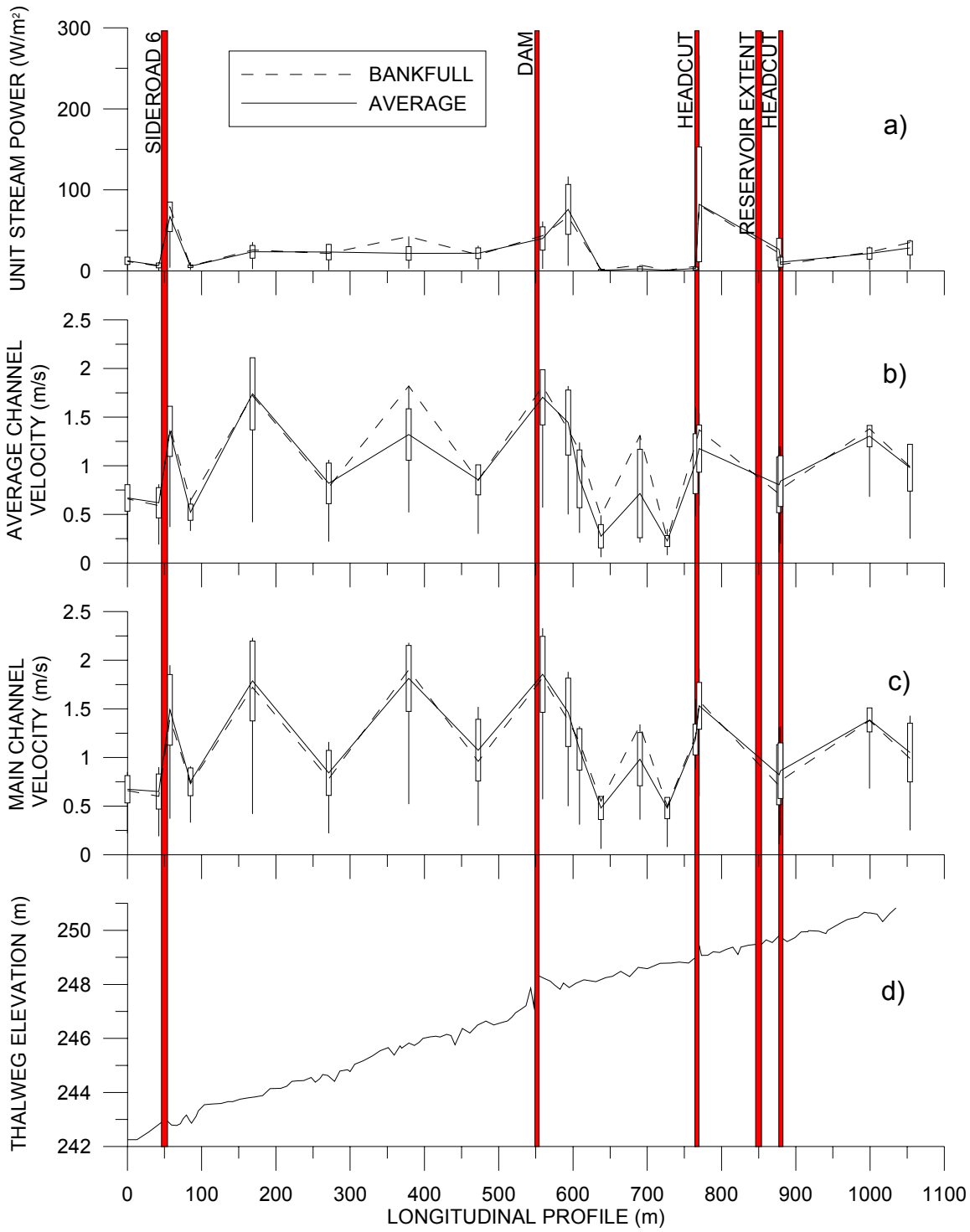

Figure H – 5. Results of a) unit stream power, b) average velocity, c) main channel velocity for incremental discharge analyses between $0 < Q \leq Q_{100}$, and d) thalweg elevation along the longitudinal profile for Walter's Creek at Bognor.

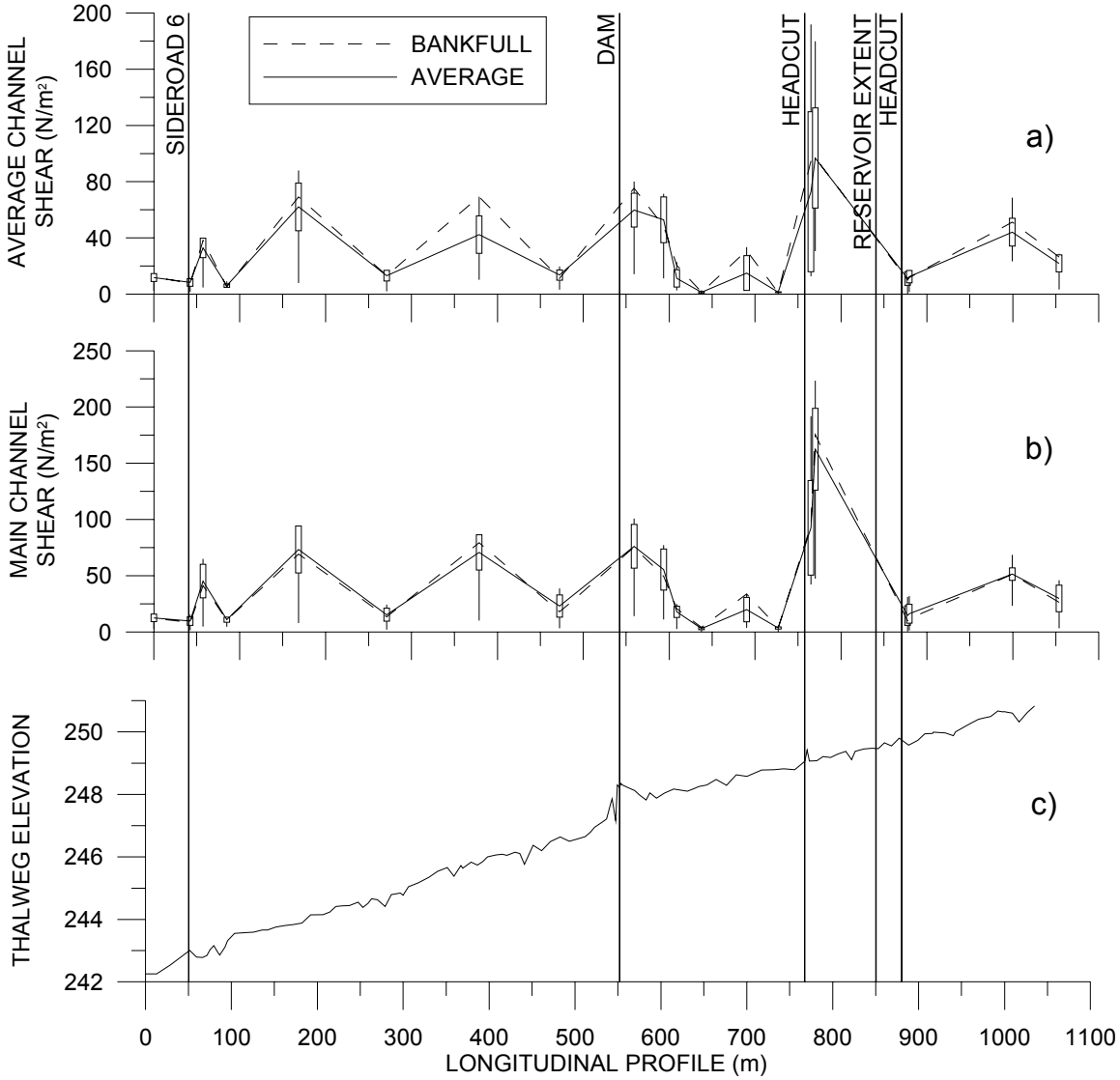

Figure H – 6. Results of a) average channel shear stress, b) main channel shear stress for incremental discharge analyses ranging between $Q < Q < Q_{100}$, and c) thalweg elevation along the longitudinal profile for Walter's Creek at Bognor.